Universitat de Lleida

Strategies for harnessing the maximum cold potential of a hybrid system for radiative cooling and solar collection

Roger Vilà Miró

http://hdl.handle.net/10803/687533

Universitat de Lleida

TESI DOCTORAL

Strategies for harnessing the maximum cold potential of a hybrid system for radiative cooling and solar collection

Roger Vilà Miró

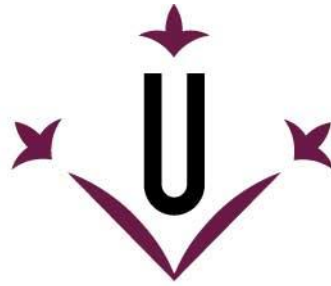Memòria presentada per optar al grau de Doctor per la Universitat de Lleida
Programa de Doctorat en Enginyeria i Tecnologies de la Informació

Directors
Prof. Dr. Albert Oriol Castell Casol
Prof. Dr. Marc Medrano Martorell

2022

This page is intentionally left blank

Agraïments

Als meus pare, la Silvia i en Lluís. Des de petit heu alimentat la meva inclinació curiosa. Sense els esforços que vàreu fer, sense la llavor de la curiositat, no hauria seguit pel camí de la investigació i avui aquesta tesi seria impensable.

Gràcies també a l'Albert i al Marc, els meus directors de tesis, pel vostre guiatge i dedicació. Gràcies per haver tingut en compte, durant tot el procés, les meves inquietuds. És gràcies als vostres consells i ajuda que avui aquesta tesi ha pogut arribar a bon port.

Vull expressar també la meva estima a tots els membres del grup SEMB, als antics i als més recents: primer per l'esforç que heu fet perquè pogués dedicar-me per complert a la recerca, però sobretot per l'ambient que s'hi respira al grup; al SEMB m'hi he sentit un més des del primer dia.

Als meus companys de fortuna i infortunis: a l'Ariadna per les converses necessàries, i a l'Alicia i el Boni per haver fet molt més senzill l'últim any de tesi.

A Tito, el meu germà, perquè aportes rauxa a la meva vida; i als meus amics, perquè encara que no sapigueu que he estat fent durant tres anys, heu sigut el màxim suport per a mi.

Finalment vull donar les gràcies a tots aquells que durant tants anys han regat el camp del coneixement. La meva és una contribució humil a la feina iniciada per molts abans que jo.

Acknowledgements

To my parents. From a young age you have nurtured my curious inclination. Without the efforts you made, without the seed of curiosity, I would have never pursued the path of research and today this thesis would be unthinkable.

Thanks to Albert and Marc, my thesis supervisors, for your guidance and dedication. Thank you for taking my concerns into consideration throughout the whole process. It is thanks to your advice and help that today this thesis has been able to come to fruition.

I would also like to express my appreciation to all the members of the SEMB group, both the oldest and the newest: first for the effort you have made so that I can dedicate myself completely to the research, but above all for the good environment created in the group; at SEMB I've felt part of the group from day one.

To my fellows in fortunes and misfortunes: to Ariadna for the necessary conversations, and to Alicia and Boni for making the last year of the thesis much easier.

To Tito, my brother, for bringing fun to my life; and to my friends, because even though you still don't know what I've been working on during these three years, you've been the ultimate support for me.

Finally, I want to thank all those who for so many years have watered the field of knowledge. Mine is a humble contribution to the work begun by many before me.

Institutional acknowledgements

Resum

La transformació i l'ús d'energies és essencial per al funcionament de les societats contemporànies. Però aquest ús va lligat, des de la Revolució Industrial, a emissions de gasos d'efecte hivernacle que han modificat el comportament del clima a nivell mundial; situació que s'ha conegut com a canvi climàtic. El nostre repte és el de construir societats capaces d'adaptar-se a aquests canvis a la vegada que en pal·lien els efectes o, si més no, no els empitjoren. Una de les estratègies d'adaptació passa per substituir les fonts d'energia, que encara avui són no-renovables, per fonts d'energia netes i renovables.

La tecnologia de refrigeració radiant, o *radiative cooling*, es presenta com una alternativa renovable per a la producció de fred per a la climatització d'espais. A més a més, investigacions prèvies han demostrat que, mitjançant un sol dispositiu, es pot produir fred i calor, en moments del dia diferents, aprofitant els fenòmens de refrigeració radiant i captació solar. Malgrat tot, la potència de producció de fred és considerablement baixa en comparació amb, per exemple, la producció de calor.

L'objectiu perseguit en aquesta tesi és el d'identificar estratègies que maximitzin el potencial de les tecnologies combinades de refrigeració radiant i captació solar. Al llarg de la tesi s'estudien tres estratègies consistents en: (1) la utilització de cobertes convectives que redueixin les pèrdues paràsites de convecció; (2) l'aprofitament del fred produït per refrigeració radiant per tal de millorar el rendiment de sistemes energètics convencionals, reduint el consum d'electricitat; i (3) la identificació de les regions europees on el potencial de producció de fred i calor és màxim.

Resumen

La transformación y uso de la energía es esencial para el funcionamiento de las sociedades contemporáneas. Pero este uso va ligado, desde la Revolución Industrial, a emisiones de gases de efecto invernadero que han modificado el comportamiento del clima a nivel mundial; situación que se ha conocido como cambio climático. Nuestro reto es el de construir sociedades capaces de adaptarse a estos cambios a la vez que palian sus efectos o, al menos, no los empeoran. Una de las estrategias de adaptación pasa por sustituir las fuentes de energía, que todavía hoy son no renovables, por fuentes de energía limpias y renovables.

La tecnología de refrigeración radiante, o *radiative cooling,* se presenta como una alternativa renovable para la producción de frío para la climatización de espacios. Además, investigaciones previas han demostrado que, mediante un solo dispositivo, se puede producir frío y calor, en momentos del día distintos, aprovechando los fenómenos de refrigeración radiante y captación solar. Sin embargo, la potencia de producción de frío es considerablemente baja en comparación con, por ejemplo, la producción de calor.

El objetivo perseguido en esta tesis es el de identificar estrategias que maximicen el potencial de las tecnologías combinadas de refrigeración radiante y captación solar. A lo largo de la tesis se estudian tres estrategias consistentes en: (1) la utilización de cubiertas convectivas que reduzcan las pérdidas parásitas de convección; (2) el aprovechamiento del frío producido por refrigeración radiante para mejorar el rendimiento de sistemas energéticos convencionales, reduciendo el consumo de electricidad; y (3) la identificación de las regiones europeas donde el potencial de producción de frío y calor es máximo.

Summary

The transformation and use of energy is essential for the functioning of contemporary societies. But this use has been linked, since the Industrial Revolution, to greenhouse gas emissions that have changed the global climate behaviour; this situation is known as the climate change. Our challenge is to build societies that can adapt to these changes while mitigating their effects, or at least not worsening them. One of the adaptation strategies is to replace energy sources, which are still non-renewable, with clean and renewable energy sources.

Radiative cooling technology is presented as a renewable alternative for the production of cold for space conditioning. In addition, previous research has shown that, using a single device, cold and heat can be produced at different times of the day, taking advantage of the phenomena of radiative cooling and solar heating. Nevertheless, the power of cold production is considerably low compared to, for example, heat production.

The aim of this thesis is to identify strategies that maximize the potential of combined radiative cooling and solar heating technologies. Throughout the thesis, three strategies are studied, consisting of: (1) the use of convective covers that reduce parasitic convection losses; (2) the use of cold produced by radiative cooling in order to improve the performance of conventional energy systems, reducing the consumption of electricity; and (3) the identification of the European regions where the potential for cold and heat production is maximized.

Nomenclature

NOTE: Nomenclature used in the papers are defined in the corresponding chapters and are not included in the following list.

ABBREVIATIONS

BB	Black Body
DHW	Domestic Hot Water
EU	European Union
HDPE	High Density Polyethylene
HP	Heat Pump
IPCC	Intergovernmental Panel on Climate Change
IR	Infrared Radiation
LDPE	Low Density Polyethylene
PE	Polyethylene
PMMA	Poly(methyl Methacrylate)
PP	Polypropylene
PPO	Polyphenylene Oxide
PV	Photovoltaic
PVC	Polyvinyl Chloride
RC	Radiative Cooling
RCE	Radiative Collector and Emitter
SH	Solar Heating
TRL	Technology Readiness Level
UV	Ultraviolet Radiation

SYMBOL DESCRIPTION

c	Speed of light in the vacuum [m/s^2]
$e_{rc,annual}$	Average annual radiative cooling energy [kWh/m^2]
h	Planck's constant [J·s]
I	Spectral radiation [W/m^2]

CONTENTS

k	Boltzmann's constant [J·K^{-1}]
N	Number of points [-]
t	Timestep [h]
T	Temperature [K]
T_{atm}	Temperature of the atmosphere [K]
T_{sun}	Temperature of the sun [K]
q_{cond}	Conductive heat exchanges with the environment [W/m^2]
q_{conv}	Convective heat exchanges with the environment [W/m^2]
q_{net}	Net balance per surface unit[1] [W/m^2]
$q_{rc,annual}$	Average annual radiative cooling power [W/m^2]
Q_{atm}	Atmospheric radiation [W]
Q_{cond}	Conductive heat exchanges with the environment [W]
Q_{conv}	Convective heat exchanges with the environment [W]
Q_{net}	Net balance [W]
Q_s	Radiation emitted by a surface [W]
Q_{sun}	Solar radiation [W]
R^2	Coefficient of determination [-]
$RMSE$	Root Mean Square Error [*^{2}]
α	Optical absorptivity [-]
ε	Optical emissivity [-]
λ	Wavelength [m]
λ_i	Vector of weights [-]
ρ	Optical reflectivity [-]
σ	Stefan-Boltzmann's constant [W/m^2·K]
τ	Optical transmissivity [-]

---

[1] The term net balance refers to the balance of a radiative surface, which is in direct contact with a system to be cooled, and the ambient (see equation 4 in page 6). In the consulted literature this term is referred to q_{net} or q_{cool}, here I prefer to use the term q_{net}, as the balance can have a negative value, resulting in a heating flux rather than a cooling one.
[2] The units of the RMSE depend on the units of the variable used to calculate the RMSE

Index

CONTENTS

CONTENTS

List of figures

NOTE: Figures presented in each paper of the thesis are not listed in this section.

Universitat de Lleida

List of tables

NOTE: Tables presented in each paper of the thesis are not listed in this section.

Chapter I. Introduction

1. Motivation of the thesis

The transformation and use of energy is essential for the functioning of today's societies; most human activities are possible thanks to the ability to extract energy from different sources and use them to our advantage. The various Industrial Revolutions, beginning in the second half of the 18th century, led to the replacement of the energy sources available at that time by coal, oil, natural gas and electricity. Since then, energy consumption continues growing, driven by population increase and industrial and economic growth, as well as improvements in standards of life.

Fossil fuels represent 70% of the energy sources used today [1]. The emissions of gases into the atmosphere associated with the consumption of these fossil fuels have contributed to the long-term risk of climate change. This latest statement has reached a consensus among the scientific community [2] and currently represents a world-wide major concern, which forces us to rethink the fossil fuel-based energy model.

In the European Union this challenge is being addressed in the latest public directives. The most recent one, European Green Deal, signed in 2020, expresses the will of the member countries to reduce the EU's emissions. The plan approved a financing equivalent to 1.8 trillion to suppress CO_2 emissions by 2050 and decouple the region's economic growth from material resources [3].

1.1. Energy consumption in Buildings

The building sector is one of the sectors which consumes more energy. In 2019, the consumption of final energy was estimated to be 40%, accounting for 36% of the CO_2 emissions [4] in the EU. Energy loads in residential buildings are mainly covered by gas (32.1%) and electricity (24.7%), while renewables represent a 19.5% of the total share (**Fig 1**). The energy consumption used in space heating accounts for the 63.6% of the total consumption; 14.8%, for water heating; 0.4%, for space cooling, and the rest is dedicated to other usages such as lighting, appliances or cooking. Almost 80% of the energy consumed in homes is used for thermal conditioning (**Fig 2**) [5]. Space heating is done

using different sources: mainly gas, but with a high impact of renewable energies (**Fig 3**). On the other hand, space cooling is all achieved by means of electricity consumption: in 2016 refrigeration accounted for 18.5% of the electricity consumption worldwide [6].
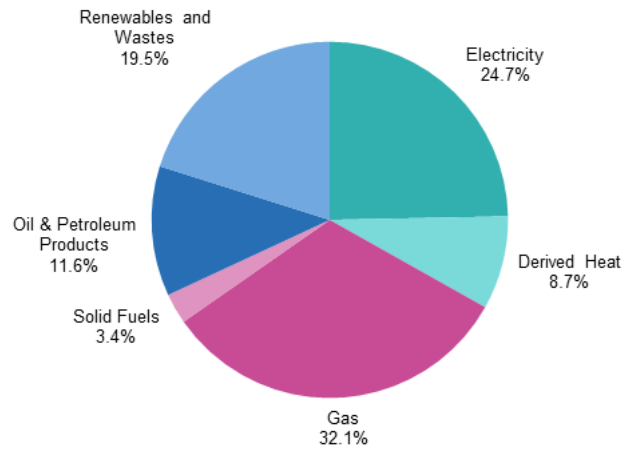
Fig 1. Final energy consumption in the residential sector by fuel in the European Union (2019) [4].
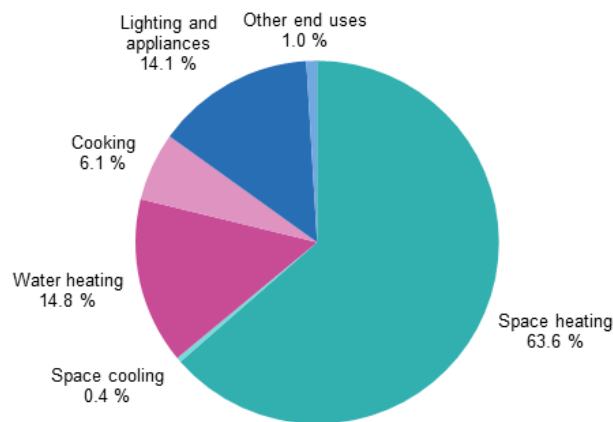
Fig 2. Final energy consumption in the residential sector by use in the European Union (2019) [4].
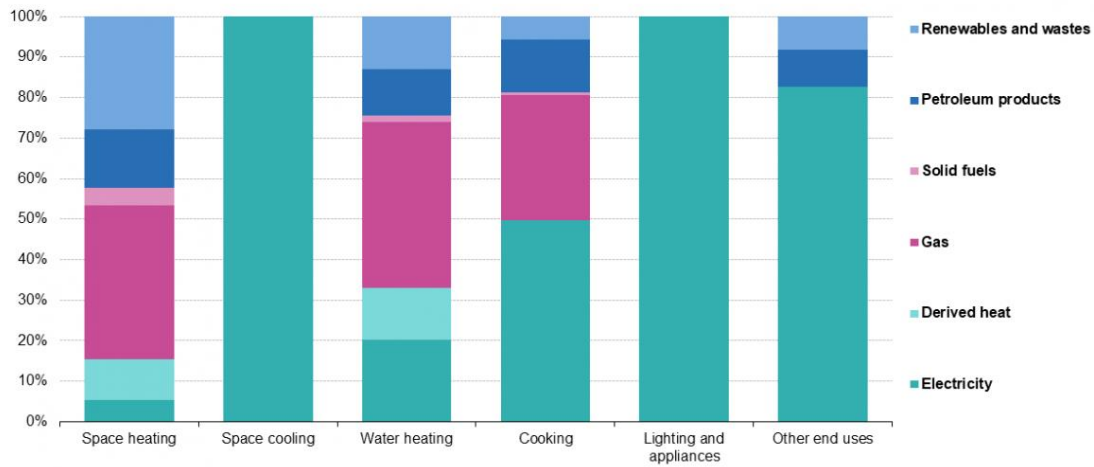
Fig 3. Part of the main energy products in the final energy consumption in the residential sector for each type of end-use in the European Union (2019) [4].

It is foreseeable that, continuing the same path, the energy consumption used in refrigeration in household increases as a result of the rising of the global temperatures and the new episodes of heat waves which, in turn, implies new CO_2 emissions to the atmosphere; contributing to a vicious circle. To meet the thermal energy requirements in buildings, two types of strategies should be adopted: passive strategies to reduce to total requirements (thermally insulated envelopes, suppression of thermal bridges, facades orientation, etc.) and active strategies such as the usage of energy from efficient and renewable sources.

Nowadays, there already exists technologies, with commercial applications, to renewably fulfil heating and DHW needs by taking advantage of solar heating [7]. For space cooling, the compression heat pump is the most widely used technology, which consumes a large amount of electricity and involves the use of refrigerants that can be leaked into the environment, causing damage to it [8]. Another technology for refrigeration is absorption cooling, which uses heat to produce cooling energy [9]. However, this latter technology is a more complex solution that has low performance and is not valid for all types of buildings due to its volume and weight.

In the last years, technologies based on the phenomena of radiative cooling (RC) have emerged as a feasible alternative for the renewable production of cold [10]–[12].

Moreover, RC can be combined with other functionalities such as solar heating or photovoltaics. The present thesis focuses in the combination of radiative cooling and solar heating to generate both cold and heat for space conditioning purposes, studying strategies to harness its maximum cold production.

2. State of the art

2.1 Theoretical background of radiative cooling

Radiative cooling is the natural process by which terrestrial bodies reduce their temperature by emitting infrared radiation towards space, which is at near 3K [13]), used as a thermal sink. The peaks of radiation emitted by the terrestrial bodies fall in the wavelength range of 7-14 μm. In this range, the Earth's atmosphere is highly transparent, allowing radiation to escape from the atmosphere and dissipate into the outer space [14], [15].

Temperatures below ambient can be achieved as a result of radiative cooling phenomenon [16], [17]. In 400 BC, people in ancient Iran already took advantage of radiative cooling to produce ice during clear nights in icehouces structures named *Yakchals* [18]. In the current era this phenomenon has begun to be studied systematically and it has gained attention, in the last years, as it is considered an attractive solution for renewable cold production.

All bodies emit electromagnetic radiation whose characteristics depend on its temperature. The spectral radiation of a black body at temperature T is expressed according to Planck's law (eq. 1), where T is the temperature, λ is the wavelength, h is the Planck's constant, k is the Boltzmann constant and c is the speed of light in the vacuum.

$$I_{BB}(T,\lambda) = \frac{2\pi hc^2}{\lambda^5} \frac{1}{e^{\frac{hc}{\lambda kT}} - 1} \tag{1}$$

The total power emitted by a surface is related to the integral of the spectral radiance I_{BB} (eq. 2). Where $\int d\Omega cos\theta$ is the integral of the solid angle on the hemi-sphere and ε is the average emissivity of the emitting surface. On the report of the Kirchoff's law of thermal

radiation, for a body in thermodynamic equilibrium, the spectral emissivity is equal to the spectral absorptivity (eq. 3).

$$P_{rad}(T) = A \int d\Omega cos\theta \int_0^\infty d\lambda\, I_{BB}(T,\lambda)\varepsilon(\lambda,\theta) \tag{2}$$

$$\varepsilon_\lambda = \alpha_\lambda \tag{3}$$

Surfaces at near ambient temperatures (~ 300 K) radiate long-wave energy. This spectral intensity in the mid-infrared range has peaks in the range of 7-14 μm. In this range the atmosphere is highly transparent (**Fig 4**), which is known as atmospheric window [19]. The radiation emitted partially matches the atmospheric window and can escape the atmosphere and dissipate into outer space. In mid-infrared there are two smaller atmospheric windows, at 3.2–4.8 and 16–23 μm wavelengths, which complement the heat dissipation process.
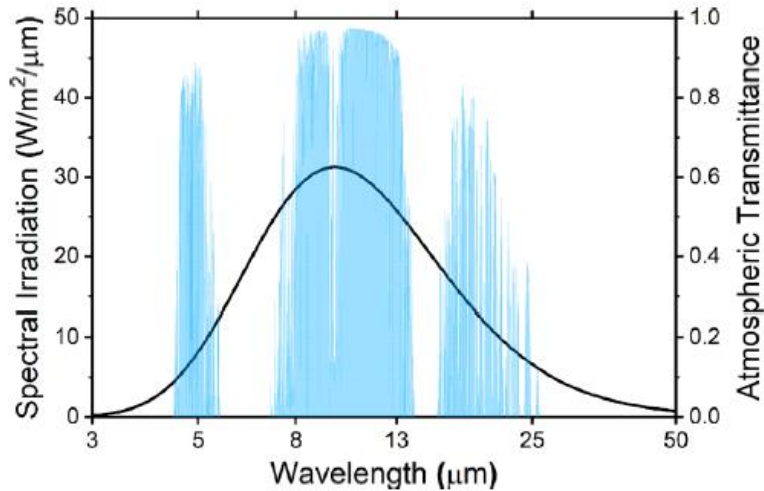
Fig 4. Spectral radiation of a blackbody surface of 300K (black curve) and the atmospheric windows – principal and secondary - in the mid-infrared regions (in blue). The radiation peak of the surfaces matches the regions of the atmosphere with higher transparency [20].

Radiative cooling occurs when an imbalance exists between the emitted and the absorbed heat, allowing to reach temperatures below room temperature (eq. 4). Radiation absorbed by the surface includes solar radiation, atmospheric radiation, and non-desired parasitic losses with the environment (convection and conduction) (**Fig 5**).

5

$$Q_{net} = Q_s(T_s) - Q_{atm}(T_{atm}) - Q_{sun}(T_{sun}) - Q_{cond} - Q_{conv} \qquad (4)^3$$

Atmospheric IR radiation (Q_{atm})

Solar radiation (Q_{sun})

Surface emitted radiation (Q_s)

Convective heat exchange (Q_{conv})

Conductive heat exchange (Q_{cond})
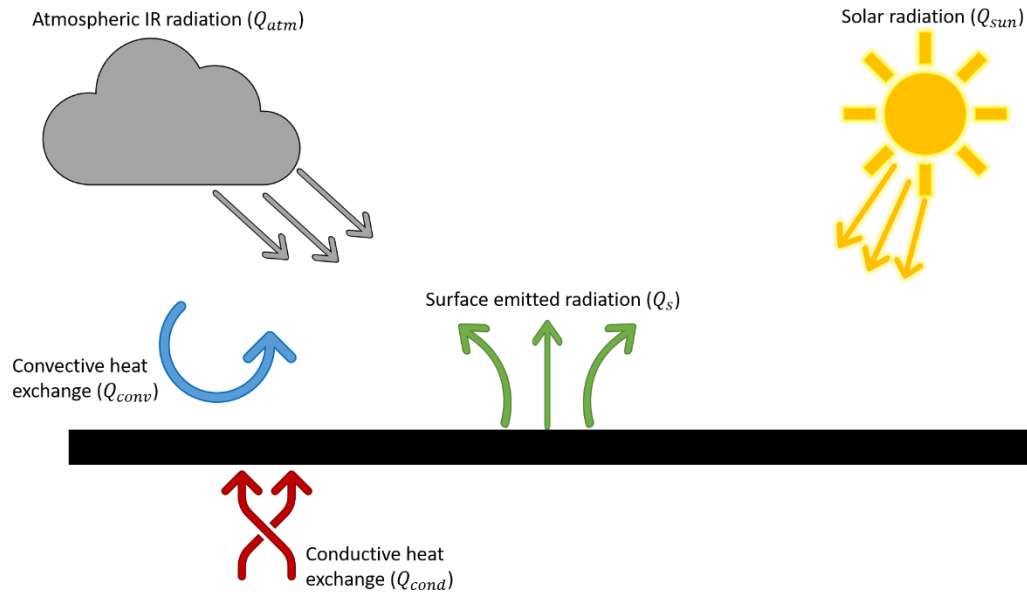
Fig 5. Scheme of the thermal exchanges between the radiative surface (black) and its surroundings.

This phenomenon occurs mainly during clear nights, in the absence of solar radiation. However, with the development of new metamaterials - which can reflect more than 90% of solar radiation - it has been possible to produce cold by radiative cooling during daylight hours [21]–[24].

2.2   Classification of radiative cooling systems

In the literature the radiative cooling systems are classified according to different criteria depending on the needs of the authors. This section contextualizes the different criteria and presents an overall view of the different systems.

---

[3] At first sight this equation might seem to violate the first law of thermodynamics. The terms at the right of the equation represent the entering and exiting heat fluxes from the control volume and, in stationary state, the value of q_{net} should be zero. Nevertheless, there exists another flux - which is intrinsictly represented by the term q_{net} – which is the heat exchange from the system to be cooled by means of radiative cooling. This system, in direct contact with the radiative cooling surface (either through the enclosures of a building or through a liquid flowrate inside pipes in contact with the surface), dissipates heat to this surface which, in turn, dissipates heat by means of radiative cooling. This invisible apportion of energy validates the law of conservation. In the literature the balance is expressed as in equation 4 and, to be consistent with the literature, in this thesis I will be using this notation.

2.2.1 Nocturnal and Daytime Radiative Cooling

Radiative cooling-based technologies can be classified into two major groups based on the targeted operation time. Nocturnal radiative cooling systems operate only during the night hours, while daytime radiative cooling systems (also named all-day radiative cooling) operate both during day and night.

The difference between the nocturnal and daytime RC systems is due to the materials used on the emitting surface. Due to the strong influence of the solar radiation the phenomenon of radiative cooling was only achieved during the night, in the absence of solar radiation. However, in recent years, materials science has succeeded in developing new materials that have properties that do not exist in nature [21], [22]. In the field of study of radiative cooling, materials have been developed that have a high reflectivity to solar radiation, allowing radiative cooling even during the daytime, in the presence of peaks of solar radiation [24], [25].

2.2.2 Broadband and Selective emitters

Radiative cooling surfaces can be categorized into two major groups depending on the emissivity properties: selective emitters and broadband emitters [26]. Selective emitters have high emissivity- with values close to 1 - only in the atmospheric window. Broadband emitters, instead, behave like a black body with close-to-unit emissivity in all the mid-infrared wavelength, benefiting from the other smaller atmospheric windows. When emitting in a greater range the emitted radiation will be greater in a broadband surface; however, according to Kirchoff's law (eq 3) the radiation absorbed by the surroundings will also be higher. In **Fig 6** it can be seen the differences between the two types of radiators.
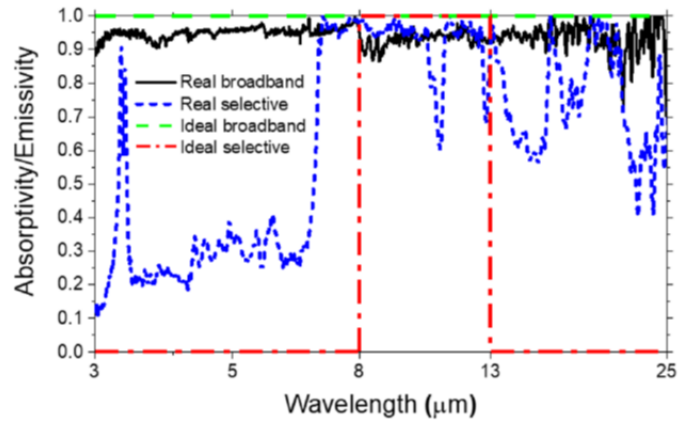
Fig 6. Spectrum of emissivity for broadband and selective surfaces (ideal and real cases) [20].

Literature points out that depending on the application one surface or the other is preferable. Broadband emitters produce higher cooling powers for above ambient temperatures applications [20], between 100 and 130 W/m^2 [27]; while the average power dissipated in selective emitters is between 60-80 W/m^2. The largest temperature difference is achieved, however, in a selective surface [27]. For sub-ambient temperature applications, a selective surface is more appropriate (**Fig 7**).
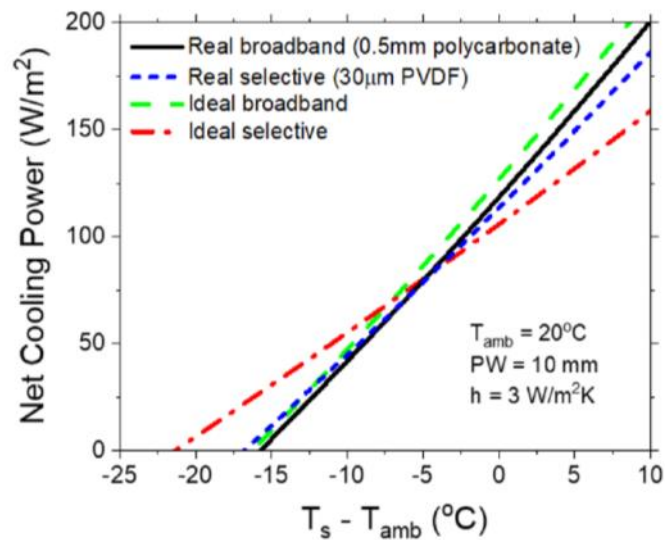
Fig 7. Net cooling power emitted by the radiator, as a function of the temperature difference between radiative cooling surface and ambient, for broadband and selective surfaces (ideal and real cases) [20].

2.2.3   Active and passive systems

To reduce the temperature of a surface by dissipating excess heating to the outer space is a passive cooling strategy. On the other hand, if the cooling power at the radiator is transmitted to a heat transfer fluid flowing through pipes in contact with a radiative panel, then it is considered an active strategy.

Passive RC is used in building envelopes, especially in selective paints and roofs [28] that allow energy to radiate to the outside; the cooled roof helps to reduce conductive heat gains from the outside, preserving a more adequate interior temperature. Active strategies have been studied to be more versatile: the cooled fluid can be stored and used to deliver cold to inner spaces [29]–[33].

2.3   Combination of radiative cooling with solar energy

Nocturnal radiative cooling only occurs during a short period of the day; this makes the technology inefficient in terms of space and operation. As suggested by Vall et al [34], combining radiative cooling with other technologies, which do not operate during the night, could make the technology more cost-effective. In this section the different ways of combining RC with other technologies available in the literature are exposed

2.3.1   Photovoltaic

Some authors have proposed to combine RC with photovoltaic (PV) systems. Solar cells absorb solar energy and convert it into electricity through the photoelectric effect. In 2019, Zaho et al [35] developed a new PV-RC hybrid system capable of producing electricity during the day and nocturnal RC. The device exhibited high solar absorption in the PV band (0.3-1.1 μm) and high emissivity in the range between 4-25 μm. The results showed that the device was able to provide both electricity and cold: it achieved an average electrical conversion of 12.4% in PV mode and a reduction of surface temperature equivalent to 12.7 ºC, although not all the reduction was attributable to RC effect.

Another achievement in this field has been the use of the RC phenomenon in order to improve the efficiency of solar cells. The electrical conversion efficiencies of photovoltaic panels are 15-22% [36]. Part of the radiation is absorbed and transformed

into heat: for every 1ºC increase in the cell temperature, its conversion efficiency can be reduced by 0.45% in Si-based solar cells. Safi and Munday [37] stated that solar cells could be cooled to sub ambient temperatures thanks to radiative cooling. Li et al [36] combined a multilayer film-based daytime radiative cooler into a photovoltaic cell; the results showed a difference in cell temperature of 5.7 ºC with and without the radiative cooling film, improving its absolute efficiency up to 0.56%.

2.3.2   *Solar Heating*

Despite radiative cooling and solar heating have different behaviours, the operations are analogous (both are achieved in the surface by means of absorbing/emitting of electromagnetic radiation). Because of this, various authors have proposed the combination of both functionalities in one single device, enabling the production of both heat and cold [34], [38]–[40]. This device has received different names but in this thesis we are using the denomination Radiative Collector and Emitter (RCE) proposed by Vall et al [34].

Matsuta et al. [38] and later Erell and Etzion [42],[43] were the first to propose a combination of solar heating and radiative cooling functionalities. The first results showed lower performance in combined system than in separate systems. The findings by Erell and Etzion, and Zhao et al. pointed out the negative effects of convection during solar heating [42] and sub-ambient radiative cooling [33]; revealing the importance of supressing this heat exchange.

Convective cover – a cover which separates the emitting/absorbing surface from the environment –is a solution to supress convective heat exchanges. Each functionality relies on different wavelength from the electromagnetic spectrum: nocturnal radiative coolers emit in the range of the mid-infrared while daytime solar collectors absorb in the range 0.2-3 μm and block infrared radiation, necessary to achieve radiative cooling. Polymeric covers are transparent to infrared and solar radiation; it implies that the RCE in solar heating mode would worsen the heating performance (the greenhouse effect achieved with glass cover is lost). Thus, the cover must be able to tune its optical properties to operate in different working modes, allowing it to absorb sunlight in heating mode and to emit mid-infrared radiation in cooling mode. The latter makes the design of the RCE more

complex. Glass has become a standard for solar heating applications, but it is not suitable for RC as it blocks infrared radiation during night. There is not yet a standard solution for RC applications. The most common are the polymeric covers, however they present structural degradation.

Vall et al. [34] proposed a design for an adaptive cover consisting of two elements: a fixed polyethylene cover and a glass cover capable of sliding over the device depending to the operating mode (**Fig 8**). Liu et al. [43] alternatively designed a combined device made of 10 μm polyethylene film, a porous cooling material with near unity infrared emissivity in the 8–13 μm range, aluminium conductor substrate, providing heat conductivity, and a solar absorbing material coated with chromium plating (solar absorptivity of 95%) (**Fig 9a** and **Fig 9b**). Radiative cooling was achieved on one layer of the device while solar collection was done on the other layer of the device; the switching between modes was achieved with a rotating shaft (**Fig 9c**).
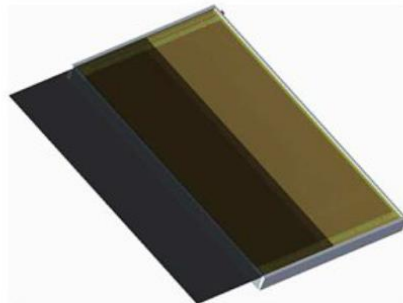
Fig 8. Sliding adaptive cover proposed by Vall et al. [34].
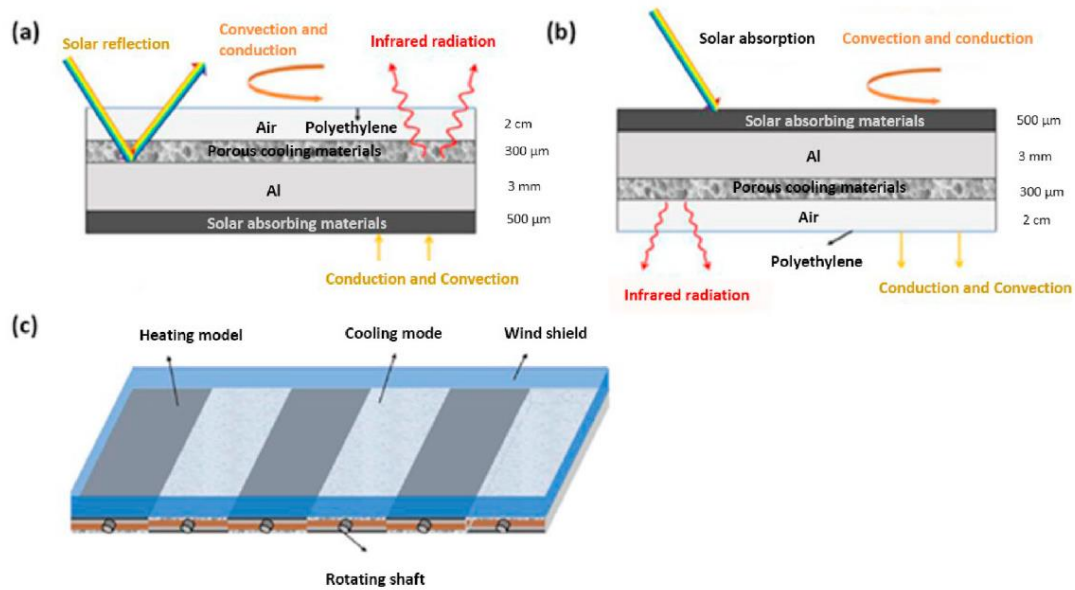
Fig 9. Mixed radiative cooler and solar heater proposed by Liu et al. [43]. (a) Radiative cooling mode, (b) Solar heating mode and (c) rotating structure.

Taking advantage of solar heating and radiative cooling can reduce the dependence to non-renewable energy sources for space conditioning and domestic hot water. Combining both functionalities in one single device will make the investment more cost-effective. The payback of this technology could be of a period of 8 years [44].

This last concept of radiative collectors and emitters (RCE) is the central technology studied in this thesis, which will be further discussed in the next chapters.

2.4   Current research trends in radiative cooling

Although radiative cooling has been studied systematically since the middle of the last century, in the last few years it has developed a new interest. After reviewing the literature two main research trends have been identified: the development of new materials and the integration with the built environment.

2.4.1   Development of new materials
The vast majority of scientific papers published recently in the field of radiative cooling focus on the development of new materials (especially for daytime RC). Radiative cooling materials can be classified as materials for the emitting surface or cover materials

to prevent convective exchanges and enable or avoid radiative exchanges, named convective covers.

Selective surface materials can be classified into: (1) polymer thin films placed on top of a metallic surface (PVC, PMMA, PPO, pigmented polymeric foils) [45]–[47], (2) silicone-based thin films (SiO, SiO_2, SiO_xN_y, SiN) [16], [48]–[50], (3) gas confined in gas slabs (spectrometry techniques found that ethylene (C_2H_4), ethyl oxide (C_2H_4O) and ammonia (NH_3) are three gases which in the presence of low humidity show high emissivity in the atmospheric window range) [51], [51], [52] and (4) metamaterials and photonic materials for daytime applications, consisting on optimized patterned structures designed in a scale lower than the wavelength of the solar light, which proved emittances in the atmospheric window higher than 90% - with records of 99% [53] - and solar reflectance close to 99% [53]–[55].

In Vilà et al. [56] we proposed a classification of materials for convective covers which distinguished the polymeric covers, pigmented covers, deposited film, zinc crystal-based covers, and cadmium films. We also suggested that smart materials could become another solution for convective covers, but the literature analysed did not offer a characterization of the infrared range.

As it is discussed in **Chapter IV**, much attention has been put to the development of new materials for selective surfaces, especially metamaterials for daytime application. However, there is not much research done on the development of materials for convective covers.

2.4.2   Integration with the built environment

The integration of radiative cooling in different energy systems in order to use the cold produced, and the benefits derived from the integration, is another outstanding line of research in the field of radiative cooling.

Wang et al. [57] simulated a photonic radiative cooler integrated in a radiant floor cooling system in a medium office building, showing electricity savings equal of 42%, in comparison with a reference conventional system. Vall et al. [34] studied the capacity of

an RCE to meet the energy demands in hotels, residential and commercial buildings in different climatic zones.

Cui et al. [58] manufactured a passive radiative sky cooling envelope for a telecommunication base station, the energy savings derived are between 6.77% and 64.29%, which corresponded to a saving of between 21.94 kWh/m^2 – 52.74 kWh/m^2. Medrano et al. [59] numerically analysed the improvement of the integration of RCE panels in seven food industries, the results showed potential electricity savings between 13% up to 62%. Zhang et al [60] modelled a hybrid daytime radiative cooler coupled to a tank to store cold, which could later be used to precool the air in an air-conditioner for a single-family house in four locations in the USA; electricity savings in the range from 26% to 46% were expected.

The combination of radiative coolers with phase-change materials has been proposed by various authors [61]–[63]. Large energy storage associated with phase-change materials allows to maintain an isothermal process during the cooling process, which would allow to maintain higher and nearly constant efficiencies throughout the process [63].

Another possibility of integration is the coupling of radiative cooling systems on the condenser side of a compression heat pump (HP), which could improve its seasonal coefficient of performance (COP), contributing to the reduction of the electricity consumed by the system. The electricity consumed is reduced by approximately 3.5% for every ºC reduced in the condenser [64]. Cold water produced during night-time by the RC is used to reduce the thermal difference between the condenser and the evaporator in a water-water heat pump. Goldstein et al. [65] simulated a two-storey office building, in Las Vegas, with a combined RC+HP system; the results showed electricity savings of 21% during summer. Finally, a novel design was proposed by Hu et al.[66], combining a traditional solar absorption chiller with radiative cooling, to provide continuously cold during 24h. The authors stated that this design could reduce the demanding space of the system and the storage tank of absorption chillers, while making it more stable through the whole day.

3. Limitations in RC and RCE

From the review of the existing literature, limitations have been detected that affect the radiative cooling process and may worsen its performance.

Radiative coolers have low cooling rates, between 20 and 80 W/m^2 with peak values of 120 W/m^2 [34], which represent an order of magnitude lower than those achieved in solar heating.

Various authors have proposed the use of convective barriers which separate the emitting surface from the environment, cutting down convective heat exchanges [44] and enabling surface cooling below ambient temperature [21], [33]. In order to illustrate the above, we can use as an example the case of Zhao et al. [33] , who, when experimentally studying the effects of wind in a radiative cooler, observed a difference between the heat transfer fluid and the environment equal to 7º C with the use of convective cover, and only 4.3ºC without convective cover.

Moreover, radiative cooling is highly dependent on the climatology. Studies can be found in the literature evaluating the potential of radiative cooling in various climates and regions. Argiriou et al. [67] estimated the sky temperature depression and the night time performance of a RC flat plate in different countries in southern Europe, concluding that this region exhibited potential to apply this technology. Bijarniya et al. [68] studied the radiative cooling potential in five cities in India; cities with low humidity presented better performance of radiative cooling.

Li et al., using a deterministic interpolation model, presented radiative cooling resource maps in the USA [69], showing an average power of 50.5 W/m^2. Chang and Zhang used a stochastic interpolation model, called Kriging, to generate maps based on weather data from 351 stations in China [70]. The model presented high accuracy. Aili et al.[71] produced global maps of net cooling power density, showing an uneven distribution of the cooling potential: the regions with the highest potential are uninhabited regions whereas dense areas present a low cooling potential in the order of 10~10^3 Watts per capita (WpP).

Up until this time it does not exist a detailed study of the potential of radiative cooling in Europe. Moreover, nobody has studied the evolution of this potential under the context of climate change, due to the rise of the global temperature associated to it. Finally, there is not yet a characterization, and comparison, of the potential of all-day radiative cooling with different solar reflectivities. The thesis aims to close these knowledge gaps. It investigates the potential for the implementation of RC and RCE-based technologies in Europe, identifying the areas and seasons with the greatest potential, understanding the potential as a function of the solar reflectivity, as well as studying the resilience of these technologies in the context of climate change.

Chapter II.   Objectives and Hypothesis

The cold produced in Radiative Collector and Emitter (RCE) systems is an order of magnitude lower than the heat produced. The main objective of this thesis is to study strategies to take profit of the maximum potential of the cold produced by RCE systems.

The research is based on the following hypotheses:

- H1. Materials for convective covers in radiative cooling and solar heating applications, which reduce parasitic losses and increase the net power balance, have been identified in separate applications. However, materials for convective covers in combined applications are yet to be identified.
- H2. Cold generated in the RCE can be used in combination with other cooling systems to improve the performances.
- H3. There are more suitable regions to use radiative cooling-based systems.
- H4. There is a relationship between local climatic conditions and the potential of radiative cooling.

The general objective of the thesis is divided into the following specific objectives:

- O1. To review on adaptive covers for combined radiative cooling and solar heating.
- O2. To study candidate materials for radiative cooling covers that minimize convective heat exchanges and maximize radiative exchanges.
- O3. To identify the best configurations to integrate RCE in combination with conventional cooling systems to meet the cooling demands in buildings.
- O4. To generate radiative cooling potential maps in Europe in order to identify suitable regions to implement technology based on RC and RCE systems.
- O5. To analyse the difference in the potential between nocturnal and all-day radiative cooling-based technologies.
- O6. To study the resilience in the implementation of RC technologies under the context of climate change.

Chapter III.   Methodology and PhD thesis structure

This chapter presents the methodology followed to answer the hypothesis of the thesis and fulfil the objectives. The core of the thesis is divided into three main parts – convective cover to improve the efficiency, integration with other systems, and potential of the technology – which reflect one or two of the hypotheses described in the previous chapter. The methodology followed in the thesis consisted on two major strategies: first a deep review of the state of the art and, secondly, the use of simulation tools to emulate practical implementations of the RCE and to evaluate the performance under different climates.

The thesis is developed in the frame of the project *"Development and evaluation of a radiative cooling and solar heating system for combined heat and cold production"* RAD-CHC (RTI2018-097669-A-I00) of the SEMB group of the University of Lleida.

The document consists of 5 scientific papers. At the time of writing the document, two of the papers (papers P1 and P4) have already been published in Journal Citation Report (JCR) journals, while the remaining three (papers P2, P3 and P5) are in the process of peer review in the corresponding indexed journals.

The literature conceptualization consisted in a review of more than 120 scientific papers, from 1975 to the current time. This process helped the author to identify the major research contributions in the field of radiative cooling, the research trends and the literature gap, as has been exposed in **Chapter I**. During this process, special attention was given to convective covers used to reduce the parasitic heat exchanges and to improve the efficiency of the system; also, the possibility of using convective covers for combined solar heating and radiative cooling applications was evaluated during the literature conceptualization. This is discussed in **Chapter IV**.

The simulation studies were divided into two types of simulations. The first ones used TRNSYS software [72] to evaluate the transitory evolution of different systems consisting on an RCE device coupled with a water-water heat pump (see **Chapter V**). The simulations were based on a mathematical model of an RCE. The second ones are based on Kriging interpolation algorithms to generate contiguous maps. Kriging, which

is a stochastic interpolation method for values prediction at different points from known reference values, is used in **Chapter VI**, **Chapter VII** and **Chapter VIII**.

1. RCE model

In the thesis a mathematical model of an RCE was used to simulate the transient evolution of a system combining RCE and water-water heat pumps. The model was developed and validated with experimental data by Vall et al [73] and is compatible with TRNSYS tools.

The model calculates the heat entering or leaving the RCE by applying an energy balance between the RCE, the ambient air and the sky. The radiative balance is discretized into four ranges of wavelength (0-4 μm, 4-7 μm, 7-14 μm and >14 μm), which allows to use two different types of convective covers for different types of applications in the same device: solar heating and radiative cooling.

Inside the RCE, the model divides it into five nodes (**Fig 10**), corresponding to different parts of the RCE, and then computes the temperature of each node. The nodes correspond to the convective cover, the radiative surface, the pipes in contact with the radiative surface, the insulation and the fluid flowing through the pipe. The model transforms the relations between nodes into an equivalent one-dimensional electrical circuit which includes some 2D effects based on simulations in Comsol Multiphysics. The electrical analogy is a simplification which results in a more flexible and less time-consuming model. Energy balance includes ordinary first-order differential equations that are solved by means of an iterative Euler's implicit method until the converging of the system.
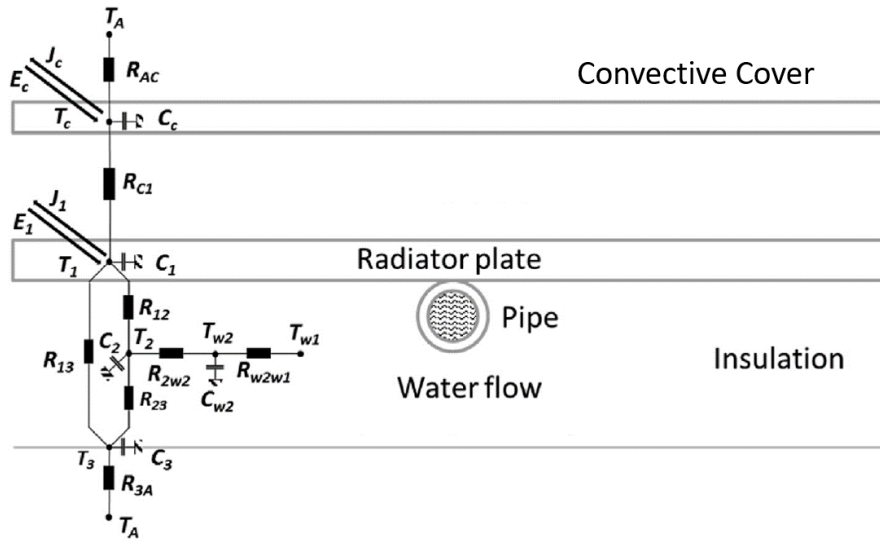
Fig 10. Scheme of the thermal model, its nodes and the 1-D electrical analogy. Modified from Vall et al. [73].

2. Kriging interpolator

Kriging interpolation has been used to generate solar heating (**Chapter VI**) and radiative cooling potential resource maps in Europe (**Chapter VI**, **Chapter VII** and **Chapter VIII**). The interpolation allows to predict the radiative cooling potential at unknown points based on the meteorological data from more than 1800 weather stations in the continent. The three simulations used the same datasets obtained from the Meteonorm's database [74].

Each paper (corresponding to one of the three chapters) presents variations in the methodology compared to the other papers; these methodologies are described in the corresponding chapter. Nevertheless, they share a similar underlying approach. In the three cases we can identify the following steps: a pre-processing of the data, the calculation of maximum radiative cooling potential in the corresponding weather station, splitting the dataset into training and test sets, the application of the Kriging interpolation, and the evaluation of the model's performance (**Fig 11**). R programming language and Rstudio (version 1.3) were used in the whole process. The packages *sp* and *gstat*, which are implemented in Rstudio, were applied for the geospatial prediction.
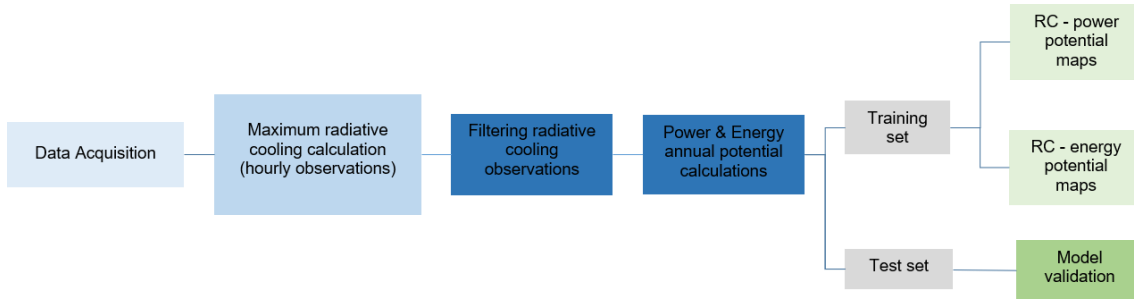
Fig 11. General workflow to generate power and energy potential resource maps

2.1 Data pre-processing

The pre-processing of the data included the standardization of variables, the filtration of diurnal and nocturnal values and the cleaning of *NA* and unusual values.

The processed dataset collected hourly data for the 365 days of the year which is arranged in a set of variables which includes ambient temperature, global horizontal solar radiation, infrared radiation, relative humidity, clearness of the sky or atmospheric pressure.

2.2 Radiative cooling calculations

The radiative cooling phenomenon is the result of the balance between the infrared radiation emitted by the radiative cooling surface and the heat exchanges absorbed by the surface. The radiative cooling power potential was calculated using the equation 4 (**Chapter I.2.1**). This equation can be further developed as (eq 5):

$$q_{net} = \varepsilon_s \sigma T_s^4 - \alpha_s \varepsilon_{sky} \sigma T_{amb}^4 - (1 - \rho_{sun}) \cdot \varepsilon_{sun} \sigma T_{sun}^4 - q_{cond} - q_{conv} \quad (5^4)$$

---

[4] At first sight this equation might seem to violate the first law of thermodynamics. The terms at the right of the equation represent the entering and exiting heat fluxes from the control volume and, in stationary state, the value of q_{net} should be zero. Nevertheless, there exists another flux - which is intrinsictly represented by the term q_{net} – which is the heat exchange from the system to be cooled by means of radiative cooling. This system, in direct contact with the radiative cooling surface (either through the enclosures of a building or through a liquid flowrate inside pipes in contact with the surface), dissipates heat to this surface which, in turn, dissipates heat by means of radiative cooling. This invisible apportion of energy validates the law of conservation. In the literature the balance is expressed as in equation 4 and, to be consistent with the literature, in this thesis I will be using this notation.

To calculate the maximum radiative cooling power of an ideal surface, the following premises were assumed and equation 5 was simplified to equation 6.

a. The surface behaved as a black body ($\varepsilon_s = \alpha_s = 1$).

b. The surface reflected all the sunlight in radiative cooling mode (with $\rho_{sun} = 1$).

c. Parasitic thermal exchanges were minimized in the RC surface ($q_{cond} = q_{conv} = 0$).

   - The device was thermally isolated ($q_{cond} = 0$).

   - The device had a convective cover ($q_{conv} = 0$). Losses related to the optical properties of the cover were neglected.

d. The RC surface was placed horizontally; all the emitted radiation was projected towards the atmosphere. Infrared radiation absorbed by the device was coincident with the atmospheric radiation.

e. Temperature of the RC device was equal to the ambient temperature (T_{amb}).

$$q_{net,bb} = \sigma T_{amb}^4 - \varepsilon_{sky}\sigma T_{amb}^4 = \sigma T_{amb}^4 - L_{in} \ (W/m^2) \qquad (6)$$

Once the hourly maximum radiative cooling power of an ideal surface was known, it was calculated the annual average power potential on each point of the sample[5] (eq. 7).

$$q_{rc,annual} = \frac{\sum_i^n q_{net,bb}^{\ +}}{N} \ (W/m^2) \qquad (7)$$

Every observation corresponded to a one-hour observation *(t = 1 h)*. The energy potential produced in a year was calculated according to eq. 8.

$$e_{rc,annual} = \frac{\sum_i^n (q_{net,bb}^{\ +} \cdot t)}{1000} \ \left(\frac{kWh}{m^2 \cdot year}\right) \qquad (8)$$

---

[5] Depending on the simulation, only nocturnal values were filtered; this is where the main differences between the three papers happen. In paper P3, data was filtered and two new datasets were created: one for nocturnal data and one for diurnal. In paper P4 the filtering was done only for those observations where radiative cooling was achieved. In paper P4 two new datasets were also created: one corresponding to nocturnal values and a second one corresponding to all-day radiative cooling values. This is further explained in the methodology section of each paper.

2.3   Training set and test set

The dataset was randomly divided into two new datasets: a training set and a test set. The training set was used to generate the interpolation model and contained 80% of the sample data. The remaining 20% of the data corresponded to the test set, which was used to evaluate the performance of the interpolation model. **Fig 12** shows the spatial distribution of the sample points in each dataset.
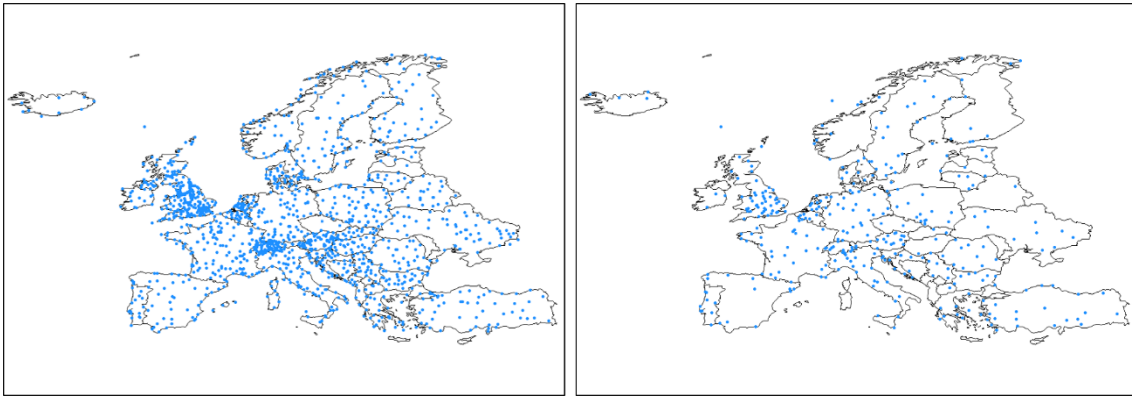
Fig 12. Spatial distribution of the sample points in the training set (left) and the test set (right).

2.4   Kriging interpolation and maps generation

In the three papers ordinary Kriging was applied. Ordinary Kriging is the general version of Kriging. This method is a non-linear estimator which decomposes the regressor into a stationary (μ) and a residual part (ε'), corresponding to the spatially correlated part (eq. 9). Ordinary Kriging assumes that the value of the variable can be predicted as a linear regression of N random variables applied to spatial data in a sample (eq. 10).

$$Z(s) = \mu + \varepsilon' \qquad (9)$$

The models trained by Kriging used the distance to the known points, $Z(s_i)$, as a regressor to predict a dependent variable at a given location, $\hat{Z}(s_0)$. The dependent variable was the radiative cooling power and energy potential, respectively.

The weight that the model gives to each of the points were determined according to the function of the variogram (eq. 11); where λ_i is the vector of the Kriging weights, N is the number of sample points and γ is the semivariance of the sample.

$$\hat{Z}(s_0) = \sum_{i=1}^{N} \lambda_i Z(s_i) \tag{10}$$

$$\begin{pmatrix} \gamma(s_1 - s_1) & \cdots & \gamma(s_1 - s_n) & 1 \\ \vdots & \ddots & \vdots & 1 \\ \gamma(s_n - s_1) & \cdots & \gamma(s_n - s_n) & 1 \\ 1 & \cdots & 1 & 0 \end{pmatrix} \cdot \lambda_i = \begin{pmatrix} \gamma(s_1 - s_0) \\ \vdots \\ \gamma(s_n - s_0) \\ 1 \end{pmatrix} \tag{11}$$

The experimental semivariance of the sample was calculated for each pair of points according to eq. 12, where $Z(s_i)$ is the value of the target variable at the point s_i, $Z(s_i + h)$ is the value of the neighbor point at a distance $s_i + h$ and E corresponds to the expected value.

$$\gamma(h) = \frac{1}{2} E[(Z(s_i) - Z(s_i + h))^2] \tag{12}$$

From eq. 12 it was obtained the experimental variogram[6]. An important step in the creation of the model was to fit a theoretical variogram, as they presented a known distribution, to the experimental variogram so that the error of the fitting was minimum (**Fig 13**). The best variogram was chosen between seven theoretical variograms (Spherical, Circular, Gaussian, Exponential, Pentaspherical, Matern and Stein); the variograms were defined by three parameters: the nugget, the sill and the range.

The training set data was used to generate the interpolation models. The model was then applied to a grid of points, identified by a longitude and a latitude, corresponding to European geographic points. The values obtained were used to generated the contiguous maps. The spatial resolution of the pixels of the maps was 6 x 8 km.

---

[6] A variogram is a representation of the spatial behavior of the studied variable. The variogram shows the influence of the distance between points to the variance of the studied variable: the closer the points are, the bigger the influence is and the lower is the variance between points.
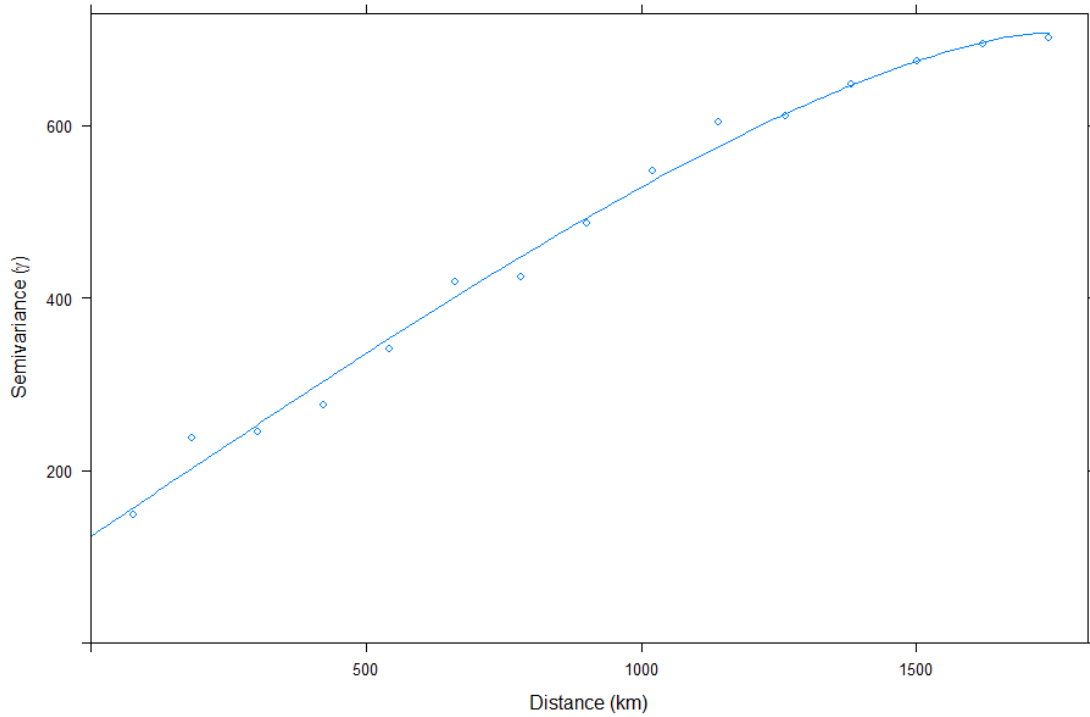
Fig 13. Example of one variogram obtained during the interpolations. The points represent the experimental variogram and the line is the theoretical variogram that minimizes the fitting error.

2.5   Model validation

To evaluate the performance of the Kriging, the interpolation model was applied to the sample points in the test set. This allowed compare the predicted value by the model with the observed value in the weather station (calculated in **2.2**).

The performance was quantitatively assessed with the coefficient of determination (R^2) and the root mean square error (RMSE) (eq. 13 and eq. 14).

$$R^2 = 1 - \frac{\sum_{i=1}^{N}\left(X_{i,m} - X_{i,p}\right)^2}{\sum_{i=1}^{N}\left(X_{i,m} - X_{avg,m}\right)^2} \tag{13}$$

$$RMSE = \sqrt{\frac{1}{N}\sum_{i=1}^{N}\left(X_{i,m} - X_{i,p}\right)^2} \tag{14}$$

Where N is the total number of locations; $X_{i,m}$ is the observed value of the sample; $X_{i,p}$ is the value estimated in the model and $X_{avg,m}$ is the average of the observed values at the weather stations. RMSE has the same units as the variable at interpolation while R^2 is dimensionless.

3. Structure of the document

The thesis is structured as follows in **Fig 14**. The chapters of the thesis are organized as follows:

- Chapter I: the first part of the thesis introduces the topic of radiative cooling. It is developed the theoretical background and the state-of-the-art through a review of the literature. It presents the research lines in the field of radiative cooling and the limitations of the technology.

- Chapter II: presents the hypothesis and objectives defined for this PhD thesis

- Chapter III: presents the methodology followed to answer the hypothesis of the thesis and sets out the structure followed in the present PhD thesis.

- Chapter IV: presents research paper P1. This paper introduces the reader to the phenomenon of radiative cooling and the possibility of combining systems based on this phenomenon with solar heating systems. A literature review of adaptive covers for combined radiative cooling and solar heating is presented and the main materials used in both applications are discussed. This chapter focuses on the H1 hypothesis and aims to answer the objectives O1 and O2.

- Chapter V: includes research paper P2. Chapter V proposes two ways to combine an RCE system with a water-to-water heat pump. The improvement of the performance is analysed. This chapter focuses on the hypothesis H2, and partially H3, and aims to answer the O3 objective.

- Chapter VI: in this chapter, paper P3 is included. This paper presents source maps for combined radiative cooling and solar heating in Europe and identifies the most suitable regions to apply RCE technology. This chapter focuses on the hypothesis H3 and H4 and aims to answer the O4 objective.

- Chapter VII: this chapter introduces research paper P4. Chapter VII presents a parametric study of the potential of radiative cooling in Europe, depending on the

reflectivity of the system to the solar range. The differences between all-day Radiative Cooling and night-time Radiative Cooling potential are presented. This chapter focuses on hypotheses H3 and H4 and aims to answer the objective O4 and O6.

- Chapter VIII: includes research paper P5. This article analyses the potential for radiative cooling in each season of the year and evaluates the evolution of the potential over the years in the context of climate change. This chapter focuses on hypotheses H3 and H4 and aims to answer the objective O4 and O5.

- Chapter IX: presents the conclusions obtained in this thesis and proposes future work on this topic.

- Chapter X: lists other contributions of the author during the PhD thesis.

Part 1. Introduction to the thesis

Chapter I. Introduction

Chapter II. Objectives and Hypothesis

Chapter III. Methodology and PhD thesis structure

Part 2. Convective cover

Chapter IV. Adaptive covers for combined radiative cooling and solar heating. A review of existing technology and materials
▶ Paper P1

Part 3. Integration of RCE

Chapter V. Numerical Analysis of the Combination of Radiative Collectors and Emitters to Improve the Performance of Water-Water Compression Heat Pumps under Different Climates
▶ Paper P2

Part 4. Potential of implementation

Chapter VI. Potential Maps for Combined Nocturnal Radiative Cooling and Diurnal Solar Heating Applications in Europe
▶ Paper P3

Chapter VII. Mapping Nighttime and All-Day Radiative Cooling Potential in Europe and the Influence of Solar Reflectivity
▶ Paper P4

Chapter VIII. Climate Change Influences in the Determination of the Maximum Power Potential of Radiative Cooling. Evolution and Seasonal Study in Europe
▶ Paper P5

Part 5. Conclusions

Chapter IX. Conclusions and future research

Chapter X. Other Contributions

Fig 14. Structure of the thesis.

CHAPTER IV

Adaptive covers for combined radiative cooling and solar heating. A review of existing technology and materials

Chapter IV.   P1: Adaptive covers for combined radiative cooling and solar heating. A review of existing technology and materials

1. Introduction

The combination of radiative cooling effect with solar heating in a single device has been proposed, in the last years, by diverse authors. This device, referred here as RCE, can provide both cooling and heating for space conditioning purposes.

One of the lines of research in the field of radiative cooling with the fastest growing of publications is the development of materials for radiative cooling. Authors such as Vall and Castell [14], Ko et al. [24] or Granqvist et al. [75] reviewed the existent literature referred to materials for emitting/absorbing surfaces to achieve sub-ambient temperatures with radiative cooling.

In combined applications of RCE two main issues must be taken into account. Firstly, radiative cooling power rates are low (on average, values between 20 and 80 W/m^2 with peaks at 120 W/m^2 could be achieved [34]) and, for sub-ambient temperature applications, convective heat exchanges worsen the performance of the emitter. Etzion and Erell [76] were the first to point out that the effect of ambient air was a limitation to maximize radiative cooling power; a convective cover which separates the emitting surface and the ambient air reduces the convective heat exchanges. Secondly, nocturnal radiative cooling and diurnal solar heating absorb/emit different wavelengths. One of the proposed solutions is the use of an adaptive cover which enables to change the optical properties of the device. An ideal cover should present a perfect transmittance in the solar spectrum and block all the infrared radiation during the day, while, during the night, it should have a perfect transmittance in the mid-infrared range. An adaptive cover addresses the two mentioned issues at the same time: it reduces the parasitic losses while it adapts the optical properties of the device according to the functionality.

CHAPTER IV

Adaptive covers for combined radiative cooling and solar heating. A review of existing technology and materials

In previous studies performed in the research group [29], [77], [78], polyethylene was used as convective cover in experiments but it presented structural degradation over the days.

In order to identify a proper solution to use in experimental studies of combined applications, it was necessary to identify materials, or combination of materials, which exhibited the described properties. Because of this, the authors performed a review and compilation of the available research done in the development of materials for convective covers in radiative cooling and solar heating applications.

2. Contribution to the state of the art

Research on materials for radiative cooling surface is one of the hot topics in this field of study. In many of the published papers convective covers are used in radiative cooling and RCE applications. However, after reviewing the state of the art it was concluded that, when convective covers are used, they are just presented as a complement to reduce the heat losses but their effects are not studied systematically. Moreover, the results are dispersed among all the literature. This paper contributes to order and summarise the progresses done in this line, presenting a classification of them.

This first part of the paper discusses the importance of convective covers and presents empirical correlations for convection coefficients in radiators and collectors. It also presents different approach designs of adaptive covers for combined solar heating and radiative cooling.

The core of the chapter is the review and classification on the main materials used in solar collector and radiative cooling. The first part of the core discusses polymeric covers. This type of covers is widely used in RC as it presents high transmittance in the atmospheric window – and high transmittance in the solar range –, but the structural degradation of the materials is still a problem. In the second part, pigmented and deposited films are covered; these materials block a big portion of the solar radiation and are not suitable in RCE applications. In the third part, we review non-polymeric covers made of cadmium or zinc-based crystals. Zinc-based crystals show high transmittance in the atmospheric window and medium transmittance in the solar range and have good structural

performance – but they are expensive –, while cadmium covers block most of the solar radiation. The optical transmittance of these materials is summarized in **Fig 15**. Finally, we extended the review to smart chromic materials which, despite they have not been studied in RC or RCE applications, they show properties that could make them suitable; however, more research has to be done.

At the moment of publishing the paper, there was not a systematic review of convective covers for combined radiative cooling and solar heating. In parallel, Zhang et al. [79] and later Farooq et al. [25] published a review of materials for convective covers in radiative cooling applications. In both papers, the study of the combination of solar heating and radiative cooling, and the proposal of smart materials for covers was overlooked.

As a conclusion for this chapter, authors proposed to characterize the optical properties of smart chromic materials in both ranges of interest (solar range and atmospheric window), as the following step to improve the performance of combined solar heating and radiative cooling applications.
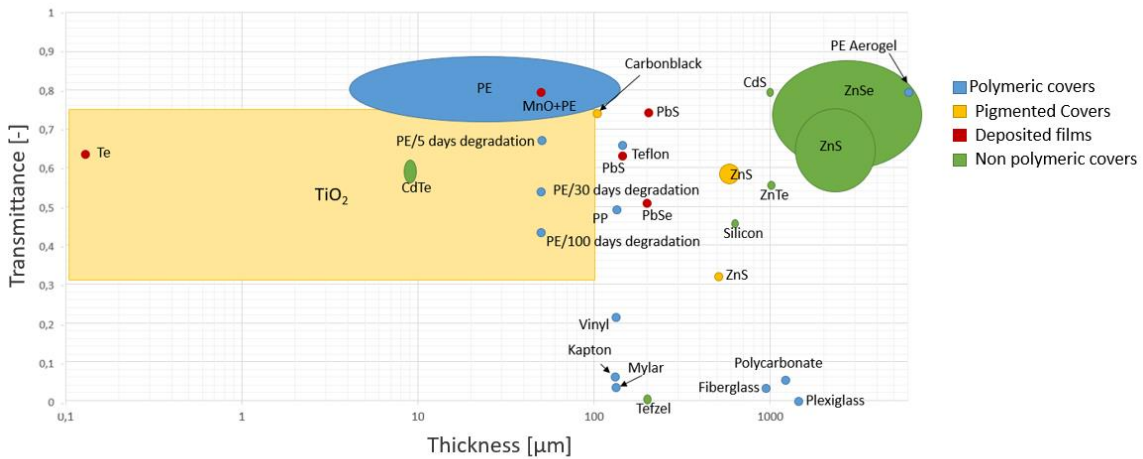
Fig 15. Comparison of experimental transmittances in the atmospheric window of different materials grouped in: polymeric, deposited films, pigmented covers and non-polymeric materials.

3. Contribution to the objective of the PhD

This chapter starts from hypothesis H1 and contributes to answer objectives O1 and O2, confirming the benefits of using a convective cover in both RC and RCE applications.
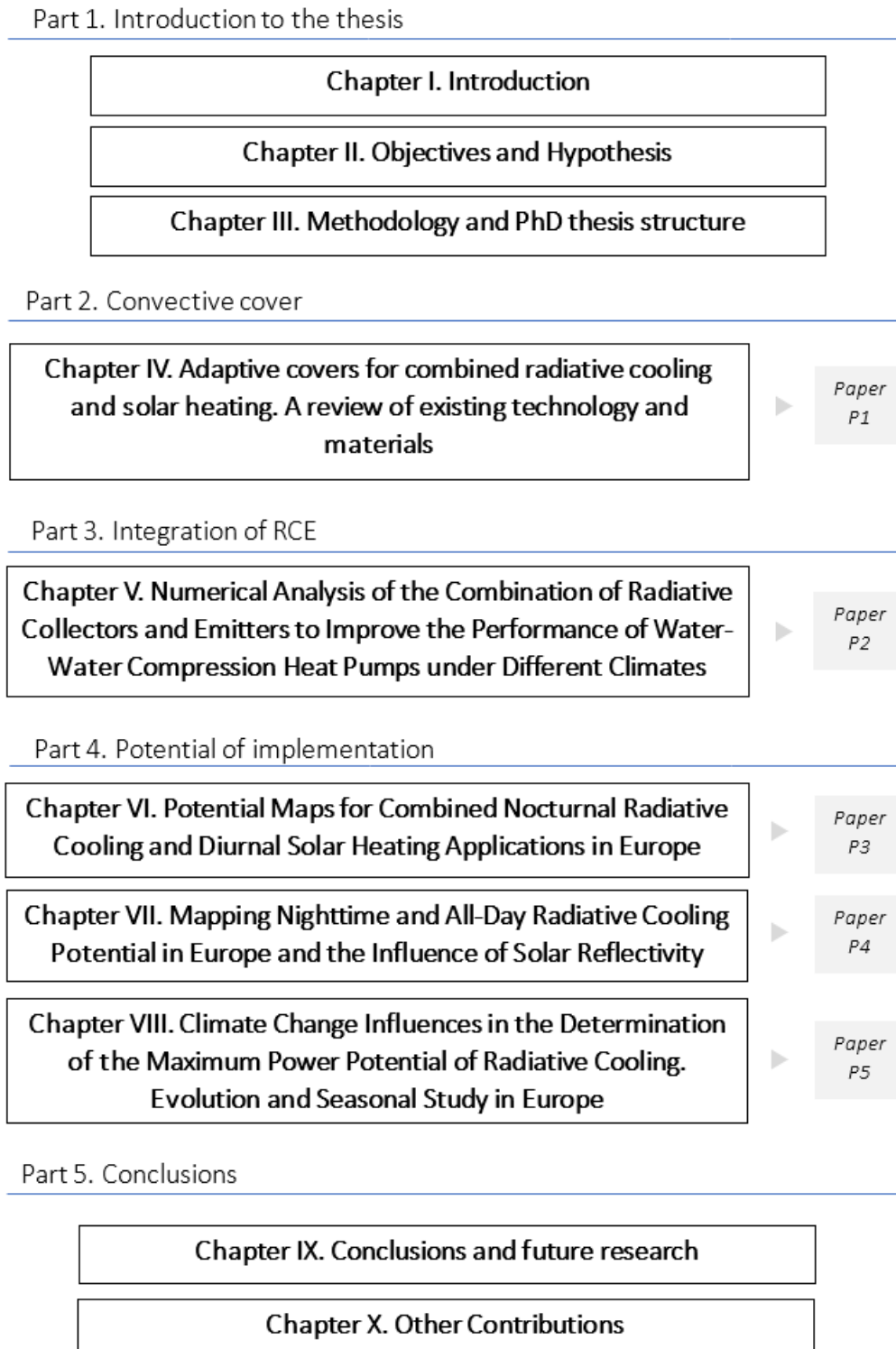
CHAPTER IV

Adaptive covers for combined radiative cooling and solar heating. A review of existing technology and materials

From this literature review, the authors detected low-density and high-density polyethylene, polypropylene, Teflon, and zinc-based crystals as good candidates to use in RCE applications in combinations with glass covers.

The paper summarises in tables the optical properties of different materials, making it easier the election of materials. This study has been used as a starting point for other investigations, in the context of a national research project, in the SEMB research team.

4. Contribution of the candidate

During the research exposed in this chapter, the candidate reviewed more than two hundred papers existing in the literature and proposed the structure and the different classifications exposed in the paper. The conclusions of the research were leaded by the candidate. Finally, the candidate was in charge of writing the final version of the paper.

5. Journal Paper

This chapter was published in *Solar Energy Materials and Solar Cells 230 (2021) 111275*, https://doi.org/10.1016/j.solmat.2021.111275.
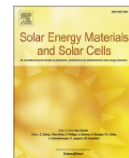
Adaptive covers for combined radiative cooling and solar heating. A review of existing technology and materials

Roger Vilà, Ingrid Martorell, Marc Medrano [*], Albert Castell

Sustainable Energy, Machinery and Buildings (SEMB) Research Group, INSPIRES Research Centre, Universitat de Lleida, Pere de Cabrera s/n, 25001, Lleida, Spain

ARTICLE INFO

ABSTRACT

Radiative cooling is a promising technology for space cooling. This technology can be combined with solar heating applications, enabling the production of both energy demands –heat during daytime and cold during nighttime– in a single device; thus, reducing the non-renewable primary energy consumption for space conditioning and domestic hot water. Radiative cooling and solar heating appear in different wavelength ranges, 8–14 μm and 0.25–2.5 μm respectively, thus the device must be able to switch between ranges in each mode. An adaptive cover placed on top of the radiator/absorber can provide this switch by combining materials with suitable optical properties for each mode. Another effect derived from the usage of covers is the reduction of convective heat losses, enhancing the performance of the device. This paper aims to review the existing materials used in solar collectors, and radiative coolers as well as available smart materials used in other fields for its potential use as adaptive covers for combined radiative cooling and solar heating applications.

Adaptive covers for combined radiative cooling and solar heating. A review of existing technology and materials

Roger Vilà, Ingrid Martorell, Marc Medrano [*], Albert Castell

Sustainable Energy, Machinery and Buildings (SEMB) Research Group, INSPIRES Research Centre, Universitat de Lleida, Pere de Cabrera s/n, 25001, Lleida, Spain

A B S T R A C T

Radiative cooling is a promising technology for space cooling. This technology can be combined with solar heating applications, enabling the production of both energy demands –heat during daytime and cold during nighttime– in a single device; thus, reducing the non-renewable primary energy consumption for space conditioning and domestic hot water. Radiative cooling and solar heating appear in different wavelength ranges, 8–14 µm and 0.25–2.5 µm respectively, thus the device must be able to switch between ranges in each mode. An adaptive cover placed on top of the radiator/absorber can provide this switch by combining materials with suitable optical properties for each mode. Another effect derived from the usage of covers is the reduction of convective heat losses, enhancing the performance of the device. This paper aims to review the existing materials used in solar collectors, and radiative coolers as well as available smart materials used in other fields for its potential use as adaptive covers for combined radiative cooling and solar heating applications.

1. Introduction

Energy transformation is indispensable for the functioning of today's societies; almost everything we do is possible due to the human capacity to extract energy from other sources to take advantage of it in our favor. Social and economic transformations resulting from Industrial Revolutions were a consequence of the replacement of energy sources available at the time by coal and later by oil, natural gas and electricity. Demand for the current model of energy consumption continues growing year after year – driven by population and industrial growth, as well as a rising in the living standards – while fossil resources still account for the 70% of the total of that growth [1].

One of the problems arising from the current energy model is the high volumes of greenhouse gases emitted into the atmosphere. The contribution of these gases to climate change as a result of human activity has reached a consensus among the scientific community [2] and global environmental awareness is currently increasing in society.

This challenge is being considered in recent public policies. In the case of the European Union it is determined to become an economy based on a low energy consumption, stable and secure, competitive, locally produced and sustainable. This is expressed in Directive 2009/28/CE on the promotion of energy from renewable resources [3], Directive 2018/844 [4] –amending Directive 2010/31/UE, concerning

energy efficiency of buildings, and Directive 2012/27/EU on energy efficiency–, and recommendations 2019/786 on the renovation of buildings [5]. Moreover, Project Europe 2030 [6], which replaces the Europe 2020 Project, sets out three key goals by 2030: (a) a reduction of at least 40% of greenhouse gas emissions with respect to 1990 values, (b) a share of at least 32% in renewable energy and (c) an improvement of at least 32.5% in energy efficiency.

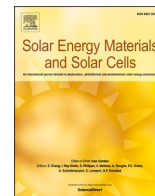The above mentioned relates to the high potential for reduction in energy consumption in buildings. In the EU, energy consumption in buildings is estimated to account for 40% of the total energy consumption, while accounting for 36% of CO_2 emissions [7]. The demand in residential sector is mostly covered by natural gas (36%) and electricity (24.1%), while renewables only account for 17.5%. Specifically, 64.1% of the total consumption in buildings is dedicated to space heating, 14.8% to Domestic Hot Water (DHW), and 0.3% to space cooling; accounting for almost 80% of the energy consumed [8]. As for space heating, the energy sources are quite diverse: natural gas dominates, but renewable sources already account for more than 20% and in a smaller proportion in DHW. According to data from Eurostat, space cooling is still entirely achieved by electricity consumption [8].

Currently, solar heating is a renewable technology which already has commercial applications in the field of energy production of heat and/or DHW. Cold generation is relegated to the use of nonrenewable air conditioning units which operate through compression or absorption

Nomenclature		Re	Reynolds Number ($-$)
		T_a	Ambient temperature (K)
A	Radiator/Absorber surface (m^2)	T_s	Surface temperature (K)
$E_b(T)$	Power absorbed/emitted by a blackbody surface at	∇T	Temperature gradient (K)
	temperature T (W)	σ	Stefan-Boltzmann's constant: 5.6704·10^{-8} (W/m^2·K^4)
$E(T)$	Power absorbed/emitted by a surface at temperature T (W)	ε	Emissivity ($-$)
h_c	Film coefficient (W/m^2·K)	ε_s	Surface emissivity ($-$)
k_{air}	Thermal conductivity of air (W/m·K)	ε_{sky}	Effective sky emissivity ($-$)
k_s	Thermal conductivity of the surface (W/m·K)	τ	Transmittance ($-$)
L	Characteristic length (m)	τ_{atm}	Transmittance in the atmospheric window's range ($-$)
P	Perimeter of the surface (m)	τ_{sol}	Transmittance in the solar range ($-$)
Pr	Prandtl Number ($-$)	ρ	Reflectivity ($-$)
Q_a	Absorbed infrared radiation from atmosphere (W)	ρ_{atm}	Reflectivity in the atmospheric window's range ($-$)
Q_{cond}	Conduction heat power (W)	ρ_{sol}	Reflectivity in the solar range ($-$)
Q_{conv}	Convective heat power (W)	α	Absorptivity ($-$)
Q_{net}	Net balance radiation power (W)	α_{atm}	Absorptivity in the atmospheric window's range ($-$)
Q_s	Infrared radiation power emitted by a radiative surface (W)	α_{sol}	Absorptivity in the solar range ($-$)
Q_{sun}	Incident solar radiation power (W)		

processes. Literature points out that radiative cooling can become a feasible possibility for renewable cooling production for space conditioning purposes [9,10].

Radiative cooling is a process by which a surface reduces its temperature by emitting thermal radiation towards the outer space taking advantage of the infrared atmospheric window transparency in the 8–14 μm range. Initially radiative cooling occurred at night only, as the energy balance during the day results in energy gains by solar radiation; however, with the development of new photonic materials and metamaterials, daytime surface cooling has been achieved [11–13]. Under clear sky conditions radiative cooling is maximized [14]. Ambient conditions and optical properties of materials play a role on the total performance of radiative cooler devices; currently they present low cooling rates (between 20 and 80 W/m^2 on average with peaks at 120 W/m^2) [15]. Total cooling rates are influenced by conduction and convection heat gains. In order to achieve higher cooling rates, various authors have proposed the use of convective barriers which separate the emitting surface from the environment, cutting down convective heat exchanges [16] and enabling surface cooling below ambient temperature [17,18].

The operation of radiative cooling is totally opposite to that of solar heating, since it occurs at different times of the day and in a different wavelengths range. Nevertheless, both functions are analogous so that combination of both functionalities has been proposed by various authors [15,19,20,21], thus enabling the production of both energy demands (heat and cold)– in a single device. As stated by Vall et al. [15], the use of both technologies may substantially reduce the non-renewable primary energy consumption for space conditioning and domestic hot water and it will make the investment more cost-effective. The payback of this technology could be of a period of 8 years [22].

Vall et al. simulated a mixed solar collector/radiative cooling system in order to evaluate the potential coverage of the demand in different building typologies and climates. The results showed that in five of the studied cities (representing five different climates in the world) it could achieve a minimum coverage of 25% of cooling and 75% of DHW in residential and hotel building typologies. In literature there is not a consensus name for this combined system: The authors named this device *Radiative Collector and Emitter (RCE)*. For the sake of simplicity, this paper also refers to it as RCE.

RCE works in two differenced modes in different wavelengths ranges: nighttime radiative cooler emits in the 3–25 μm range (long wave) while daytime collector absorbs solar radiation in the 0.2–3 μm range and blocks long waves. This will be further discussed in section 2;

however, the key is to know that RCE must have different optical properties which depend on the working mode.

To achieve this dual function two strategies have been identified: (1) to place an adaptive cover with selective transmittances on top of a black surface. The black surface absorbs/emits all the radiation while the cover filters the desired wavelengths. Covers, at the same time, can diminish the effects of convective exchanges, named convective covers. There are two typologies of adaptive covers: an exchangeable cover [23] which uses different materials depending on each working mode, or a smart material cover which is able to switch its optical properties depending on the working mode. Alternatively, (2) a second strategy is to use a selective surface, which controls the emissive/absorbance properties of the surface in different wavelengths ranges. As it has been previously stated, metamaterials with selective emissivity/absorptivity have already been proposed for all day radiative cooling applications [11–13]. However, up until this point, more complex metamaterials for combined radiative cooling and solar heating applications have not been investigated. These selective surfaces could also make use of a cover to diminish the effects of convection.

This paper puts the focus on the first mentioned strategy. Different reviews have been published on radiative cooling technology, including those by Lu et al. [24], Vall et al. [25], Nwaji et al. [26] and Zhao et al. [27]. Other reviews have focused specifically on materials for radiative cooling purposes, such as Granqvist and Niklasson [28], Ko [12] or Santamouris and Feng [9], placing its focus on emitter surfaces. However, to our knowledge, no revision of materials used in convective suppression applied to radiative cooling and solar heating has been presented. In this paper we review the different approaches presented in literature for RCE covers which allow the combination of both radiative collectors and emitters, while reducing the negative convection gains.

2. Background

2.1. Solar and infrared range

All the bodies being at a temperature above absolute zero are continuously radiating thermal energy. The energy emitted per unit surface area is according to Boltzmann's law (eq (1)). The amount of energy emitted from a surface, at a given wavelength, will depend on the material and conditions of the surface as well as the temperature of the surface. For a blackbody surface, the energy absorbed and emitted is maximum (Eq. (2)).

$$E(T) = \varepsilon\sigma T^4 \tag{1}$$

$$E_b(T) = \sigma T^4 \tag{2}$$

The Sun, being at near 5800 K, is considered to be a black body emitting shortwave radiation between the ultraviolet and the near-infrared band with its peaks falling in the visible range; collectors absorb energy within these wavelengths. Then again, cold bodies at ambient temperature (~300K) emit longwave radiation in the infrared band towards the outer space, which is at 3K [29]. Due to this large difference in temperatures, space becomes an energy sink. This process is possible due to the high transparency of the atmosphere at 0.3–3, 3.2–4.8, 8–14 and 16–23 μm wavelengths (Fig. 1). These transparent ranges are known as atmospheric windows. In the 8–14 μm range of wavelengths, atmospheric window matches a high portion of the infrared energy radiated by the bodies, enabling a temperature reduction.

It is noted that each mode of the RCE operates in different wavelengths ranges. For an RCE cover, during heating mode, it is desired to allow all the solar radiation to pass through the cover while blocking the infrared radiation. During cooling mode, it is desired to allow all the 8–14 μm radiation emitted by the surface to pass through the cover. Table 1 summarizes the optical properties of and ideal cover of an RCE.

2.2. Nonradiative heat gains

When a surface is not in an isolated environment, it is exposed to the following energy exchanges (Fig. 2):

1. Incoming short wavelength (0.3–2.5 μm) solar radiation which is absorbed by the surface. This energy flux is only present during daytime.
2. Infrared radiation emitted by the atmosphere and absorbed by the surface.
3. Infrared radiation emitted by the surface to the atmosphere.
4. Thermal gains/losses by exchange with the surrounding air or adjacent solids in the form of convection or conduction, respectively.

The total energy exchanged in the form of heat can be expressed according to Eq. (3). Due to the small value of σ, at low temperatures the effect of radiation is negligible compared to the conduction and convection effects. When temperature increases, due to the effect of T^4, the contribution of radiation is dominant. RCE systems at near ambient temperatures fall in a range where the three effects have to be considered.

When the surface temperature (T_s) is different from the ambient temperature (T_a), nonradiative exchanges with the environment (conduction and convection) exist. During nighttime radiative cooling applications, if the cooler is designed to work at $T_s > T_a$, it would benefit from convective and conductive heat exchanges [31] while for $T_s < T_a$, nonradiative exchanges would reduce the total performance of the RCE [32]. In contrast, during daytime solar heating applications,
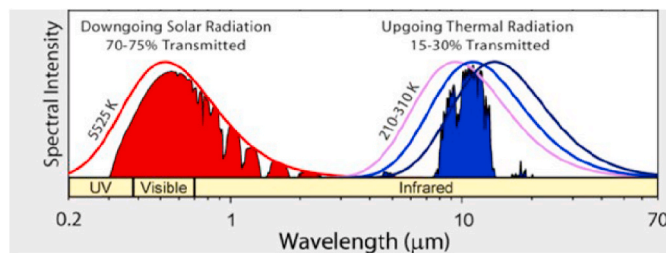
Fig. 1. Solar radiation (red) and radiation through the atmospheric window (blue). Modified from Ref. [30]. (For interpretation of the references to color in this figure legend, the reader is referred to the Web version of this article.)

Table 1
Ideal optical properties of a RCE cover.

	Solar Spectrum		Atmospheric Window	
	Transmittance	Emittance	Transmittance	Emittance
Heating mode	100%	0%	0%	0%
Cooling mode	–	–	100%	0%

nonradiative heat exchanges would enhance the overall performance of the RCE when $T_s < T_a$ while it would be reduced when $T_s > T_a$, the most usual situation. For an RCE with overambient daytime temperatures and subambient nighttime temperatures, energy will be maximum when the convection and conduction gains are minimal (Eq. (4)).

$$Q_{net} = Q_s(T_s) - Q_a(T_a) + Q_{sun}(T_{sun}) - Q_{cond} - Q_{conv} \tag{3}$$

$$Q_{net} = A \cdot \sigma \cdot \varepsilon_s \left(T_s^4 - \varepsilon_{sky}T_a^4\right) + Q_{sun}(T_{sun}) \tag{4}$$

Conduction heat gains are the consequence of thermal energy exchanging processes between bodies in contact at different temperatures (Eq. (5)). In the case of a radiative cooler, heat gains will appear on the emitter/absorber's walls and can be minimized with thermal insulation.

$$Q_{cond} = -k_s \cdot A \cdot \nabla T \tag{5}$$

Convection is a thermal energy transfer between areas of the same fluid at different temperatures through the movement of the molecules inside these areas. In the case of the radiative cooler, this movement occurs between the air particles in contact with the surface at a lower temperature and the air particles at room temperature. The convective heat gains can be expressed with Eq. (6).

$$Q_{conv} = h_c \cdot A \cdot (T_s - T_a) \tag{6}$$

The convection heat transfer coefficient on a flat plate can be expressed based on the Nusselt number (Eq. (7)) which takes into account both free and forced convection effects. Different authors have fitted empirical correlations to convection heat transfer coefficient as a function of wind speed, increasing as the velocity increases [33]. Table 2 shows the approximations used by authors in different contexts.

$$h_c = \frac{Nu \cdot k_{air}}{L} \tag{7}$$

Zhao et al. [18] experimentally studied the effects of wind speed on radiative surface performance. The results showed that the difference in temperatures between the circulating water and the environment decreased from 7 °C to 4.3 °C (Fig. 3) due to a change of wind speed when the convective cover was removed.

3. Exchangeable adaptive cover

An exchangeable adaptive cover concept can be viewed as a combination of two different covers that can be swapped, one for solar heating mode and the other for radiative cooling mode, providing low spectral transmittance in the infrared band and high spectral transmittance in the solar range during the daytime solar collection mode, and high spectral transmittance in the 8–14 μm wavelength range during nighttime radiative cooling mode.

Commercial flat plate solar collectors are provided with low emissivity glass covers with the aim of letting solar radiation pass through, while preventing heat loss to the environment. Moreover, thanks to the very low transmittance on the whole infrared (IR) spectrum of this glass, it blocks thermal radiation to escape from the surface while acting as a convective suppressor for the collector, enhancing the total performance. Glass by itself is not a good candidate for RCE applications, as it would prevent radiative cooling at night. Alternatively, polyethylene film has high transmittance both in the infrared and the solar spectrum (Table 3), allowing radiative cooling during night. Glass can be placed
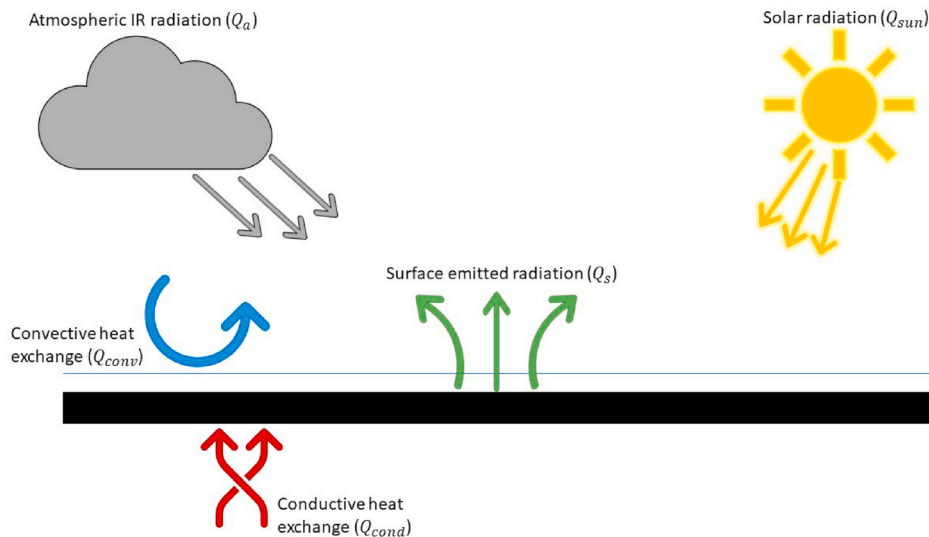
Fig. 2. Thermal exchanges between the radiative surface and its surroundings.

on top of polyethylene during daytime to improve the RCE performance and be removed during nighttime. Vall et al. [15] proposed to slide the glass on top of polyethylene films (Fig. 4), enabling the automation of the process. Liu et al. [22] alternatively designed a combined device made of 10 μm polyethylene film, a porous cooling material with near unity infrared emissivity in the 8–13 μm range, aluminum conductor substrate, providing heat conductivity, and a solar absorbing material (Fig. 5) coated with chromium plating (solar absorptivity of 95%). Radiative cooling was achieved on one layer of the device while solar collection was done on the other layer of the device; the switching between modes was achieved with a rotating shaft.

In solar collection applications glass is widely used [42,43] and has become the standard material. In contrast, there is not yet a standard material in radiative cooling applications and it is still a subject of study.

3.1. Convective covers based on polymers

The main feature for convective covers, also named windscreens, in radiative cooling applications is its high transmittance in the far-infrared (FIR) spectrum. Due to this characteristic, windscreens are placed on top of emitters, separating the radiator from the environment conditions. In 1975, Johnsons [16] investigated the use of a 0.0005 in (0.0127 mm) cover of fluorinated ethylene propylene (FEP or Teflon) film. Film was protected against water attack and structurally reinforced with aluminum ribs. The author measured a transparency of 70%, but he stated that the film was too thin to withstand environmental conditions. Orel et al. [44] used a polyester foil with a thickness of 50 μm. Authors only affirmed that it was transparently enough for infrared radiation to cover an aluminum radiator.

Despite the two materials described above, the material most commonly used as a windscreen has been polyethylene due to its high transmittance in the atmospheric window (Fig. 6). To reduce conductive and convective heat exchanges, Bartoli et al. [45] built in 1977 an insulating styrophoam box covering the radiator with a polyethylene sheet of 50 μm thickness on top; although it was presented to have almost ideal transparency, it had quite low mechanical properties and, under high humidity conditions, it showed moisture condensation, decreasing the optical properties.

Tsilingris [46] studied the infrared transmittances of various polymers for their utilization as a suppressor for the convective losses/gains in solar collector/emitting surfaces. Of the ten samples analyzed – plexiglass, fiberglass, polycarbonate, polyethylene, polypropylene, tedlar, mylar, kapton and vinyl – Tsilingris sentenced that polyethylene and

polypropylene had the highest transmission, making them suitable for radiative cooling applications; while fiberglass, kapton and mylar showed the lowest coefficients, being suitable for solar collector applications.

Leroy et al. [47] used a polyethylene aerogel as a cover: it showed low thermal conductivity, high transmittance in the atmospheric window (0.799) and high reflectance of solar radiation (0.922). This offers the possibility to achieve daytime radiative cooling. Raman et al. [17] covered a photonic solar reflector and thermal emitter with a 12.5 μm thick LDPE to obtain daytime radiative cooling. The system, which had a 97% reflectance in the solar band and high emittance in the longwave range, was able to cool to 4.9 °C below ambient. In the last decade, various authors have used polyethylene foils –both high density polyethylene (HDPE) and low density polyethylene (LDPE)– as convective windscreen materials combined with new structures such as crystals, metamaterials and photonic crystal, which serve as emitting surface, to achieve daytime radiative cooling. Xu et al. covered with polyethylene a new crystal with 87% emittance in the atmospheric window and 88% solar reflective [48]. Zhao et al. combined a polymer metamaterial film with a PE cover achieving a difference of 10 °C between circulating water and ambient temperature under solar radiation [18]. Anodic aluminum oxide covered with PE presented cooling power of 64 W/m^2 and cooling temperatures of 2.6 °C below ambient [49].

Because of the optical properties and also the low cost and availability of polyethylene, it has been tested in mixed heating and cooling applications. In 1987, Matsuta et al. [19] used a selective solar heating/radiative cooling surface covered with a polyethylene film to prevent convective exchanges achieving maximum values of 610 W/m^2 in collection mode and 51 W/m^2 in radiative mode. Long et al. [21] developed a composite surface made of silica micro-grating and p-doped Si, covered with polyethylene, to enable both solar collection and radiative cooling. Hu et al. developed a selective surface highly emitting/absorbing in both the solar range and atmospheric window band covered with a PE convective cover; the system had a cooling power of 50.3 W/m^2, under clear night conditions, and a solar collector efficiency of 62.7% [20,50]. A combined radiative cooling/solar heating system based on water circulating under a black surface –protected with LDPE film– presented a daily thermal efficiency between 26.8 and 40.7% and a cooling efficiency of 58.3% [51].

Radiative cooling simulations also make use of polyethylene covers in the models. Mihalakakou et al. [41] modeled, using TRNSYS, the performance of a radiative cooling system in a building. The system consisted of a stainless steel radiative cooler covered with a

Table 2
Summary of convection coefficient correlations.

Reference	Coefficient correlation	Units	Characteristic dimensions in the study	Observations and Applications
[18]	$h_c = 8.3 + 2.5v$	W/m²K	A = 0.58 m × 0.58 m	Radiative cooler without windscreen $0 < v < 8$ m/s
[18]	$h_c = 2.5 + 2v$	W/m²K	A = 0.58 m × 0.58 m	Radiative cooler with windscreen $0 < v < 8$ m/s
[34]	$h_c = 5.7 + 3.8v$	W/m²K	L = 2.9	Small flat plate solar collectors
[35]	$h_c = 2.8 + 3v$	W/m²K	A = 2 m × 1 m	Thermal simulation of solar energy systems
Berdahl and Clark quoted in [36]	$h_c = 0.8$	W/m²K	–	$T_s < T_a$ Free convection (v < 0.076 m/s)
Berdahl and Clark quoted in [36]	$h_c = 3.5$	W/m²K	–	Ts > Ta Free convection (v < 0.45 m/s)
Berdahl and Clark quoted in [36]	$h_c = 0.054 \cdot Re^{0.8} Pr^{0.33} \cdot k_S/L$	W/m²K	–	Turbulent flow
Berdahl and Clark quoted in [36]	$h_c = 1.8 + 3.8v$	W/m²K	–	Turbulent flow (1,3 < v < 4,5 m/s)
[37]	$h_c = 5.7 + 3.8v$	W/m²K	L < 0.5 m	–
Sparrow (1979) quoted in [38]	$h_c = 4.6v^{0.5} L^{-0.5}$	W/m²K	$L = \dfrac{4 \cdot A}{P}$	Horizontal flat plate
Lunde (1980) quoted in [38]	$h_c = 4.5 + 2.9v$	W/m²K	–	–
[39]	$h_c = 9.4v^{0.5}$	W/m²K	–	Fitted equation to experimental data
[40]	$h_c = 0.6 + 3.5v^{0.5}$	W/m²K	–	Without windscreen
[40]	$h_c = 0.5 + 1.2v^{0.5}$	W/m²K	–	Single polyethylene layer windscreen
[40]	$h_c = 0.3 + 0.8v^{0.5}$	W/m²K	–	Double windscreen
[41]	$h_c = 3.1 + 4.1v$	W/m²K	A = 14 m × 7 m	Forced convection 0.1 < v < 2 m/s
[41]	$h_c = 5.7 + 3.8v$	W/m²K	A = 14 m × 7 m	Without windscreen v < 4 m/s
[41]	$h_c = 7.3v^{0.8}$	W/m²K	A = 14 m × 7 m	Without windscreen v > 4 m/s
[41]	$h_c = 0.5 + 1.2v^{0.5}$	W/m²K	A = 14 m × 7 m	Single polyethylene layer windscreen

polyethylene film of 60–100 μm of thickness. Daily energies varied between 29.7 and 55.8 W h/m² under clear sky and between 26.7 and 44.9 W h/m² for a cloudy day.

In 1998, Al-Nimr et al. [52] developed a mathematical model which described the dynamic thermal behavior of a radiative cooling system consisting of a black surface and a polyethylene thin film of 40 μm on top. This model assumed that the polyethylene cover had perfect radiative properties. The analytical solution showed lower outlet temperature predictions compared to experimental results.

Due to the transparency of polyethylene in the solar range, it has not only been used in radiative cooling and RCE applications but also in photovoltaic/radiative cooling mixed systems (PV/RC) for the combined generation of electricity during daytime and cold during night. Zhao et al. were able to achieve 12.7 °C reduction below ambient nighttime temperature with an average electrical conversion efficiency of 12.4% [53]. The PV/RC performance is strongly dependent on climate areas and seasons [54–56].

3.1.1. Pigmented covers

Andretta et al. [65] in 1981 made a lowcost cover blending in two layers of polyethylene with commercial standard pigments, such as TiO₂ and carbon black, with the aim of reflexing part of the solar radiation while absorbing the rest through the carbon black. The authors achieved subambient temperatures under these films even during daytime. Single layers of polyethylene pigmented with TiO₂ were also studied by Niklasson and Erikson [66]. Authors concluded that these covers were able to achieve radiative cooling for more than 19 h of the day. Using hot pressing technique with small particles of TiO₂ (diameter of 60 nm) into two polyethylene foils Mastai et al. [67] could obtain transmittance in the atmospheric window regions of 0.54–0.765 and high solar reflectances (Table 4).

Zinc based pigments blended into two polyethylene foils have also been used as convective covers. The performance of polyethylene with different pigments, including ZnS, ZnSe, ZrO₂ and ZnO where studied by Nilsson et al. [68]. Results showed that ZnS is the best pigment among the others to be used in selective covers [68–71].

3.1.2. PbS, PbSe and Te deposited films

PbS, PbSe and Te deposited on polyethylene films can also act as shields. Dobson et al. [71] compared different films produced by

chemical solution deposition (CSD) techniques: in particular they produced PbSe and PbS films on polyethylene films and on ZnS and ZnO pigmented polyethylene films. The films showed a variety of optical properties based on the deposition parameters: in the case of the PbS, the films deposited from potassium nitrilotriacetate (NTA) showed high transmittance in the atmospheric window (Table 5) while with trisodium citrate (TSC) depositions the transmittance was slightly lower. In the case of the PbSe, transmittance in the atmospheric range was lower, as well as the reflectance in the solar spectrum due to the NTA baths. PbS films presented high absorption in the solar range. Authors also studied the behavior of PbS semiconductor laminates deposited on pigmented polyethylene with ZnS and ZnO. Transmittance values in the solar range were very low (0.04 and 0.03), while absorption values in this range were higher than 0.62. Engelhard et al. [72] developed an easy method to deposit Te films on a polyethylene substrate –pretreated with KMnO₄– using the room temperature decomposition of electrochemically
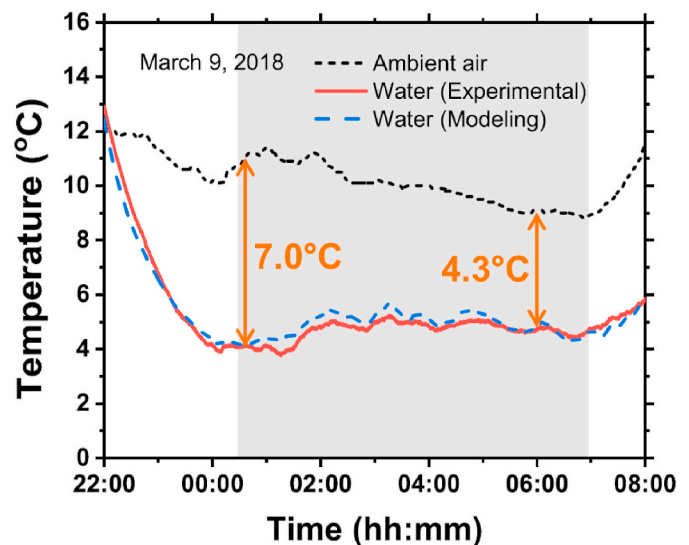
Fig. 3. Experimental temperatures obtained from a radiative cooling test, showing the effect of wind. During the colored grey period PE windscreen was not used on top of the emitting surface [18].

37

Table 3
Summary of transmittances of polymeric covers.

Cover material	Reference	Thickness	τ_{atm}	τ_{sol}	Application	Comment
Teflon	[16]	127 μm	~0.7	–	RC	–
LDPE	[17]	12.5 μm	–	–	Daytime RC	–
LDPE	[20,50,55]	20 μm	0.83[a]	0.85[1]	SH/RC	–
LDPE	[54]	6 μm	0.87[1]	0.89[1]	PV/SH/RC	–
LDPE	[46,62]	6 μm	0.87	0.89	SH/RC	–
LDPE	[53]	–	High	High	RC/PV	–
LDPE	[57]	20 μm	–	–	Daytime RC	–
LDPE	[58]	–	–	–	Daytime RC	–
PE	[19]	30 μm	0.86[b]	0.85[1]	SH/RC	–
PE	[46]	130 μm	0.79[1]	–	–	–
PE	[46]	50 μm	0.88[1]	0.87[1]	SH/RC	–
PE	[48]	–	–	–	Daytime RC	–
PE	[49]	50 μm	–	–	Daytime RC	–
PE	[52]	40 μm	High	–	RC	–
PE	[59]	50 μm	0.72	–	RC	New film
			0.69			5 days exposition
			0.57			30 days exposition
			0.42			100 days exposition
PE	[60]	50 μm	0.74[1]	–	RC	–
PE	[61]	1 μm	0.92	–	SH/RC	–
PE	[62]	Ø150 μm	0.872	–	RC	Fibermesh cover
PE	[63]	30 μm	0.85	–	RC	–
PE	[64]	–	0.92	<0.45	Daytime RC	–
PE aerogel	[47]	6 mm	0.80	0.11	Daytime RC	–
Polyester	[44]	50 μm	High	–	RC	–
Polycarbonate	[46]	1.22 mm	0.06[1]	–	–	–
Kapton	[46]	130 μm	0.08[1]	–	–	–
Mylar	[46]	130 μm	0.05[1]	–	–	–
PP	[46]	130 μm	0.50[1]	–	–	–
Plexiglass	[46]	1.52 mm	0.01[1]	–	–	–
Vinyl	[46]	125 μm	0.21[1]	–	–	–
Fiberglass	[46]	960 μm	0.04[1]	–	–	–

[a] Value obtained digitalizing transmittance graphs of materials using WebPlotDigitizer tool. Wavelenghts from 0,38 to 2,5.
[b] Value obtained digitalizing transmittance graphs of materials using WebPlotDigitizer tool.
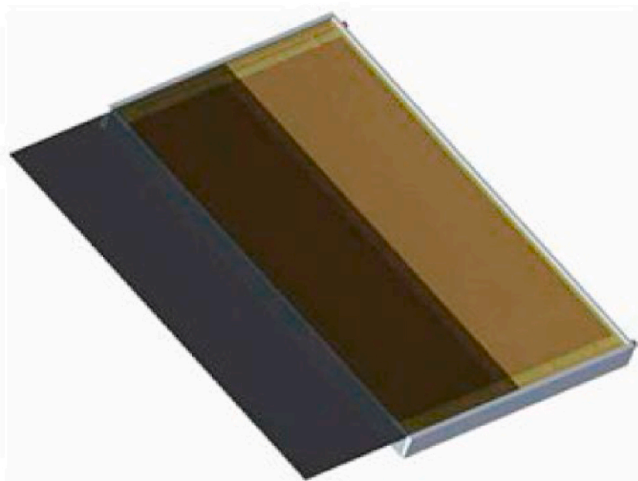
Fig. 4. Sliding adaptive cover proposed by Vall et al. [15].

generated H₂Te. The film had a relatively lower transmittance in the atmospheric windows compared to polyethylene (0.652 vs. 0.813) but also a higher decrease in transmittance in the solar range (0.047 vs. 0.891). For this reason, it is suitable to use it as a daytime radiative cooler shield.

3.1.3. Effect of aging

The continuous exposition to the atmosphere has a deteriorating effect in the optical properties of the polymers. Ali et al. [59] studied the degradation on the transparency of films of polyethylene of 50 μm under atmospheric conditions in Assiut (Egypt). The transmittance of the film dropped 41.7%, from 0.72 to 0.42 after 100 days of outdoor exposition; the radiative cooling performance decreased a 33.3%.

Carrasco et al. [73] analyzed HDPE exposed under artificial UV light with FTIR technology. Samples were prepared following the ASTM-D638 standard 0 type V. Analysis shows that the polymer undergoes chemical and structural changes that modify its mechanical properties: stiffness of HDPE increased after 120 days of exposition, Young's modulus changed from 604 MPa to 855 MPa (Fig. 7), tensile strength is reduced from 23.1 to 17.1 MPa (Fig. 7), and the strain is reduced from 231% to 7.4% (Fig. 7).

3.1.4. Effect of thickness

The thickness of the cover material has an effect on its optical properties. Ali et al. [59,60] studied the transmittances of polyethylene with different thickness, concluding that a foil of 25 μm of thickness showed better transparency than a foil of 50 μm. They verified that the decrease in the thickness of the PE foil, from 50 μm to 25 μm, supposed and increase of the performance of the radiative cooler by 8.6%.

Nwaji et al. [61] carried out a finite element analysis of the performance of a RCE system applied in five Nigerian cities. The authors modeled a flat titanium absorber coated with PET and covered with a polyethylene windscreen. Results showed that, during daytime solar collection, as the number of polyethylene windscreens increased, the circulating water temperature decreased progressively (Fig. 8).

3.1.5. Mechanical problems

Despite the favorable optical properties of polymeric covers described above, their weak mechanical properties become an inconvenient for their application outdoors: the cover has to withstand wind, tearing, rainwater [62] and snow. Dust and humidity can affect both the mechanical behavior and the optical properties of the cover [16]. Due to
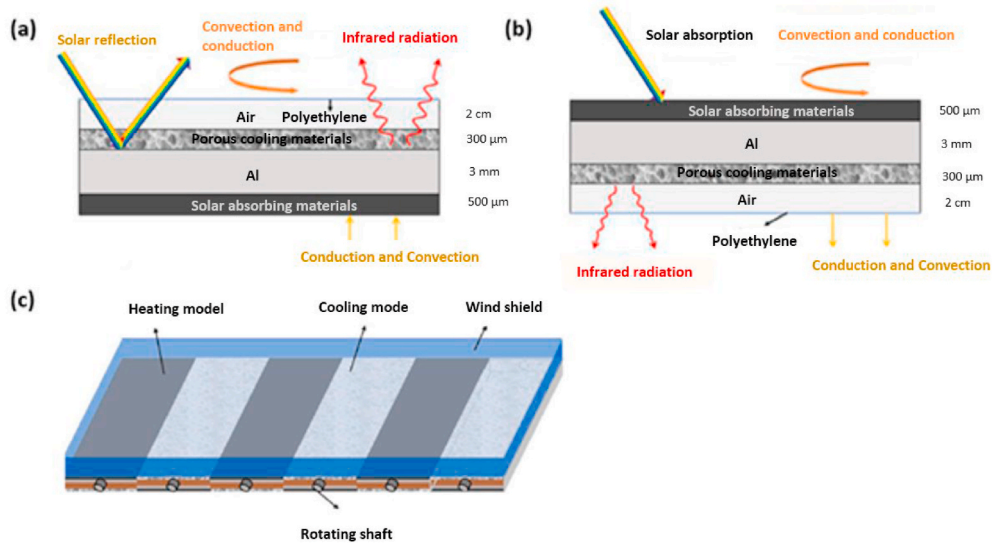
Fig. 5. Mixed radiative cooler and solar heater proposed by Liu et al. [22]. (a) Radiative cooling mode, (b) Solar heating mode and (c) rotating structure.
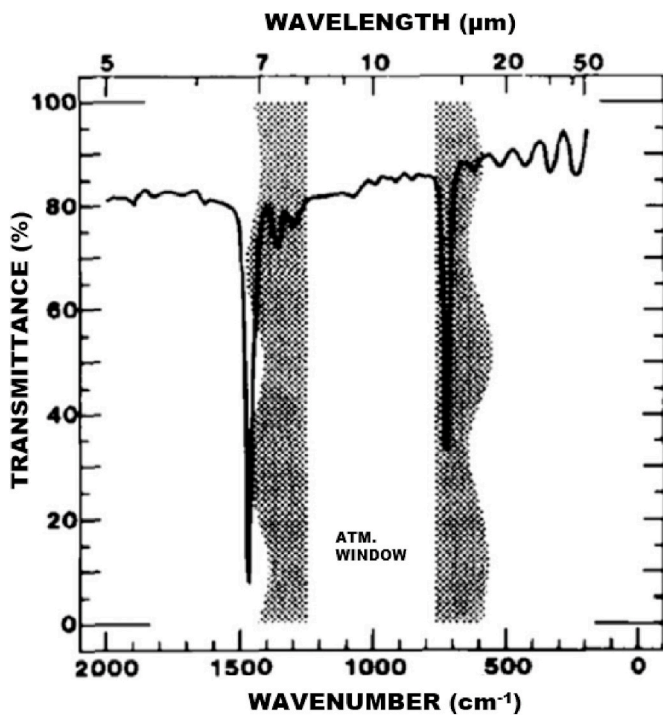
Fig. 6. Spectral transmittance of a 30 μm thick foil of HDPE [53].

its thinness, the wind can cause the fluttering of the foil. Finally, the covers are exposed to the presence of animals – birds and insects – which can damage the structure.

A new configuration for the polyethylene shape was studied by Nilsson et al. [63] in 1985. They used a screen made of three layers of corrugated polyethylene in a V-shaped arrangement (Fig. 9). When transmittance and thermal insulation was analyzed, this configuration presented a better convective performance than a flat cover, with a transmittance of 0.73. Moreover, this cover had a characteristic thickness of 4.5 cm; although it was not studied, it could add an extra structural resistance compared to flat covers.

Golaka and Exell [74] simulated a theoretical convective shield, a grid made of slats, which could deal with the previous described structural weakness. Authors performed finite elements simulations of the airflow through diverse obstacles over a radiative cooling surface: on top of the surface it was placed a grid consisting of metallic perpendicular strips (Fig. 10). The grid acts as a barrier for the airflow, reducing the total heat transferred by convective movements. A small windshield could increase the turbulence over a surface, increasing the convective heat transfer but a higher windshield avoids these problems. However, a high shield can interfere with the radiation of the surface. Authors concluded that it makes sense to use this structure where the winds produce unfavorable heat fluxes to the surface [74]. As mentioned by Gentle et al., the previous study overestimated the reduction potential of the convective heat transfer [62].

Gentle et al. proposed the use of a polymeric mesh made of UV stabilized HDPE fibers of 150 μm diameter (Fig. 11). The mesh had an effective transparency of 87% while suppressing the convection transfer

Table 4
Summary of optical properties of pigmented covers.

Pigment	Reference	Thickness	τ_{atm}	τ_{sol}	ρ_{atm}	ρ_{sol}	α_{atm}	α_{sol}
TiO$_2$	[65]	100 μm	0.74	0.57	–	–	–	–
TiO$_2$	[67]	0.12 μm	0.765	0.61	0.765	0.381	0.063	0.009
TiO$_2$	[67]	0.45 μm	0.731	0.412	0.731	0.581	0.115	0.007
TiO$_2$	[67]	0.75 μm	0.681	0.273	0.681	0.712	0.157	0.015
TiO$_2$	[67]	1.08 μm	0.651	0.22	0.651	0.684	0.196	0.096
TiO$_2$	[67]	1.82 μm	0.546	0.166	0.546	0.763	0.276	0.071
TiO$_2$	[67]	submicrometer	0.323	0.391	0.601	0.435	0.076	
TiO$_2$	[68]	100 μm	0.75	0.09		0,67		
Carbonblack	[65]	100 μm	0.74	0.24	–	–	–	–
ZnO	[68]	–	0.68	0.31		0.69		
ZnS	[68]	400 μm	0.33	0.013	0.09	0.849	0.58	0.138
ZnS	[70]	420 μm	~0.6	–	–	0.8	–	–

Table 5
Summary of optical properties of deposited films.

Film material	Reference	Thickness	τatm	τsol	ρatm	ρsol	αatm	αsol
PbSe (HC NTA)	[71]	200 μm	0.508	0.09	0.186	0.274	0.306	0.636
PbS (HC NTA)	[71]	200 μm	0.741	0.168	0.154	0.468	0.105	0.364
PbS (HC TSC)	[71]	150 μm	0.642	0.138	0.143	0.372	0.215	0.490
ZnS pigment + PbS film	[71]	–	0.488	0.162	0.331	0.35	0.629	0.629
ZnO pigment + LDPE coated with PbS film	[71]	–	0.406	0.03	0.155	0.286	0.439	0.684
MnO coated PE	[72]	50 μm	0.801	0.725	0.17	0.173	0.029	0.102
Te	[72]	0.12 μm	0.652	0.047	0.221	0.123	0.137	0.83
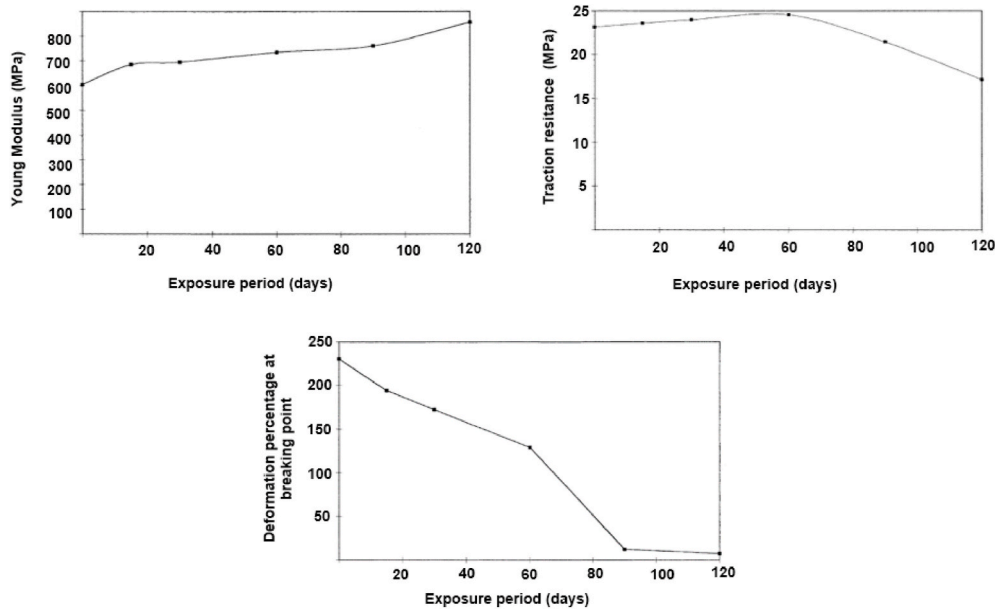
Fig. 7. Variation of Young modulus, traction resistance and strain. Modification of [73].
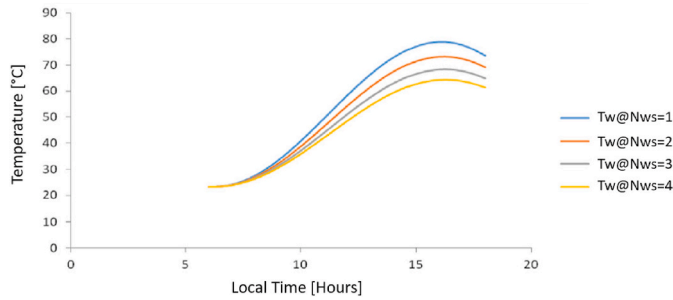
Fig. 8. Effect of number of polyethylene windscreens, under solar collection, simulated by Nwaji et al. [61].

[62]. Based on the existing use of UV stabilized mesh in the field of agriculture, authors affirmed that this configuration was expected to have a lifespan of 5 years.

3.2. Non-polymeric convective covers

3.2.1. Zinc crystals

Zinc compounds have also been investigated in the form of crystals. Compared to zinc pigments, where zinc compound constituted a small portion of the whole cover, zinc crystals are big structures constituted mainly by zinc. With the aim of obtaining a robust cover, Bathgate and Bosi [75,76] studied the thermal performance of ZnS shield. Authors compared ZnS cover with a polyethylene cover: ZnS had similar radiative cooling performances to polyethylene. Nevertheless, ZnS crystal
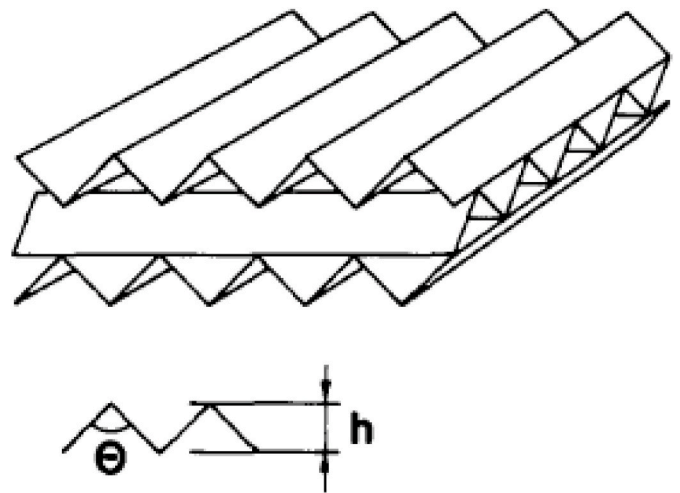
Fig. 9. Three layered corrugated foils (v-shapped) of polyethylene with high infrared transmittance and low nonradiative heat exchange [63].

covers are a durable solution. ZnS is a low toxic material, outdoor resistant and available in 4 mm thickness – 40 times thicker than PE – which provided an atmospheric window's transmittance of 64%.

Chen et al. [77] combined a highly selective emitter with a ZnSe cover to minimize solar radiation; the passive radiative cooling system was backed with a shading system which minimizes solar radiation exposition and a vacuum chamber which minimizes parasitic conductive
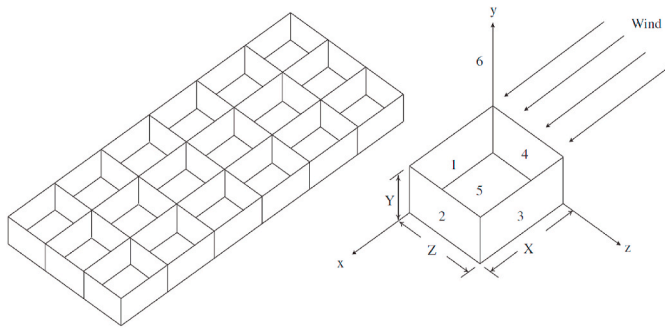
Fig. 10. Wind shield proposed by Golaka and Exell and an enlarged view of a cell unit [74].

Fig. 11. Segment of the HDPE mesh [59].

Fig. 12. Large temperature reduction below ambient through radiative cooling in a 24-h day-night cycle. A maximal cooling of 42.2 °C synchronizes with the peak of the solar irradiances [77].

and convective loses. The whole system achieved a record decrease of the surface temperature of 42 °C below ambient coinciding with the peak of solar irradiance (Fig. 12). Laatioui et al. [78] calculated the optical properties in the solar and atmospheric windows' range of the following shields: ZnS, ZnSe and ZnTe. The shields had a transmittance between 0.66 and 0.77 in the atmospheric windows and between 0.61 and 0.66 in the solar range. The transmittance was lower in the visible range (0.22–0.37).

ZnSe and ZnS crystals are materials that have a high price. Reduction of thickness and purity of the crystal would represent a reduction in cost. Nevertheless, Yashina et al. [79] described three processes of manufacturing ZnS polycrystals: chemical vapor deposition (CVD), hot pressing, and vapor deposition. The first method is based on the reaction of Zn with H_2S, while the other two processes make use of ZnS powder, which is less expensive than crystal. According to the authors, CVD is the most appealing process to fabricate ZnS crystals due to its better optical homogeneity and low impurity content [79,80].

3.2.2. Cadmium films

Benlattar et al. [81] studied the use of CdTe films (9.7 μm) on a 1 mm silicon substrate. The film had a relatively high reflectivity (0.38) and an elevated absorption (0.42) in the solar band and was transparent in the 8–13 μm region (0.62). One year later, in 2006, the authors presented a similar experiment, this time using a CdS sheet (1 mm). The sheet had a high transmittance in the 8–13 μm range (0.8) and a high absorptivity in the solar range (0.68) [82]. Table 6 summarizes these properties. Fig. 13 presents a visual comparison of the atmospheric window transmittance of the previous materials. It can be seen visually that polyethylene covers, CdS and zinc-based materials presented the highest
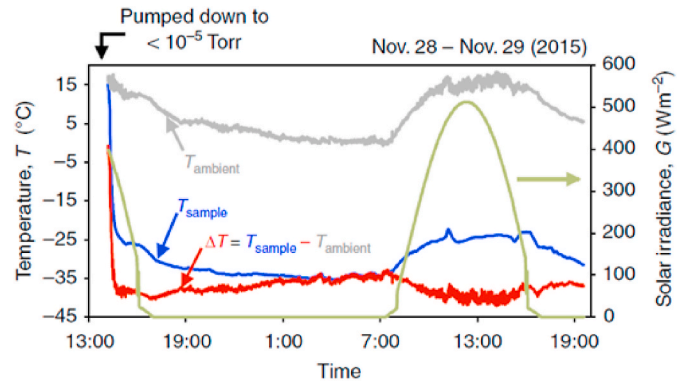
transmittance.

4. Smart material adaptive cover

A smart material for RCE windscreen applications would switch its optical properties depending on the working mode: during daytime it should present a strong transmittance in the solar band and opacity in the infrared band; during nighttime it should be highly transparent to the infrared range. In the following sections several types of chromic materials (electrochromic, thermochromic, gasochromic and photochromic) are reviewed in order to know their suitability for RCE, as they can change their optical properties under exposure to external stimuli. These materials have been used in thermal control but, despite being widely studied in the glazing and smart window industries [83–85], the wavelength range of interest of these materials is restricted to solar range and no insights on the infrared are provided. To our knowledge, only few researches have studied the infrared range.

4.1. Electrochromic materials

Under the application of low magnitude voltage, electrochromic materials exhibit tunability of their optical properties [86]. These properties have been studied since the 1970s [87], mostly in the visible spectrum [88]. This technology has most of its applications in the field of smart windows [89], although they are also noteworthy in camouflage [90,91], automotive and aircraft [87,89], and thermal regulation [83].

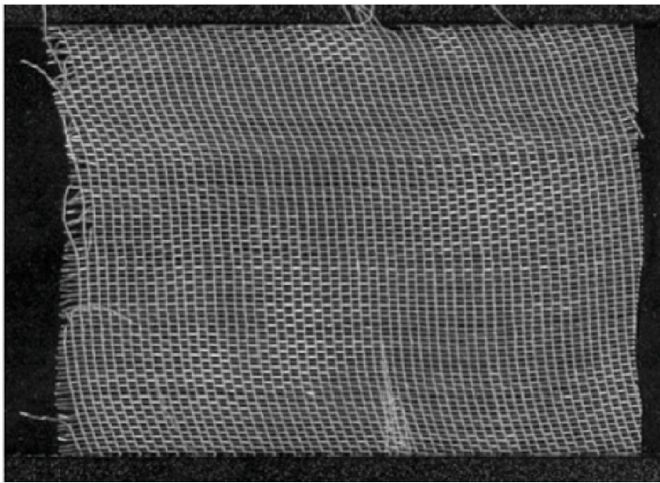Electrochromic materials show a battery-shaped structure (Fig. 13) consisting of five layers interspersed with transparent conductive materials, an electrolyte conducting material, an electrochromic sheet and an electron accumulation layer [92]. The working principle of this material is the redox reactions that occur when the current flows. The ions, usually Li^+ or H^+, move from the accumulation layer to the electrode, generating new energy bands in which the compound interacts with the light and, as a consequence, modifies the optical properties of the material.

Metal oxides such as WO, TiO_2, Nb_2O_5, MoO_3, NiO, IrO_2 and V_2O_5 [93] have been used as electrochromic materials to control the transmittance and emissivity properties in the visible, especially wolfram compounds being also able to act on the NIR spectrum [94].

Mandal et al. [95] studied the existing change in the infrared spectrum of a lithium-titanium-oxygen material. In the $Li_4Ti_5O_{12}$ form it exhibits low visible and long-infrared absorbance; in the $Li_7Ti_5O_{12}$ form it has high emission throughout the IR, thus allowing thermal regulation. According to the authors, this material may have application as radiative surfaces for radiative cooling and solar heating devices. Franke et al. [96] studied the optical properties of electrochromic surfaces based on wolfram and achieved a modulation of their emissivity. Xu

Table 6
Summary of optical properties of non-polymeric covers.

Cover material	Reference	Thickness	τ_{atm}	τ_{sol}	ρ_{atm}	ρ_{sol}	α_{atm}	α_{sol}
ZnS	[75]	4 mm	0.64	–	–	–	–	–
ZnS	[76]	4 mm	0.64	–	–	–	–	–
ZnS	[78]	1 mm	0.77	0.66	0.12	0.21	0.11	0.13
ZnSe	[76]	7.1 mm	0.7	–	–	–	–	–
ZnSe	[77]	–	0.87	–	–	–	–	–
ZnSe	[78]	1 mm	0.71	0.65	0.17	0.20	0.12	0.15
ZnTe	[78]	1 mm	0.66	0.61	0.21	0.22	0.13	0.17
Tefzel	[76]	200 μm	0.1	–	–	–	–	–
Silicon	[76]	0.6 mm	0.47	–	–	–	–	–
CdTe film + Si substrate	[81]	9.7 μm + 1 mm	0.58	0.3	0.3	0.38	0.42	0.22
CdTe film + Si substrate	[81]	9.7 μm + 1 mm	0.62	0.28	0.01	0.07	0.37	0.71
CdS film	[82]	1 mm	0.8	0.3	0.01	0.02	0.19	0.68
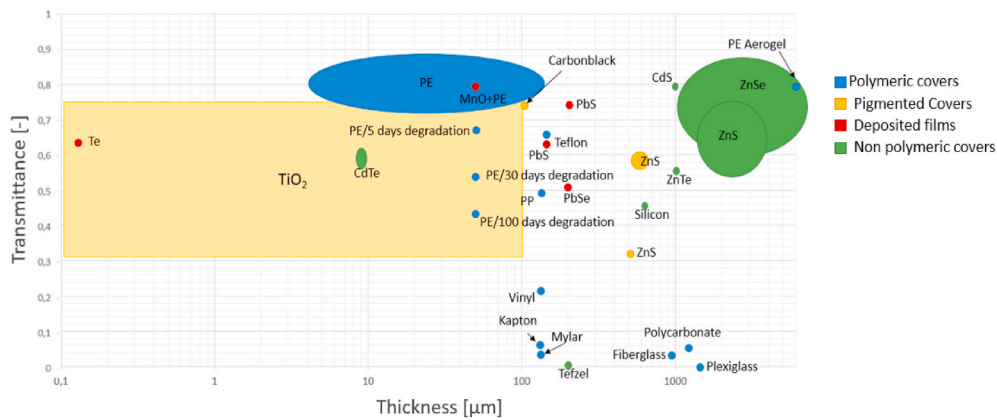
Fig. 13. Comparison of experimental transmittances in the atmospheric window of different materials grouped in: polymeric, deposited films, pigmented covers and non-polymeric materials.

et al. [97] achieved changes of 0.4 of emissivity in the 8–14 μm range -atmospheric window-in a device based on H_2SO_4-doped polyaniline films, allowing radiative cooling under low voltage.

4.2. Thermochromic materials

Thermochromic materials respond to temperature changes by modifying their optical properties [93]. Thermochromic materials maintain a highly emissive or transmitting semiconductor structure in the infrared; when the transition point (T_c) is reached, the material behaves like a semi metal, with high reflectivity in the infrared band [98]. These materials find their applications in the fields of energy saving, thermal control and camouflage [99] and glazing [100].

Vanadium dioxide (VO_2) is a phase change material usually studied in thermochromic applications. At a temperature below 68 °C, vanadium dioxide presents high emissivity in the IR, whereas when the temperature is above the transition point, it is highly reflective to IR wavelengths. According to Liu et al. [98], a 900 nm VO_2 thin film exhibited 0.8–0.9 emittance in the IR below transition conditions whereas for above conditions the emittance fell between 0.2 and 0.3. In comparison, thicker films of vanadium dioxide offer better thermochromic properties between modes than thin films.

Doping vanadium dioxide the transition temperature can be controlled. When doped with wolfram transition temperature can be reduced to 30 °C [101]. Other authors have doped vanadium dioxide with terbium cation (Tb^{3+}). Although an improvement in transmittance was shown, the transition temperature reduction was much lower (from 67.5 °C to 60 °C) [102]. Alternatively, Chen et al. [103] reduced transition temperature to 35 °C with an undoped VO_2 multilayered structure.

Thermochromic material, such as vanadium dioxide, can be used as

switchers to control the effective emissivity surfaces in order to achieve a turning "on-off" radiative cooler [104]. Metamaterial configurations of thermochromic materials enhance radiative cooling properties [105]. Sun et al. [106] demonstrated that, at room temperature, an VO_2 metamaterial emitter radiated in 3–5 μm and 8–14 μm range; at high temperature strong radiation was gathered in the 5–8 μm range. Tazawa et al. [107,108] estimated a maximum cooling power of near 50 W/m^2 for a vanadium-doped surface. Ono et al. [109] simulated the performance of a VO_2 metamaterial based radiative cooler which initiated when ambient temperature was above a transition point; the results showed a maximum cooling power peak of 120 W/m^2 (Fig. 14). Kort-Kamp et al. [110] also simulated the performance of a photonic VO_2 radiator; the results showed that a 6 °C reduction from the ambient could be achieved under ~100 W/m^2 cooling rates (see Fig. 15).

Polymer can also exhibit thermochromism [111]. La et al. [112] studied a polyampolyte hydrogel which showed a high contrast of 80% in the visible band: from opaque at low temperature to transparent at high temperature. The transmittance in the mid-infrared and long-infrared was lower in both cases.

4.3. Gasochromic materials and gas slab

Gasochromic materials exhibit a change in coloration of films based on wolfram due to the presence of hydrogen [88,113]. These materials have favorable points over electrochromic and thermochromic material: gasochromic are cheaper and simpler and allow better modulation of the transmittance, being able to achieve intermediate transmittances [100]. Gasochromic smart windows' switching properties can decrease the annual thermal HVAC consumptions by 25%–35% [85]. Nevertheless, they may still not have an application in radiative cooling or solar heating fields, as the infrared range has not been studied.

Fig. 14. Illustration of an electrochromic window bleached (a) and colored (b) [92].

Fig. 15. Thermal performance of a VO_2 metamaterial based radiative cooler (black curve) over a 24h cycle. Blue curve represents the cooling power of the radiative cooler [109]. (For interpretation of the references to color in this figure legend, the reader is referred to the Web version of this article.)
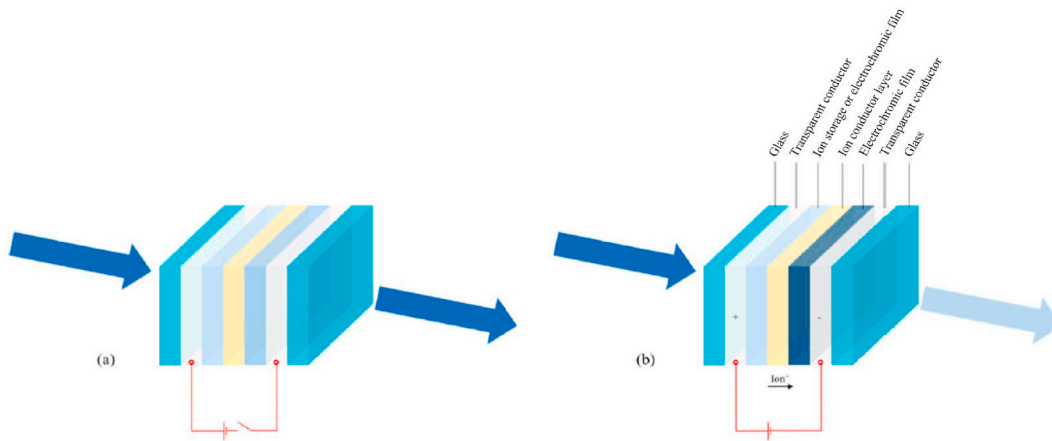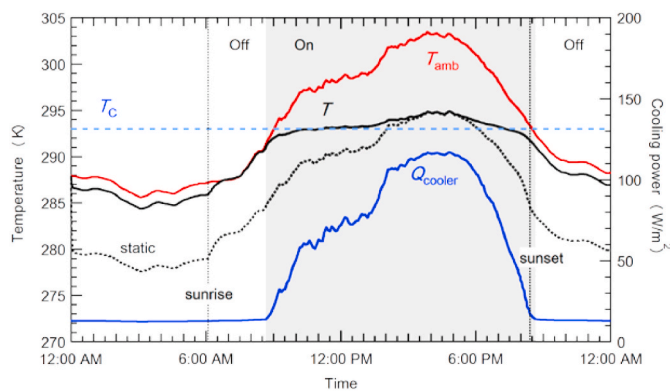
Radiative cooling has been tested with selectively emitting infrared gases confined in the air gap between the emitting/absorbing surface and the infrared transparent convective cover [114]. However, little research has been conducted. Spectrometry techniques found that ethylene (C_2H_4), ethyl oxide (C_2H_4O) and ammonia (NH_3) [115–117] are three gases which –in the presence of low humidity– show high emissivity in the atmospheric window wavelengths (8–14 µm). In an experiment with ethylene gas, under daytime conditions, authors measured a drop of 10 °C with respect to the environment [117].

4.4. Photochromic materials

Under exposure to ultraviolet light photochromic materials turn dark [28]. This photochromic switching is a fast and reversible process [88]. To our knowledge, photochromic materials do not present yet applications in the radiative cooling field.

Photochromism occurs when a transition in a molecule, such as azobenzene, spiropyran, furylfulgide, and diarylethene [93], between two isomers with different optical properties exists [118]. Other metal oxides –MoO_3, WO_3, V_2O_5, Nb_2O_5, ZnO, and TiO_2 [93]– also exhibit photochromism.

5. Conclusions

In this study the concept of RCE has been presented. Covers, or

windscreens, with switching optical properties placed on top of absorber/emitter surface can be used in order to achieve mixed solar heating and radiative cooling.

This paper has also discussed the influence of convection phenomena on radiative cooling and solar heating surfaces and the different approaches used by various authors to calculate this contribution as a direct function of wind speed. In order to achieve subambient temperatures through radiative cooling, the need to reduce these negative gains through windscreens or convective shields has been emphasized. Then, adaptive windscreens in RCE devices allow the switching between working modes and a reduction of thermal exchanges, enhancing the performance.

Windscreens can be found in many of experimental research in the fields of radiative cooling and RCE analyzed in this paper. However, they are presented as an additional complement, meaning that the effects of using a windscreen are, in general, not examined.

The article reviewed and classified the different types of adaptive covers used in order to reduce convective gains/losses, for later use in mixed applications of both radiative cooling and solar heating. These mixed applications have been classified into two major groups depending on whether they rely on a single smart material or a combination of different materials (exchangeable covers). Polyethylene is the most widely used material in radiative cooling and RCE applications due to its high transmittance in the 8–14 µm band, the main atmospheric window. Different prototypes have been developed that allow both night radiation and daytime collection and the ability of these devices to meet the demands of thermal loads has also been modeled. Polyethylene presents serious structural and aging disadvantages. Increasing the thickness of the material is not considered an optimal solution as it worsens the total transmittance. Pigmented covers block a big portion of the sunlight and are not appropriate for RCE applications. Alternatively, zinc crystals offer some transmittance in the solar range and could be used as thick windscreen in RCE applications. However, they are an expensive solution.

Finally, authors suggest that chromic materials could become a durable solution for windscreen in radiative cooling-solar heating applications. These materials are of high interest in smart windows and glazing technologies. Due to this fact, papers analyzed do not present information of the performance in the infrared region. On the other hand, the chromic materials already studied in radiative cooling applications have been used as emitters so these materials have no seemingly useful properties as windscreen. After this review, authors propose the characterization of the optical properties, in both the solar range and the atmospheric windows' range, of chromic materials as the next research step on the path of improving the performance of combined solar heating and radiative cooling applications.

CRediT authorship contribution statement

Roger Vilà: Conceptualization, Investigation, Data curation, Visualization, Writing – original draft. **Ingrid Martorell:** Conceptualization, Investigation, Writing – review & editing. **Marc Medrano:** Conceptualization, Investigation, Writing – review & editing, Supervision. **Albert Castell:** Conceptualization, Writing – review & editing, Supervision, Project administration, Funding acquisition.

Declaration of competing interest

The authors declare that they have no known competing financial interests or personal relationships that could have appeared to influence the work reported in this paper.

Acknowledgements

References

[1] IEA, "Global energy demand rose by 2.3% in 2018, its fastest pace in the last decade," IEA, Mar. 26, accessed Jan. 23, 2020, https://www.iea.org/news/global-energy-demand-rose-by-23-in-2018-its-fastest-pace-in-the-last-decade, 2019.

[2] J. Cook, et al., Consensus on consensus: a synthesis of consensus estimates on human-caused global warming, Environ. Res. Lett. 11 (4) (Apr. 2016), 048002, https://doi.org/10.1088/1748-9326/11/4/048002.

[3] Directive 2009/28/EC of the European Parliament and of the Council of 23 April 2009 on the Promotion of the Use of Energy from Renewable Sources and Amending and Subsequently Repealing Directives 2001/77/EC and 2003/30/EC, Jun. 2009, https://doi.org/10.1007/978-1-137-54507-7_21.

[4] Directive (EU), Of the European Parliament and of the Council of 30 May 2018 Amending Directive 2010/31/EU on the Energy Performance of Buildings and Directive 2012/27, EU on energy efficiency, 2018, p. 17.

[5] Commission recommendatoin (EU), on Building Renovation - (Notified under Document C(2019) 3352), 786 - of 8 May 2019, 2019, p. 46.

[6] Project Europe 2030: Challenges and Opportunities : a Report to the European Council by the Reflection Group on the Future of the EU 2030, Publications Office of the European Union, Luxemburg, 2010.

[7] European Comission, Energy performance of buildings directive. https://ec.europa.eu/energy/en/topics/energy-efficiency/energy-performance-of-buildings/energy-performance-buildings-directive#documents, 2018 accessed Jan. 23,.

[8] Eurostat, Energy Consumption in Households, May 2019. https://ec.europa.eu/eurostat/statistics-explained/index.php?title=Energy_consumption_in_households#Use_of_energy_products_in_households_by_purpose.

[9] M. Santamouris, J. Feng, Recent progress in daytime radiative cooling: is it the air conditioner of the future? Buildings 8 (12) (Dec. 2018) 168, https://doi.org/10.3390/buildings8120168.

[10] S.Y. Jeong, C.Y. Tso, M. Zouagui, Y.M. Wong, C.Y.H. Chao, A numerical study of daytime passive radiative coolers for space cooling in buildings, Build. Simul. 11 (5) (Oct. 2018) 1011–1028, https://doi.org/10.1007/s12273-018-0474-4.

[11] E. Rephaeli, A. Raman, S. Fan, Ultrabroadband photonic structures to achieve high-performance daytime radiative cooling, Nano Lett. 13 (4) (Apr. 2013) 1457–1461, https://doi.org/10.1021/nl4004283.

[12] B. Ko, D. Lee, T. Badloe, J. Rho, Metamaterial-based radiative cooling: towards energy-free all-day cooling, Energies 12 (1) (Dec. 2018) 89, https://doi.org/10.3390/en12010089.

[13] M.M. Hossain, B. Jia, M. Gu, A metamaterial emitter for highly efficient radiative cooling, Adv. Opt. Mater. 3 (8) (Aug. 2015) 1047–1051, https://doi.org/10.1002/adom.201500119.

[14] P. Berdahl, R. Fromberg, The thermal radiance of clear skies, Sol. Energy 29 (4) (1982) 299–314, https://doi.org/10.1016/0038-092X(82)90245-6.

[15] S. Vall, A. Castell, M. Medrano, Energy savings potential of a novel radiative cooling and solar thermal collection concept in buildings for various world climates, Energy Technol. 6 (11) (Nov. 2018) 2200–2209, https://doi.org/10.1002/ente.201800164.

[16] T.E. Johnson, Radiation cooling of structures with infrared transparent wind screens, Sol. Energy 17 (3) (1975) 173–178, https://doi.org/10.1016/0038-092X(75)90056-0.

[17] A.P. Raman, M.A. Anoma, L. Zhu, E. Rephaeli, S. Fan, Passive radiative cooling below ambient air temperature under direct sunlight, Nature 515 (7528) (Nov. 2014) 540–544, https://doi.org/10.1038/nature13883.

[18] D. Zhao, et al., Subambient cooling of water: toward real-world applications of daytime radiative cooling, Joule 3 (1) (Jan. 2019) 111–123, https://doi.org/10.1016/j.joule.2018.10.006.

[19] M. Matsuta, S. Terada, H. Ito, Solar Heating and radiative cooling using a solar collector-sky radiator with a spectrally selective surface, Sol. Energy 39 (3) (1987) 183–186.

[20] M. Hu, G. Pei, Q. Wang, J. Li, Y. Wang, J. Ji, Field test and preliminary analysis of a combined diurnal solar heating and nocturnal radiative cooling system, Appl. Energy 179 (2016) 899–908, https://doi.org/10.1016/j.apenergy.2016.07.066.

[21] L. Long, Y. Yang, L. Wang, Simultaneously enhanced solar absorption and radiative cooling with thin silica micro-grating coatings for silicon solar cells, Sol. Energy Mater. Sol. Cells 197 (Aug. 2019) 19–24, https://doi.org/10.1016/j.solmat.2019.04.006.

[22] J. Liu, et al., Research on the performance of radiative cooling and solar heating coupling module to direct control indoor temperature, Energy Convers. Manag. 205 (Feb. 2020) 112395, https://doi.org/10.1016/j.enconman.2019.112395.

[23] S. Vall, M. Medrano, C. Solé, A. Castell, Combined radiative cooling and solar thermal collection: experimental proof of concept, Energies 13 (4) (Feb. 2020) 893, https://doi.org/10.3390/en13040893.

[24] X. Lu, P. Xu, H. Wang, T. Yang, J. Hou, Cooling potential and applications prospects of passive radiative cooling in buildings: the current state-of-the-art, Renew. Sustain. Energy Rev. 65 (Nov. 2016) 1079–1097, https://doi.org/10.1016/j.rser.2016.07.058.

[25] S. Vall, A. Castell, Radiative cooling as low-grade energy source: a literature review, Renew. Sustain. Energy Rev. 77 (Sep. 2017) 803–820, https://doi.org/10.1016/j.rser.2017.04.010.

[26] G.N. Nwaji, C.A. Okoronkwo, N.V. Ogueke, E.E. Anyanwu, Hybrid solar water heating/nocturnal radiation cooling system I: a review of the progress, prospects and challenges, Energy Build. 198 (Sep. 2019) 412–430, https://doi.org/10.1016/j.enbuild.2019.06.017.

[27] D. Zhao, et al., Radiative sky cooling: fundamental principles, materials, and applications, Appl. Phys. Rev. 6 (Jun. 2019), 021306, https://doi.org/10.1063/1.5087281.

[28] C.G. Granqvist, G.A. Niklasson, Solar energy materials for thermal applications: a primer, Sol. Energy Mater. Sol. Cells 180 (Jun. 2018) 213–226, https://doi.org/10.1016/j.solmat.2018.02.004.

[29] S. Buddhiraju, P. Santhanam, S. Fan, Thermodynamic limits of energy harvesting from outgoing thermal radiation, Proc. Natl. Acad. Sci. Unit. States Am. 115 (16) (Apr. 2018) E3609–E3615, https://doi.org/10.1073/pnas.1717595115.

[30] R. Zevenhoven, M. Fält, Radiative cooling through the atmospheric window: a third, less intrusive geoengineering approach, Energy 152 (Jun. 2018) 27–33, https://doi.org/10.1016/j.energy.2018.03.084.

[31] M.G. Meir, J.B. Rekstad, O.M. LØvvik, A study of a polymer-based radiative cooling system, Sol. Energy 73 (6) (Dec. 2002) 403–417, https://doi.org/10.1016/S0038-092X(03)00019-7.

[32] M. Zeyghami, D.Y. Goswami, E. Stefanakos, A review of clear sky radiative cooling developments and applications in renewable power systems and passive building cooling, Sol. Energy Mater. Sol. Cells 178 (May 2018) 115–128, https://doi.org/10.1016/j.solmat.2018.01.015.

[33] Y. Cui, Y. Wang, Q. Huang, S. Wei, Effect of radiation and convection heat transfer on cooling performance of radiative panel, Renew. Energy 99 (Dec. 2016) 10–17, https://doi.org/10.1016/j.renene.2016.06.025.

[34] J.A. Duffie, W.A. Beckman, Solar Engineering of Thermal Processes, John Wiley & Sons, Inc., Hoboken, NJ, USA, 2013, https://doi.org/10.1002/9781118671603.

[35] J. Li, et al., Experimental study on a novel photovoltaic thermal system using amorphous silicon cells deposited on stainless steel, Energy 159 (Sep. 2018) 786–798, https://doi.org/10.1016/j.energy.2018.06.127.

[36] E. Erell, D. Pearlmutter, T. Williamson, Urban Microclimate: Designing the Spaces between Buildings, Routledge, 2012.

[37] K.W. Böer, J.A. Duffie, Advances in Solar Energy: an Annual Review of Research and Development, Springer Science & Business Media, 2012.

[38] E. Sartori, Convection coefficient equations for forced air flow over flat surfaces, Sol. Energy 80 (9) (Sep. 2006) 1063–1071, https://doi.org/10.1016/j.solener.2005.11.001.

[39] S. Sharples and P. S. Charlesworth, "Full Scale Measurements of Wind Induced Convective Heat Transfer from a Roof Mounted Flat-Plate Solar Collector," p. 9.

[40] B. Givoni, Passive Low Energy Cooling of Buildings. John Wiley & Sons.

[41] G. Mihalakakou, A. Ferrante, J.O. Lewis, The cooling potential of a metallic nocturnal radiator, Energy Build. 28 (3) (Nov. 1998) 251–256, https://doi.org/10.1016/S0378-7788(98)00006-1.

[42] Y. Choi, M. Mae, H. Bae Kim, Thermal performance improvement method for air-based solar heating systems, Sol. Energy 186 (Jul. 2019) 277–290, https://doi.org/10.1016/j.solener.2019.04.061.

[43] S. Furbo, L. Jivan Shah, Thermal advantages for solar heating systems with a glass cover with antireflection surfaces, Sol. Energy 74 (6) (Jun. 2003) 513–523, https://doi.org/10.1016/S0038-092X(03)00186-5.

[44] B. Orel, M. Klanjsek Gunde, A. Krainer, Radiative cooling efficiency of white pigmented paints, Sol. Energy 50 (6) (1993) 477–482.

[45] B. Bartoli, S. Catalanotti, B. Coluzzi, V. Cuomo, V. Silvestrini, G. Troise, Nocturnal and diurnal performances of selective radiators, Appl. Energy 3 (4) (1977) 267–286, https://doi.org/10.1016/0306-2619(77)90015-0.

[46] P.T. Tsilingiris, Comparative evaluation of the infrared transmission of polymer films, Energy Convers. Manag. 44 (18) (Nov. 2003) 2839–2856, https://doi.org/10.1016/S0196-8904(03)00066-9.

[47] A. Leroy, et al., High-performance subambient radiative cooling enabled by optically selective and thermally insulating polyethylene aerogel, Sci. Adv. 5 (10) (Oct. 2019), eaat9480, https://doi.org/10.1126/sciadv.aat9480.

[48] Z. Xu, et al., A new crystal Mg11(HPO3)8(OH)6 for daytime radiative cooling, Sol. Energy Mater. Sol. Cells 185 (Oct. 2018) 536–541, https://doi.org/10.1016/j.solmat.2018.06.012.

[49] Y. Fu, J. Yang, Y.S. Su, W. Du, Y.G. Ma, Daytime passive radiative cooler using porous alumina, Sol. Energy Mater. Sol. Cells 191 (Mar. 2019) 50–54, https://doi.org/10.1016/j.solmat.2018.10.027.

[50] M. Hu, B. Zhao, X. Ao, Y. Su, G. Pei, Numerical study and experimental validation of a combined diurnal solar heating and nocturnal radiative cooling collector, Appl. Therm. Eng. 145 (Dec. 2018) 1–13, https://doi.org/10.1016/j.applthermaleng.2018.08.097.

[51] M. Hu, et al., Experimental study on a hybrid photo-thermal and radiative cooling collector using black acrylic paint as the panel coating, Renew. Energy 139 (Aug. 2019) 1217–1226, https://doi.org/10.1016/j.renene.2019.03.013.

[52] M.A. Al-Nimr, Z. Kodah, B. Nassar, A theoretical and experimental investigation of a radiative cooling system, Sol. Energy 63 (6) (Dec. 1998) 367–373, https://doi.org/10.1016/S0038-092X(98)00098-X.

[53] B. Zhao, M. Hu, X. Ao, X. Huang, X. Ren, G. Pei, Conventional photovoltaic panel for nocturnal radiative cooling and preliminary performance analysis, Energy 175 (May 2019) 677–686, https://doi.org/10.1016/j.energy.2019.03.106.

[54] M. Hu, B. Zhao, X. li, Y. Wang, G. Pei, Preliminary Thermal Analysis of a Combined Photovoltaic-Photothermic-Nocturnal Radiative Cooling System, " *Energy*, Jan. 2016, https://doi.org/10.1016/j.energy.2017.03.075.

[55] M. Hu, G. Pei, L. Li, R. Zheng, J. Li, J. Ji, Theoretical and experimental study of spectral selectivity surface for both solar heating and radiative cooling, Int. J. Photoenergy 2015 (2015) 1–9, https://doi.org/10.1155/2015/807875.

[56] M. Hu, et al., Feasibility research on a double-covered hybrid photo-thermal and radiative sky cooling module, Sol. Energy 197 (Feb. 2020) 332–343, https://doi.org/10.1016/j.solener.2020.01.022.

[57] X. Ao, M. Hu, B. Zhao, N. Chen, G. Pei, C. Zou, Preliminary experimental study of a specular and a diffuse surface for daytime radiative cooling, Sol. Energy Mater. Sol. Cells 191 (Mar. 2019) 290–296, https://doi.org/10.1016/j.solmat.2018.11.032.

[58] C. Liu, Y. Wu, B. Wang, C.Y. Zhao, H. Bao, Effect of atmospheric water vapor on radiative cooling performance of different surfaces, Sol. Energy 183 (May 2019) 218–225, https://doi.org/10.1016/j.solener.2019.03.011.

[59] A.H.H. Ali, H. Saito, I.M.S. Taha, K. Kishinami, I.M. Ismail, Effect of aging, thickness and color on both the radiative properties of polyethylene films and performance of the nocturnal cooling unit, Energy Convers. Manag. 39 (1–2) (Jan. 1998) 87–93, https://doi.org/10.1016/S0196-8904(96)00174-4.

[60] A. Hamza H. Ali, I.M.S. Taha, I.M. Ismail, Cooling of water flowing through a night sky radiator, Sol. Energy 55 (4) (1995) 235–253, https://doi.org/10.1016/0038-092X(95)00030-U.

[61] G.N. Nwaji, C.A. Okoronkwo, N.V. Ogueke, E.E. Anyanwu, Investigation of a hybrid solar collector/nocturnal radiator for water heating/cooling in selected Nigerian cities, Renew. Energy 145 (Jan. 2020) 2561–2574, https://doi.org/10.1016/j.renene.2019.07.144.

[62] A.R. Gentle, K.L. Dybdal, G.B. Smith, Polymeric mesh for durable infra-red transparent convection shields: applications in cool roofs and sky cooling, Sol. Energy Mater. Sol. Cells 115 (Aug. 2013) 79–85, https://doi.org/10.1016/j.solmat.2013.03.001.

[63] N.A. Nilsson, T.S. Eriksson, C.G. Granqvist, Infrared-transparent convection shields for radiative cooling: initial results on corrugated polyethylene foils, Sol. Energy Mater. 12 (5) (1985) 327–333, https://doi.org/10.1016/0165-1633(85)90002-4.

[64] B. Bhatia, et al., Passive directional sub-ambient daytime radiative cooling, Nat. Commun. 9 (1) (2018) 5001, https://doi.org/10.1038/s41467-018-07293-9. Nov.

[65] A. Andretta, B. Bartoli, B. Coluzzi, V. Cuomo, Selective surfaces for natural cooling devices, J. Phys. Colloq. 42 (C1) (Jan. 1981) C1-423–C1-430, https://doi.org/10.1051/jphyscol:1981131.

[66] G. A. Niklasson and T. S. Eriksson, "Radiative Cooling with Pigmented Polyethylene Foils".

[67] Y. Mastai, Y. Diamant, S.T. Aruna, A. Zaban, TiO2 nanocrystalline pigmented polyethylene foils for radiative cooling applications: synthesis and characterization, Langmuir 17 (22) (2001) 7118–7123.

[68] T.M.J. Nilsson, G.A. Niklasson, Radiative cooling during the day: simulations and experiments on pigmented polyethylene cover foils, Sol. Energy Mater. Sol. Cells 37 (1) (Apr. 1995) 93–118, https://doi.org/10.1016/0927-0248(94)00200-2.

[69] T.M. Nilsson, W.E. Vargas, G.A. Niklasson, "Pigmented Foils for Radiative Cooling and Condensation Irrigation," Freiburg, Federal Republic of Germany, Sep. 1994, pp. 193–204, https://doi.org/10.1117/12.185370.

[70] T.M.J. Nilsson, G.A. Niklasson, C.G. Granqvist, A solar reflecting material for radiative cooling applications: ZnS pigmented polyethylene, Sol. Energy Mater. Sol. Cells 28 (2) (1992) 175–193, https://doi.org/10.1016/0927-0248(92)90010-M.

[71] K.D. Dobson, G. Hodes, Y. Mastai, Thin semiconductor films for radiative cooling applications, Sol. Energy Mater. Sol. Cells 80 (3) (2003) 283–296, https://doi.org/10.1016/j.solmat.2003.06.007.

[72] T. Engelhard, E.D. Jones, I. Viney, Y. Mastai, G. Hodes, "Deposition of tellurium films by decomposition of electrochemically- generated H 2 Te : application to radiative cooling devices 370 (2000) 101–105.

[73] F. Carrasco, P. Pag, Artificial aging of high-density polyethylene by ultraviolet irradiation, Eur. Polym. J. 8 (2001).

[74] A. Golaka, R.H.B. Exell, An investigation into the use of a wind shield to reduce the convective heat flux to a nocturnal radiative cooling surface, Renew. Energy 32 (4) (Apr. 2007) 593–608, https://doi.org/10.1016/j.renene.2006.03.007.

[75] S.G. Bosi, S.N. Bathgate, D.R. Mills, At last! A durable convection cover for atmospheric window radiative cooling applications 57 (2014) 1997–2004, https://doi.org/10.1016/j.egypro.2014.10.064.

[76] S.N. Bathgate, S.G. Bosi, A robust convection cover material for selective radiative cooling applications, Sol. Energy Mater. Sol. Cells 95 (10) (Oct. 2011) 2778–2785, https://doi.org/10.1016/j.solmat.2011.05.027.

[77] Z. Chen, L. Zhu, A. Raman, S. Fan, "Radiative cooling to deep sub-freezing temperatures through a 24-h day–night cycle, Nat. Commun. 7 (2016) 13729, https://doi.org/10.1038/ncomms13729. Dec.

[78] S. Laatioui, M. Benlattar, M. Mazroui, K. Saadouni, Zinc monochalcogenide thin films ZnX (X = S, Se, Te) as radiative cooling materials, Optik 166 (Aug. 2018) 24–30, https://doi.org/10.1016/j.ijleo.2018.04.004.

[79] E.V. Yashina, Preparation and properties of polycrystalline ZnS for IR applications 39 (7) (2003) 6.

[80] P. Biswas, P. Ramavath, R. Johnson, K.V. Ravi, Fabrication of IR transparent zinc sulphide plate by chemical vapour deposition (CVD), Indian J. Chem. Technol. 5 (2016).

[81] M. Benlattar, E.M. Oualim, M. Harmouchi, A. Mouhsen, A. Belafhal, Radiative properties of cadmium telluride thin film as radiative cooling materials, Opt Commun. 256 (1–3) (2005) 10–15, https://doi.org/10.1016/j.optcom.2005.06.033.

[82] M. Benlattar, E.M. Oualim, T. Mouhib, M. Harmouchi, A. Mouhsen, A. Belafhal, Thin cadmium sulphide film for radiative cooling application, Opt Commun. 267 (1) (Nov. 2006) 65–68, https://doi.org/10.1016/j.optcom.2006.06.050.

[83] L. Giovannini, F. Favoino, V. Serra, M. Zinzi, Thermo-chromic glazing in buildings: a novel methodological framework for a multi-objective performance evaluation, Energy Procedia 158 (Feb. 2019) 4115–4122, https://doi.org/10.1016/j.egypro.2019.01.822.

[84] J. Hoon Lee, J. Jeong, Y. Tae Chae, Optimal control parameter for electrochromic glazing operation in commercial buildings under different climatic conditions, Appl. Energy 260 (Feb. 2020) 114338, https://doi.org/10.1016/j.apenergy.2019.114338.

[85] W. Feng, L. Zou, G. Gao, G. Wu, J. Shen, W. Li, Gasochromic smart window: optical and thermal properties, energy simulation and feasibility analysis, Sol. Energy Mater. Sol. Cells 144 (Jan. 2016) 316–323, https://doi.org/10.1016/j.solmat.2015.09.029.

[86] C.M. Lampert, Innovative solar optical materials, Opt. Eng. 23 (1) (Feb. 1984), https://doi.org/10.1117/12.7973260.

[87] G.A. Niklasson, C.G. Granqvist, Electrochromics for smart windows: thin films of tungsten oxide and nickel oxide, and devices based on these, J. Mater. Chem. 17 (2) (2007) 127–156, https://doi.org/10.1039/B612174H.

[88] C.M. Lampert, Chromogenic smart materials, Mater. Today 7 (3) (Mar. 2004) 28–35, https://doi.org/10.1016/S1369-7021(04)00123-3.

[89] G. Gorgolis, D. Karamanis, Solar energy materials for glazing technologies, Sol. Energy Mater. Sol. Cells 144 (Jan. 2016) 559–578, https://doi.org/10.1016/j.solmat.2015.09.040.

[90] H. Yu, et al., A feasible strategy for the fabrication of camouflage electrochromic fabric and unconventional devices, Electrochem. Commun. 102 (May 2019) 31–36, https://doi.org/10.1016/j.elecom.2019.03.006.

[91] L. Zhang, Q. Zhang, H. Ye, Design of infrared camouflage cloak for underground silos, Def. Technol. (Nov. 2019), https://doi.org/10.1016/j.dt.2019.11.001. S2214914719308177.

[92] S.D. Rezaei, S. Shannigrahi, S. Ramakrishna, A review of conventional, advanced, and smart glazing technologies and materials for improving indoor environment, Sol. Energy Mater. Sol. Cells 159 (Jan. 2017) 26–51, https://doi.org/10.1016/j.solmat.2016.08.026.

[93] Y. Wang, E.L. Runnerstrom, D.J. Milliron, Switchable materials for smart windows, Annu. Rev. Chem. Biomol. Eng. 7 (1) (Jun. 2016) 283–304, https://doi.org/10.1146/annurev-chembioeng-080615-034647.

[94] C. Guo, S. Yin, M. Yan, T. Sato, Facile synthesis of homogeneous CsxWO3 nanorods with excellent low-emissivity and NIR shielding property by a water controlled-release process, J. Mater. Chem. 21 (13) (2011) 5099, https://doi.org/10.1039/c0jm04379f.

[95] J. Mandal, S. Du, M. Dontigny, K. Zaghib, N. Yu, Y. Yang, "Li 4 Ti 5 O 12 : a visible-to-infrared broadband electrochromic material for optical and thermal management, Adv. Funct. Mater. 28 (36) (Sep. 2018) 1802180, https://doi.org/10.1002/adfm.201802180.

[96] E.B. Franke, C.L. Trimble, J.S. Hale, M. Schubert, J.A. Woollam, Infrared switching electrochromic devices based on tungsten oxide, J. Appl. Phys. 88 (10) (Nov. 2000) 5777–5784, https://doi.org/10.1063/1.1319325.

[97] G. Xu, et al., A visible-to-infrared broadband flexible electrochromic device based polyaniline for simultaneously variable optical and thermal management, Sol. Energy Mater. Sol. Cells 208 (May 2020) 110356, https://doi.org/10.1016/j.solmat.2019.110356.

[98] D. Liu, H. Cheng, W. Zheng, C. Zhang, Infrared thermochromic properties of VO2 thin films prepared through aqueous sol-gel process, J. Wuhan Univ. Technol.-Materials Sci. Ed. 27 (5) (Oct. 2012) 861–865, https://doi.org/10.1007/s11595-012-0563-7.

[99] D. Liu, H. Ji, R. Peng, H. Cheng, C. Zhang, Infrared chameleon-like behavior from VO2(M) thin films prepared by transformation of metastable VO2(B) for adaptive camouflage in both thermal atmospheric windows, Sol. Energy Mater. Sol. Cells 185 (Oct. 2018) 210–217, https://doi.org/10.1016/j.solmat.2018.05.042.

[100] A. Frattolillo, G. Loddo, C.C. Mastino, R. Baccoli, Heating and cooling loads with electrochromic glazing in Mediterranean climate, Energy Build. 201 (Oct. 2019) 174–182, https://doi.org/10.1016/j.enbuild.2019.06.042.

[101] D. Liu, H. Cheng, X. Xing, C. Zhang, W. Zheng, Thermochromic properties of W-doped VO 2 thin films deposited by aqueous sol-gel method for adaptive infrared stealth application, Infrared Phys. Technol. 77 (Jul. 2016) 339–343, https://doi.org/10.1016/j.infrared.2016.06.019.

[102] N. Wang, et al., Terbium-doped VO 2 thin films: reduced phase transition temperature and largely enhanced luminous transmittance, Langmuir 32 (3) (Jan. 2016) 759–764, https://doi.org/10.1021/acs.langmuir.5b04212.

[103] X. Chen, Q. Lv, X. Yi, Smart window coating based on nanostructured VO2 thin film, Optik 123 (13) (Jul. 2012) 1187–1189, https://doi.org/10.1016/j.ijleo.2011.07.048.

[104] S. Taylor, Y. Yang, L. Wang, Vanadium dioxide based Fabry-Perot emitter for dynamic radiative cooling applications, J. Quant. Spectrosc. Radiat. Transf. 197 (Aug. 2017) 76–83, https://doi.org/10.1016/j.jqsrt.2017.01.014.

[105] S.-R. Wu, K.-L. Lai, C.-M. Wang, Passive temperature control based on a phase change metasurface, Sci. Rep. 8 (1) (Dec. 2018) 7684, https://doi.org/10.1038/s41598-018-26150-9.

[106] R. Sun, et al., Broadband switching of mid-infrared atmospheric windows by VO 2 -based thermal emitter, Opt Express 27 (8) (Apr. 2019) 11537, https://doi.org/10.1364/OE.27.011537.

[107] M. Tazawa, P. Jin, T. Miki, K. Yoshimura, K. Igrashi, IR Properties of SiO Deposited on V1yxWxO2 Thermochromic FIlms by Vacuum Evaporation, 2000, p. 4.

[108] M. Tazawa, P. Jin, S. Tanemura, Thin film used to obtain a constant temperature lower than the ambient, Thin Solid Films 281–282 (Aug. 1996) 232–234, https://doi.org/10.1016/0040-6090(96)08620-8.

[109] M. Ono, K. Chen, W. Li, S. Fan, Self-adaptive radiative cooling based on phase change materials, Opt Express 26 (18) (Sep. 2018) A777, https://doi.org/10.1364/OE.26.00A777.

[110] W.J.M. Kort-Kamp, S. Kramadhati, A.K. Azad, M.T. Reiten, D.A.R. Dalvit, "Passive radiative 'thermostat' enabled by phase-change photonic nanostructures, ACS Photonics 5 (11) (Nov. 2018) 4554–4560, https://doi.org/10.1021/acsphotonics.8b01026.

[111] A. Seeboth, R. Ruhmann, O. Mühling, Thermotropic and thermochromic polymer based materials for adaptive solar control, Materials 3 (12) (Dec. 2010) 5143–5168, https://doi.org/10.3390/ma3125143.

[112] T.-G. La, X. Li, A. Kumar, Y. Fu, S. Yang, H.-J. Chung, Highly flexible, multipixelated thermosensitive smart windows made of tough hydrogels, ACS Appl. Mater. Interfaces 9 (38) (Sep. 2017) 33100–33106, https://doi.org/10.1021/acsami.7b08907.

[113] H. Ye, X. Meng, L. Long, B. Xu, The route to a perfect window, Renew. Energy 55 (Jul. 2013) 448–455, https://doi.org/10.1016/j.renene.2013.01.003.

[114] T.S. Eriksson, E.M. Lushiku, C.G. Granqvist, Materials for radiative cooling to low temperature, Sol. Energy Mater. 11 (1984) 149–161.

[115] E.M. Lushiku, C.G. Granqvist, Radiative cooling with selectively infrared-emitting gases, J. Appl. Phys. 53 (8) (1982) 5526–5530, https://doi.org/10.1364/AO.23.001835.

[116] E.M. Lushiku, T.S. Eriksson, A. Hjortsberg, C.G. Granqvist, Radiative cooling to low temperatures with selectively infrared-emitting gases, Sol. Wind Technol. 1 (2) (1984) 115–121, https://doi.org/10.1016/0741-983X(84)90013-4.

[117] A. Hjortsberg, C.G. Granqvist, Radiative cooling with selectively emitting ethylene gas, Appl. Phys. Lett. 39 (6) (1981) 507–509, https://doi.org/10.1063/1.92783.

[118] H. Tian, S. Yang, Recent progresses on diarylethene based photochromic switches, Chem. Soc. Rev. 33 (2) (2004) 85, https://doi.org/10.1039/b302356g.

Chapter V.   P2: Numerical analysis of the combination of radiative collectors and emitters to improve the performance of water-water compression heat pumps under different climates

1. Introduction

Global environmental awareness is increasing, and energy consumption is one of the main issues to pay attention to. For instance, the European Union aims to suppress CO_2 emissions by 2050 [3]. Shifting towards an energy system based on renewable and clean energy is currently a challenge. Technologies such as photovoltaics and solar thermal collection have consolidated in the market and its implementation in buildings is growing year after year.

In buildings, space cooling is mainly achieved by means of electricity consumption. Compression heat pump is the most widely used technology worldwide [8]. Despite some directives consider it to be a renewable technology when the COP is high, heat pumps consume a large amount of electricity.

Radiative cooling is presented as a renewable technology to meet the cooling demands in buildings. The energy savings of radiative cooling and RCE technologies has been studied by several authors [58], [60]. Vall et al numerically studied the usage of RCE systems to meet cooling demands and DHW in hotels, commercial and residential buildings in different climatic zones [34]; the results showed that the percentage of cold coverage with RC ranged between 0-40% in the majority of cases. According to Medrano et al [59], integrating RCE panels in food industries could save upon 13%-62% of electricity.

However, the integration of active RC and RCE technologies in buildings is still in early stages. Moreover, experimental results showed that the radiative cooling density power is low [29], [77], and new strategies must be planned in order to make it a feasible technology. The combination of radiative cooling with other technologies could foster its development and implementation in the market.

Coupling radiative cooling systems to the condenser of a water-water heat pump could improve its performance, contributing to save the electricity consumed. A heat carrier fluid can be cooled down by means of radiative cooling which then can be circulated through the condenser of the heat pump. Theoretically, for each ºC reduced in the condenser, it can be saved 3.5% of electricity [64].

In the context of the national project (RTI2018-097669-A-I00), a numerical model of an RCE was developed in the research group by Vall et al [73]. Using this model and the optical properties of polyethylene described in **Chapter IV**, the objective of this study was to simulate the coupling of RCE with water-water heat pumps in order to determine the potential improvements of their COP.

2. Contribution to the state of the art

Goldstein et al. [56] simulated a two-storey office building with a combined radiative cooling and heat pump system in Las Vegas. In this chapter the candidate proposes two different coupling designs of RCE and heat pump. The study of the performance is extended to nine locations corresponding to eight different world climates, analysing the COP of both the HP and the whole system taking into account the consumptions of all the active elements, and comparing them to a reference system of a single heat pump (**Fig 16**). The performance of both designs is simulated in a single-house building using TRNSYS. Finally, this system, compared to the one proposed by Goldstein et al, enables the production of hot water.
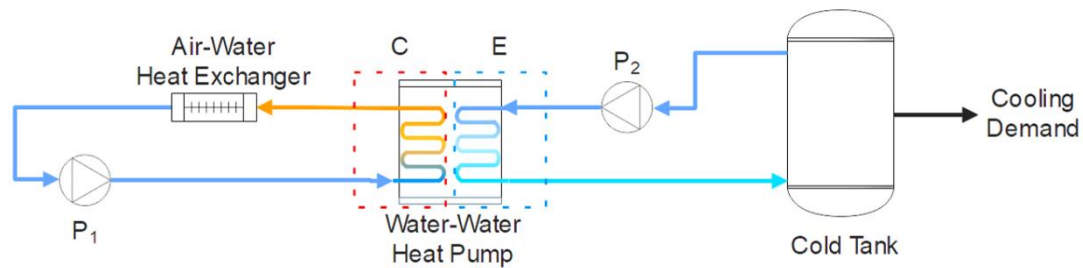
Fig 16. Conceptual scheme of the reference system.

During the day, both configurations used RCE fields to heat water which was stored in a coiled tank. When a DHW demand occurred, the hot water in the tank was replaced with tap water.

Regarding cold production, in the first configuration, named Intermediate Tank configuration (IT), the cold produced during the night by the RCE is stored in an intermediate tank. During the day, this tank acts as a heat sink for the condenser of the heat pump. The heat pump absorbs heat from the cooling tank (where heat from the building is rejected by the cooling distribution system) and releases it to the intermediate tank, heating it up. An air-water heat exchanger is used as a support to dissipate heat to the ambient air during daytime to avoid overheating. A conceptual scheme of the configuration is presented in **Fig 17**.
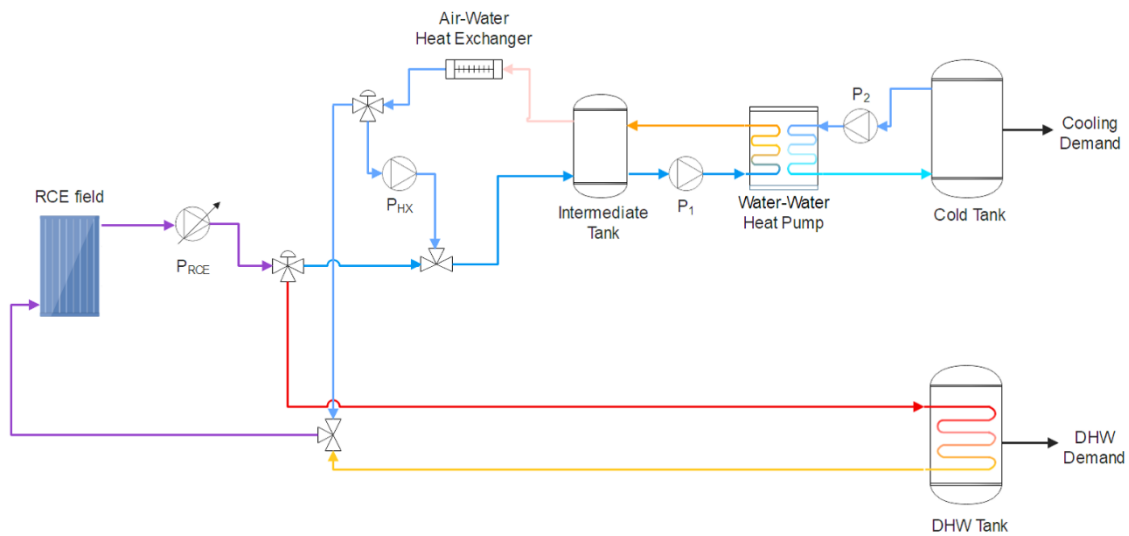
Fig 17. Conceptual scheme of the combination of RCE+HP in the Intermediate Tank configuration (IT).

The second configuration uses the concept of peak load shifting as a base of design, coupling both the production of cold in the RCE and the production of cold in the heat pump, which is latter used for space cooling. To reduce the diurnal peaks of the demand, part of the production is displaced to the previous night. During the night the RCE cools down a heat transfer fluid which is then circulated through the condenser of the heat pump, improving its performance. At the outside of the evaporator, the cold generated is stored in a cold tank. This configuration simplifies the previous system, removing one speed pump and the intermediate tank. The conceptual scheme of the system is presented in **Fig 18**.

The results in paper P2 proved that the cold generated in the RCE could be a useful heat sink for the condenser of the heat pump, improving its performance and saving electricity. In cities with dry climate and low cooling loads the improvement of the coefficient of performance was greater, while in humid climates or with high cooling demands, the improvement of the performance is not as high.

This paper brings more knowledge, diminishing the gap that currently exists in the literature, in the line of implementing and integrating RC and RCE in buildings with different characteristics and load profiles.
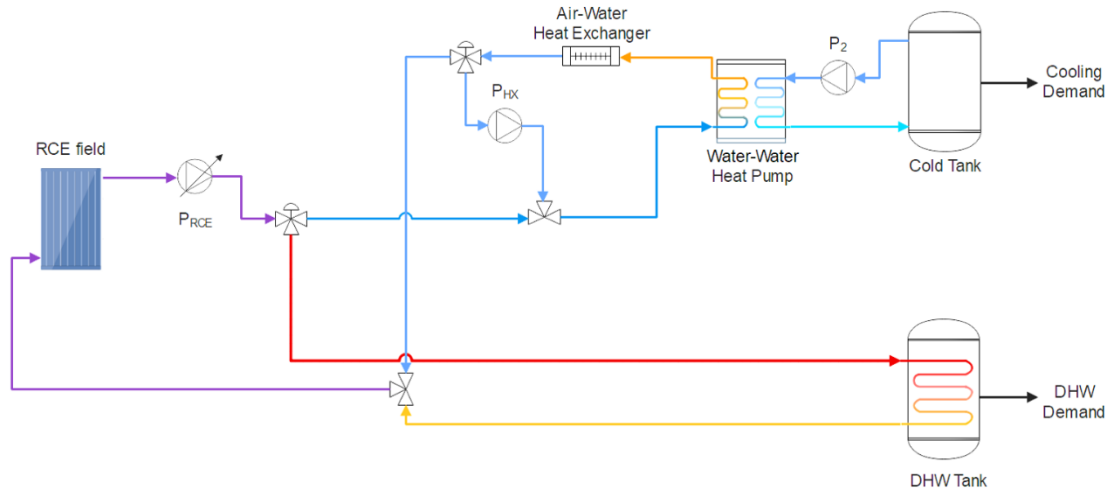
Fig 18. Conceptual scheme of the combination of RCE+HP in the Peak Load Shifting configuration (PL).

3. Contribution to the objectives of the thesis

This chapter starts from hypothesis H2 and H3 and contributes to fulfil objective O3, proving that RCE combined with a heat pump increases the overall performance of the system producing cold, while producing heat at the same time.

The results showed a better performance of the heat pump in IT configuration in most of the cases studied. However, when taking into consideration the consumption of the active elements of the systems, PL configurations show a better performance in most of the cases.

The results showed an underutilization of the facility in solar heating mode. The candidate considers that more focus should be put on this issue in future steps of the project.

4. Contribution of the candidate

Roger Vilà Miró was in charge of defining and implementing the configurations in TRNSYS, developing the controls of the systems and performing the simulations on the established locations. He was also in charge of the troubleshooting derived during the simulations

After the simulations, the candidate performed the data analysis of the results. Finally, he also led the writing of the paper.

5. Journal Paper

This chapter was submitted to the journal *Energy,* published by Elsevier, and it is currently under a peer-review process.

Vilà, Roger and Medrano, Marc and Castell, Albert, Numerical Analysis of the Combination of Radiative Collectors and Emitters to Improve the Performance of Water-Water Compression Heat Pumps Under Different Climates. Available at SSRN: https://ssrn.com/abstract=4166504 or http://dx.doi.org/10.2139/ssrn.4166504

Numerical Analysis of the Combination of Radiative Collectors and Emitters to Improve the Performance of Water-Water Compression Heat Pumps under Different Climates

Roger Vilà, Marc Medrano*, Albert Castell

Sustainable Energy, Machinery and Buildings (SEMB) Research Group, INSPIRES Research Centre, Universitat de Lleida, Pere de Cabrera s/n, 25001 Lleida, Spain; roger.vila@udl.cat (R.V.); albert.castell@udl.cat (A.C.)

* = corresponding author details: marc.medrano@udl.cat

Abstract

Radiative cooling allows to cool down surfaces in a renewable way. It can be combined with solar collection functionality to produce heat and cold in a single device known as Radiative Collector and Emitter (RCE). In this paper we propose to combine a RCE with compression heat pumps to improve its performance, producing both heat and cold. Two combined systems are studied: a peak load shifting configuration where radiative cooling and cold production for demand occur simultaneously, and a decoupled configuration with an intermediate tank. The research numerically simulates both systems in different cities and climates, and compares them to a reference system based on a conventional heat pump. The results reveal and improvement of the performance in both configurations: a greater performance of the heat pump is found in the intermediate tank configuration; but after considering the electrical consumptions of all components of the system, peak load shifting configurations exhibit the best performance in most of the cities. Denver, Lleida and Rome – cities with dry climate and moderate cooling requirements – are the top cities with the greatest improvement of the performance. In the solar heating mode, the facilities show an underutilization of the collection field.

Keywords: radiative cooling; solar thermal collector; heat pump; coefficient of performance; numerical simulation; building integration; TRNSYS

Nomenclature

$c_{p,w}$	specific heat capacity of water at constant pressure	kJ/kg·K
C	cold side of a heat pump (evaporator)	-
E_c	cooling energy demand	kJ
E_{DHW}	DHW energy demand	kJ
h	film coefficient	W/m²·K
H	Hot side of a heat pump (condenser)	-
$\dot{m}$	flowrate	kg/h
$\dot{m}_{DHW}$	domestic hot water (DHW) flowrate	kg/h
N	opaque sky cover	tenths
Q_c	heat extracted in the heat pump	W
R_{atm}	infrared radiation from the atmosphere	W/m²
R_{net}	infrared radiation net balance	W/m²
T_c	temperature of the cold side of the Heat pump	K
T_{db}	dry bulb temperature	K
T_{dp}	dew point temperature	K
T_h	temperature of the hot side of the Heat pump	K
t	time step	h
v	wind speed	m/s
W	electricity power consumption	W
ΔT_{tank}	temperature differences in the tank	K
ε_{sky}	emissivity of the sky	-
ε_s	emissivity of the surface	-
σ	Stefan-Boltzmann constant: 5.67·10⁻⁸	W/m²·K⁴

Abbreviations

COP	Coefficient of Performance
DHW	Domestic Hot Water
HX	Heat Exchanger
HP	Heat Pump/ Heat Pump Alone Configuration
IT	Intermediate Tank Configuration
P_1	Pump nº 1
P_2	Pump nº 2
P_{RCE}	Pump of the RCE field
P_{HX}	Pump of the Heat Exchanger
PL	Peak Load Shifting Configuration
RC	Radiative Cooling
RCE	Radiative Collector and Emitter
SCOP	Seasonal Coefficient of Performance
SH	Solar Heating

1. Introduction

The climate emergency has become a major concern, forcing us to rethink the current energy system based on fossil fuels. This challenge is being considered in recent public policies. In the case of the European Union, this was expressed in Directive 2009/28/CE [1] on the promotion of energy from renewable resources, Directive 2018/844 [2] and recommendations 2019/786 [3] on the renovation of buildings. Project Europe 2030 [4] set out three key goals by 2030: (a) a reduction of at least 40% of greenhouse gas emissions with respect to 1990 values, (b) a share of at least 32% in renewable energy and (c) an improvement of at least 32.5% in energy efficiency. This is lately reaffirmed in the European Green Deal, certified in 2020, which approved a financing plan equivalent to 1.8 trillion to suppress CO_2 emissions by 2050 and decouple the region's economic growth from material resources [5].

One of the sectors with the greatest impact on energy consumption is the building sector. Consumption in buildings is estimated to be 40% of final energy consumption in Europe, accounting for 36% of CO_2 emissions [6]. The biggest part of this energy (80%) is used to meet the energy demands for space conditioning (DHW, Cooling and Heating). It is foreseeable that, continuing the same path, the energy consumption used in refrigeration in household increases as a result of the rising of the global temperatures and the new episodes of heat waves which, in turn, implies new CO_2 emissions to the atmosphere; contributing to a vicious circle.

In recent decades, renewable energies – with zero or minimal greenhouse gases' emissions– have begun to play a new role, being more important in the total energy mix. Technologies such as photovoltaics and solar thermal collection have experienced a great development and they are now available in the market as consolidated commercial applications. Despite this, the cooling comfort is still achieved by means of electricity consumption [6]. In the last years, new technologies based on the natural phenomenon of radiative cooling have been studied [7]–[9]. These technologies enable to produces cold in a renewable way.

Radiative cooling is the natural process by which the terrestrial bodies reduce their surface temperature by emitting infrared radiation towards the outer space. The peaks of the emitted radiation fall between the range of 7-14 μm of wavelength. The terrestrial atmosphere is transparent to this wavelength; the energy can escape and dissipate into the outer space, which is approximately at 3K. During clear nights, the net balance between the radiation emitted by the objects and the radiation absorbed from their surroundings allows to cool them down to temperatures below ambient. With the development of new materials in the past years, nowadays radiative cooling can also be achieved during the day, under the exposure of solar radiation [8], [10]–[14].

Another notable achievement in this line has been the combination of nocturnal radiative cooling and diurnal solar heating applications in a single device, hereinafter referred as Radiative Collector and Emitter (RCE) in this paper (see section 2.1). Solar heating is a long-researched renewable technology [15], [16] with commercial applications in building and industrial sectors for years. While radiative cooling happens in wavelengths between 7-14 μm, solar heating is due to the 0.25-2.5 μm wavelength range. Despite their behaviour are totally opposite they are analogous: both are achieved, during different times of the day, in the surface by means of absorbing/emitting of electromagnetic radiation. This novel technology is still under development and has not reach yet the market. Thermodynamic limitations prevent radiative cooling-based technologies from achieving higher cooling powers. On average, experimental values between 20 and 80 W/m^2 with peaks at 120 W/m^2 were achieved [18], which falls an order of magnitude below the powers that can be obtained by solar collection. Nevertheless, this cold generated can still be used to cool spaces. Moreover, according to Fernandez et al. [19], climates where night-time hours are warm and humid may limit the impact of radiative cooling, while climates with warm days, cool nights and low humidity are identified as favourable targets.

The combination of a heat pump and an RCE could improve the seasonal coefficient of performance (COP) of the heat pump. An increase in the COP contributes to the reduction of the electricity consumed in the operation of the machine. The electricity consumed by HP is reduced by approximately 3.5% for every ºC reduced in the condenser [20]. Cold water produced during night-time by the RCE can be used to reduce the thermal difference between the condenser and the evaporator in a water-water heat pump. Coupling RCE with commercial cooling systems could make this technology more attractive for the market.

To our knowledge, there is little research done examining the impact of combining technology based on radiative cooling with conventional cooling technologies. Medrano et al. [21] numerically analysed the improvement of the integration of RCE panels in seven food industries. The results showed potential electricity savings between 13% and 62%. Fernandez et al. [19]

simulated a system based on daytime radiative cooling coupled to a radiant floor, in an office building, with electricity savings between 45% to 68%. Goldstein et al. [22] simulated a two-storey office building with a system combining radiative cooling and heat pumps; the results showed electricity savings of 21% during summer. The previous studies are limited to meet the cooling needs of a building, this study expands the focus to meet the cooling and the DHW needs of a building. The paper also widens the number of configurations and climates studied, proposing two possible combinations of RCE and heat pump (RCE+HP).

The aim of this study is to evaluate the improvement of the COP of a heat pump, and the potential energy savings, when combining it with the cooling function of the RCE. The systems are compared with a reference case with no RCE. The study presents a numerical analysis of the improvement of the performance and the energy savings in a single-family house. The study is extended to nine different locations, with different weather conditions, and different energy loads.

2. Background
    2.1. RCE background

The combination of solar collection and radiative cooling functionalities in a single RCE device has been proposed by several authors. Matsuta et al. [23] were the first to propose a selective absorber/emitter capable of achieving diurnal solar capture and nocturnal radiative cooling. The results showed that the powers achieved in the combined system were lower than in separate systems. Lately, Erell and Etzion studied the capacity to collect solar energy on a radiative cooling surface [24] and the capacity of a solar collector to dissipate heat by radiative cooling [25]. The authors pointed out that the convective effects were negative during the solar collection. Zhao et al. [26] investigated the effects of wind speed on an RC surface. In sub-ambient temperatures applications, the convective transfers have a negative effect on the surface performance.

The findings of the studies by Erell and Etzion and Zhao et al. reveal the importance of a convective cover in this type of combined applications. The problem lies in the ranges of the electromagnetic spectrum in which each of the functionalities works: nocturnal radiative coolers emit in the range of 3-25 μm (long wave) - with peaks between 8-14 μm -, while daytime solar collectors absorb in the range 0.2-3 μm and block long-wave radiation (Fig 1). A cover for RCE should be transparent to solar radiation and opaque to infrared radiation during the day, while at night it should be transparent to infrared radiation. The latter implies complex designs. Vilà et al. [27] presented a review of existing covering solutions in combined applications. In commercial solar heating applications, glass covers - transparent to solar radiation and opaque to other wavelengths - are the main solution; in radiative cooling applications the most common solution are plastic covers -transparent both in the atmospheric window and the solar radiation-, especially

polyethylene. Vall et al [18] proposed a device that uses an adaptive cover for each of the two RCE modes. The cover consists of two elements: a fixed polyethylene cover, located above the emitting/absorbing surface, and an outer glass cover capable of sliding over the device according to the operating mode (Fig 2).
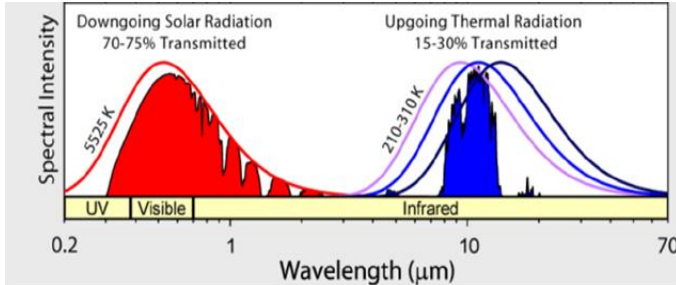
Fig 1. Solar radiation spectrum (red) and infrared radiation through the atmospheric window (blue). Modified from [28].
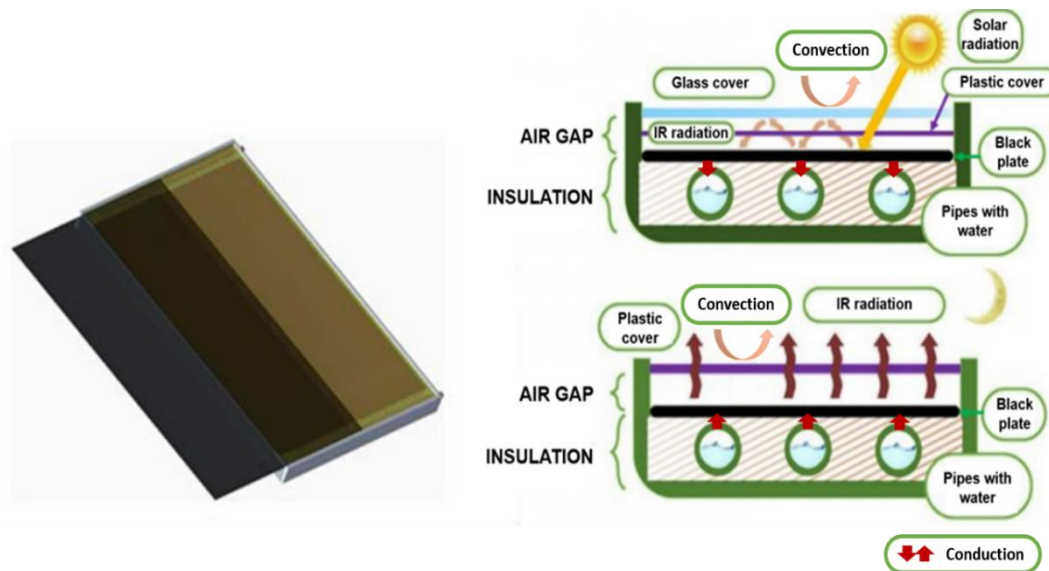
Fig 2. Design of an RCE composed by an emitter surface with a fixed polyethylene cover (in yellow) and a sliding glass cover (in dark grey) proposed by Vall et al. [18] (left). Parts of the RCE and main heat exchanges in the different modes of operation: diurnal heating mode and nocturnal cooling mode, with movable cover proposed by Vall et al. (right).

Hu et al. [29] developed a mathematical model of a system combining solar heating and radiative cooling, but it didn't simulated an adaptive cover which changed its optical properties. Vall et al. [30] also presented a new model capable of simulating a combined RCE system that included the adaptive cover. This model allows to vary the optical properties of the cover depending on the operating system. This system is based on the adaptive cover proposed in Vall et al. [18]   (Fig 2). The adaptive cover by Vall et al. consisted on a film cover of polyethylene placed on top of the absorber/emitter, enabling the transmittance of both solar and infrared radiation, and a sliding glass cover. During the day the glass cover was placed on top of the polyethylene film and the

absorber, achieving solar heating; during the night it was removed to obtain radiative cooling. The mathematical model was experimentally validated and implemented in TRNSYS and is the one used in this study.

2.2. Compression heat pumps

Compression heat pumps (HP) is the most widely used technology in the world for cold and heat production in buildings. It is a technology that uses large amounts of electricity in order to extract heat - in the cooling cycle - on the side of the evaporator (cold focus) and dissipate it on the side of the condenser (hot focus).

COP is a measure of HP's efficiency and is defined as the ratio between the heat extracted and the electrical energy required as input (eq (1)).

$$COP = \frac{Q_c}{W_{net}} \tag{1}$$

In an ideal cooling cycle, eq (1) can be expressed as eq (2). According to this equation, the performance of the HP is related to the temperature gap between the hot focus (T_h) and the cold focus (T_c) of the machine. The lower the temperature of heat rejection, the higher the efficiency is:

$$COP = \frac{T_c}{T_h - T_c} \tag{2}$$

HP in cooling cycles is mainly used under hot weather conditions, especially during the hottest hours of the day, increasing the temperature of the condenser and reducing its efficiency. Combining the HP with nocturnal RC is intended to reduce the temperature of the hot focus, using the cold of the RC as a heat sink.

3. Methods of Simulation

In this study we proposed two configurations for combined RCE + HP systems. These systems allow to produce heat by means of solar collection and to improve the performance of heat pump, in cooling mode, due to radiative cooling. Both configurations are compared to a reference case.

Three cooling systems were simulated in this study. The first one is based on a conventional heat pump system which has been used as a reference system. The other two systems combine compression heat pump systems with RCE technology. The configurations are described in section 3.1.

Simulations have been performed in a total of nine cities, corresponding to eight different climates according to the Köppen-Geiger classification [31]. The transient behaviour of the systems were simulated using TRNSYS software.

3.1. Description of refrigeration systems

In this section, the different refrigeration system configurations studied, as well as their operation are presented. Three configurations are studied: Heat Pump (HP) alone (used as the reference configuration), Intermediate Tank configuration (IT), and Peak Load Shifting configuration (PL). While the HP alone configuration is used as the reference configuration, both the IT and the PL configurations combine the heat pump with the RCE to improve the COP. Fig 3, Fig 4 and Fig 5 show the TRNSYS models used in HP, IT and PL configurations, respectively.
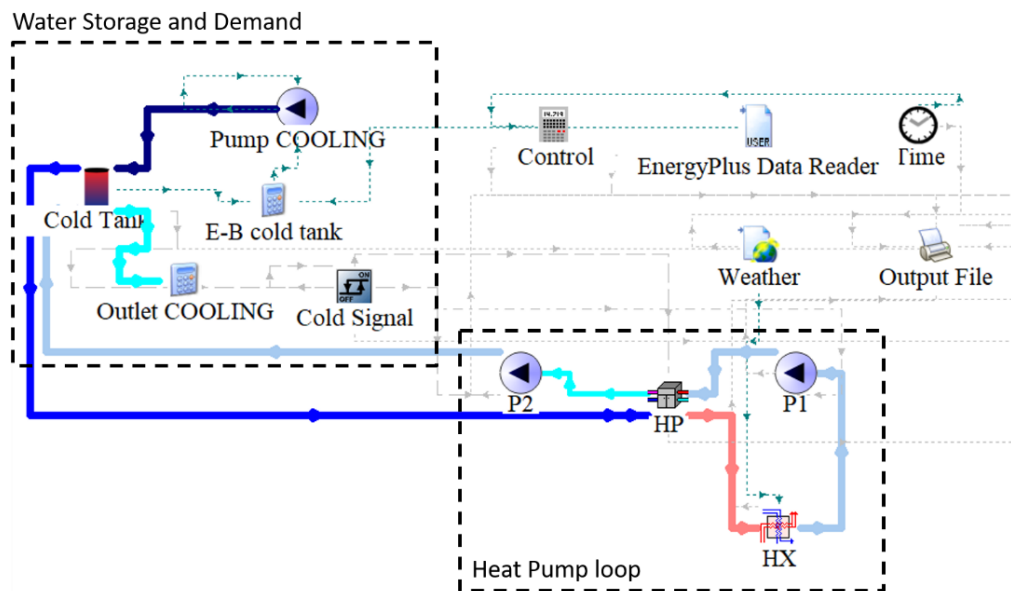
Fig 3. Transient energy model of the Heat Pump alone configuration (HP) in TRNSYS.
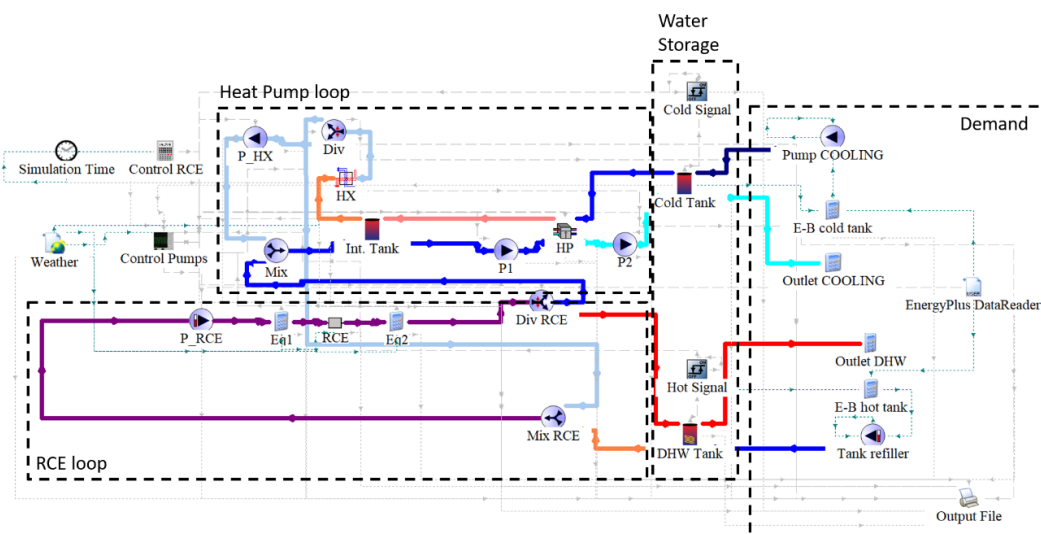
Fig 4. Transient energy model of the Intermediate tank configuration (IT) in TRNSYS.
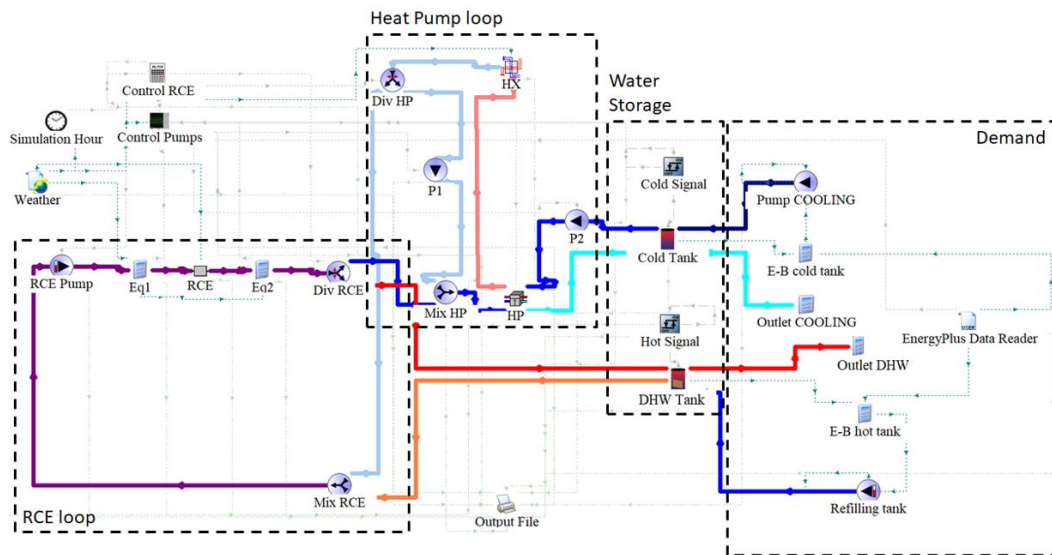
Fig 5. Transient energy model of the Peak Load Shifting configuration (PL) in TRNSYS.

The heat pump is a single-stage water-to-water heat pump simulated using Type 927 from the Trnsys TESS library in all configurations [32]. The type simulates the heat pump based on the data provided in an external file, relating the rated cooling capacity, the rated consumption, the condenser flowrate, and the evaporator flow rate. These parameters are sized for each studied city (see 4.3Table 3).

The RCE operates under radiative cooling mode during night-time, while it operates under solar heating mode during daytime, depending of the hour of the day and the sunset and sunrise hours.

3.1.1. Heat Pump (HP) alone configuration

The conventional cooling circuit based on a water-to-water heat pump has been used as a reference system to evaluate the improvement of the RCE (Fig 6).

On the side of the condenser, we modelled a closed circuit consisting of a single speed pump and an air-water heat exchanger. In the heat exchanger the heat transfer fluid is cooled down to temperatures close to ambient, dissipating the heat of condensation to air.

A tank is connected to the side of the evaporator to store the cold water coming out of the heat pump. The circuit operates until an average set point temperature of 7 ℃ inside the tank is reached. The tank acts as a buffer tank to extract cold from during demand hours. During the demanding hours the tank heats up, when it reaches a limit temperature of 17 ℃, the heat pump is reactivated.
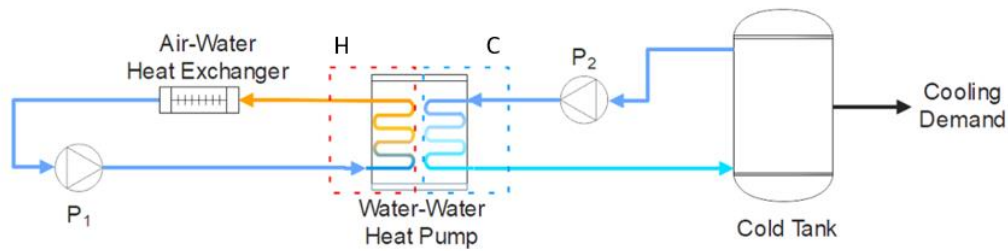
Fig 6. Conceptual scheme of the HP Alone configuration used as the reference case in the simulations. The heat pump is composed of the condenser (hot side, H) and the evaporator (cold side, C).

3.1.2. RCE+ Heat Pump in Intermediate Tank configuration (IT)

In this improvement system, when the solar radiation is higher than 100 W/m^2, the RCE produces heat during the day which is stored in a hot water tank, with an internal coil, for later use in DHW. The tank is emptied during DHW demand hours and refilled with mains water.

During the night, if the net balance between the radiation emitted by the RCE surface and the radiation absorbed from the atmosphere is higher than 25 W/m^2, the system is activated. The RCE field, formed by the RCE panels in parallel and a variable speed pump, cools water which is stored in an intermediate cold tank. This tank is used as a heat sink for the HP condenser. In the condenser side of the heat pump is connected, in addition, a single speed pump and an air-water heat exchanger. In the heat exchanger water is forced to a pre-cooling process: the water is cooled down to a few degrees above the ambient before it enters to the RCE field.

Next to the evaporator side of the heat pump there is a single speed pump and a third tank, the cold tank, that is used as a buffer tank to store the cooled water from the HP. The control activates the heat pump during the day, and the system starts removing heat from the cold tank, cooling it down, and releases it into the intermediate tank. The HP operates during the day until the cold tank reaches an average temperature of 7 ℃. Similar to the reference circuit, cold is extracted from the cold tank during demand hours and, when the cold tank reaches a set point temperature of 17 ℃ during the daytime, the system operates like the reference case, dissipating heat to the ambient. A conceptual scheme of the system is presented in Fig 7.
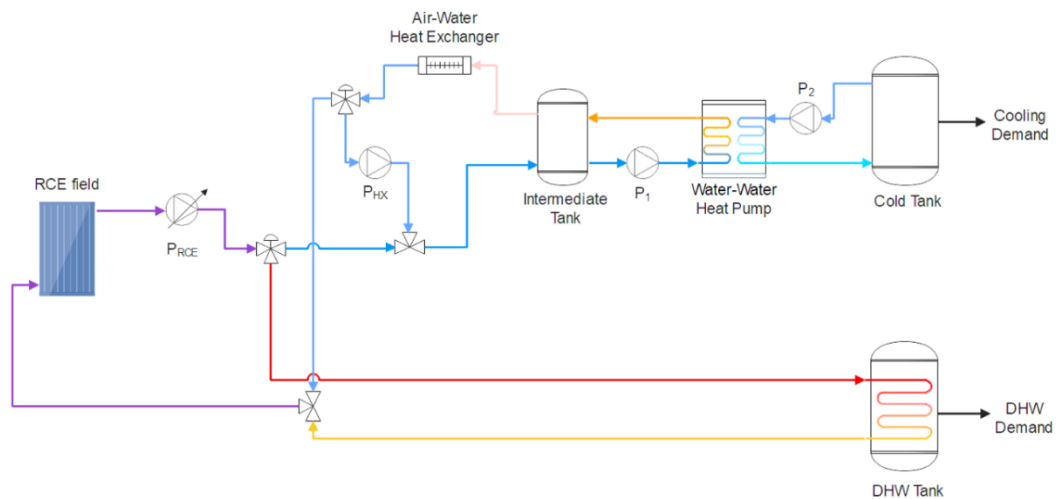
Fig 7. Conceptual scheme of the combination RCE+HP in the Intermediate Tank configuration (IT).

3.1.3. RCE + Heat Pump in Peak Load Shifting Configuration (PL)

The second proposed improvement system is based on a peak load shifting process for cold production. In order to reduce the peak in the cold demand during the day, part of the cold production is advanced to the previous night. This configuration is a simplification of the previous system, in which one speed pump and the intermediate tank is removed. Similarly to IT, in this configuration the heat produced during the day is stored in a hot water tank with coil and later used in DHW. During the night, on the side of the condenser, the heat transfer fluid is subjected to a pre-cooling process through the air-water heat exchanger - which lowers the temperature close to ambient temperature - and is then circulated through the RCE circuit. The cooled fluid in the RCE is immediately used as the condenser heat sink.

On the side of the evaporator, the water is cooled and stored in the cold tank, which works as a buffer tank, until a set-point temperature of 7ºC inside the tank is reached. When there is a demand for cooling, the cold is extracted from the tank, heating it up. Once the cold tank reaches a temperature of 17 ºC, the heat pump is reactivated to cold down the water of the cold tank. If the heat pump is operated during daytime, heat is dissipated to the air through the heat exchanger. The conceptual scheme of the system is presented in Fig 8.
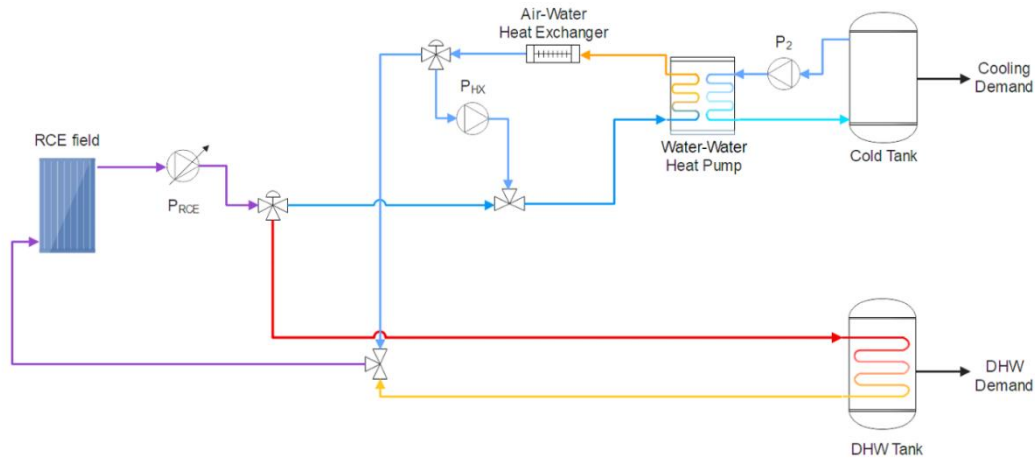
Fig 8. Conceptual scheme of the combination RCE+HP in the Peak Load Shifting configuration (PL).

3.2. Simulation Conditions

3.2.1. Cities

Each of the three facilities, described in section 3.1, were simulated for each of the nine cities, corresponding to eight different climates according to Köppen-Geiger classification (

Table 1). Cities were selected in order to represent most of the climates of Köppen-Geiger classifications; cold climates or without cooling demands were not considered in the analysis.

Table 1. Cities of simulation and equivalences betwen the Köppen-Geiger climate classification and the International Energy Conservation Code (IECC) climate zones.

City	Coordinates	Köppen-Geiger classification	IECC climate zone model
Lleida	41,61674N – 0,62218E	Bsk	3
Caracas	10,48801N – 66,87919W	Aw	1
Chicago	41,85003N – 87,65005W	Dfa	5
Denver	39,73915N – 104,9847W	Bsk	3
London	51,50853N – 0,12574W	Cfb	5
Ottawa	45,41117N – 75,69812W	Dfb	6
Riyadh	24,68773N – 46,72185E	BWh	2
Rome	41,89193N – 12,51133E	Csa	2
Tokyo	35,6895N – 139,69171E	Cfa	3

3.2.2. Simulation Season

The study simulated the warmest months in the northern hemisphere. The simulation period included June, July and August (between 01/06 00:00 and 01/09 00:00). The time step chosen in the simulation was 5 minutes.

3.2.3. Building Load Demands

The studied facilities were designed to meet the load demand for cooling and DHW - the latter only in the two RCE facilities - of a single-family detached house with crawlspace (Fig 9).
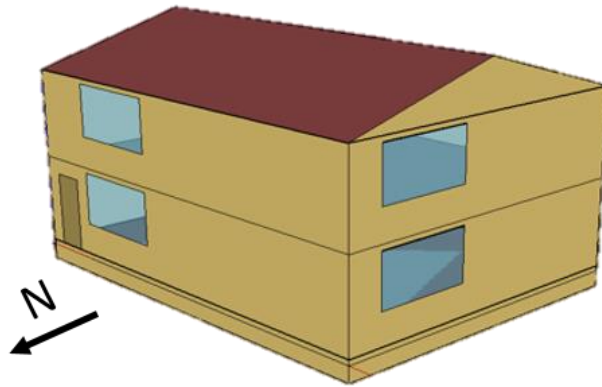
Fig 9. Model of a single-family house used to simulate the energy loads in EnergyPlus. North-West orientation.

Energy demands have been generated using numerical simulations in EnergyPlus [33]. The building models used in the EnergyPlus simulation were modifications of the models published by the USA Department of Energy (DOE). Models are typified for different cities in the USA and their constructive characteristics vary according to the climatic region, which are based on the International Energy Conservation Code (IECC) [34]. In this research Köppen-Geiger climate regions were assimilated to an IECC climate zone with close characteristics (

Table 1) in order to simulate the energy loads in different cities of the world.

The model of the single-family house consists of a double-decked building with a rectangular floor plan and a gabled roof. The facades are oriented towards each of the four cardinal points. It has a total of eight windows, four windows on each floor (one on each facade). The access door is located on the northern facade of the house.

Additional improvements have been added to the original model to reduce demand. The additional improvements were:

- Schedules set point temperature set at 25ºC.
- Summer night ventilation schedule set between 20h and 8h.
- Solar protections (overhangs).

The energy demands file generated in EnergyPlus is, afterwards, read by each of the TRNSYS models. The energy loads for the summer months are shown in Fig 10 for each simulated city. As it was expected, the cooling requirements are much higher than the rest of the energy needs. Heating loads are smaller in comparison, and they are not considered in the TRNSYS simulations. Riyadh and Caracas present more stringent cold requirements compared with the other cities of the simulation.
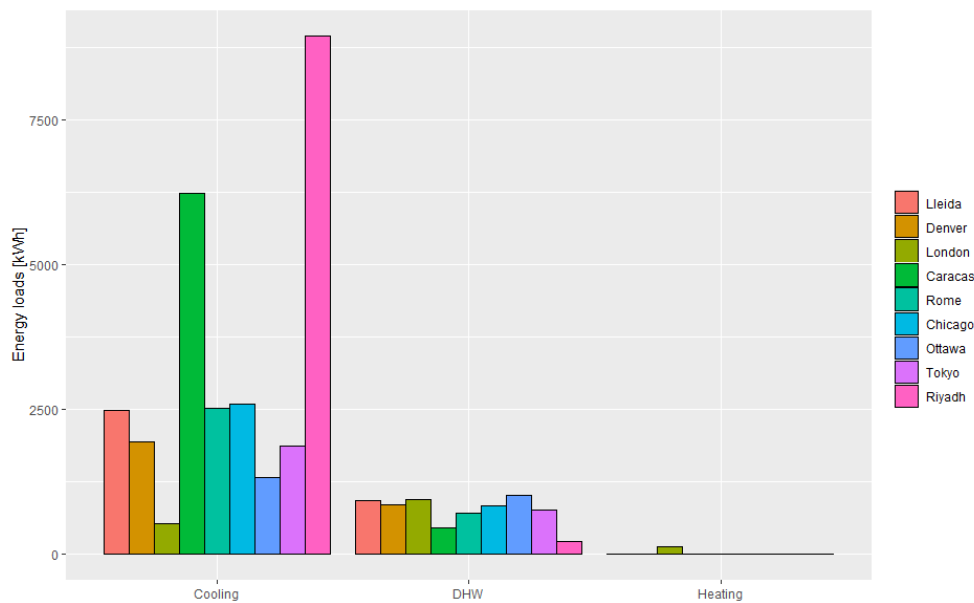
Fig 10. Energy loads (DHW, Heating and Cooling) of a single-family house during the warmest months (June to August) in the nine studied cities. Cooling energy demands are one order of magnitude above DHW. Heating demands are much lower in comparison and are overlooked.

3.3. Calculations

3.3.1. COP of the heat pump

The COP of the heat pump is calculated in TRNSYS as the ratio between the heat extracted in the evaporator side and the electrical consumption of the heat pump (eq (1)).

3.3.2. COP of the system

The study only compares the performance of the proposed configurations when they are working in the cold production mode (the reference system is only able to generate cold in this simulation).

The COP of the system represents the ratio of heat extracted on the cold side of the heat pump – in this case, the evaporator – and the electric consumption of all the active elements of the system (speed pumps and heat pumps). The number of active elements varied depending on whether the heat pump operates during the night, in combination with RC phenomenon, or during the day. Equations eq (3) and eq (4) were used to calculate the COP of the full system, taking into account the energy consumptions of all the active elements, of the Peak Load Shifting configuration and

65

the Intermediate Tank configuration, respectively, when the HP operates during the night; eq (5) and eq (6) were used when HP operates during the day for Peak Load Shifting configuration and the Intermediate Tank configuration, respectively. Eq (7) represented the COP of the reference system.

$$COP = \frac{Q_c}{W_{P_2} + W_{P_{RCE}} + W_{HP}} \tag{3}$$

$$COP = \frac{Q_c}{W_{P_2} + W_{P_{HX}} + W_{P_{RCE}} + W_{HP}} \tag{4}$$

$$COP = \frac{Q_c}{W_{P_2} + W_{P_1} + W_{HP}} \tag{5}$$

$$COP = \frac{Q_c}{W_{P_2} + W_{P_{HX}} + W_{P_1} + W_{HP}} \tag{6}$$

$$COP = \frac{Q_c}{W_{P_2} + W_{P_1} + W_{HP}} \tag{7}$$

Where Q_c represents the ratio of heat extracted on the cold side of the heat pump, and W_x respresents the electricity power consumption of the different speed pumps and the heat pump (described in the nomenclature), which were provided by TRNSYS tool.

The coefficient of performance of the HP and the full system was calculated for each observation. An average value was used as an indicator of the seasonal coefficient of performance (SCOP).

3.3.3. TRNSYS equations
3.3.3.1. Sky emissivity and IR radiation

In the calculation of atmospheric radiation, it was assumed that the sky was at the dry bulb temperature (T_{db}) of ambient air and that the effective sky emissivity could be determined according to the Walton correlation (eq (8)) [35], where T_{dp} is the dew point temperature in Kelvins, and N is the opaque sky cover in tenths.

$$\varepsilon_{sky} = \left(0.787 + 0.764 \cdot ln\left(\frac{T_{dp}}{273}\right)\right)$$
$$\cdot (1 + 0.0224 \cdot N - 0.0035 \cdot N^2 + 0.00028 \cdot N^3) \tag{8}$$

Using the effective sky emissivity, the incoming infrared radiation was expressed as eq (9).

$$R_{atm} = \varepsilon_{sky} \cdot \sigma \cdot T_{db}^4 \tag{9}$$

3.3.3.2. Net Balance

The radiative cooling power was determined by the net infrared radiation balance. This balance is defined as the difference between the radiation emitted by the surface - at surface temperature of the RCE, T_s - and the incoming atmospheric infrared radiation absorbed by the surface (eq (8)).

$$R_{net} = \varepsilon_s \cdot \sigma \cdot T_s^4 - R_{atm} \qquad (10)$$

4. Systems modelling

4.1. Energy loads simulation

The building model was not included in the TRNSYS simulations, but the demands were calculated separately using EnergyPlus (see section 3.2.3). In TRNSYS simulations we implemented the reading of the demand file generated in EnergyPlus and two auxiliary sub-circuits, DHW and cooling, which simulate the fulfilling of this load demand.

The file generated in EnergyPlus was arranged as a table consisting on observations, every five minutes from Jan 1st 00:00 to Dec 31st 23:59, for the demands of DHW, heating and cooling, expressed in Joules. A fourth column of the file expressed the time group of the observation. At the beginning of the simulation the tanks had no accumulated energy to supply the demand. In order to prevent the overworking of the facility, for the first day of simulation (Jun 1st) the energy demands of the building were set to zero.

The DHW and cooling outputs of the file are connected to the DHW sub-circuit and the cooling sub-circuit. The DHW sub-circuit simulates an open circuit consisting of the DHW tank and a variable speed pump. When there is hot water demand, part of the water in the tank (hot water) is replaced by mains water. The mains water is set at 13 °C. The flow rate by which the water in the tank is replaced is determined by an energy balance according to eq (11).

$$\dot{m}_{DHW} = \frac{E_{DHW}}{c_{p,w} \cdot \Delta T_{tank} \cdot t} \qquad (11)$$

Where E_{DHW} is the DHW energy requirements at a given timestep obtained from EnergyPlus simulations, $c_{p,w}$ is the water specific heat, ΔT_{tank} is the temperature difference between the tank and the mains water, and t is the timestep (set to 5 minutes).

The cooling sub-circuit simulates a closed circuit consisting of the cold tank and a constant flow pump. When there is a cooling demand, the speed pump activates and circulates water from the cold tank. The return temperature to the tank is calculated according to eq (12):

$$T_{ret} = T_{out} + \frac{E_c}{c_{p,w} \cdot \dot{m}_C \cdot t} \tag{12}$$

Where E_c is the cooling requirements at a given timestep obtained from EnergyPlus simulations, T_{out} is the temperature of the water at the outlet of the cold tank and $\dot{m}_C$ is the cooling flowrate.

4.2. Description of the types

The main characteristics of each type models are summarized in Table 2. The following sections describe the important types (RCE, Heat Pump and Control) used in the simulations.

Table 2. Summary of the TRNSYS' types used in the simulations of the different configurations.

Name	Type	Main Parameters	Input variables	Output Variables
RCE	Type 800	67 parameters including: - geometry of the panel - thermodynamic properties of air, water and insulator - optical properties of cover materials and radiator	Inlet temperature Inlet flowrate Ambient temperature Wind velocity Global horizontal solar radiation and infrared radiation	Outlet temperature Outlet flowrate Useful gain Temperature of the cover Temperature of the radiator Temperature of the pipe Temperature of the insulator
Control RCE	Type 807	Sunrise and sunset time for each month of the year	Month Simulation time	Control signal
Control pumps (IT)	Type 809	Gamma variable pump Solar radiation limit Infrared radiation limit	Global horizontal solar radiation and infrared radiation RCE net radiation Cold tank signal DHW tank signal Energy load demand Ambient temperature RCE outlet temperature RCE mode work	Variable speed pump control signal Heat Pump control signal Heat exchanger control signal
Control pumps (PL)	Type 808	Gamma variable pump Solar radiation limit Infrared radiation limit	Global horizontal solar radiation and infrared radiation RCE net radiation Cold tank signal DHW tank signal Energy load demand Ambient temperature Cold tank average temperature RCE mode work	Variable speed pump control signal Heat Pump control signal Heat exchanger control signal
Heat Pump	Type 927	Rated Cooling Capacity Rated Consumption	Inlet flowrate Inlet temperature Cooling control signal	Outlet flowrate Outlet temperature Heat transfer Power consumption
Differential Controller	Type 2b	High limit cut-out temperature	Input temperature Monitoring temperature Dead bands Input control function	Output control function

Air-water Heat Exchanger	Type 5c	Specific heat of water Specific heat of air	Inlet temperatures Inlet flowrates Overall heat transfer coefficient	Outlet temperatures Outlet flowrates Heat transfer rate Effectiveness
Storage tank	Type 158	Tank volume Tank height Number of ports Height of ports Number of tank nodes Loss coefficient	Inlet temperatures Inlet flowrates Loss temperatures	Outlet temperatures Outlet flowrates Average tank temperatures Tank losses
Storage tank with coil	Type 156	Tank volume Tank height Number of ports Height of ports Number of tank nodes Number of coil nodes Loss coefficient	Inlet temperature Inlet flow rate Control signal Pump efficiency Motor efficiency	Outlet temperatures Outlet flowrates Average tank temperatures Average coil temperatures Tank losses
Variable Speed Pump	Type 110	Rated flow rate Rated power Fluid specific heat Power coefficients	Inlet temperature Inlet flow rate Control signal Pump efficiency Motor efficiency	Outlet temperature Power consumption Fluid heat transfer Environmental heat transfer
Single Speed Pump	Type 114	Rated flow rate Rated power Fluid specific heat	Inlet temperature Inlet flow rate Control signal Overall pump efficiency Motor efficiency	Outlet temperature Power consumption Fluid heat transfer Environmental heat transfer
Controlled Flow Diverter and Tee	Type 11	-	Inlet Temperatures Inlet Flowrates Control Signal	Outlet Temperatures Outlet Flowrates
Data Reader	Type 9	-	-	DHW loads Cooling loads
Weather Data Processor	Type 15	-	-	Dry bulb temperature Dew point temperature Wind velocity Opaque sky cover Global horizontal radiation
Output printer	Type 25	-	Outputs to read	External File
Time value	Type 21	-	-	Time of simulation Day of simulation Month of simulation

4.2.1. RCE

This is an own Type based on the model developed and experimentally validated by Vall et al. [30]. It consists on a global energy balance between the RCE, the ambient air and the sky in order to determine the net heat flow entering or leaving the RCE. On the other hand, the RCE is discretized in different nodes using a one-dimensional electrical analogy (1D), which includes some 2D effects based on detailed simulations of these effects using Comsol Multiphysics. The radiative balance is performed for four different wavelength ranges (0-4 μm, 4-7 μm, 7-14 μm and >14 μm). The model allows the use of two cover materials. This allows to distinguish between different wavelength ranges, with special interest in the infrared atmospheric window (7-14 μm), to integrate the dual functionality solar collector/radiative cooler. Energy balance equations are

ordinary first-order differential equations that are solved numerically using Euler's implicit method.

4.2.2.   Heat Pump (Type 927)

This Type belongs to the TRNSYS TESS library and simulates a single-stage water-to-water heat pump. The model is controlled by a signal that turns the pump on or off and receives as inputs the flows and temperatures in the condenser and evaporator. The outputs (flowrate and temperature of the fluid, heat transfer and power consumption of the heat pump) of the model are based on information contained in a data file supplied by the user which contains catalogue data for the capacity and power [32] (see 4.3.1). These values are determined by the temperatures and flowrates at the inlet of the condenser and evaporator.

4.2.3.   Control

Three types were developed ad-hoc to control the combined RCE + HP facilities. The first one controls the operation mode of the RCE (radiative cooling or solar heating) depending of the time of the simulation. The second type controls the operation of the Peak Load Shifting system, and the last type controls the Intermediate Tank system.

The types use as inputs the solar radiation and the net RC balance of the RCE surface, the ambient temperatures and the temperatures of the different tanks and the energy demand of the simulated building. These inputs determine the operating status (ON / OFF) of the speed pumps and heat pump, and the flowrate control signal of the variable speed pump. To filter low radiation values, the system is OFF in RC mode if the net radiation balance is below 25 W/m^2 and below 100 W/m^2 in SH mode.

4.3. Sizing
4.3.1.   Heat Pump

In order to compare the different configurations, the heat pump had the same characteristics in the three systems, but was specifically sized for each studied city. As a criterion to size the water-water heat pump we chose a maximum cooling capacity equivalent to the peak cooling loads of the building.

The sizing of the heat pumps is based on Airlan's commercial heat pumps [36]. The sizing parameters were scaled in order to meet the worst case observation, which was previously simulated. Table 3 summarizes the main parameters of the heat pump for each of the representative locations.

Table 3. Design parameters of the water-water heat pump.

	Rated Cooling Capacity [kW]	Electricity Consumption [kW]	Condenser Flowrate [kg/h]	Evaporator Flowrate [kg/h]	Worst case observation time	Heat Pump model
Lleida	6.28	1.73	1362	1086	19:00 19/07	WRL-H 026
Caracas	6.42	1.88	1368	1116	16:10 26/08	WRL-H 031
Chicago	5.65	1.56	1224	972	18:15 01/07	WRL-H 026
Denver	5.05	1.39	1080	864	19:00 26/06	WRL-H 026
London	3.94	1.09	864	684	19:00 19/07	WRL-H 026
Ottawa	5.71	1.57	1224	972	18:25 20/07	WRL-H 026
Riyadh	9.02	2.19	1908	1548	19:55 29/06	WRL-H 041
Rome	5.71	1.57	1224	972	18:25 23/07	WRL-H 026
Tokyo	5.50	1.52	1188	936	18:15 01/07	WRL-H 026

4.3.2. Cold tank

The criterion used to size the cold tank is that the tank must meet the totality of the cooling demand of the 75% of the days. The other 25% of days, with higher demands, are only partially met. Table 3 summarizes the storage volume of the cold tank.

Table 4. Cold tank capacity.

City	Cold tank volume [m^3]
Lleida	2.5
Caracas	6.5
Chicago	3.5
Denver	2.5
London	1
Ottawa	1.8
Riyadh	9
Rome	2
Tokyo	2.9

4.3.3. RCE area

The proposed systems have been sized for an RCE area of 30 m^2, equivalent to 15 RCE panels in parallel configuration. Assuming an average radiative cooling capacity of 50 W/m^2 ([37], [38]), 1500 W of radiative cooling power are estimated.

4.3.4. Solar heating mode characteristics

The Spanish Technical Code (CTE) [39] and the Spanish Institute for the Diversification of Energy Saving (IDAE) [40] recommend that the storage volume for a solar thermal collection system lays between 50-180 l/m^2 of capturing surface and the flowrate remains between 40-60 l/h·m^2 of capturing surface. The storage volume of the DHW tank was set at 1.5 m^3 and the flowrate of the fluid through the RCE fields was set at 1500 kg/h.

4.3.5. Radiative cooling mode characteristics

Radiative cooling characteristics are different among PL and IT configurations. In the PL configuration, the RCE flowrate is determined by the characteristics of the chosen heat pump: it was set to be equal to the flowrate required in the condenser of the heat pump (Table 3).

In IT configuration the intermediate tank was sized with a volume of 2 m^3, assuming an average cooling power of 50 W/m^2 during 7 working hours at night and a thermal decrease of 5 ºC at the end of the night. In this configuration, the flowrate through the RCE can be decoupled from the HP's condenser. This means that a lower flowrate, which maximizes the thermal differences between the inlet and the outlet in the RCE, can be selected. In all the cities this flowrate was set to 450 kg/h, about 3 times smaller than the PL flow rate, in order to achieve temperature differences of 2-3 ºC between the inlet and the outlet of the RCE.

5. Results and Discussion

5.1. Cold Production

5.1.1. Analysis of the performance

Fig 11 shows the comparison of the performance of the different configurations in each studied city. This figure shows both the seasonal COP of the heat pump and the system. The combination of RCE with heat pumps showed and improvement of the seasonal COP of the heat pump in all the studied locations

Differences in the performance between different configurations tend to be similar when considering the seasonal COP of the system. After accounting all the electrical consumptions (COP of the system), the PL configuration has lower efficiency than the reference model in Caracas, and the IT configuration behaves similarly to the reference in Caracas, Chicago and Riyadh.

In seven of the nine cities (Lleida, Ottawa, London, Tokyo, Rome, Chicago and Caracas) the improvement in HP's performance is greater in IT configuration than PL. However, after accounting the consumption of all the elements, the improvement of the COP of the system is greater in PL configuration in most cities (Denver, Rome, London, Riyadh and Tokyo). The intermediate tank configuration (IT), despite being the most complex system of all, and having one more tank and one more pump than the peak load shifting configuration (PL), and two more pumps than the reference configuration, improves the COP of the system in Caracas, Lleida and Ottawa.
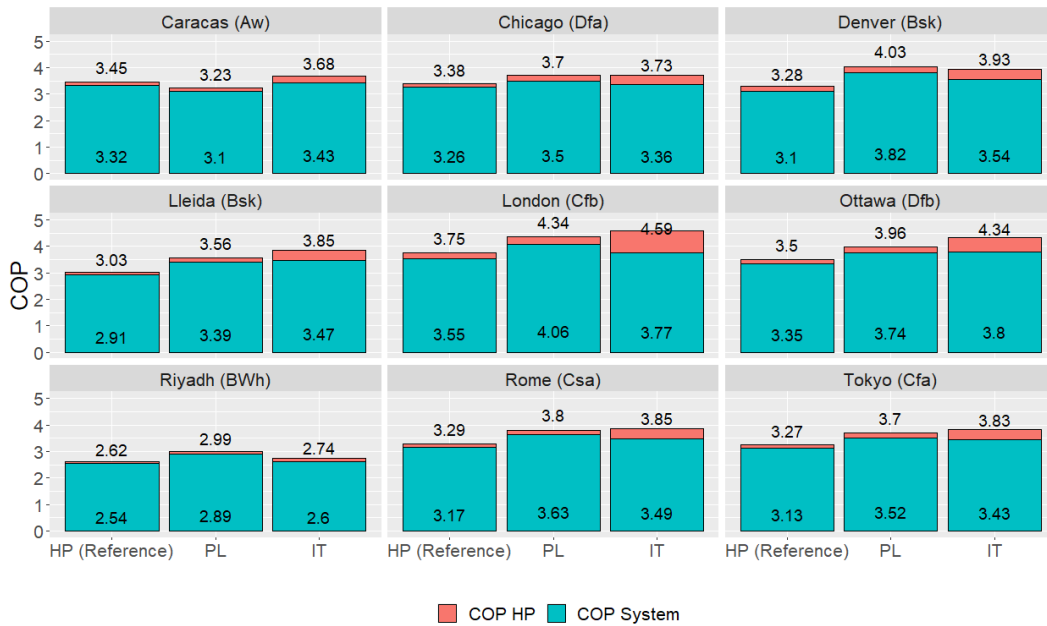
Fig 11. Seasonal coefficient of performance (SCOP) in cooling mode of the water-water heat pump and the system for the three configurations: HP Alone, Peak Load Shifting (PL) and Intermediate Tank (IT) configuration

Denver (PL), Lleida (PL and IT) and Rome (PL) are the top three cities where the improvement of the whole system is greater (23.09%, 16.59%, 16.09% and 14.56%, respectively). The three cities are ranked in the middle of the table in terms of cooling requirements (Fig 10). According to the Köppen-Geigger, Denver and Lleida are classified in Bsk climate which is characterized for being dry climate and for having cold or very cold winters and hot summers. Rome is classified in Csa climate which is represented by dry and hot summers. The three cities are subjected to low humidity conditions; these results are in agreement with the stated by Fernandez et al. [19].

On the other hand, Caracas (PL and IT), Riyadh (IT), Chicago (PL) and London (IT) are the cities where the system performed worst. Climates in Caracas, Chicago and London are distinguished by humid weathers. Riyadh, despite being in a dry climate area, presents the highest cooling demands of all the nine studied cities and the cooling contribution of the RCE is small in comparison with the total heat to dissipate. The poor performance of humid climates and highly demanding locations is also in agreement with the results of Fernandez et al. [19].

In Riyadh the size of the cold tank is significantly larger compared to other cities due to the sizing criteria (Table 3). The added difficulty to cool down a large tank means that in Riyadh the system is constantly working during the night (Table 5). In the rest of the cities, in the PL configuration, the number of hours when the HP is working does not exceed 44% of nocturnal hours. In the IT configuration, the cities of Lleida, Caracas, Chicago and Tokyo also work for the majority of the night. We can see differences in the nocturnal behaviour of both configurations: in IT, the aim is to maximize the operational time of RC in order to store the maximum cold in the intermediate

73

tank. In PL the goal is to produce the required cold for the next day in the shortest possible time in order to minimize the electricity consumption. Table 5 shows that the heat pump in the PL configuration works most of the time in combination with radiative cooling, while the rest of the time it works as a conventional HP. The above indicates that the sizing criteria used is appropriate for this type of combined system.

Table 5. Summary of the number of working hours when radiative cooling is achieved and the heat pump is working. Ratio between the number of hours when radiative cooling is achieved and the total amount of nocturnal hours in PL and IT configurations, and ratio between the number of hours where the heat pump operates in combination with radiative cooling in PL configuration.

		Peak Load Shifting			Intermediate Tank
	Nocturnal hours [h]	HP ON [h]	RC hours / nocturnal hours ratio [%]	RC+HP hours / HP hours ratio [%]	RC hours / nocturnal hours ratio [%]
Lleida	879,00	381,00	37,82	87,25	90,34
Caracas	1092,00	217,25	15,15	76,14	93,29
Chicago	849,00	102,08	10,57	87,92	72,33
Denver	879,00	375,17	38,17	89,43	37,37
London	719,50	131,50	64,70	57,03	42,58
Ottawa	849,00	226,92	18,40	68,86	46,49
Riyadh	1001,00	998,25	95,30	95,57	95,19
Rome	849,00	430,67	43,95	86,65	61,86
Tokyo	910,00	335,58	30,96	83,96	78,85

In PL configurations, the COP of the whole system is higher when the heat pump works at night combined with the RCE. When the tank no longer contains usable stored cold, and the heat pump has to work during the day like a conventional heat pump, the performance worsens (Fig 12). The biggest differences between nocturnal and diurnal operation are found in Riyadh (19.18%), Caracas (16.23%) and Denver (16.51%), while the differences are lower in Lleida (5.58%) and Tokyo (8.32%).
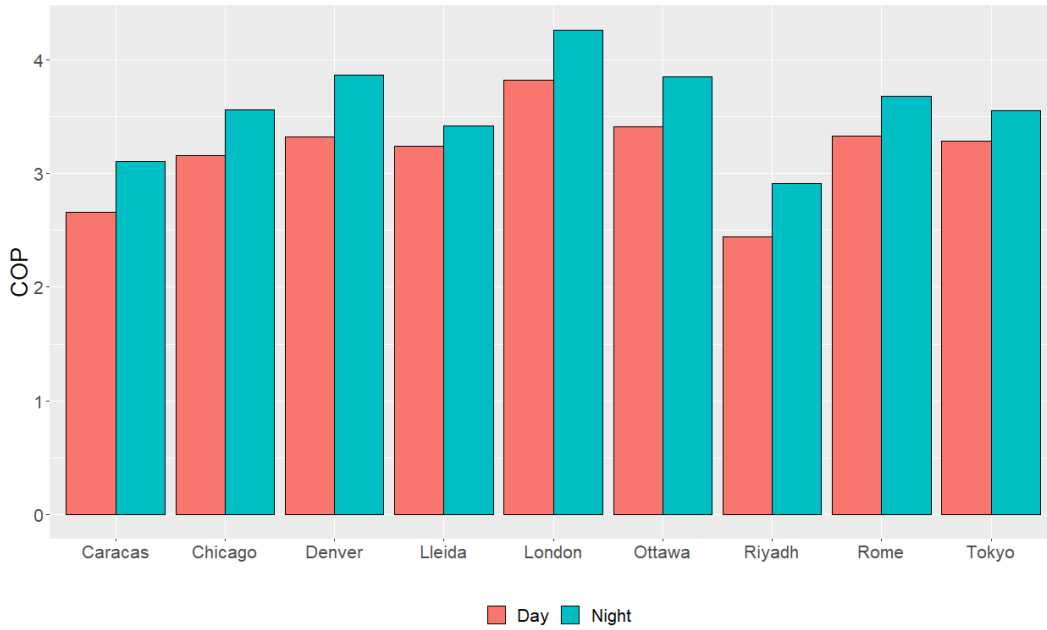
Fig 12. Differences between the nocturnal and diurnal seasonal COP of the Peak Load Shifting configuration

In Table 6 it is presented the average difference between the outlet temperature of the RCE and the ambient temperature when the RCE operates in radiative cooling mode. In the PL configuration, water cannot reach sub-ambient temperature at the outlet, while in all the IT simulations, at the outlet of the RCE, the water is at a colder temperature than the ambient.

Table 6. Average differences between the temperature at the outlet of the RCE and the ambient temperature. In the Intermediate Tank configuration, sub-ambient temperatures are reached at the output of the RCE.

City	Peak Load Shifting	Intermediate tank
Lleida	3.41 ± 0.33 ºC	-0.28 ± 0.33 ºC
Denver	2.24 ± 0.25 ºC	-0.10 ± 0.27 ºC
London	1.28 ± 0.29 ºC	-0.52 ± 0.36 ºC
Rome	2.53 ± 0.34 ºC	-0.70 ± 0.59 ºC
Caracas	3.27 ± 0.36 ºC	-0.31 ± 0.48 ºC
Chicago	2.76 ± 0.38 ºC	-0.26 ± 0.42 ºC
Ottawa	2.86 ± 0.35 ºC	-0.36 ± 0.38 ºC
Tokyo	2.72 ± 0.26 ºC	-0.25 ± 0.28 ºC
Riyadh	4.96 ± 0.50 ºC	-0.04 ± 0.53 ºC

In the PL configuration, the flowrate through the RCE is determined by the condenser's flowrate of the heat pump. In the IT configuration, the radiative cooling flowrate is decoupled from the heat pump flowrate, so that a lower flow can be selected, which allows a higher difference between RCE's inlet and outlet temperatures. In both combined systems the average inlet temperature at the condenser is lower than in the reference configuration (HP Alone) (Table 7), reaching a higher COP.

Table 7. Average inlet temperature at the condenser of the water-water heat pump

City	HP Alone	Peak Load Shifting	Intermediate tank
Lleida	33,73 ± 3,57 ºC	28,47 ± 3,83 ºC	27,08 ± 5,22 ºC
Denver	33,22 ± 4,59 ºC	23,33 ± 3,56 ºC	25,87 ± 5,24 ºC
London	25,33 ± 3,29 ºC	20,81 ± 4,57 ºC	19,96 ± 3,70 ºC
Rome	30,64 ± 2,18 ºC	25,32 ± 2,67 ºC	26,41 ± 3,62 ºC
Caracas	32,43 ± 2,05 ºC	29,92 ± 1,49 ºC	31,81 ± 2,83 ºC
Chicago	31,70 ± 3,65 ºC	27,31 ± 3,74 ºC	27,86 ± 4,94 ºC
Ottawa	28,21 ± 3,62 ºC	24,11 ± 4,62 ºC	22,14 ± 5,18 ºC
Tokyo	30,76 ± 3,21 ºC	26,56 ± 3,10 ºC	26,72 ± 4,56 ºC
Riyadh	45,08 ± 4,37 ºC	38,65 ± 3,87 ºC	45,03 ± 3,97 ºC

5.1.2. Efficiency of the RCE

Fig 13 shows the average radiative cooling power achieved in the fluid (defined by the temperature change between the inlet and outlet of the RCE) and the net radiation balance in the surface (defined by the surface temperature of the RCE and the absorbed infrared radiation from the atmosphere).

The power potential in the surface in both configurations present similar trends. It is observed that in the PL configuration the radiative cooling power achieved is higher than in the IT configuration. The average efficiency of the RCE in radiative cooling mode, defined as the ratio between the achieved power and the potential power, is higher in the peak load shifting configuration (36-74%) than in the intermediate tank configuration (17-40%) (Fig 14).

The power achieved is influenced by the flowrate inside the RCE, the working temperatures the time of operation and the total amount of hours of operation. Each configuration has a different control (section 3.1) resulting in a different operation for each case. It makes it difficult to compare the efficiencies of the systems directly. The results shown in Fig 13 should only be used as an illustration of the performance but not as a proof that PL configurations are more efficient than IT configurations.
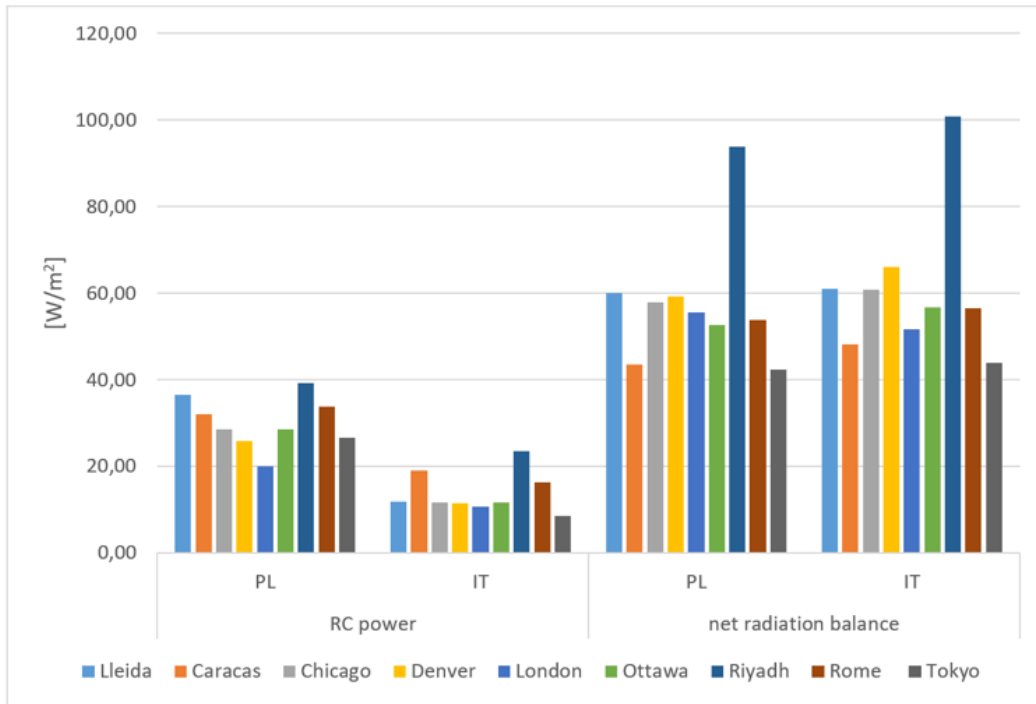
Fig 13. Average seasonal radiative cooling power and net power in the surface of the RCE
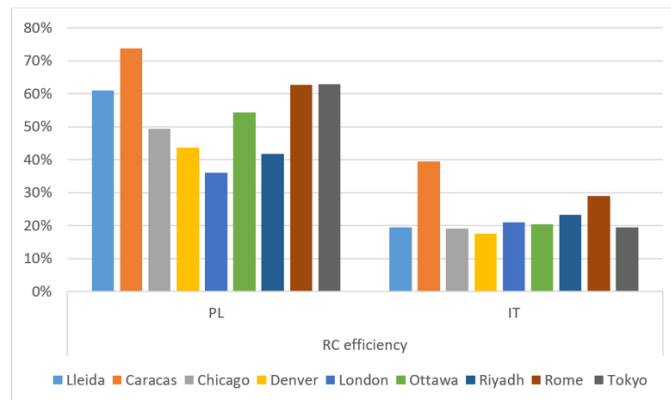
Fig 14. Average seasonal efficiency of the RCE operating in radiative cooling mode.

5.1.3. Energy Savings

Energy savings in the electricity consumption of the active elements, during the months of summer (June-August), of the different systems are presented in Fig 15. Results show energy savings from 3% up to 20% in all the configurations except from PL systems in Caracas, where the it requires 118.27 kWh more than in the reference case. There is not a big difference between PL and IT configurations in Tokyo, London and Ottawa. The biggest difference between the energy savings in the two configurations are found in Riyadh (PL) and Rome (IT) (5.4 and 2.5 times higher, respectively). It is notable that, in Riyadh, a small improvement in the coefficient

of performance translates into big energy savings. Denver and Lleida also present energy savings close or higher than 100 kWh in both configurations.

IT configuration and the configuration by Fernandez et al. [19] make use of a tank between the radiative cooling loop and the demand loop. However, the present simulation predicts lower electricity savings than in Fernandez et al. The biggest difference comes from the capacity to generate daytime radiative cooling in Fernandez's model. The savings obtained in Riyadh in PL configurations are comparable with the electricity savings predicted by Goldstein [22], as both Riyadh and Las Vegas correspond to hot desert climates in the Köppen-Geigger classification (BWh). In this case, the peak-load shifting configuration can be assimilated to Goldstein's configuration, as in both systems the radiative cooling panels are directly coupled to the condenser of the heat-pump. The energy savings in Riyadh obtained in this study (12%) are lower compared to those obtained by Goldstein in Las Vegas (21%). The greatest energy savings in Goldstein's study, compared to the present ones, is due to the capacity of Goldstein's model to produce daytime radiative cooling. This suggests that an all-day radiative cooling system is a better option to meet the cooling demands when combined with a heat pump. Nevertheless, an all-day radiative cooler doesn't have the capacity to achieve solar heating, not being able to fulfil the DHW demands. This is later studied in section 5.2.
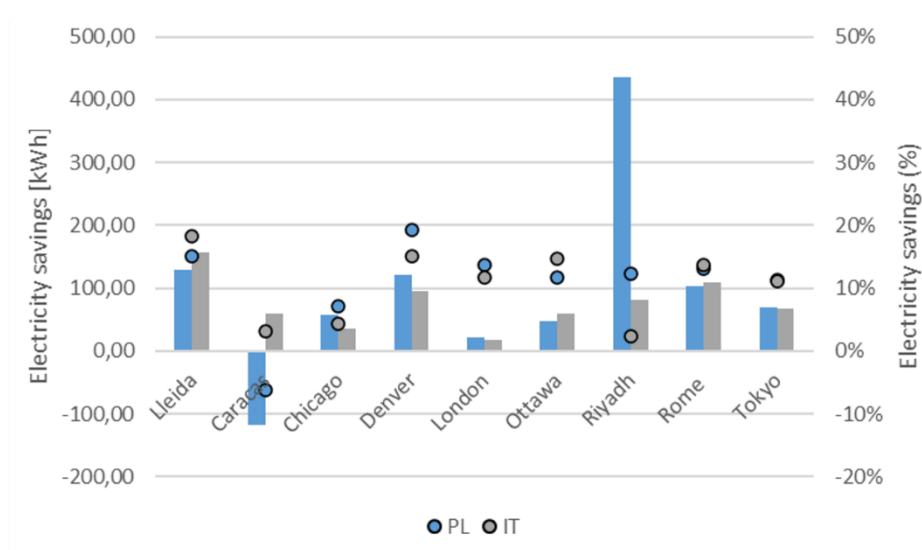
Fig 15. Electricity saved in two RCE+HP configurations: peak load shifting configuration (PL) and intermediate tank configuration (IT). The bars represent the total amount of energy saved (in kWh) and the dots represent the corresponding percentage (%).

5.2. Heat Production

Due to the dual functionality of the RCE both proposed configurations incorporate the possibility of achieving solar collection during the day. The tank stores energy between 40-60°C which is used to meet the DHW demands of the building. Table 8 summarizes the average temperatures

achieved in the tank at the end of a day of solar collection. The behaviour in both systems is similar and the small differences are due to the differences in the inertia of the RCE when switching from cooling mode to solar collection mode.

Table 8. Average temperature of the DHW tank at the end of the day in the different improvement configurations proposed during the months of summer (June – August).

	Average DHW tank temperature [ºC]	
	PL	IT
Caracas	52.57	52.01
Chicago	49.85	49.95
Denver	50.7	50.33
Lleida	51.52	51.70
London	49.75	50.10
Ottawa	49.71	50.65
Riyadh	51.6	51.12
Rome	51.12	51.29
Tokyo	50.52	51.54

Diurnal average solar collector efficiencies of 33%–49% are achieved in the RCE panels (Fig 16). Only in London, the system operates in more than 50% of the available hours for solar collection. In the other studied cities, the results show an underutilization of the solar system. In the case of Lleida, for example, the energy stored for one day is used to cover DHW demands for the next three days (Fig 17). As it has been previously discussed, the 30 m^2 collection area are needed to improve the performance of the heat pump in the radiative cooling mode, but they are excessive to meet DHW demand of the building. This results, and the results discussed in section 5.1.3, suggests that a collection field composed of all-day radiative coolers and less surface of RCE may be optimal to meet both cooling and DHW needs.
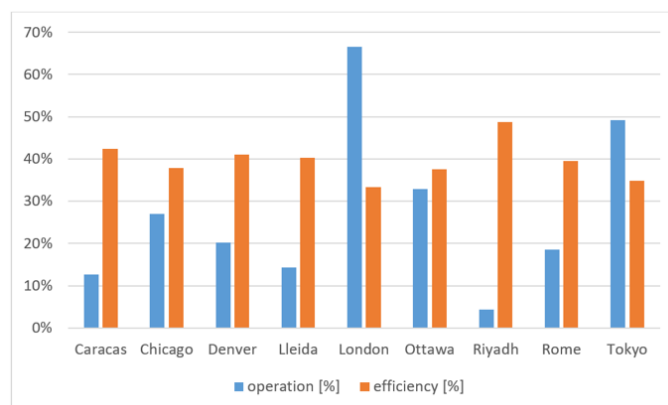
Fig 16. Efficiency of the solar collector (orange) and ratio between the operating hours and the solar collection hours available (blue).
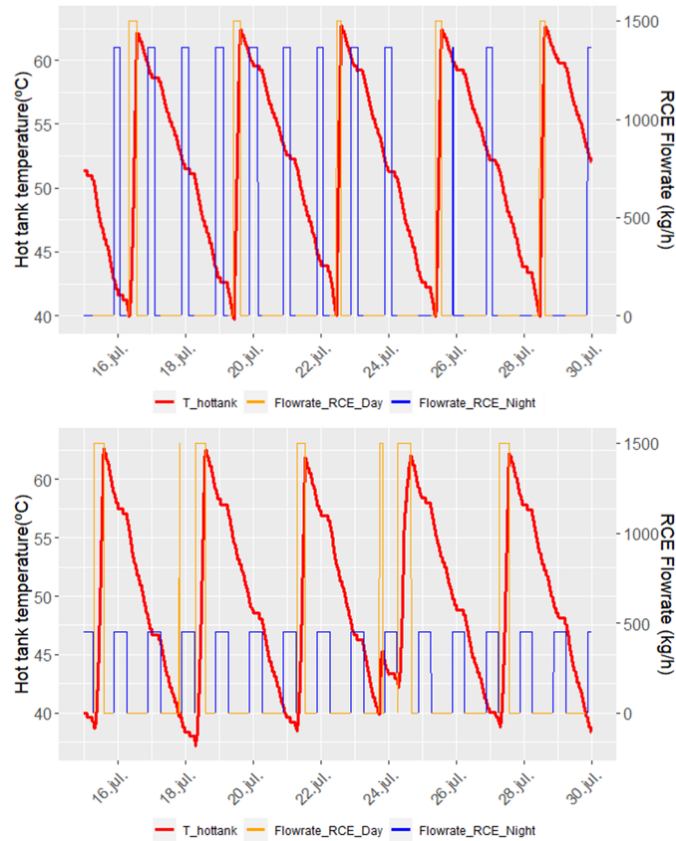
Fig 17. Evolution of the DHW temperature (red) and the flowrate flowing through the RCE in solar collection mode (orange) and radiative cooling mode (blue) in PL configuration (top) and IT configuration (bottom). Energy stored in the hot water tank during one day is used to cover DHW demands for the next three days. Case of Lleida.

6. Conclusions

The present research proved numerically that the use of RCE can achieve both solar heating and radiative cooling functionalities during the hottest month of the year in different cities of the northern hemisphere, corresponding to different Köppen-Geiger climate classification regions. The cold generated demonstrated to be a useful heat sink for the condenser of a heat pump, increasing its COP and, as a result, saving electricity. In this paper we proposed two possible combinations of 15 RCE panels, corresponding to an emitting/collecting surface equal to 30 m^2: a peak load shifting configuration (PL), based on the direct coupling of the radiative cooling and the cold production for consumption, and an intermediate tank configuration (IT) where both productions are decoupled by means of an intermediate tank.

Both systems, despite being more complex in terms of the number of elements, improve their performance compared to a reference case with a single heat pump. Intermediate Tank configuration shows greater improvements of the performance of the heat pump in most of the cities studied. Peak Load shifting configuration shows greater improvements of the whole system in five cities. Cities with dry climate and middle or low cooling loads are the cities where the

improvement of the system is greater (Denver, Lleida and Rome). Humid climates or climates with high cooling demands performed worst.

On average, in IT configurations, sub-ambient temperature water is obtained at the outlet of the RCE. Sub-ambient temperatures are not observed in PL configurations. The radiative cooling efficiency in the RCE was higher in PL configuration (36-74%) than in IT configuration (17-40%). However, the discussion revealed that the efficiencies can't be directly compared.

The proposed systems allow to obtain hot water at a temperature between 40 and 60ºC during the day. The results show an underutilization of the facilities if they have to meet only DHW. In this case the facilities only work between 4 and 49% of the available time, except in London (67%). During these hours of operation, the performance of the RCE is 33%–49%.

Acknowledgment

References

[1] European Parliament, "Directive 2009/28/EC of the European Parliament and of the Council of 23 April 2009 on the promotion of the use of energy from renewable sources and amending and subsequently repealing Directives 2001/77/EC and 2003/30/EC," *Official Journal of the European Union*, vol. 140, pp. 16–62, 2009, doi: 10.3000/17252555.L_2009.140.eng.

[2] "Directive (EU) 2018/ of the European Parliament and of the Council of 30 May 2018 amending Directive 2010/31/EU on the energy performance of buildings and Directive 2012/27/EU on energy efficiency," p. 17.

[3] "COMMISSION RECOMMENDATION (EU) 2019/ 786 - of 8 May 2019 - on building renovation - (notified under document C(2019) 3352)".

[4] *Project Europe 2030: challenges and opportunities : a report to the European Council by the Reflection Group on the Future of the EU 2030*. Luxemburg: Publications Office of the European Union, 2010.

[5] "A European Green Deal," *European Commission - European Commission*. https://ec.europa.eu/info/strategy/priorities-2019-2024/european-green-deal_en (accessed Apr. 25, 2022).

[6] Eurostat, "Energy consumption in households," May 2019. https://ec.europa.eu/eurostat/statistics-explained/index.php?title=Energy_consumption_in_households#Use_of_energy_products _in_households_by_purpose

[7] S. Vall and A. Castell, "Radiative cooling as low-grade energy source: A literature review," *Renewable and Sustainable Energy Reviews*, vol. 77, pp. 803–820, Sep. 2017, doi: 10.1016/j.rser.2017.04.010.

[8]   B. Ko, D. Lee, T. Badloe, and J. Rho, "Metamaterial-Based Radiative Cooling: Towards Energy-Free All-Day Cooling," *Energies*, vol. 12, no. 1, p. 89, Dec. 2018, doi: 10.3390/en12010089.

[9]   G. N. Nwaji, C. A. Okoronkwo, N. V. Ogueke, and E. E. Anyanwu, "Hybrid Solar Water Heating/Nocturnal Radiation Cooling System I: A Review of the Progress, Prospects and Challenges," *Energy and Buildings*, p. S0378778818338179, Jun. 2019, doi: 10.1016/j.enbuild.2019.06.017.

[10]   S. Catalanotti, V. Cuomo, G. Piro, D. Ruggi, V. Silvestrini, and G. Troise, "The radiative cooling of selective surfaces," *Solar Energy*, vol. 17, no. 2, pp. 83–89, May 1975, doi: 10.1016/0038-092X(75)90062-6.

[11]   M. A. Kecebas, M. P. Menguc, A. Kosar, and K. Sendur, "Passive radiative cooling design with broadband optical thin-film filters," *Journal of Quantitative Spectroscopy and Radiative Transfer*, vol. 198, pp. 179–186, Sep. 2017, doi: 10.1016/j.jqsrt.2017.03.046.

[12]   J. Mandal *et al.*, "Hierarchically porous polymer coatings for highly efficient passive daytime radiative cooling," *Science*, vol. 362, no. 6412, pp. 315–319, Oct. 2018, doi: 10.1126/science.aat9513.

[13]   J.-W. Cho, T.-I. Lee, D.-S. Kim, K.-H. Park, Y.-S. Kim, and S.-K. Kim, "Visible to near-infrared thermal radiation from nanostructured tungsten anntennas," *J. Opt.*, vol. 20, no. 9, p. 09LT01, Aug. 2018, doi: 10.1088/2040-8986/aad708.

[14]   Y. Cui, X. Luo, F. Zhang, L. Sun, N. Jin, and W. Yang, "Progress of passive daytime radiative cooling technologies towards commercial applications," *Particuology*, vol. 67, pp. 57–67, Aug. 2022, doi: 10.1016/j.partic.2021.10.004.

[15]   W. Carrión-Chamba, W. Murillo-Torres, and A. Montero-Izquierdo, "A review of the state-of-the-art of solar thermal collectors applied in the industry," *ings*, no. 27, Dec. 2021, doi: 10.17163/ings.n27.2022.06.

[16]   O. E. da Silva Júnior, J. A. de Lima, R. Abrahão, M. H. A. de Lima, E. P. Santos Júnior, and L. M. Coelho Junior, "Solar Heating with Flat-Plate Collectors in Residential Buildings: A Review," *Energies*, vol. 15, no. 17, p. 6130, Aug. 2022, doi: 10.3390/en15176130.

[17]   S. Buddhiraju, P. Santhanam, and S. Fan, "Thermodynamic limits of energy harvesting from outgoing thermal radiation," 2018, vol. 10759. doi: 10.1117/12.2323951.

[18]   S. Vall, A. Castell, and M. Medrano, "Energy Savings Potential of a Novel Radiative Cooling and Solar Thermal Collection Concept in Buildings for Various World Climates," *Energy Technol.*, vol. 6, no. 11, pp. 2200–2209, Nov. 2018, doi: 10.1002/ente.201800164.

[19]   N. Fernandez, W. Wang, K. J. Alvine, and S. Katipamula, "Energy Savings Potential of Radiative Cooling Technologies," PNNL--24904, 1234791, Nov. 2015. doi: 10.2172/1234791.

[20]   T. Facius and B. Aircoil, "Benefits of Water Cooled vs Air Cooled Equipment in Air Conditioning Applications," *Cooling Technology Institute*, p. 50, 2011.

[21]   M. Medrano, A. Salandin, C. Solé, I. Martorell, R. Vilà, and A. Castell, "Potential for Integration of a Renewable Combined Heating and Cooling System in Food Industries requiring Heat and Cold," *ISES Solar World Congress 2021*, 2021.

[22]   E. A. Goldstein, A. P. Raman, and S. Fan, "Sub-ambient non-evaporative fluid cooling with the sky," *Nature Energy*, vol. 2, no. 9, p. 17143, Sep. 2017, doi: 10.1038/nenergy.2017.143.

[23]   M. Matsuta, S. Terada, and H. Ito, "Solar Heating and radiative cooling using a solar collector-sky radiator with a spectrally selective surface," *Solar Energy*, vol. 39, no. 3, pp. 183–186, 1987.

[24]   E. Erell and Y. Etzion, "Heating experiments with a radiative cooling system," *Building and Environment*, vol. 31, no. 6, pp. 509–517, Nov. 1996, doi: 10.1016/0360-1323(96)00030-3.

[25]   E. Erell and Y. Etzion, "Radiative cooling of buildings with flat-plate solar collectors," *Building and Environment*, vol. 35, no. 4, pp. 297–305, May 2000, doi: 10.1016/S0360-1323(99)00019-0.

[26] D. Zhao *et al.*, "Subambient Cooling of Water: Toward Real-World Applications of Daytime Radiative Cooling," *Joule*, vol. 3, no. 1, pp. 111–123, Jan. 2019, doi: 10.1016/j.joule.2018.10.006.

[27] R. Vilà, I. Martorell, M. Medrano, and A. Castell, "Adaptive covers for combined radiative cooling and solar heating. A review of existing technology and materials," *Solar Energy Materials and Solar Cells*, vol. 230, p. 111275, Sep. 2021, doi: 10.1016/j.solmat.2021.111275.

[28] R. Zevenhoven and M. Fält, "Radiative cooling through the atmospheric window: A third, less intrusive geoengineering approach," *Energy*, vol. 152, pp. 27–33, Jun. 2018, doi: 10.1016/j.energy.2018.03.084.

[29] M. Hu, B. Zhao, X. Ao, Y. Su, and G. Pei, "Numerical study and experimental validation of a combined diurnal solar heating and nocturnal radiative cooling collector," *Applied Thermal Engineering*, vol. 145, pp. 1–13, Dec. 2018, doi: 10.1016/j.applthermaleng.2018.08.097.

[30] S. Vall, K. Johannes, D. David, and A. Castell, "A new flat-plate radiative cooling and solar collector numerical model: Evaluation and metamodeling," *Energy*, vol. 202, p. 117750, Jul. 2020, doi: 10.1016/j.energy.2020.117750.

[31] M. C. Peel, B. L. Finlayson, and T. A. McMahon, "Updated world map of the Köppen-Geiger climate classification," *Hydrol. Earth Syst. Sci.*, vol. 11, no. 5, pp. 1633–1644, Oct. 2007, doi: 10.5194/hess-11-1633-2007.

[32] "HVAC Library Mathematical Reference," p. 262.

[33] D. B. Crawley *et al.*, "EnergyPlus: creating a new-generation building energy simulation program," *Energy and Buildings*, vol. 33, no. 4, pp. 319–331, Apr. 2001, doi: 10.1016/S0378-7788(00)00114-6.

[34] US Office of Energy Efficiency & Renewable Energy, "Prototype Building Models," *Building Energy Codes Program*. https://www.energycodes.gov/prototype-building-models (accessed Jan. 20, 2022).

[35] G. N. Walton, "Thermal Analysis Research Program reference manual," *National Bureau of Standards*, vol. NBSSIR 83-2655, p. 21, 1983.

[36] "AIRLAN - Tecnología del Confort," *Airlan*. https://www.airlan.es/ (accessed May 20, 2022).

[37] S. Vall, A. Castell, and M. Medrano, "Energy Savings Potential of a Novel Radiative Cooling and Solar Thermal Collection Concept in Buildings for Various World Climates," *Energy Technol.*, vol. 6, no. 11, pp. 2200–2209, Nov. 2018, doi: 10.1002/ente.201800164.

[38] R. Vilà, I. Martorell, M. Medrano, and A. Castell, "Adaptive covers for combined radiative cooling and solar heating. A review of existing technology and materials," *Solar Energy Materials and Solar Cells*, vol. 230, p. 111275, Sep. 2021, doi: 10.1016/j.solmat.2021.111275.

[39] Ministerio de Fomento, "Código Técnico de la Edificación. Documento básico de ahorro de energía." Gobierno de España. [Online]. Available: https://www.codigotecnico.org/

[40] Instituto para la Diversificación y Ahorro de la Energía (IDAE), "Guía Técnica de Energía Solar Térmica." 2020.

CHAPTER VI
Potential maps for combined nocturnal radiative cooling
and diurnal solar heating applications in Europe

![Universitat de Lleida logo]
Universitat de Lleida

Chapter VI.   P3: Potential maps for combined nocturnal radiative cooling and diurnal solar heating applications in Europe

1. Introduction

Radiative cooling uses the outer space as a sink to dissipate heat from terrestrial bodies, allowing to achieve sub-ambient temperatures in the surface of these bodies. In this thesis it has been proposed to combine radiative cooling with solar heating process to obtain both heat and cold in a single device.

Nevertheless, radiative cooling and solar heating power strongly depend on the climatological conditions [14], [80]–[82]: for humid or cloudy regions, the heat rejection capacity is lower. According to the previous literature, there exists a variability between regions.

In **Chapter V** we have already seen that the improvement of the heat pump combined with an RCE field is different in each of the analysed climates. In this paper, cities with dry climates have been identified as the cities where the improvement was greater.

According to Vall and Castell [14], very little research has been conducted on evaluating the radiative cooling power potential for various climates and regions; instead, the majority of papers published in the literature evaluate the power potential in a certain location. There was a need of a tool that could bring broader information of the potential of this technology. This tool could become an aid to drive public policies on the usage of renewable energies.

The potential of radiative cooling had already been evaluated in the United States [69] and China [70] using geostatistical methods to obtain radiative cooling potential maps. In Europe, the first attempt to evaluate the radiative cooling power potential was done by Argiriou et al. [67] in 1992; in the research, authors estimated the nocturnal radiative cooling performance of 28 locations of southern Europe. In 2021, Aili et al. [71] mapped the average summer and winter potential worldwide; the researchers also crossed the

CHAPTER VI
Potential maps for combined nocturnal radiative cooling
and diurnal solar heating applications in Europe

cooling potential with the population density. However, the maps presented by Aili et al. presented low scale resolution due to the size of the map.

There was still a need to evaluate the potential in Europe. Moreover, the potential of combined technologies (RCE) had not been evaluated yet. **Chapter VI** presents nocturnal radiative cooling and diurnal solar heating potential resource maps for contiguous Europe. A methodology to combine both potential maps is presented and the most suitable regions to apply both combined systems are identified.

2. Contribution to the state of the art

In paper P3, nocturnal radiative cooling source maps for power and energy potential are presented for the first time in contiguous Europe. The maps were generated by Kriging geostatistical interpolation using meteorological data from more than 1700 weather station distributed all-over the region (**Fig 19**).
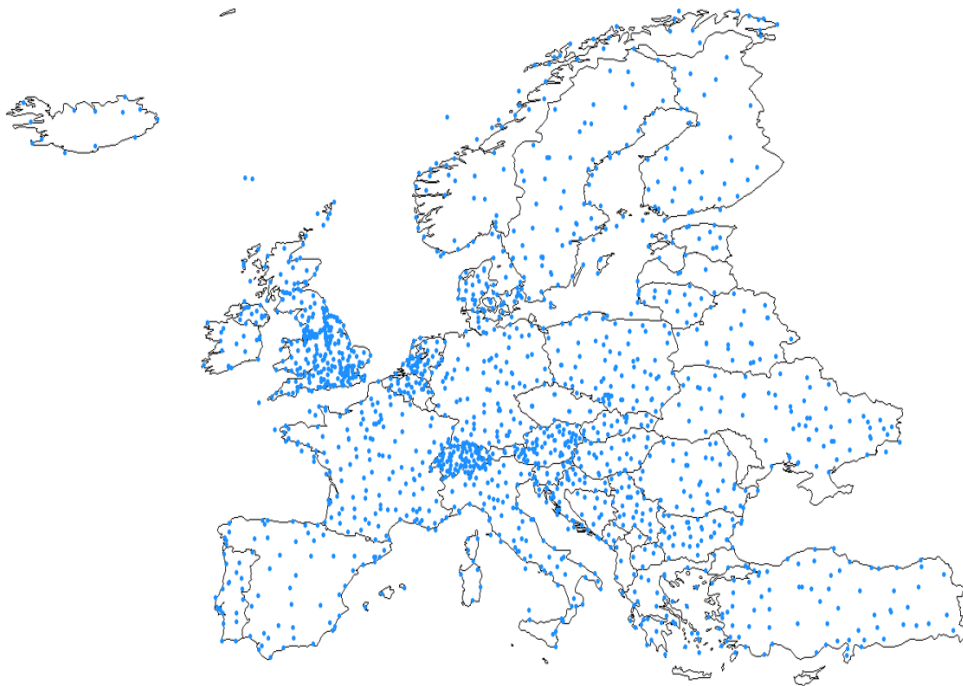
Fig 19. Distribution of the meteorological sample points.

The model was validated by means of a Leave-one-out-validation (LOOCV). Coefficient of determination (R^2), root mean square error (RMSE) and normalized root mean square error (NRMSE) were the metrics chosen to evaluate the performance of the interpolations.

The results of the metrics are summarised in **Table 1**. R^2 presented values higher than 0.84 in all the cases while the NRMSE was lower than 7%. The models were demonstrated to perform well and were suitable to predict solar heating and radiative cooling potential in unknown locations.

Table 1. Performance of the Kriging models in radiative cooling and solar heating maps.

	R2	RMSE	NRMSE
RC - Power	0.84	2.43 W/m²	6.45%
RC - Energy	0.84	10.75 kWh/m²·year	6.96%
SH - Power	0.98	7.64 W/m²	3.01%
SH - Energy	0.98	35.27 kWh/m²·year	2.73%

The paper proposed a suitability index (*SI*), based on the formula of eq.5 to combine values of solar heating and radiative cooling production with different orders of magnitude. *SI* is used to identify suitable regions to apply RCE technologies.

$$SI = \left(\frac{x_{rc} - x_{rc,min}}{x_{rc,max} - x_{rc,min}} \cdot \omega_1 + \frac{x_{sh} - x_{sh,min}}{x_{sh,max} - x_{sh,min}} \cdot \omega_2 \right) \cdot 100$$

$$\omega_1 + \omega_2 = 1$$

(5)

Where x_{rc} is the predicted value of radiative cooling at a given location; $x_{rc,min}$, the lowest radiative cooling observation; $x_{rc,max}$, the highest radiative cooling observation; x_{sh} is the predicted value of solar heating at a given location; $x_{sh,min}$, the lowest solar heating observation; $x_{sh,max}$, the highest solar heating observation; and ω_1 and ω_2 are the weights factors for each functionality. In this study, weight factors were chosen to have the same weight ($\omega_1 = \omega_2 = 0.5$).

Suitability Index could be mapped, and regions were filtered according to more or less strict criteria both for power and energy. **Fig 20** and **Fig 21** are a sample of the SI maps generated.

CHAPTER VI
Potential maps for combined nocturnal radiative cooling
and diurnal solar heating applications in Europe
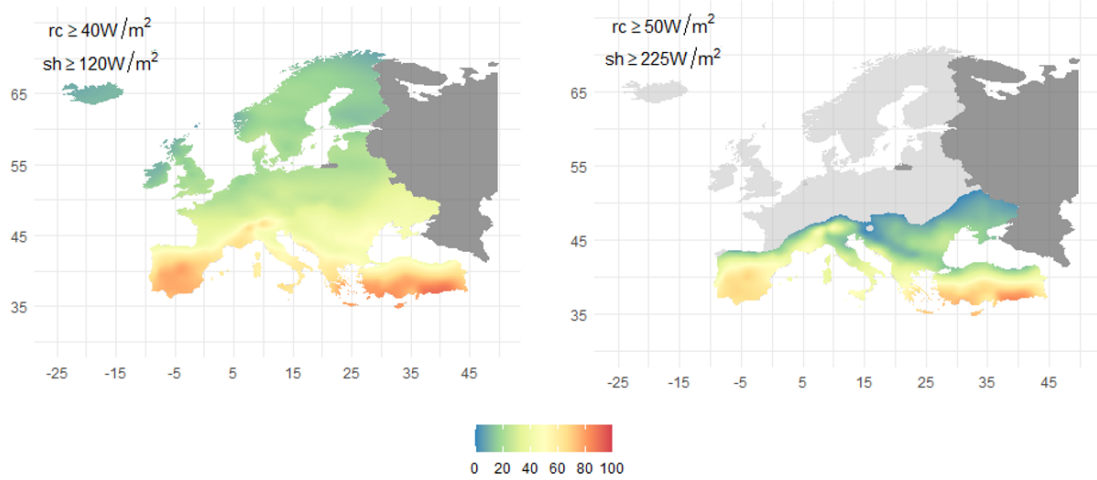
Fig 20. Suitability Index (%) for combined radiative cooling and solar heating applications for different power criteria. According to the criteria bright grey regions are not suitable for RCE applications. Zones coloured in dark grey have been excluded in this research.
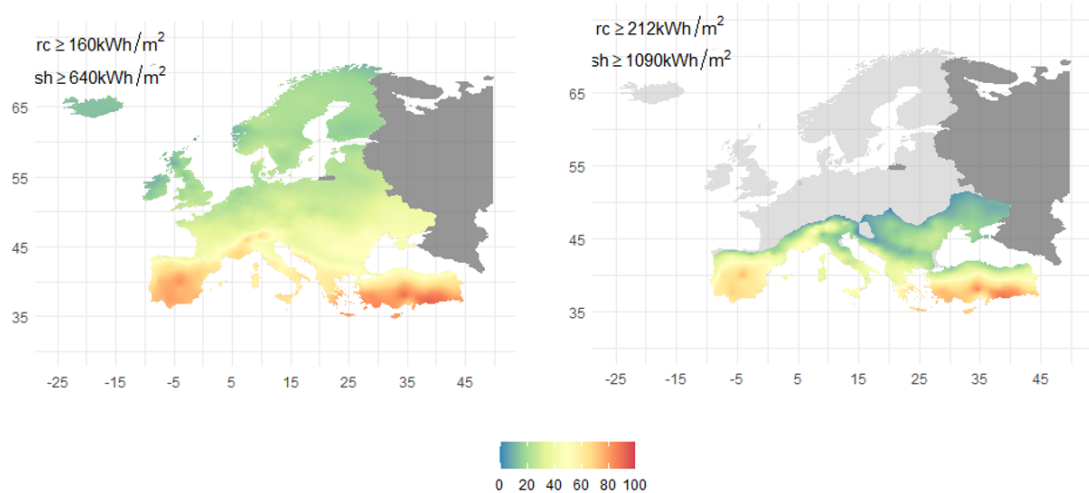
Fig 21. Suitability Index (%) for combined radiative cooling and solar heating applications for different energy criteria. According to the criteria bright grey regions are not suitable for RCE applications. Zones coloured in dark grey have been excluded in this research.

The previous maps, which allow the characterization of the different zones, are a step forward in the determination of the potential of RCE technologies. The maps can be used as a tool for the generation of policies that allow a faster implementation of this type of technology.

CHAPTER VI
Potential maps for combined nocturnal radiative cooling
and diurnal solar heating applications in Europe

3. Contribution to the objectives of the thesis

This chapter starts from hypothesis H3 and H4 and contributes to fulfil objective O4. Kriging proved to be a reliable tool to predict the radiative cooling potential in Europe.

On average, the annual power potential in Europe is 50.24 W/m^2, with peak values of 75.01 W/m^2, and the energy potential is 212.21 kWh/m^2·year. For solar heating, the average annual potential is 225.08 W/m^2 and 1152.36 kWh/m^2·year. After applying the presented *SI* index, the south was identified as the region in Europe where is more suitable to use RCE technologies.

4. Contribution of the candidate

Roger Vilà Miró was in charge of the conceptualization and the definition of the methodology, the interpolation, the data validation and the analysis of the results. The candidate also led the discussion of the results and the writing of the paper.

5. Journal Paper

This chapter was submitted to the journal *Renewable Energy*, published by Elsevier, and it is currently under a peer-review process

Potential Maps for Combined Nocturnal Radiative Cooling and Diurnal Solar Heating Applications in Europe

R. Vilà[1], L. Rincón[1], M. Medrano[1*] and A. Castell[1]

[1]Sustainable Energy, Machinery and Buildings (SEMB) Research Group, INSPIRES Research Centre, Universitat de Lleida,
Pere de Cabrera s/n, 25001 Lleida, Spain

[*]Corresponding author: marc.medrano@udl.cat

Abstract

Radiative cooling is a process by which a surface reduces its temperature by emitting thermal radiation towards the outer space. Radiative cooling technology can be combined, in a single device, with the existing technology of solar heating. A Radiative Collector and Emitter (RCE) can produce heat during the day and cold during the night in order to supply both cold and heat demands for temperature conditioning of spaces in a renewable way. The power generated by these devices strongly depends on the weather conditions of the place where it is used. Based on climatological data from 1791 weather stations in Europe, we predict the potential of power and energy production using Kriging interpolations. Detailed prediction maps of solar heating and radiative cooling potential are presented. Both potentials have been combined in order to obtain suitability maps of the RCE technology. The maps reveal the south as the European region where there is greater potential for the implementation of RCE technology.

Keywords: *radiative cooling, solar heating, potential map, renewable energy, spatial interpolation, Kriging, Europe.*

1. Introduction

In recent years, technologies based on the phenomenon of radiative cooling (RC) are starting to be considered as a renewable alternative, still under development, for the production of energy for cooling purposes.

Radiative cooling is the natural process by which terrestrial bodies reduce their surface temperature by emitting infrared radiation into the outer space, at a temperature of 3K [1]. All bodies emit electromagnetic radiation whose characteristics depend on its temperature. The peaks of radiation emitted by the terrestrial bodies (~ 300 K) fall in the wavelength range of 7-14 μm. In this range, the Earth's atmosphere is highly transparent (known as the atmospheric window), allowing the radiation to escape from the atmosphere and dissipate into the outer space [2].

Radiative cooling occurs when a positive imbalance exists between the emitted and the absorbed radiation. Surface temperatures below ambient temperature can be reached as a result of this imbalance. The thermal energy absorbed by the surface includes solar radiation, atmospheric radiation, and parasitic losses (convection and conduction). This phenomenon occurs mainly during clear nights, in the absence of solar radiation. However, in the last years, with the development of new metamaterials – which can reflect more than 90% of solar radiation– it has been possible to produce cold by radiative cooling during daylight hours [3]–[6].

Another research trend in the field of radiative cooling is the combination of RC technologies with solar heating (SH) applications. Although heat production is an opposed functionality, as it works in a different wavelength range (0.2-3 μm), the operation is analogous to radiative cooling [7]. Both functionalities lay in the same principle: the transfer of heat between a heat transfer fluid

and a capturing/emitting surface. In the solar heating mode, the surface captures incident solar radiation and transfers it to the heat transfer fluid; while, in the radiative cooling mode, the heat transfer fluid transfers heat to the surface which emits radiation to the outer space. This combination of functionalities allows to harvest both thermal energy demands on buildings and industrial processes. Liu et al. [8] stated that the payback of this technology could be of a period of 8 years.

In the literature, several experimental researches on the combination of radiative cooling and solar heating can be found. In 1987 Matsuta et al. [9] designed a selective solar collector and sky radiator with maximum heat fluxes of 610 W/m^2 of solar heating and 51 W/m^2 of radiative cooling. Hu et al. [10] manufactured a combined system based on an optical selective surface. Zhao et al. [11] designed a combined device that consisted of a transparent silica cavity, ultrapure single-walled carbon nanotubes aqueous dispersion, a solar reflective film and deionized water. An experimental proof of concept of a combined system by Vall et al. [12] demonstrated diurnal/nocturnal efficiencies up to 49% and 32%, respectively. The combination of both functionalities involves difficulties in the design of the working mode switching. To achieve this switching Liu et al. [8] proposed a rotating device where the different functionalities are achieved on the two sides of a flat surface. Vall et al. [12], [13] proposed an adaptive cover consisting on a sliding glass cover and a fixed polyethylene cover.

Radiative cooling provides a low cooling power range: between 20 and 80 W/m^2, with peaks of 120 W/m^2. This powers fall one order of magnitude below the power obtained by solar collection [14], [15]. The result of the radiation balance, both for radiative cooling and for solar heating, depends on the optical properties of the capturing/emitting surface, as well as on the meteorological conditions [16]–[18]. As a result of this last statement, the performance of a radiative collector and emitter (RCE) varies with the location.

Determining the maximum potential of solar heating and radiative cooling, as a result of the location, can be of great interest. The Global Solar Atlas is a well-known resource, developed by Solargis and the World Bank that aims *to provide access to solar resource and photovoltaic power potential data globally* [19]. The information of the Global Solar Atlas is presented in form of a contiguous map. Similar maps have been developed for other regions such as America and the USA [20], Europe [21] or Spain [22]. These maps are based on weather satellite measures [19], [20], [22] or the interpolation of data from ground weather stations [21], [23], [24] . To interpolate radiation data obtained from weather stations, Kriging is a recommended interpolator [21].

In the case of radiative cooling, Argiriou et al. [25] was the first to estimate the performance of a nocturnal radiative cooling in 28 locations in southern Europe. In the last years this study has been extended to bigger areas using geostatistical algorithms which have been used to map the radiative cooling potential in unknown regions based on the potential in a known region. Chang et al.[26] and Li et al.[27] used geostatisical interpolation methods to obtain radiative cooling potential maps in China and USA, respectively. Vilà et al. [28] compared the annual potential in Europe of a night-time radiative cooling surface and an all-day radiative cooling surface. Finally, Aili et al. [29] generated worldwide seasonal radiative cooling potential and global radiative cooling potential per capita maps.

Resource maps for solar radiation that can be found in the literature are commonly used for the identification of suitable locations for solar radiation implementation, as well as for the design of solar systems. Similarly, radiative cooling maps can be found in the literature, which can help the identification of suitable locations and the design of such systems. However, there is no attempt in the literature to combine both solar radiation and radiative cooling maps in order to determine the most suitable locations for a combined solar heating and radiative cooling (RCE) technology.

The main objective and innovation of this work is to propose a methodology to generate combined maps of radiative cooling and solar heating in order to identify the optimal regions in Europe with higher potential production of the RCE technology. For such purpose, both nocturnal radiative cooling and diurnal solar heating potential maps will be generated, based on Kriging interpolations, as the two natural outputs of the RCE device.

2. Methods

To obtain potential maps for both radiative cooling and solar heating, the geostatistical Kriging interpolation was used. Meteorological data from different weather stations in Europe were used as predictors. After an initial process of preparing the data sets, Kriging predictions were assessed. The performance of the model was estimated by means of a Leave-One-Out Cross-Validation (LOOCV) study. The next sections describe the steps followed in the research which include the data acquisition from European weather stations, the standardization of these data, calculation of the radiative cooling and solar heating potential, the training and testing of the Kriging model, the calculation of an index to combine both potentials, and the generation of the resource maps. **Fig 1** summarizes these steps.
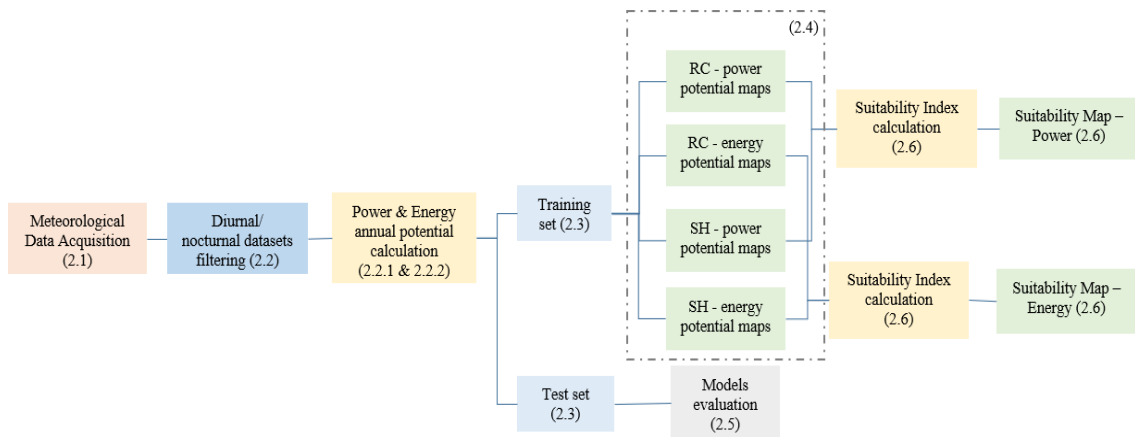
Fig 1. Illustration of the workflow followed in this research. Each step corresponds to one section, in brackets, of the Methods.

2.1. Data Acquisition

Weather data was obtained from the Meteonorm database. Meteonorm is a software that combines global meteorological data, space interpolations and stochastic weather generation [30] to provide access to typical years and historical time series.

Data corresponded to 1791 weather stations distributed in 46 European countries (**Fig 2**). The data used in the study belonged to the last set of measured data available for the year 2005. This dataset collected hourly data for the 365 days of the year. Study variables included ambient temperature, atmospheric infrared radiation and global horizontal solar radiation, relative humidity, clearness of the sky or atmospheric pressure. Ambient temperature, global horizontal solar radiation, relative humidity or atmospheric pressure were data measured at the weather station while atmospheric radiation was calculated by Metonorm based on the Aubinet model [31]. The datasets also provided geographic information (latitude, longitude and elevation) of each of the weather stations.
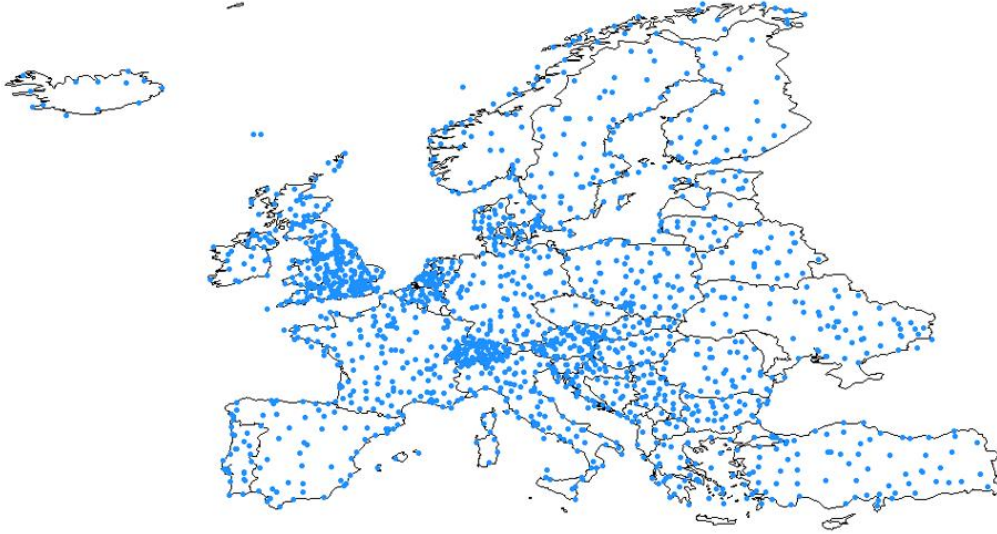
Data Pre-processing

Data pre-processing and data cleaning, as well as statistical analysis and spatial predictions, were done with Rstudio version 1.3. For geospatial predictions, the *sp* and *gstat* packages, available for R, were used.

The pre-processing of the data includes the standardization of variables with characters, filtering nocturnal and diurnal values and cleaning of NA and abnormal values. After the pre-processing the data was divided into two new datasets, corresponding to nocturnal data or diurnal data.

To calculate the maximum potential at a given point, the commonly used premises ([25]–[29]) were assumed as follows:

- Results from the literature [12] demonstrate that radiative cooling powers are one order of magnitude lower than solar heating ones. Thus, in this work the absorbing/emitting surface was placed horizontally to maximize the infrared emission towards the atmosphere.
- The absorbing/emitting surface behaved as a black-body surface ($\varepsilon_s = \alpha_s = 1$) in order to maximize infrared emissivity during night, and maximize solar collection during daytime.
- During daytime, infrared radiation emitted by the surface was totally blocked with a glass cover, providing greenhouse effect, as commonly done in solar thermal collectors. Losses related to the optical properties of the cover were neglected.
- Parasitic losses of conduction and convection were minimized ($q_{cond} = q_{conv} = 0$).
- The radiative surface is at ambient temperature.

2.2.1. Radiative cooling calculations

To calculate the radiative cooling power and energy, the nocturnal dataset of filtered data was used. Under steady conditions, the nocturnal net radiative cooling power of a surface can be calculated as a balance of the different incoming and outgoing radiations:

$$q_{net} = q_s(T_s) - q_a(T_a) - q_{cond} - q_{conv} \qquad (1)$$

Where q_s is the emitted radiation power on a surface at temperature T_s, q_a is the radiation emitted by the ambient at temperature T_a, and q_{cond} and q_{conv} are the parasitic losses of conduction and

convection. The units of power values are W/m^2 and temperatures are expressed in K. With the assumptions in 2.2, Eq.1 is simplified and the maximum radiative cooling potential is expressed as follows (Eq.2):

$$q_{net\_max,bb} = \sigma T_a^4 - q_{atm} = \sigma T_a^4 - L_{in} \ (W/m^2) \quad (2)$$

In Eq.2 $q_{net,bb}$ represents the net balance radiation of the black-body surface, expressed in W/m^2; q_{atm}, the radiation emitted by the atmosphere and absorbed by the surface, expressed in W/m^2; σ, the Stefan – Boltzmann constant, expressed in $W/(m^2 \cdot K^4)$; and L_{in} is the atmospheric radiation according to the Aubinet model (Eq.3) [31], expressed in W/m^2.

$$L_{in} = \sigma[94 + 12.6\log(100 \cdot e_s) - 13 \cdot KT_d + 0.341(T_{a\_C} + 273.15)^4 \quad (3)$$

Where σ is the Stefan-Boltzmann constant $\left(\frac{W}{m^2 \cdot K^4}\right)$; e_s is the saturated vapour pressure (hPa); KT_d is the clearness index (-) and T_{a_C} is the ambient temperature expressed in Celsius (^oC).

Eq. 2 was used to predict the hourly potential of nocturnal radiative cooling. Only positive values were used to predict the potential, corresponding to observations where radiative cooling could actually be achieved. The average annual potential was calculated according to Eq.4, where *n* is the total number of positive observations at each location.

$$q_{rc,annual} = \frac{\sum_i^n q_{net,bb}^+}{n} \ (W/m^2) \quad (4)$$

Every observation corresponded to a one-hour observation *(t = 1 h)*. Thus, the energy produced in a year was calculated as Eq.5.

$$e_{rc,annual} = \frac{\sum_i^n(q_{net,bb}^+ \cdot t)}{1000} \ \left(\frac{kWh}{m^2 \cdot year}\right) \quad (5)$$

2.2.2. Solar heating calculations

For solar heating calculations, diurnal dataset was used. Solar heating power was calculated assuming that maximum solar heating power at a certain time corresponded to the Global Horizontal radiation at that time. Only positive values were used in the calculation.

Annual average solar heating power potential and produced energy was calculated using Eq.6 and Eq.7. GHR corresponds to the Global Horizontal Radiation value.

$$q_{sh,annual} = \frac{\sum_i^n GHR}{n} (W/m^2) \quad (6)$$

$$e_{sh,annual} = \frac{\sum_i^n(GHR \cdot t)}{1000} \ \left(\frac{kWh}{m^2 \cdot year}\right) \quad (7)$$

2.3. Training and Test Datasets

Diurnal and nocturnal datasets were randomly divided into two new subsets: training set and test set. The training sets contained information from 80% of the locations and were used in the construction of the interpolation models for each mode of operation (radiative cooling or solar

heating). Test sets were used to evaluate the performance of each model. **Fig 3** shows and spatial distribution sample points used for the training and the test of the model.

2.4. Kriging Interpolation

Kriging is a method for predicting unknown values at different points based on known data [32]. In this study, Kriging was used as a geographic interpolation technique to generate continuous radiative cooling and solar heating resource maps (spatial resolution of the pixel of 6 x 8 km).

The Kriging methodology functions as a linear regression applied to spatial data which is used as regressor, $Z(s)$, in order to predict a dependent variable, $\hat{Z}(s_0)$, in a given point (Eq.8).

$$\hat{Z}(s_0) = \lambda_0 \, Z(s) \tag{8}$$

Weights (λ_0) are determined as a function of the difference between the neighbouring values of the different points of the sample. Kriging is considered to be a stochastic interpolation method that, in addition to the prediction surface, also provides a measure of the reliability of the predictions. The models trained by Kriging used the distance to the known points as the independent variable. The dependent variables were the radiative cooling and solar heating power potentials and energy potentials in each case.

2.5. Performance of the Model

To evaluate the accuracy of the Kriging model, predictions were made in the test dataset and the results were compared with the observed values. The coefficient of determination (R^2), and the root mean square error (RMSE) and the normalized root mean square error (NRMSE) were calculated (Eq.9) (Eq.10) (Eq.11).

$$R^2 = 1 - \frac{\sum_{i=1}^{N}\left(X_{i,m} - X_{i,p}\right)^2}{\sum_{i=1}^{N}\left(X_{i,m} - X_{avg,m}\right)^2} \tag{9}$$

$$RMSE = \sqrt{\frac{1}{N}\sum_{i=1}^{N}\left(X_{i,m} - X_{i,p}\right)^2} \tag{10}$$

$$NRMSE = \frac{RMSE}{X_{max,m} - X_{min,m}} \tag{11}$$

Where N is the total number of locations; $X_{i,m}$ is the observed value of the sample; $X_{i,p}$ is the value estimated in the model and $X_{avg,m}$ is the average of the observed values at the weather

stations. RMSE has the same units as the variable at interpolation while R^2 and NRSME are dimensionless.

2.6. Suitability Index (SI)

We propose a methodology to combine values of solar heating and radiative cooling production with different orders of magnitude. The suitability index is a qualitative value which allowed to identify the adequate regions to apply RCE technologies.

To reduce the influence of the higher values of solar heating compared to those of radiative cooling, feature scaling was applied to both solar heating and radiative cooling data. Feature scaling (Eq.12) reduces all values into a range between 0 and 1. Both potentials can then be weighted according to Eq.13.

$$x' = \frac{x - x_{min}}{x_{max} - x_{min}} \tag{12}$$

$$SI = \left(\frac{x_{rc} - x_{rc,min}}{x_{rc,max} - x_{rc,min}} \cdot \omega_1 + \frac{x_{sh} - x_{sh,min}}{x_{sh,max} - x_{sh,min}} \cdot \omega_2 \right) \cdot 100 \tag{13}$$

$$where\ \omega_1 + \omega_2 = 1$$

Where x' is the value of the variable after applying feature scaling; x is the predicted value x_{min} is the lowest predicted value and x_{max} is the highest predicted value. For radiative cooling interpolations, x_{rc} is the predicted value and $x_{rc,min}$ and $x_{rc,max}$ are the minimum and maximum predictions, respectively. In the case of the solar heating interpolations, x_{sh} is the predicted value and $x_{sh,min}$ and $x_{sh,max}$ are the minimum and the maximum. The variables ω_1 and ω_2 represent the weight that each interpolation has in the SI index in a considered location.

3. Results and Discussion
3.1. Model validation

The model validation was first conducted using the data of the test set, 20% of the data collected, equivalent to 352 locations of the sample. **Fig 4** shows the comparison between the predicted values and the observed values of the test set. The coefficient of determination (R^2) and the RMSE are shown in Table 1. High values of the coefficient of determination indicate that the model is able to explain a high proportion of the variability of the observations. The RMSE coefficient is a measure of the accuracy with which the model predicts the response, low values indicate a higher proportion. RMSE values are difficult to interpret without any reference, which is why we also include the normalized RMSE value (NRMSE).
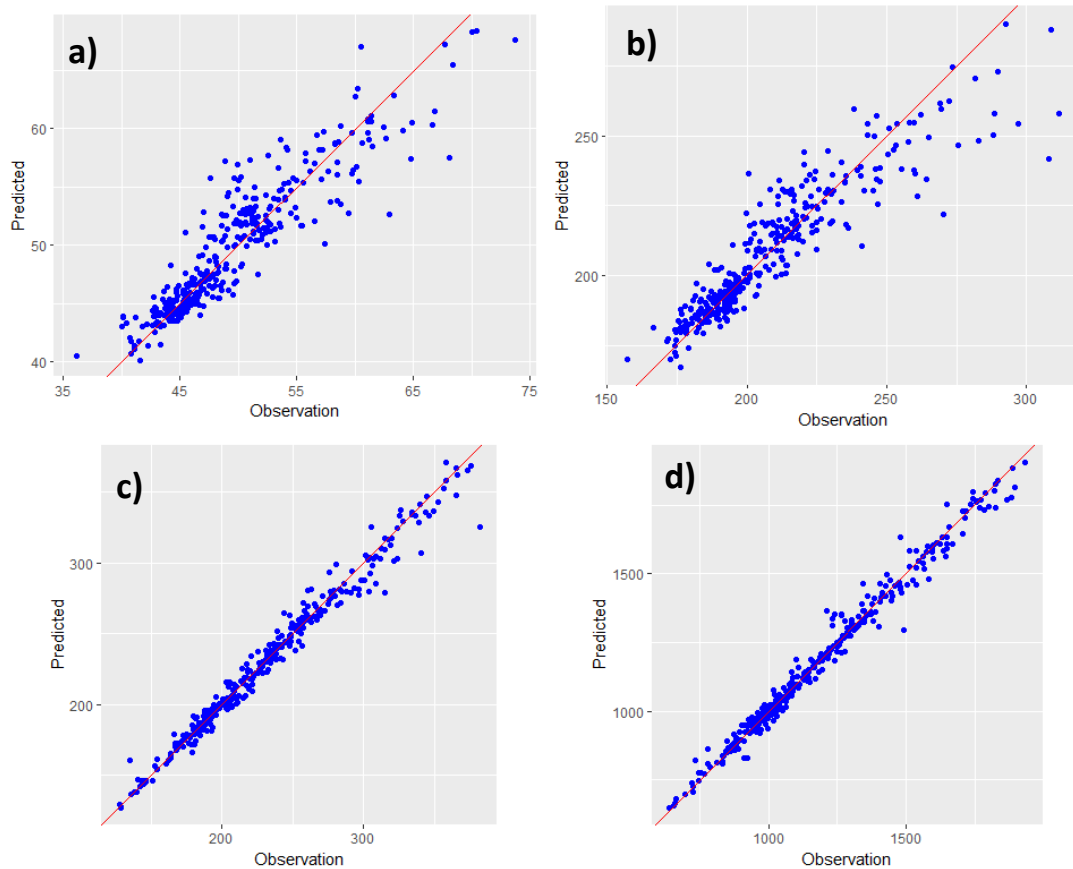
Fig 4. Scatterplots of observed values versus predicted values: (a) radiative cooling annual power potential (W/m2), (b) radiative cooling annual energy potential (kWh/m2·year), (c) solar heating annual power potential (W/m2) and (d) solar heating annual energy potential (kWh/m2·year).

Of the four cases, we observe that "RC - Energy" prediction performed worst. However, R^2 presents high values in all the four cases, especially, the solar heating values which are higher than 0.94. On the other hand, the NRMSE values are very low in solar heating predictions (less than 3.01%), while for radiative cooling predictions they do not exceed 7% error. Therefore, the models are accepted to be suitable for application in the prediction of solar heating and radiative cooling potential.

Table 1. Performance of the Kriging models

	R^2	RMSE	NRMSE
RC - Power	0.84	2.43 W/m^2	6.45%
RC - Energy	0.84	10.75 kWh/m^2·year	6.96%

SH - Power	0.98	7.64 W/m^2	3.01%
SH - Energy	0.98	35.27 kWh/m^2·year	2.73%

3.2. Radiative Cooling Resource Maps

Fig 5 shows the resulting resource maps – annual average power and annual energy produced – of radiative cooling in Europe after the application of Kriging interpolation.
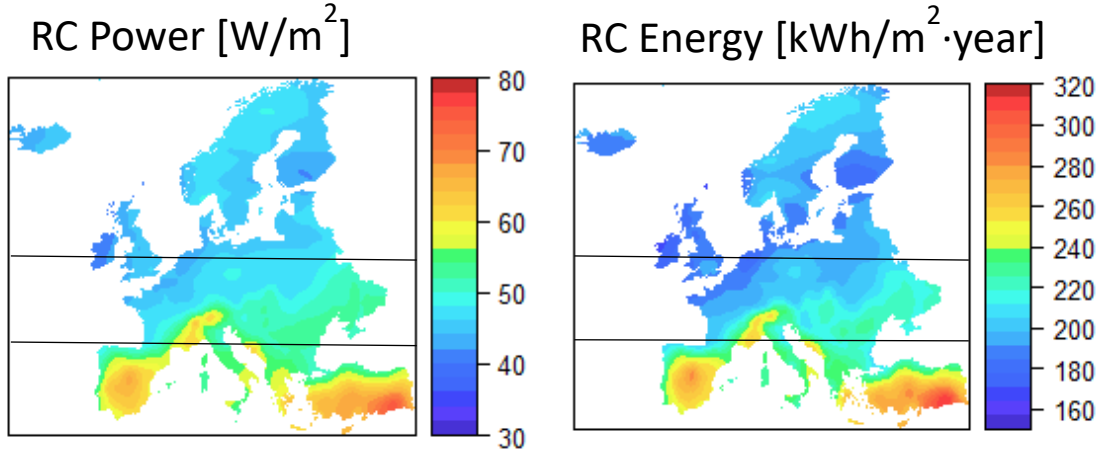
Fig 5. Radiative Cooling resource maps in Europe: annual average power potential (left) and annual energy potential (right). Horizontal lines divide the map into three regions: north (53.55 N–71.15 N), centre (43.46 N–53.55 N) and south (34.60 N–43.46 N).

The potential cooling power in Europe of an RCE surface lays between 40-75 W/m^2. The map is divided into three regions: the southern region, which covers the area between parallels 34.60 N and 43.46 N; the central region, which covers the area between the parallels 43.46 N and 53.55 N and the northern region, which covers the remaining area between the parallels 53.55 N and 71.15 N. As described in [28] the region with the highest radiative cooling potential is the Southern European region with areas where the average value can reach 75 W/m^2, and never less than 48 W/m^2 (Table 2). Northern Europe, on the other hand, is the region with the least potential. In this region the potential does not reach 50 W/m^2 per year. In central Europe, the potential ranges from 40.56 W/m^2 to 62.88 W/m^2. The centre and north have similar average potential values (49.23 and 45.32 W/m^2, respectively), while the average value for the southern region is 59.35 W/m^2.

Table 2. Minimum, average and maximum values for the predicted average annual radiative cooling power potential.

	Min [W/m^2]	Avg [W/m^2]	Max [W/m^2]
Europe	40.01	50.24	75.01
North	40.01	45.32	48.54
Centre	40.56	49.23	62.88
South	48.60	59.35	75.01

Regarding to the annual cooling energy potentials that can be obtained in an RCE surface, Table 3 shows that the average value of energy potential that can be obtained in northern Europe is 194.33 kWh/m^2·year, ranging between 166.98 kWh/m^2·year and 209.05 kWh/m^2·year; in central Europe, it is 207.01 kWh/m^2·year with valleys and peaks between 168.34 kWh/m^2·year and 258.84 kWh/m^2·year; and, in southern Europe, it is 248.08 kWh/m^2·year ranging between 204.49 kWh/m^2·year and 311.02 kWh/m^2·year. Southern Europe is the region with the highest energy potential of radiative cooling cold production. From [28] we know that in northern Europe there are many more hours of operation of a radiative cooling system, as the nights are ostensibly longer

for most part of the year, while the southern regions present shorter radiative cooling activity. We have seen that the average annual power potential and the annual energy potential are higher in the south rather than in the north. It can be concluded that longer number of hours does not mean more energy produced., as the higher radiative cooling powers in the south, with shorter nights, outperform longer nights in the north, but with smaller cooling powers.

Table 3. Minimum, average and maximum values for the predicted annual radiative cooling energy potential.

	Min [kWh/m²·year]	Avg [kWh/m²·year]	Max [kWh/m²·year]
Europe	166.98	212.21	311.02
North	166.98	194.33	209.05
Centre	168.34	207.01	258.84
South	204.49	248.08	311.02

3.3. Solar Heating Resource Maps

Solar heating potential maps in Europe are shown in **Fig 6**. The maps show a clear decreasing trend with latitude. The values of predicted solar heating power are an order of magnitude higher than those produced by radiative cooling. The annual average power potential in Europe lays between 126.66 W/m² and 376.77 W/m², with an average score of 225.08 W/m² (Table 4). The central and southern regions present average power potential above the average of the continent, 228.27 W/m² and 306.57 W/m², respectively. The annual power in the northern region ranges between 126.66 W/m² and 206.46 W/m²; the average potential is 166.28 W/m², 58.8 W/m² lower than the average of the continent.

*Table 4. Minimum, average and maximum values for the predicted annual average solar heating power potential.*
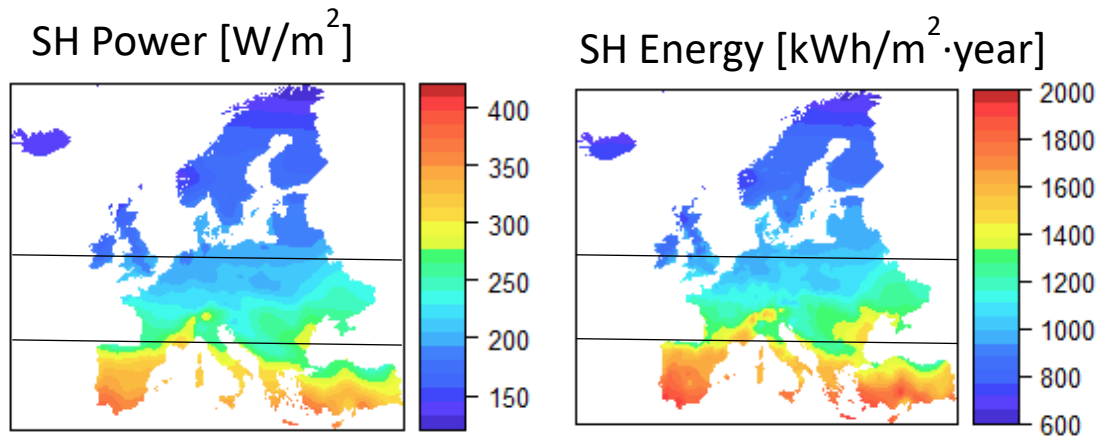
Fig 6. Solar Heating resource maps in Europe: annual average power potential (left) and annual energy potential (right). Horizontal lines divide the map into three regions: north (53.55 N–71.15 N), centre (43.46 N–53.55 N) and south (34.60 N–43.46).

	Min [W/m²]	Avg [W/m²]	Max [W/m²]
Europe	126.66	225.08	376.77
North	126.66	166.28	206.46
Centre	168.37	228.27	314.17
South	234.63	306.57	376.77

The average annual solar heating energy that can be obtained in Europe is 1152.36 kWh/m²·year. In the centre of Europe, the energy potential is close to the average of the continent (1166.05 kWh/m²·year), while the northern region is below the average (849.66 kWh/m²·year) and the south is above this value (1576.82 kWh/m²·year) (Table 5). In Turkey and Spain, most part of the

country presents average values above 1800 kWh/m^2·year; thus showing a strong availability of this natural energy resource.

Table 5. Minimum, average and maximum values for the predicted annual energy solar heating potential.

	Min [kWh/m^2·year]	Avg [kWh/m^2·year]	Max [kWh/m^2·year]
Europe	639.14	1152.36	1943.40
North	639.14	849.66	1074.06
Centre	851.22	1166.05	1624.39
South	1134.61	1576.82	1943.40

3.4. Discussion about the maximum potential

The maps presented in the previous sections represent the maximum radiative cooling and solar heating power and energy that can be potentially achieved in an RCE. The real power achieved by this technology will fall below these predictions. The difference between the maximum potential and the achieved in the RCE depend on the designing of the RCE, which includes the optical properties of its materials and the insulation of the device.

At the moment of writing this paper, the technology is still under the first stages of development and there is still a lack of available data. However, from a study by Vall et al. [12], the experimental results show that RCE presents average efficiencies of conversion of solar energy equal to 49% during the day; and average efficiencies of conversion of radiative cooling equal to 32% during the night. The latter proves that the current technology is still far from reaching the maximum potential presented in the previous maps.

3.5. Suitability index map

The combination of radiative cooling and solar heating resource maps has been done with the application of the suitability index, described in section 2.6, to each point of the prediction maps. As a result, the RCE technology' suitability index maps are presented in **Fig 7** and **Fig 8**. This index ranks the regions in a range from 0 to 100, where 0 indicates zero suitability and 100 indicates a total suitability.

Fig 7 shows the value of the index under different criteria of solar heating and radiative cooling power potential when considering the same weights ($\omega_1 = \omega_2 = 0.5$). As an example, in the second map the index has only been applied to those locations that meet the criteria that the radiative cooling power is greater than or equal to 40 W/m^2 and the solar heating power is greater than or equal to 170 W/m^2. The grey areas are the regions which do not meet the filtering criteria. Similarly, **Fig 8** shows the suitability maps under different energy filtering criteria.

Power and energy suitability maps present similar patterns among them. One might think that, using the power results, the energy maps can be directly obtained considering only the total night and day hours for radiative cooling and solar heating, respectively. But as described in section 2.2.1 and section 2.2.2, for the calculation of each of the potentials, only the positive observations of RC and SH power have been taken into account, which implies the discard of a series of observations. For this reason, both power and energy maps are plotted.

In both **Fig 7** and **Fig 8** it can be found that the most interesting regions to apply the combined technology of RCE are located in the south and the east of Europe. Of these regions, southern Turkey and southern Spain have a score in the suitability index higher than 70% in all the defined criteria. It is observed that, with a medium filtering criterion for radiative cooling production (45 W/m^2 and 185 kWh/m^2) and solar heating (170 W/m^2 and 865 kWh/m^2), the major part of the

continent is suitable for the application of RCE technology. In these cases, some regions in the north present low values but they are still suitable for the technology. If the criteria chosen are more restrictive the suitable areas are displaced to the south. It is also noted under these restrictive criteria, there is a small area in central Europe where it is still suitable to apply the technology.

A parametric study was done changing the weights from 0 to 1 in the SI index. The results are plot in the maps in Fig 9. Increasing the weight of the radiative cooling potential (ω_1) slightly diminishes the overall SI index. When the radiative cooling weight is lower than the solar heating weight – meaning that low production of RC is needed in comparison to SH – the southern coastal regions present high SI; when the radiative cooling weight is higher than solar heating weight, the highest suitability is found in the south-east of Turkey.

These maps consider the potential production of cold and heat, but they do not consider the difference in the energy demands due to the different climatology of each region. It is known, for example, that the north of Europe [33], which presents low score in the suitability index, is a cold region where there is low demand for refrigeration and high demand for heating, while southern Europe needs higher cooling rates but lower heating demands. It is proposed, as a future work, to cross the radiative cooling and solar heating resource maps presented here with the thermal energy demands of each region, in order to identify which part of the thermal energy demands can be covered by the RCE technology.

4. Conclusions

In this paper we have identified the areas of greatest potential for the application of the technology of combined radiative cooling and solar heating for heat and cooling production, named Radiative Collector and Emitter (RCE), in Europe.

Kriging interpolation of data from weather stations has proven to be a reliable tool to generate potential power and energy resource maps for nocturnal radiative cooling and solar heating of a horizontal RCE surface. The model has high performance values for both power and energy production.

On average, the annual radiative cooling potential in Europe is 50.24 W/m^2 and 212.21 kWh/m^2·year, and the solar heating potential is 225.08 W/m^2 and 1152.36 kWh/m^2·year. This potential was calculated assuming ideal conditions; in real applications, the performance of the RCE will be lower and will depend on the design of the RCE. In both heat and cold production, the southern region presents the highest potential while the north presents the lowest potential.

In the paper we have proposed a qualitative index to assess the suitability of the implementation of this technology based on the potential production capacity. No major differences were observed between the power and energy maps. Under restrictive criteria only the south and the east of the continent is suitable for the implementation of RCE. With medium restrictive criteria, the majority of the continent is suitable for the implementation. It has been proposed as future work to cross the predicted values of energy production with the thermal energy demands in buildings in order to identify the percentage of energy that RCE technology could cover.
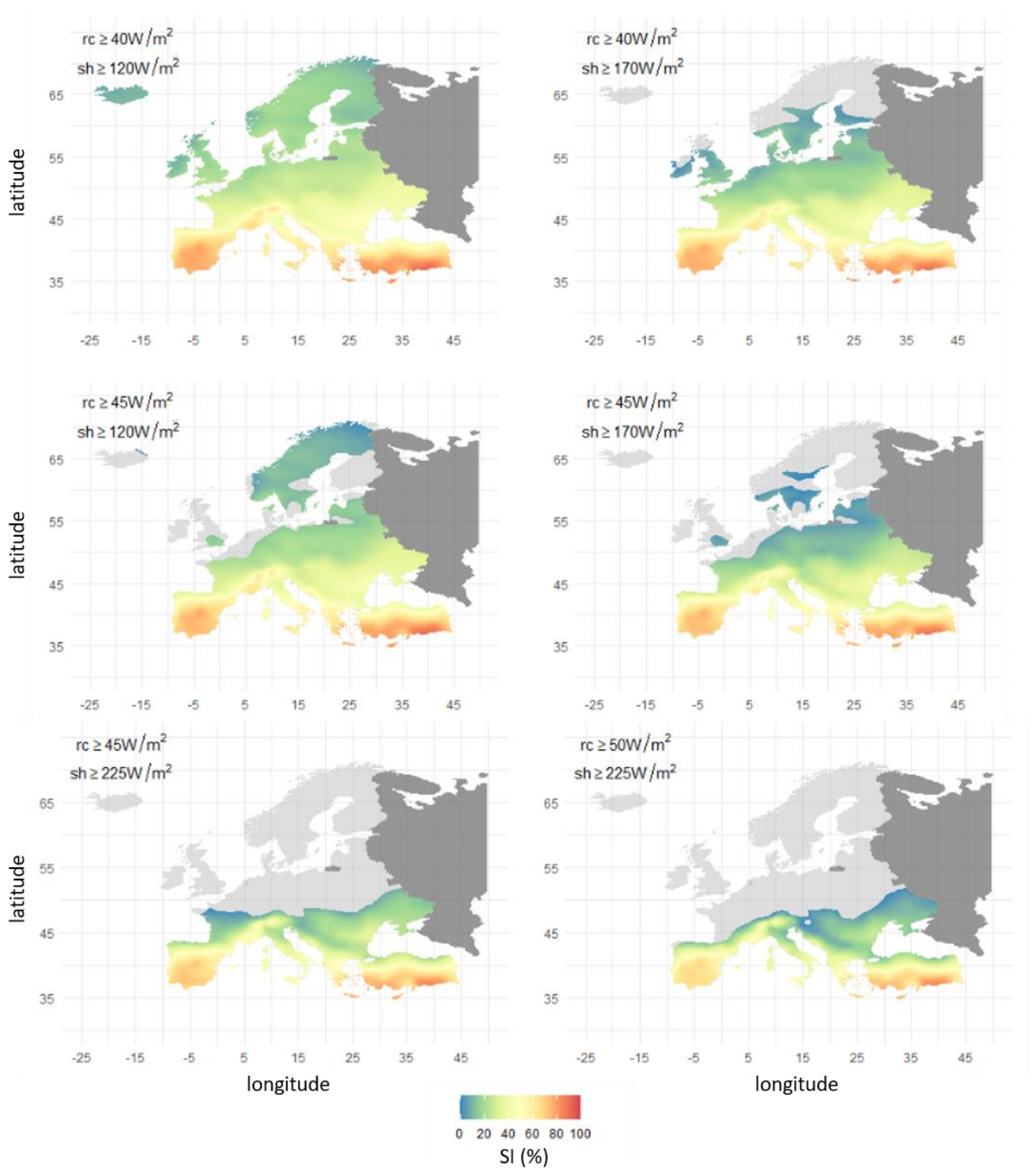
Fig 7. Suitability index (%) for combined radiative cooling and solar heating applications for different power criteria. According to the criteria bright grey regions are not suitable for RCE applications. Zones coloured in dark grey have been excluded in this research.

101
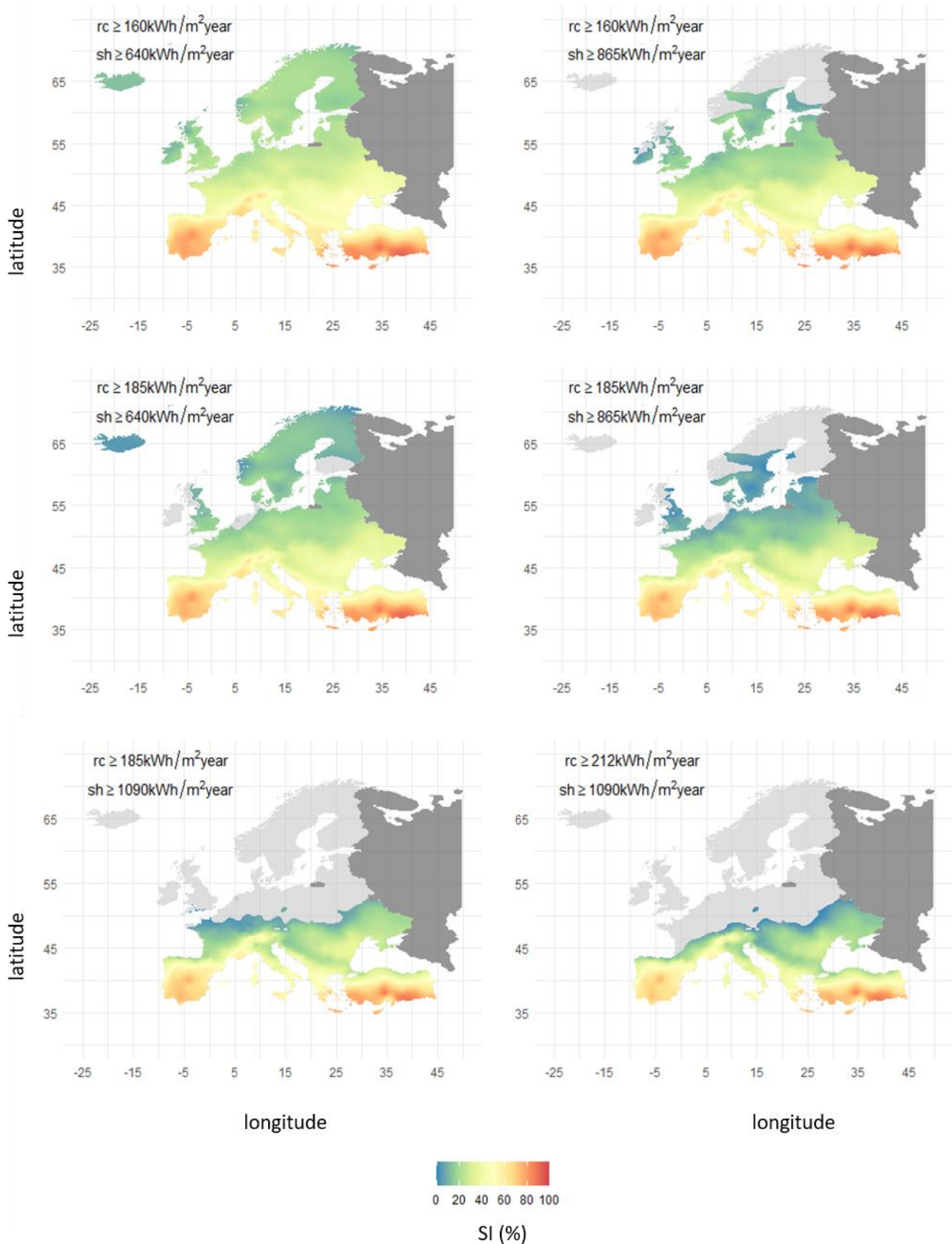
Fig 8. Suitability Index (%) for combined radiative cooling and solar heating applications for different energy criteria. According to the criteria bright grey regions are not suitable for RCE applications. Zones coloured in dark grey have been excluded in this research.
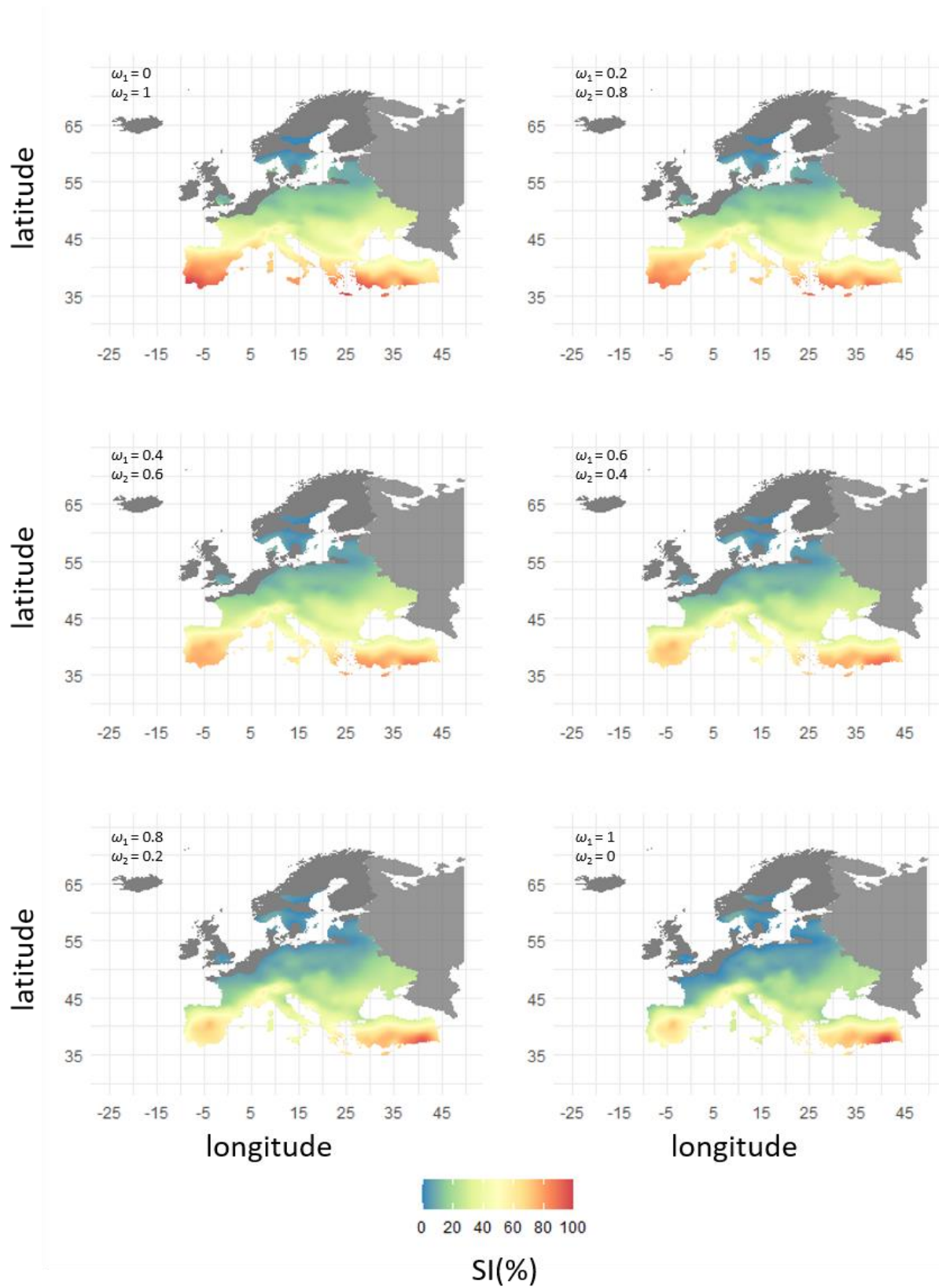
Fig 9. Suitability Index power maps for diferent weight values (ω_1 and ω_2). Radaitive cooling potential is higher than 45 W/m^2 and solar heating potential is higher than 170 W/m^2.

Bibliography

[1] D. J. Fixsen, «The temperature of the cosmic microwave background», *Astrophys. J.*, vol. 707, n.º 2, pp. 916-920, dic. 2009, doi: 10.1088/0004-637X/707/2/916.

[2] S. Vall y A. Castell, «Radiative cooling as low-grade energy source: A literature review», *Renew. Sustain. Energy Rev.*, vol. 77, pp. 803-820, sep. 2017, doi: 10.1016/j.rser.2017.04.010.

[3] A. P. Raman, M. A. Anoma, L. Zhu, E. Rephaeli, y S. Fan, «Passive radiative cooling below ambient air temperature under direct sunlight», *Nature*, vol. 515, n.º 7528, pp. 540-544, nov. 2014, doi: 10.1038/nature13883.

[4] E. Rephaeli, A. Raman, y S. Fan, «Ultrabroadband Photonic Structures To Achieve High-Performance Daytime Radiative Cooling», *Nano Lett.*, vol. 13, n.º 4, pp. 1457-1461, abr. 2013, doi: 10.1021/nl4004283.

[5] Y. Zhai *et al.*, «Scalable-manufactured randomized glass-polymer hybrid metamaterial for daytime radiative cooling», *Science*, vol. 355, n.º 6329, pp. 1062-1066, mar. 2017, doi: 10.1126/science.aai7899.

[6] B. Ko, D. Lee, T. Badloe, y J. Rho, «Metamaterial-Based Radiative Cooling: Towards Energy-Free All-Day Cooling», *Energies*, vol. 12, n.º 1, p. 89, dic. 2018, doi: 10.3390/en12010089.

[7] R. Vilà, I. Martorell, M. Medrano, y A. Castell, «Adaptive covers for combined radiative cooling and solar heating. A review of existing technology and materials», *Sol. Energy Mater. Sol. Cells*, vol. 230, p. 111275, sep. 2021, doi: 10.1016/j.solmat.2021.111275.

[8] J. Liu *et al.*, «Research on the performance of radiative cooling and solar heating coupling module to direct control indoor temperature», *Energy Convers. Manag.*, vol. 205, p. 112395, feb. 2020, doi: 10.1016/j.enconman.2019.112395.

[9] M. Matsuta, S. Terada, y H. Ito, «Solar Heating and radiative cooling using a solar collector-sky radiator with a spectrally selective surface», *Sol. Energy*, vol. 39, n.º 3, pp. 183-186, 1987.

[10] M. Hu, G. Pei, Q. Wang, J. Li, Y. Wang, y J. Ji, «Field test and preliminary analysis of a combined diurnal solar heating and nocturnal radiative cooling system», *Appl. Energy*, vol. 179, pp. 899-908, 2016, doi: 10.1016/j.apenergy.2016.07.066.

[11] B. Zhao, M. Hu, Q. Xuan, T. H. Kwan, Y. N. Dabwan, y G. Pei, «Tunable thermal management based on solar heating and radiative cooling», *Sol. Energy Mater. Sol. Cells*, vol. 235, p. 111457, ene. 2022, doi: 10.1016/j.solmat.2021.111457.

[12] S. Vall, M. Medrano, C. Solé, y A. Castell, «Combined Radiative Cooling and Solar Thermal Collection: Experimental Proof of Concept», *Energies*, vol. 13, n.º 4, p. 893, feb. 2020, doi: 10.3390/en13040893.

[13] S. Vall, K. Johannes, D. David, y A. Castell, «A new flat-plate radiative cooling and solar collector numerical model: Evaluation and metamodeling», *Energy*, vol. 202, p. 117750, jul. 2020, doi: 10.1016/j.energy.2020.117750.

[14] U. Eicker y A. Dalibard, «Photovoltaic-thermal collectors for night radiative cooling of buildings», *Sol. Energy*, vol. 85, n.º 7, pp. 1322-1335, 2011, doi: 10.1016/j.solener.2011.03.015.

[15] B. Bhatia *et al.*, «Passive directional sub-ambient daytime radiative cooling», *Nat. Commun.*, vol. 9, n.º 1, p. 5001, nov. 2018, doi: 10.1038/s41467-018-07293-9.

[16] P. Berdahl y R. Fromberg, «The thermal radiance of clear skies», *Sol. Energy*, vol. 29, n.º 4, pp. 299-314, 1982, doi: 10.1016/0038-092X(82)90245-6.

[17] R. Tang, Y. Etzion, y I. A. Meir, «Estimates of clear night sky emissivity in the Negev Highlands, Israel», *Energy Convers. Manag.*, vol. 45, n.º 11-12, pp. 1831-1843, 2004, doi: 10.1016/j.enconman.2003.09.033.

[18] M. Li y C. F. M. Coimbra, «On the effective spectral emissivity of clear skies and the radiative cooling potential of selectively designed materials», *Int. J. Heat Mass Transf.*, vol. 135, pp. 1053-1062, jun. 2019, doi: 10.1016/j.ijheatmasstransfer.2019.02.040.

[19] «Global Solar Atlas». https://globalsolaratlas.info/map (accedido 1 de septiembre de 2022).

[20] M. Sengupta, Y. Xie, A. Lopez, A. Habte, G. Maclaurin, y J. Shelby, «The National Solar Radiation Data Base (NSRDB)», *Renew. Sustain. Energy Rev.*, vol. 89, pp. 51-60, jun. 2018, doi: 10.1016/j.rser.2018.03.003.

[21] H. G. Beyer, G. Czeplak, U. Terzenbach, y L. Wald, «Assessment of the method used to construct clearness index maps for the new European Solar Radiation Atlas (ESRA)», *Sol. Energy*, vol. 61, n.º 6, pp. 389-397, dic. 1997, doi: 10.1016/S0038-092X(97)00084-4.

[22] J. M. Sancho Avila, J. Riesco, C. Jiménez, M. C. Sánchez de Cos Escuin, J. Montero, y M. López, «Atlas de Radiación Solar en España utilizando datos del SAF de Clima de EUMETSAT», *Minist. Agric. Aliment. Medio Ambiente*, vol. Agencia Estatal de Meteorología (AEMET).

[23] H. Alsamamra, J. A. Ruiz-Arias, D. Pozo-Vázquez, y J. Tovar-Pescador, «A comparative study of ordinary and residual kriging techniques for mapping global solar radiation over southern Spain», *Agric. For. Meteorol.*, vol. 149, n.º 8, pp. 1343-1357, ago. 2009, doi: 10.1016/j.agrformet.2009.03.005.

[24] A. Pettazzi y S. S. Casado, «Conselleria de Medio Ambiente, Territorio e Infraestructura (MeteoGalicia, Área de Observación e Climatología)», p. 125.

[25] A. Argiriou, M. Santamouris, C. Balaras, y S. Jeter, «Potential of radiative cooling in southern Europe», *Int. J. Sol. Energy*, vol. 13, n.º 3, pp. 189-203, ene. 1992, doi: 10.1080/01425919208909784.

[26] K. Chang y Q. Zhang, «Modeling of downward longwave radiation and radiative cooling potential in China», *J. Renew. Sustain. Energy*, vol. 11, n.º 6, p. 066501, nov. 2019, doi: 10.1063/1.5117319.

[27] M. Li, H. B. Peterson, y C. F. M. Coimbra, «Radiative cooling resource maps for the contiguous United States», *J. Renew. Sustain. Energy*, vol. 11, n.º 3, p. 036501, may 2019, doi: 10.1063/1.5094510.

[28] R. Vilà, M. Medrano, y A. Castell, «Mapping Nighttime and All-Day Radiative Cooling Potential in Europe and the Influence of Solar Reflectivity», *Atmosphere*, vol. 12, n.º 9, p. 1119, ago. 2021, doi: 10.3390/atmos12091119.

[29] A. Aili, X. Yin, y R. Yang, «Global Radiative Sky Cooling Potential Adjusted for Population Density and Cooling Demand», *Atmosphere*, vol. 12, n.º 11, p. 1379, oct. 2021, doi: 10.3390/atmos12111379.

[30] J. Remund, S. Müller, S. Kunz, B. Huguenin-Landl, C. Studer, y R. Cattin, «Meteonorm». Meteotest, Switzerland, 23 de julio de 2019. [Windows Vista/7/8/10 32/64 bit]. Disponible en: https://meteonorm.com/en/download

[31] M. Aubinet, «Longwave sky radiation parametrizations», *Sol. Energy*, vol. 53, n.º 2, pp. 147-154, 1994, doi: 10.1016/0038-092X(94)90475-8.

[32] T. Hengl, «A Practical Guide to Geostatistical Mapping of Enviromental Variables», *Off. Off. Publ. Eur. Communities*, p. 165, 2007, doi: JRC38153.

[33] U. Persson y S. Werner, «Quantifying the Heating and Cooling Demand in Europe», STRATEGO Enhanced Heating & Cooling Plans, IEE/13/650, 2015.

CHAPTER VII
Mapping night-time and all-day radiative cooling
potential in Europe and the influence of solar reflectivity

Chapter VII.   P4: Mapping night-time and all-day radiative cooling potential in Europe and the influence of solar reflectivity

1. Introduction

In recent years the research in radiative cooling - thanks to the development of metamaterials - has moved towards the production of all-day radiative cooling to fully activate its potential to generate cold. In **Chapter V** it was showed that for nocturnal radiative cooling mode a large RCE collecting surface is needed, while the RCE field is underutilized during the production of DHW. New designs could be proposed in order to adapt the production of cold or heat during the day, depending on the demand requirements, while during the night it could work as a normal night radiator.

Chapter VI presents source maps of the potential of nocturnal radiative cooling potential. **Chapter VII**, which presents paper P4, aims to go one step further and complementing the previous maps with resource maps of the potential of all-day radiative cooling. The paper provides a parametric study of the evolution of potential power and energy as a function of the solar reflectivity of the radiator.

2. Contribution to the state of the art

The paper shows for the first time a comparison between the potential of nocturnal radiative cooling and all-day radiative cooling in Europe, mapping both power and energy (**Fig 22** and **Fig 23**).

CHAPTER VII
Mapping night-time and all-day radiative cooling
potential in Europe and the influence of solar reflectivity
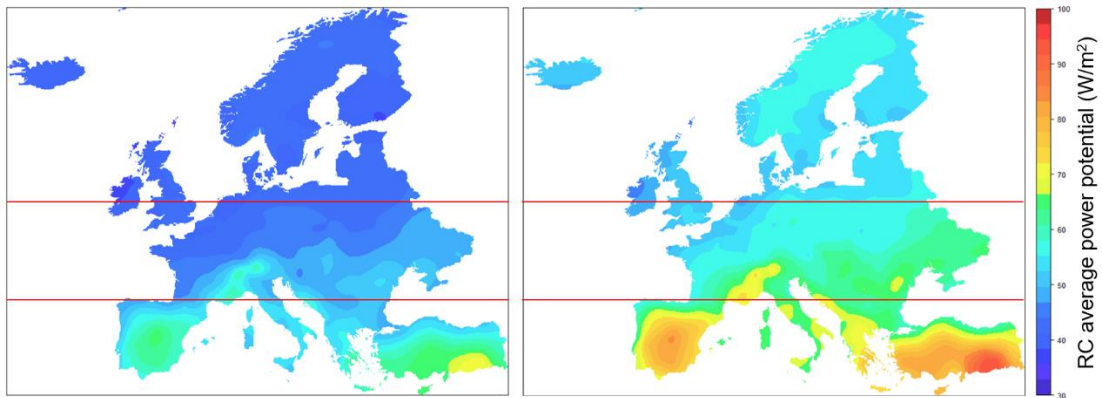
Fig 22. Map of annual power potential (kWh/m²·year) of nocturnal radiative cooling (left) and all-day radiative cooling of an ideal solar reflective surface (right). Horizontal red lines divide the map into three zones: north (53.55 N–71.15 N), centre (43.46 N–53.55 N) and south (34.60 N–43.46 N).
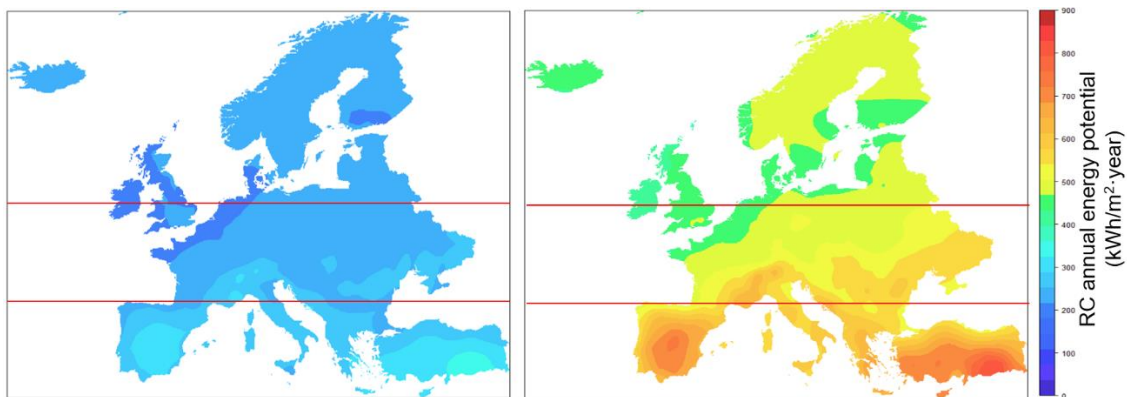
Fig 23. Map of annual energy potential (kWh/m²·year) of nocturnal radiative cooling (left) and all-day radiative cooling of an ideal solar reflective surface (right). Horizontal red lines divide the map into three zones: north (53.55 N–71.15 N), centre (43.46 N–53.55 N) and south (34.60 N–43.46 N).

The results show that shifting from nocturnal radiative cooling to all-day radiative cooling, on an ideal surface, the increasing of the average annual power potential is equivalent to 27.21%, while the increasing of the annual average energy potential is equivalent to 126.65 %.

The parametric study shows the importance of the reflectivity. When the solar reflectivity is equal to or below 50%, the emissive surface behaves like a nocturnal radiative cooler: during the day the sunlight absorbed by the surface balances the radiation emitted by it and the surface can no longer produce cold. Shifting from an ideal reflectivity of 100% to a reflectivity of 90%, the energy potential dropped 28.45%. Today, materials with 99%

reflectivity have been developed; these materials could show potentials close to the maximum predictions shown in the paper.

The paper also presents an analysis of the potential disaggregated by region, showing that southern Europe is the region where, on average, higher powers and energies can be obtained compared to central and northern Europe. **Table 2** and **Table 3** show the predicted results of the parametric study.

Table 2. Minimum, average and maximum values for each solar reflectivity. Potential maps of RC power (W/m^2).

	Latitude Range			Solar Reflectivity				
			1	0.9	0.8	0.7	0.6	0.5
Center	43.46 N–53.55 N	Min	46.43	36.31	34.20	34.65	35.09	35.82
		Avg	58.69	45.27	41.31	42.40	43.34	44.12
		Max	73.08	56.17	51.62	53.81	55.98	57.87
North	53.55 N–71.15 N	Min	43.82	35.70	33.78	33.55	33.88	34.09
		Avg	53.77	43.76	39.31	39.59	39.95	40.23
		Max	57.81	48.00	42.19	42.25	42.90	43.38
South	34.60 N–43.46 N	Min	56.36	42.23	40.80	42.43	43.67	44.41
		Avg	72.33	54.33	49.84	52.51	53.72	55.05
		Max	94.01	72.76	62.24	66.05	67.16	69.14
Europe	34.60 N–71.15 N	Min	43.82	35.70	33.76	33.55	33.88	34.09
		avg	60.18	46.87	42.61	43.79	44.59	45.32
		max	94.01	72.56	62.34	66.05	67.16	69.14

Table 3. Minimum, average and maximum values for each solar reflectivity. Potential maps of annual RC energy ($kWh/m^2 \cdot year$).

	Latitude Range			Solar Reflectivity				
			1	0.9	0.8	0.7	0.6	0.5
Center	43.46 N–53.55 N	min	406.74	312.63	254.79	228.15	220.30	213.05
		avg	514.16	396.23	309.89	278.54	263.55	254.74
		max	639.71	493.03	378.74	333.92	322.46	317.90
North	53.55 N–71.15 N	min	384.08	313.42	258.55	232.97	221.06	213.08
		avg	470.99	383.47	311.62	280.07	264.03	253.50
		max	506.40	422.26	346.71	309.46	291.11	278.34
South	34.60 N–43.46 N	min	493.88	368.86	281.38	266.07	246.96	240.26
		avg	633.56	475.55	360.98	323.36	306.98	299.93
		max	822.66	642.35	492.60	413.61	397.85	388.09
Europe	34.60 N–71.15 N	min	384.08	312.63	254.79	228.15	220.30	213.05
		avg	527.10	410.35	322.43	289.55	273.87	264.87
		max	822.66	642.35	492.60	413.61	397.85	388.09

CHAPTER VII
Mapping night-time and all-day radiative cooling
potential in Europe and the influence of solar reflectivity

3. Contribution to the objectives of the thesis

This chapter starts from hypothesis H3 and H4 and contributes to fulfil objective O4 and O5, proving a great improvement of the annual potential when shifting from a nocturnal radiative cooling surface to an ideal all-day radiative cooling surface.

Paper P4 provides resource maps of power and energy for both nocturnal and all-day radiative cooling. A parametric study of the potential was performed changing the reflectivity to solar radiation, showing that for reflectivity values close to 50% the surface behaves like a nocturnal radiator. It is also discussed that to fully take advantage of its potential, reflectivity should not be lower than 90%. Finally, the south continues being the region of Europe where the potential for all-day radiative cooling is greatest.

4. Contribution of the candidate

Roger Vilà Miró was in charge of the conceptualization and the definition of the methodology, the interpolation, the data validation and the analysis of the results. The candidate also led the discussion of the results and the writing of the paper.

5. Journal Paper

This chapter was published in *Atmosphere 12 (2021) 1119*, https://doi.org/10.3390/atmos12091119.

Mapping Nighttime and All-Day Radiative Cooling Potential in Europe and the Influence of Solar Reflectivity

Roger Vilà [iD], Marc Medrano and Albert Castell *[iD]

Sustainable Energy, Machinery and Buildings (SEMB) Research Group, INSPIRES Research Centre, Universitat de Lleida, Pere de Cabrera s/n, 25001 Lleida, Spain; roger.vila@udl.cat (R.V.); marc.medrano@udl.cat (M.M.)
* Correspondence: albert.castell@udl.cat; Tel.: +34-973003570

Article

Mapping Nighttime and All-Day Radiative Cooling Potential in Europe and the Influence of Solar Reflectivity

Roger Vilà [ID], Marc Medrano and Albert Castell *[ID]

Sustainable Energy, Machinery and Buildings (SEMB) Research Group, INSPIRES Research Centre, Universitat de Lleida, Pere de Cabrera s/n, 25001 Lleida, Spain; roger.vila@udl.cat (R.V.); marc.medrano@udl.cat (M.M.)
* Correspondence: albert.castell@udl.cat; Tel.: +34-973003570

Abstract: Radiative cooling is a natural process to cool down surfaces through the rejection of thermal radiation using the outer space as a cold sink, taking advantage of the transparency of the atmospheric windows (8–14 μm), which partially matches the infrared radiation band. With the development of new materials that have a high reflectivity of solar radiation, daytime radiative cooling can be achieved. This phenomenon depends on the optical properties of the surface and the local weather conditions. In this research, climatological data from 1791 weather stations were used to present detailed nighttime and all-day radiative cooling maps for the potential implementation of radiative cooling-based technologies. The paper offers a parametric study of the variation of the potential as a result of decreasing the solar reflectivity. The results show that southern Europe is the region with the highest potential while northern Europe holds more hours of available radiative cooling. After varying the solar reflectivity from 1 to 0.5 the average power reduces from 60.18 to 45.32 W/m^2, and energy from 527.10 to 264.87 $kWh/m^2 \cdot year$. For solar reflectivity lower than 0.5, all-day radiative coolers behave as nighttime radiative coolers, but power and energy values improve significantly for high values of solar reflectivity. Small variations of solar reflectivity have greater impacts on the potential at higher reflectivity values than at lower ones.

Keywords: radiative cooling; nighttime radiative cooling; daytime radiative cooling; all-day radiative cooling; cooling potential; potential maps; spatial interpolation; Kriging; Europe

1. Introduction

Radiative cooling (RC) is a natural cooling process already used in 400 BC in ancient Iran for ice production [1]. In recent years it has experienced a new awakening. During the 1960s and 1970s the phenomenon began to be studied systematically [2,3]. However, it is in this last decade, driven by the needs for a change in the model of energy production and consumption, when technologies based on RC are positioned as promising solutions for the production of clean and green energies for space cooling purposes.

Radiative cooling is known to be the process by which a surface reduces its temperature through the emission of thermal radiation into the outer space. It benefits from the high transparency of the atmosphere in 8–14 μm wavelength range, named atmospheric window, which partially matches the peak of infrared radiation emitted by terrestrial bodies at ambient temperatures. This cooling process occurs when a net imbalance exists between the emitted and the absorbed heat; solar radiation, atmospheric radiation and parasitic losses (convection and conduction) also accounted for in this net balance. This technique allows for achieving temperatures below ambient [4].

The first selective surfaces (also called emitters), emitting in the 8–14 μm range, were designed to achieve RC during night time [2,5]. In 1975, Catalanotti et al. [3] obtained radiative cooling during daytime, but the performance was poor. Overcoming solar radiation was a great challenge. In 2014, Raman et al. [6] demonstrated a temperature drop—4–5 °C—below ambient under direct sunlight in photonic radiative cooling, which

combined layers of SiO_2 and HfO_2 on top of a silver surface. The recent development of new multilayer thin structures [6–8], porous polymers [9–11], nanoparticle materials [12], metamaterials [13–16] and photonic crystals [17–19], allows the manufacture of selective surfaces which emit only in the 8–14 μm range while reflecting the incoming solar radiation.

Several authors have conducted simulation studies in order to predict the potential of radiative cooling technologies. Vall et al. [20] modelled the behavior of a system that combined solar collection and radiative cooling in order to determine the potential coverage of cooling and DHW requirements in residential and commercial buildings under different climates. Feng et al. [21] conducted a daytime RC simulation and experimentation and evaluated the most significate variables and concluded that, in order to maximize RC, ultra-low parasitic heat gains and maximum suppression of solar irradiance in the emitter was required. Bijarniya et al. [22] studied the radiative cooling potential in various climate conditions in five cities in India, and evaluated the performance of different RC systems (ideal emitters, broadband emitters and selective emitters). Carlosena et al. [23] studied the potential of daytime radiative cooling for mitigating the effects of urban heat islands and performed simulations of different applications and locations for a total of 15 theoretical materials and 7 existing materials used in emitters.

Prediction of radiative cooling potential in different areas could become an aid to drive public policies on the usage of renewable energies. In 1992, Argiriou et al. [24] estimated the sky temperature depression and the night time performance of a RC flat plate in different countries in southern Europe, and concluded that southern Europe exhibited a promising potential for a high application of this technology. Chang et al. [25] and Li et al. [26] used geostatistical prediction tools to model and to obtain radiative cooling potential maps in China and USA, respectively.

In this research we applied interpolation tools to generate annual nighttime and all-day radiative cooling potential maps in Europe. A comparison of results between emitters with different reflectivity in the solar range is also offered. We present twenty maps corresponding to seven maps of annual power, seven maps of annual energy production and six maps of percentage of RC hours over total annual hours.

2. Methods

The parametric study of the variation of the all-day radiative cooling potential in Europe as a function of the reflectivity in the solar range of the emitter material was conducted based on meteorological data measured in 1791 weather stations. Kriging was the interpolation technique used to obtain radiative cooling maps.

2.1. Data Acquisition

The climatological data used was available in the Meteornorm database. Meteonorm is a recognized software in the field of energy simulation of buildings and solar facilities. The downloaded data corresponded to a total of 1791 weather stations distributed in 46 European countries. The distribution of these stations is shown in Figure 1. The data is related to the last volume of measured data available in Metonorm for the year 2005. The resulting dataset included information on weather variables recorded hourly for 365 days of the year. Stored variables included ambient temperature, atmospheric IR radiation and global horizontal solar radiation, relative humidity, clearness index of the sky and atmospheric pressure. Ambient temperature, global horizontal solar radiation, relative humidity, clearness index or atmospheric pressure are data measured at the weather station while atmospheric radiation (L_{in}) is calculated based on the Aubinet model (1) [27]:

$$L_{in} = \sigma \cdot [94 + 12.6 \log(100 \cdot e_s) - 13 \cdot KT_d + 0.341 \cdot (T_a + 273.15)]^4 \tag{1}$$

where L_{in} is the atmospheric radiation (W/m^2); σ is the Stefan–Boltzman constant $\left(W \frac{m^2}{K^4}\right)$; e_s is the saturated vapor pressure (hPa); KT_d is the clearness index (-) and T_a is the ambient temperature (°C).
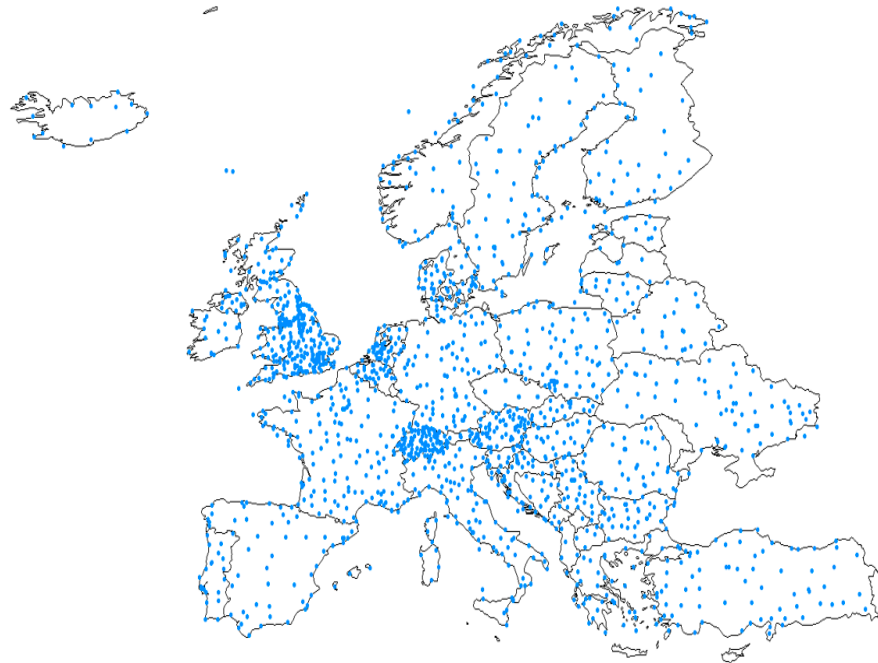
Figure 1. Spatial distribution of the sample points.

2.2. Radiative Cooling Calculation

In the research, the following premises were assumed: the greatest potential of a black-body surface (emittance of the surface (ε_s) equal to one) (a) could be achieved by minimizing the parasitic losses of conduction and convection, (b) while absorbed solar radiation depended on the reflectivity of the surface. In this study, ε_s is equal to 1 and parasitic losses are neglected. In RC applications, the emitter surface temperature is close to ambient temperature; in this case it was assumed that (c) the temperature on the surface was equal to ambient temperature. The net balance power per surface unit at each location was calculated (2).

$$q_{net,ideal}(T_a) = \sigma T_a^4 - L_{in} - (1-\rho)S_H \left(\text{W/m}^2\right) \tag{2}$$

where ρ is the solar reflectivity of the emitter (-) and S_H corresponds to the global horizontal solar radiation (W/m^2).

Only positive values of Equation (2), corresponding to observations where radiative cooling occurred, were filtered. The average annual RC potential at each location was calculated according to (3) where n is the total number of positive observations:

$$q_{rc,avg} = \frac{\sum_i^n q_{net,ideal}^+}{n} \left(\text{W/m}^2\right) \tag{3}$$

Every value from Equation (2) corresponded to a one-hour observation (t = 1 h). Thus, allowing us to calculate the RC annual energy (6):

$$e_{rc} = \frac{\sum_i^n q_{net,ideal}^+ \cdot t}{1000} \left(\frac{\text{kWh}}{\text{m}^2} \cdot \text{year}\right) \tag{4}$$

Finally, a third value was included (5). This value referred to the number of observations where radiative cooling was achieved ($N[q_{net,ideal}^+]$), compared to the total number of observations (8760).

$$coverage = \frac{N(q_{net,ideal}^+)}{8760} \, [\%] \tag{5}$$

2.3. Training and Test Datasets

Data was divided into two subsets: training set and test set. The training set contained information from 80% of the locations and was used in the construction of the interpolation model for each value of ρ. Test set data was used to evaluate the performance of each model.

2.4. Interpolation Kriging Model

Kriging is a stochastic interpolation method for values prediction at different points from known reference values. In the study we used the most general version of the methodology, ordinary Kriging, which decomposed the regressor into a stationary part (μ) and a residual (ε'), corresponding to the spatially correlated part (6) [28]:

$$Z(s) = \mu + \varepsilon'(s) \tag{6}$$

This method worked as a linear regression applied to spatial sample data which was used as regressor, $Z(s)$, in order to predict a dependent variable, $Z(s_0)$, at a given location (7). The weight given by the model to each of the points in the sample was determined by a variogram function (8).

$$\hat{Z}(s_0) = \lambda_0 Z(s) \tag{7}$$

$$\begin{pmatrix} \gamma(s_1 - s_1) & \cdots & \gamma(s_1 - s_n) & 1 \\ \vdots & \ddots & \vdots & 1 \\ \gamma(s_n - s_1) & \cdots & \gamma(s_n - s_n) & 1 \\ 1 & \cdots & 1 & 0 \end{pmatrix} \cdot \lambda_0 = \begin{pmatrix} \gamma(s_1 - s_0) \\ \vdots \\ \gamma(s_n - s_0) \\ 1 \end{pmatrix} \tag{8}$$

where λ_0 is a vector of Kriging weights, n the number of sample points and γ is the semivariance.

The semivariance of the sample was calculated for each pair of points from (9), where $Z(s_i)$ is the value of the target variable at the point s_i, $Z(s_i + h)$ is the value of the neighbor point at a distance $s_i + h$ and E corresponds to the expected value. A theoretical variogram was adjusted to the variogram so that the error of the fitting was minimum.

$$\gamma(h) = \frac{1}{2} E\left[(Z(s_i) - Z(s_i + h))^2 \right] \tag{9}$$

2.5. Assessment Metrics of the Model

Radiative cooling values were predicted using the test set locations in the Kriging model. These predictions were compared with the existing potential values at these locations. In order to evaluate the accuracy of the model, the coefficient of determination (R^2) and the root mean square error (RMSE) were calculated (10) and (11):

$$R^2 = 1 - \frac{\sum_{i=1}^{N} \left(X_{i,m} - X_{i,p} \right)^2}{\sum_{i=1}^{N} \left(X_{i,m} - X_{m,avg} \right)^2} \tag{10}$$

$$RMSE = \sqrt{\frac{1}{N} \sum_{i=1}^{N} \left(X_{i,m} - X_{i,p} \right)^2} \tag{11}$$

where N is the total number of locations; $X_{i,m}$ is the observed values of the sample; $X_{i,p}$ is the value estimated in the model and $X_{m,avg}$ is the average of the observed values at the weather stations. RMSE has the same units as the variable at interpolation (power, energy and coverage) while R^2 is dimensionless.

3. Results and Discussion

In the first part of this section we present a comparison of the prediction maps for the cases of nighttime and all-day RC of an ideal reflective surface (ρ = 1). In the second part we determine the changes that occur when varying the value of surface reflectivity in all-day RC. In both sections the performance of the interpolation models used has been evaluated.

3.1. Nighttime and All-Day Comparison

Figure 2 shows the annual potential maps of radiative cooling for night and ideal all-day cases. The maps were divided into three regions: south, center and north.
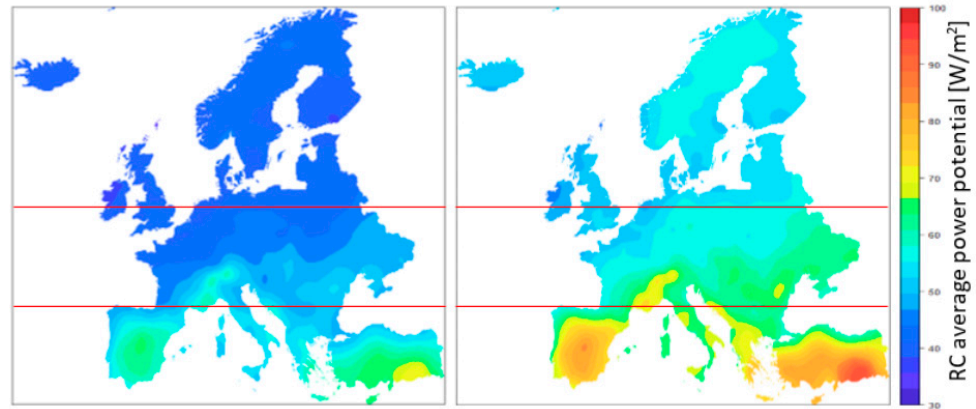

Figure 2. Map of annual average power potential (W/m^2) of nighttime RC (**left**) and all-day RC of an ideal solar reflective surface (**right**). Horizontal red lines divide the map into three zones: north (53.55 N–71.15 N), center (43.46 N–53.55 N) and south (34.60 N–43.46 N).

In all-day applications, the potential RC was greater than in night applications. On average in Europe, the change to all-day applications represented an increase of 27.21% (from 47.30 to 60.17 W/m^2). The all-day map presented more diversification of the values with respect to the night map (in all-day the range is 43.82–94.01 W/m^2 and in nighttime, 35.14–71.34 W/m^2).

It was observed that the regions with the greatest potential were located in the south of Europe (57.36 W/m^2 in nighttime map and 72.33 W/m^2 in all-day), in the Mediterranean basin, especially the cases of Turkey, Spain and Greece. These results were consistent with the findings of Argiriou et al. [24]. The areas of least potential were in the northern countries (41.51 W/m^2 in nighttime map and 53.77 W/m^2 in all-day) where the temperature is lower. The average potential in the central zone was 46.48 (nocturnal) and 58.69 (all-day) and they are values comparable to those in the north but with a wider range of variability (Table 1). In these cases, the performance of the surface is only influenced by the temperature and the atmospheric radiation and the results are coherent with the climatology of Europe where the ambient temperature decreases with the latitude.

Table 1. Minimum, average and maximum annual average power potential of the different zones of Europe.

	Latitude Range	RC Power (Nighttime)			RC Power (All-Day)		
		min (W/m^2)	avg (W/m^2)	max (W/m^2)	min (W/m^2)	avg (W/m^2)	max (W/m^2)
Center	43.46 N–53.55 N	37.95	46.48	60.11	46.43	58.69	73.08
North	53.55 N–71.15 N	35.14	41.51	45.31	43.82	53.77	57.81
South	34.60 N–43.46 N	46.67	57.36	71.34	56.36	72.33	94.01
Europe	34.60 N–71.15 N	35.14	47.30	71.34	43.82	60.17	94.01

Annual energy potential maps are shown in Figure 3. The night map presented homogeneous values with minimal differences between regions. In the all-day predictions there was an average increase of 114% (124% in the south, 116% in the center and 108% in the north) of the available annual energy potential: the average was 245.76 kWh/m^2·year in the night case and 527.1 kWh/m^2·year in the all-day case. This means that only during daytime can 281.34 kWh/m^2·year be produced. In all-day applications, southern countries can radiate, on average, 633.56 kWh/m^2·year; center countries, 514.16 kWh/m^2·year; and

northern countries, 470.99 kWh/m^2·year (Table 2). On average, nighttime RC was achieved in 59.6% of the annual observations.
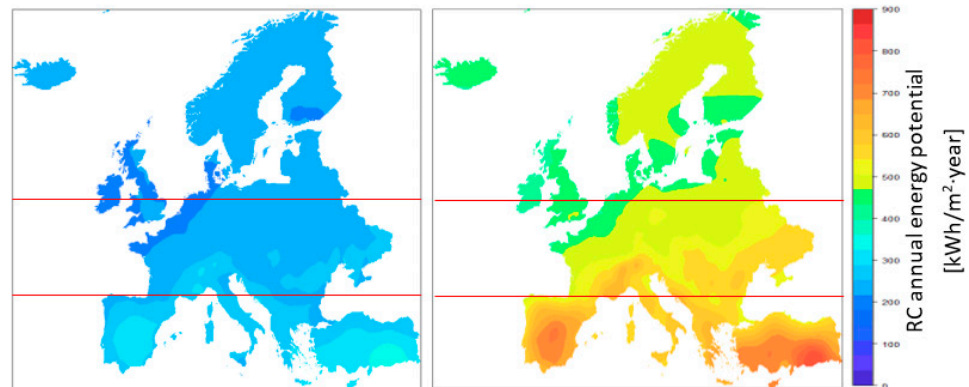
Figure 3. Map of annual energy potential (kWh/m^2·year) of nighttime RC (**left**) and all-day RC of an ideal solar reflective surface (**right**). Horizontal red lines divide the map into three zones: north (53.55 N–71.15 N), center (43.46 N–53.55 N) and south (34.60 N–43.46 N).

Table 2. Minimum, average and maximum annual energy potential of the different zones of Europe.

		Energy (Nighttime)			Energy (All-Day)		
	Latitude Range	**min (kWh/m^2·Year)**	**avg (kWh/m^2·Year)**	**max (kWh/m^2·Year)**	**min (kWh/m^2·Year)**	**avg (kWh/m^2·Year)**	**max (kWh/m^2·Year)**
Center	43.46 N–53.55 N	194.22	238.00	296.31	406.74	545.83	639.71
North	53.55 N–71.15 N	194.15	229.99	250.19	384.08	485.70	506.40
South	34.60 N–43.46 N	231.12	283.07	352.59	493.88	688.64	822.66
Europe	34.60 N–71.15 N	194.15	245.76	352.59	384.08	559.47	822.66

Table 3 lists the values of the performances of the four models. In all cases, R^2 presented high values (between 0.83 and 0.91), which indicates that the models collected more than 83% of the variability of the sample data. In the energy models, the value of RMSE presented values of one order of magnitude greater, in agreement with the values of prediction.

Table 3. Performance of the nocturnal and all-day models.

	Power		Energy	
	Nocturnal	**All-Day**	**Nocturnal**	**All-Day**
RMSE	2.28 (W/m^2)	2.46 (W/m^2)	12.38 (kWh/m^2·year)	21.58 (kWh/m^2·year)
R^2	0.89 (-)	0.91 (-)	0.83 (-)	0.91 (-)

3.2. Influence of the Solar Reflectivity on the Performance of a Radiative Surface

3.2.1. Average Power Potential

The annual RC power potential maps in Europe are displayed in Figure 4 for each value of reflectivity. The reduction of the reflectivity affects the three regions equally (25% reduction) but, in absolute values, the southern regions are especially penalized (average power reduced by 17.28 W/m^2). It is observed that the maps tend to homogenize results throughout the territory as the reflectivity is reduced: the range of values (minimum to maximum average power potential) diminished from 50.19 to 35.05 W/m^2.
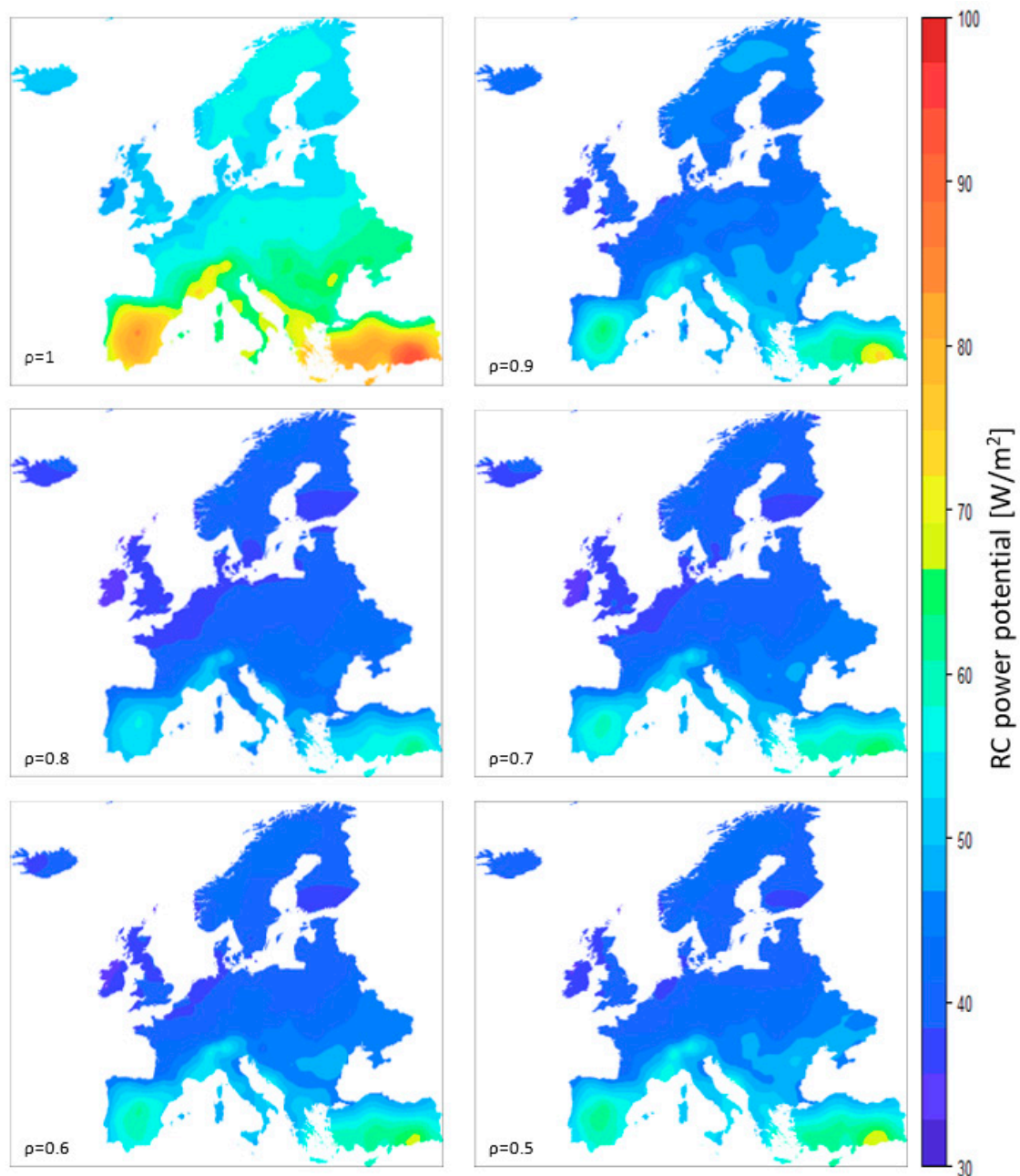
Figure 4. Map of RC power potential (W/m^2) for six values of solar radiation reflectivity.

Table 4 shows that the average value of the potential of RC power followed a decreasing trend for solar reflectivity from 1 to 0.8, while between 0.7 and 0.5 the potential increased slightly; 0.8 being the value of solar reflectivity where the average potential was minimum (42.61 W/m^2). Between 1 and 0.8 a maximum difference of potentials occurred: reducing the solar reflectivity from 1 to 0.8 caused a decrease of 29% in the potential of RC power. Between 0.8 and 0.5, the potential increased 6.4%.

The explanation behind these results is due to the number of observations with which the annual average is calculated. With the reduction of the reflectivity, the total number of RC observations also decreases (see Section 2.2). To better understand this, Figure 5 is displayed. The figure shows the power calculated in each of the observations for the month of February at the location of Batman. Observations that resulted in high power values when $\rho = 1$ remained high when $\rho = 0.5$, while those observations with low power decreased to the point of having negative values (red points) and were discarded in the

calculation of the average. As a result, the calculation of the average for solar reflectivity 0.5 and 0.6 had few observations but of higher quality than for solar reflectivity 0.7 and 0.8. This phenomenon is a result of the different heat fluxes occurring during nighttime and daytime RC. During nighttime RC, solar radiation is not present, thus solar reflectivity does not play any role. However, during daytime RC, solar reflectivity has a significant impact on the radiative balance. In Section 3.2.2. we discuss that most of the observations of RC when considering a solar reflectivity of 0.6 and 0.5 are during nighttime, and thus not affected by this parameter.
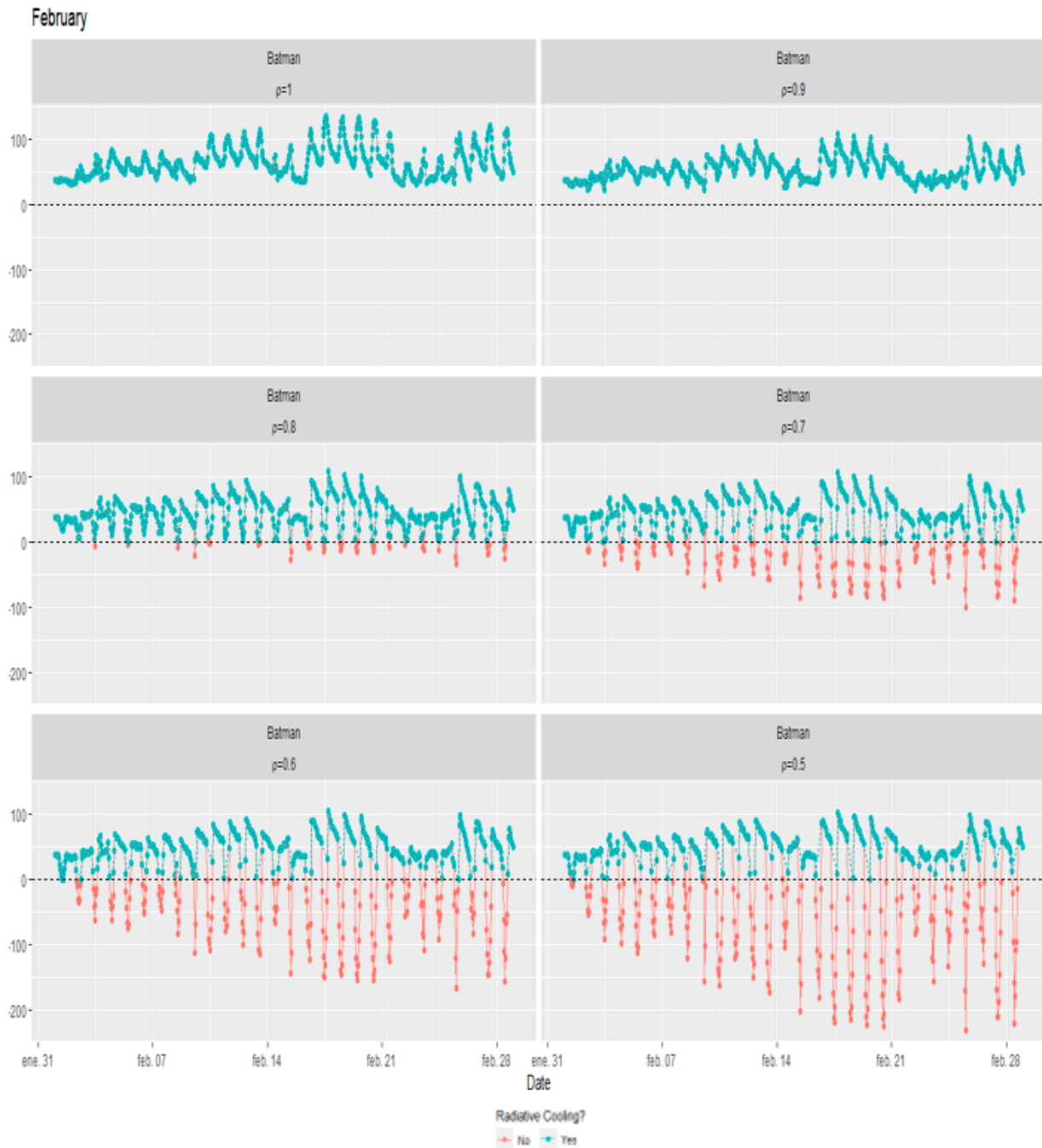
Figure 5. Power potential for each observation in Batman during the month of February and for each value of solar reflectivity. Blue points correspond to radiative cooling observations and red points correspond to solar heating observations. Red observations were discarded in calculations.

Table 4. Minimum, average and maximum values for each solar reflectivity. Potential maps of RC power (W/m^2).

	Latitude Range		Solar Reflectivity					
			1	0.9	0.8	0.7	0.6	0.5
Center	43.46 N–53.55 N	min	46.43	36.31	34.20	34.65	35.09	35.82
		avg	58.69	45.27	41.31	42.40	43.34	44.12
		max	73.08	56.17	51.62	53.81	55.98	57.87
North	53.55 N–71.15 N	min	43.82	35.70	33.78	33.55	33.88	34.09
		avg	53.77	43.76	39.31	39.59	39.95	40.23
		max	57.81	48.00	42.19	42.25	42.90	43.38
South	34.60 N–43.46 N	min	56.36	42.23	40.80	42.43	43.67	44.41
		avg	72.33	54.33	49.84	52.51	53.72	55.05
		max	94.01	72.76	62.24	66.05	67.16	69.14
Europe	34.60 N–71.15 N	min	43.82	35.70	33.76	33.55	33.88	34.09
		avg	60.18	46.87	42.61	43.79	44.59	45.32
		max	94.01	72.56	62.34	66.05	67.16	69.14

We did not observe significant differences in performance of the model for each reflectivity value (Table 5). In all six cases, the values of R^2 were greater than 0.80 which means that, in all the cases, the models could explain more than 80% of the variability of the sample values. RMSE values were small, indicating that the models had good accuracy.

Table 5. Performance of the model of the potential maps of power for different solar reflectivity values.

Reflectivity	R^2 (-)	RMSE (W/m^2)
1	0.91	2.46
0.9	0.84	2.40
0.8	0.87	1.90
0.7	0.87	2.16
0.6	0.90	2.02
0.5	0.88	2.32

3.2.2. RC Activity

The maps in Figure 6 show the percentage of hours in a year that the emitter was able to achieve radiative cooling (from now on we refer to this observation of net radiative cooling as "RC activity"). When the reflectivity in the solar range is reduced, the material decreases its behavior as a selective material: when it absorbed more solar radiation the number of observations in which the surface was unable to do radiative cooling increased. In these daytime observations the device was actually behaving as a solar thermal collector, heating up the surface.

Contrary to what the power maps showed, the percentage of RC activity of the emitter decreased as reflectivity decreased in the six cases (Table 6). For a reflectivity of 0.5, the worst-case scenario, only in 67% of cases was radiative cooling achieved; the remaining 33% were solar collection observations. Northern regions had more observations of radiative cooling, in all the cases, which means more time available to perform radiative cooling, than southern regions. In Section 3.1 it was pointed out that nighttime RC represented 59.6% of the RC activity in Europe, this means that only 7.47% of the activity occurred during daytime when $\rho = 0.5$; 10.81%, when $\rho = 0.6$; 16.18%, when $\rho = 0.7$; 26.98%, when $\rho = 0.8$; 40.29%, when $\rho = 0.9$ and 40.4%, when $\rho = 1$.
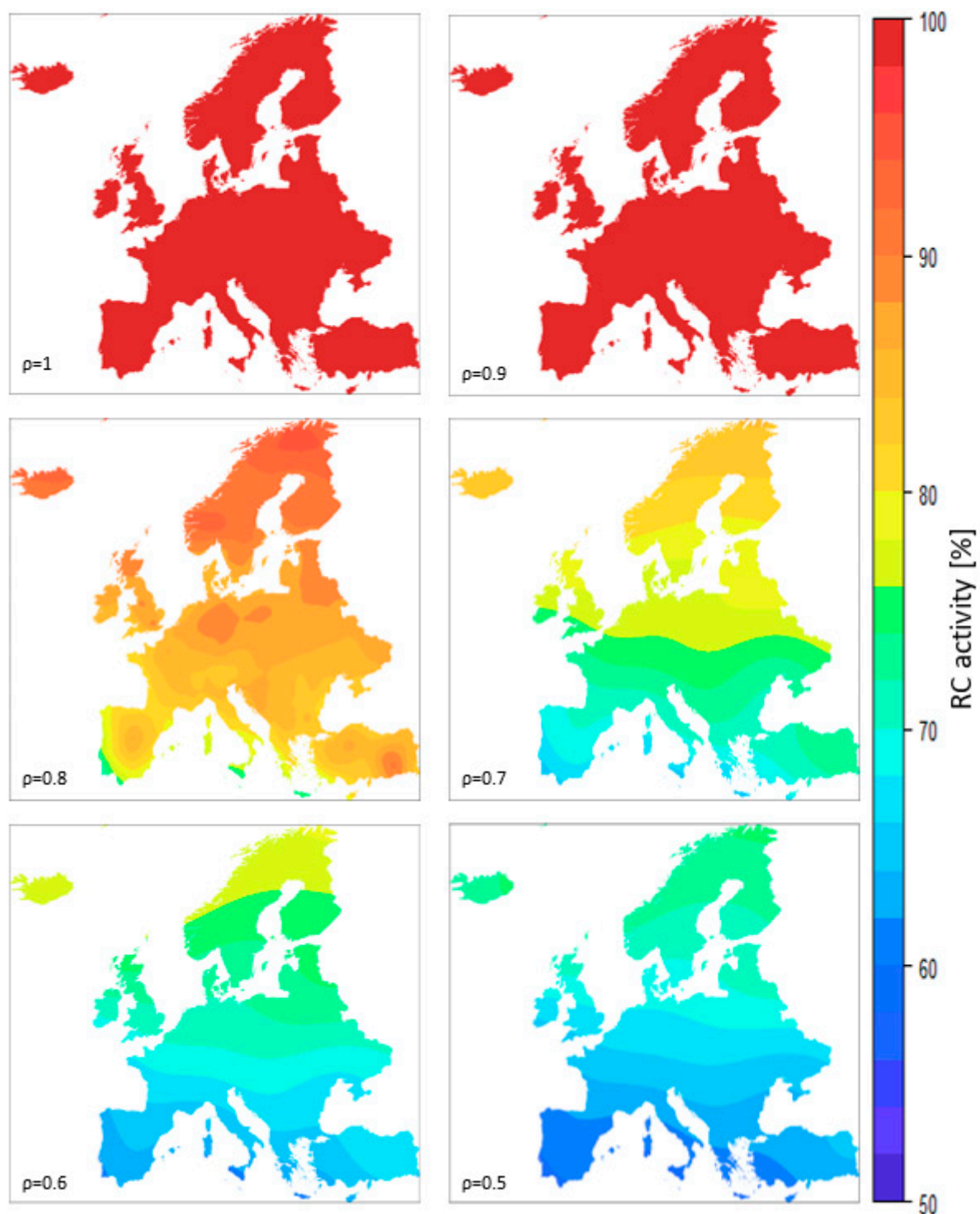
Figure 6. Map of RC activity (%) for six values of solar radiation reflectivity.

The results of RC activity for $\rho = 1$ have not been interpolated by Kriging as a variability in the values to be interpolated is required. For this case, all values were equal to 100% and Kriging could not be performed. It was assumed that in unknown locations the RC activity value was 100%.

The model for reflectivity 0.9 showed a low R^2 value and low RMSE. This model could not reproduce much of the variability of the sample but it also gives low errors of prediction. The range of the values of the sample was very small. For reflectivity values below 0.9, the models presented good metrics of R^2 and RMSE (Table 7).

Table 6. Minimum, average and maximum values for each solar reflectivity. RC Activity (%).

			Solar Reflectivity					
	Latitude Range		1	0.9	0.8	0.7	0.6	0.5
Center	43.46 N–53.55 N	min	100	100	79.04	68.52	63.76	61.29
		avg	100	99.89	85.68	74.93	69.42	65.93
		max	100	98.55	89.41	78.36	73.07	69.55
North	53.55 N–71.15 N	min	100	99.72	84.34	76.60	70.87	67.07
		avg	100	99.96	90.42	80.53	75.21	71.66
		max	100	99.99	94.48	84.12	78.33	74.53
South	34.60 N–43.46 N	min	100	99.03	72.35	64.03	60.55	58.43
		avg	100	99.78	82.50	70.25	65.08	62.07
		max	100	99.96	90.32	73.37	67.73	64.50
Europe	34.60 N–71.15 N	min	100	98.55	72.35	64.03	60.55	58.43
		avg	100	99.89	86.58	75.78	70.41	67.07
		max	100	100	94.48	84.12	78.33	74.53

Table 7. Performance of the model of the potential maps of RC activity for different solar reflectivity values.

Reflectivity	R^2 (-)	RMSE (-)
0.9	0.25	0.19
0.8	0.84	1.49
0.7	0.87	1.43
0.6	0.88	1.24
0.5	0.91	1.05

3.2.3. Annual Energy Potential

The maps in Figure 7 show the annual RC energy potential at each point in Europe. It can be seen, again, that the regions of southern Europe are the areas with the highest energy capacity for radiative cooling. For solar reflectivity values between 0.8 and 0.6, northern regions present higher energy potential than central regions. In this range, although the power potential in the north was lower than in the center (Figures 4 and 5), the north had more time available to perform RC (Figure 6 and Table 6), resulting in higher values of annual energy available.

The available energy was reduced by lowering solar reflectivity (Table 8). At low reflectivities, maps presented a homogenization pattern. When solar reflectivity is equal to 0.5 it behaves as a nighttime surface (when $\rho = 0.5$ it was able to provide, on average, 264.87 kWh/m^2·year, while a nighttime surface was able to provide 245.76 kWh/m^2·year). The largest differences in the average annual RC energy were observed between $\rho = 1$ and $\rho = 0.8$. In this range, the difference between average values in Europe was equal to 204.67 kWh/m^2·year, and it was equal to 272.58 kWh/m^2·year in southern Europe. In the range of 0.8–0.5, the existing difference in the average was equal to 57.56 kWh/m^2·year in Europe. Between $\rho = 1$ and $\rho = 0.8$, the average annual RC energy reduction for Europe was 38.83%, while between $\rho = 0.8$ and $\rho = 0.5$ it was 17.85%. Small variations in reflectivity have a greater impact on the energy potential at high reflectivity values than at low ones.
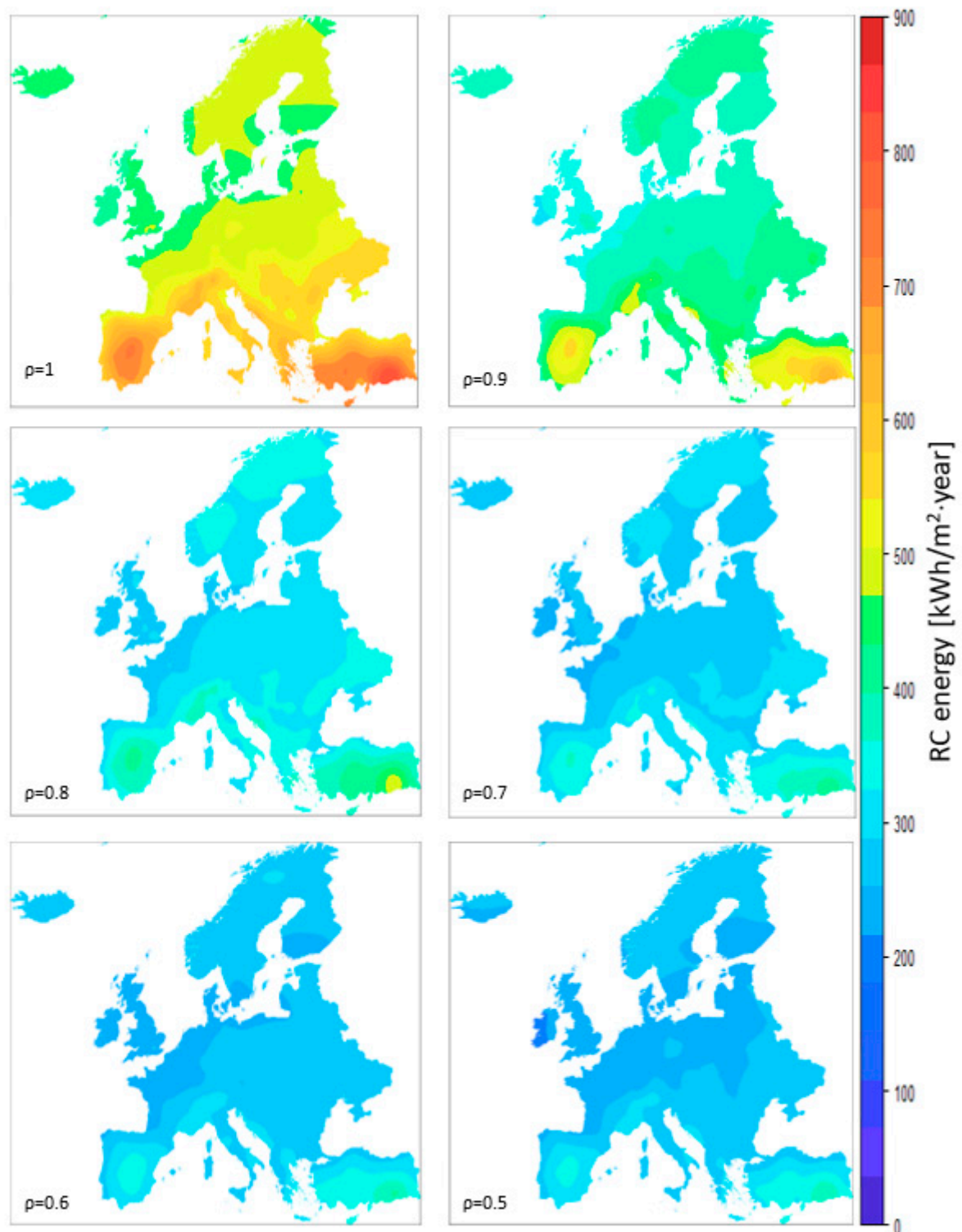
Figure 7. Map of annual RC energy (kWh/m^2·year) for six values of solar radiation reflectivity.

Southern countries were more affected by the reduction of ρ than northern and central countries: differences in the average RC energy available between $\rho = 1$ and $\rho = 0.5$ were 333.63 kWh/m^2·year in southern regions, 259.42 kWh/m^2·year in central regions and 217.49 kWh/m^2·year in northern regions. The model presented a good performance in the six cases (Table 9).

Table 8. Minimum, average and maximum values for each solar reflectivity. Potential maps of annual RC energy (kWh/m^2·year).

			Solar Reflectivity					
	latitude Range		1	0.9	0.8	0.7	0.6	0.5
Center	43.46 N–53.55 N	min	406.74	312.63	254.79	228.15	220.30	213.05
		avg	514.16	396.23	309.89	278.54	263.55	254.74
		max	639.71	493.03	378.74	333.92	322.46	317.90
North	53.55 N–71.15 N	min	384.08	313.42	258.55	232.97	221.06	213.08
		avg	470.99	383.47	311.62	280.07	264.03	253.50
		max	506.40	422.26	346.71	309.46	291.11	278.34
South	34.60 N–43.46 N	min	493.88	368.86	281.38	266.07	246.96	240.26
		avg	633.56	475.55	360.98	323.36	306.98	299.93
		max	822.66	642.35	492.60	413.61	397.85	388.09
Europe	34.60 N–71.15 N	min	384.08	312.63	254.79	228.15	220.30	213.05
		avg	527.10	410.35	322.43	289.55	273.87	264.87
		max	822.66	642.35	492.60	413.61	397.85	388.09

Table 9. Performance of the model of the potential maps of RC energy for different solar reflectivity values.

Reflectivity	R^2 (-)	RMSE (kWh/m^2·year)
1	0.91	21.58
0.9	0.83	21.34
0.8	0.81	16.24
0.7	0.74	16.04
0.6	0.81	13.30
0.5	0.78	13.82

4. Conclusions

In this article we presented the potential of implementing nighttime and all-day radiative cooling technologies in Europe for different solar reflectivity values of the RC emitting surface. Based on climatological data from weather stations and using Kriging interpolation techniques, maps of annual potential for RC power, RC energy and RC activity were displayed. The following conclusions can be drawn from the study:

- Kriging is a good methodology to predict radiative cooling values from known climatological data. The models presented high values of R^2 and low values of RMSE.
- With the implementation of new materials, all-day radiative cooling can be achieved. For solar reflectivity equal to 1, the shift from nocturnal to all-day radiative cooling can improve the average potential power from 47.30 to 60.17 W/m^2, with peak values of 94.01 W/m^2. The average annual energy increases from 245.76 to 559.47 kWh/m^2·year.
- The areas with the greatest potential of implementation are the regions of southern Europe. These regions present high values of power and energy potential.
- Compared to the other regions, the north holds more hours of available radiative cooling.
- The best performance, in all the three regions defined, is achieved when solar reflectivity is equal to one. In order to minimize the solar radiation absorbed by the surface, the reflectivity values in the solar range must be close to 1.
- For solar reflectivity values below 0.5, the behavior of the surface can be assimilated to a nighttime radiative cooler.
- Annual energy and RC activity decreases with reflectivity, while average power potential presents higher values in the 0.6–0.5 range for reflectivity, rather than in the 0.8–0.7 range. This is a result of calculating the average powers using only the observations where RC is achieved, and not for all the observations; for low solar reflectivity values, RC observations correspond mainly to nighttime values where

high-power values are obtained. On the contrary, for solar reflectivity values between 0.8 and 0.7, the same nocturnal RC values are achieved, as well as a higher number of low-power daytime observations, thus reducing the average power. Finally, when the solar reflectivity is equal to 0.9, diurnal observations present higher powers, thus increasing the average power.

- For low values of solar reflectivity, maps tend to show homogeneous patterns.
- Small variations in solar reflectivity have greater impacts on the potential at higher reflectivity values than lower ones: in the range of 1–0.8, the reduction of average power potential is 29.19% and the annual energy is 38.83%.

References

1. Bahadori, M.N. Passive Cooling Systems in Iranian Architecture. *Sci. Am.* **1978**, *238*, 144–155. [CrossRef]
2. Johnson, T.E. Radiation Cooling of Structures with Infrared Transparent Wind Screens. *Sol. Energy* **1975**, *17*, 173–178. [CrossRef]
3. Catalanotti, S.; Cuomo, V.; Piro, G.; Ruggi, D.; Silvestrini, V.; Troise, G. The Radiative Cooling of Selective Surfaces. *Sol. Energy* **1975**, *17*, 83–89. [CrossRef]
4. Vall, S.; Johannes, K.; David, D.; Castell, A. A New Flat-Plate Radiative Cooling and Solar Collector Numerical Model: Evaluation and Metamodeling. *Energy* **2020**, *202*, 117750. [CrossRef]
5. Sodha, M.S.; Singh, U.; Tiwari, G.N. A Thermal Model of a Roof Pond System with Moveable Insulation for Heating a Building. *Build. Environ.* **1982**, *17*, 135–144. [CrossRef]
6. Raman, A.P.; Anoma, M.A.; Zhu, L.; Rephaeli, E.; Fan, S. Passive Radiative Cooling below Ambient Air Temperature under Direct Sunlight. *Nature* **2014**, *515*, 540–544. [CrossRef]
7. Cunha, N.F.; AL-Rjoub, A.; Rebouta, L.; Vieira, L.G.; Lanceros-Mendez, S. Multilayer Passive Radiative Selective Cooling Coating Based on Al/SiO2/SiNx/SiO2/TiO2/SiO2 Prepared by Dc Magnetron Sputtering. *Thin Solid Film.* **2020**, *694*, 137736. [CrossRef]
8. Kecebas, M.A.; Menguc, M.P.; Kosar, A.; Sendur, K. Passive Radiative Cooling Design with Broadband Optical Thin-Film Filters. *J. Quant. Spectrosc. Radiat. Transf.* **2017**, *198*, 179–186. [CrossRef]
9. Mandal, J.; Fu, Y.; Overvig, A.C.; Jia, M.; Sun, K.; Shi, N.N.; Zhou, H.; Xiao, X.; Yu, N.; Yang, Y. Hierarchically Porous Polymer Coatings for Highly Efficient Passive Daytime Radiative Cooling. *Science* **2018**, *362*, 315–319. [CrossRef] [PubMed]
10. Peng, L.; Liu, D.; Cheng, H. Design and Fabrication of the Ultrathin Metallic Film Based Infrared Selective Radiator. *Sol. Energy Mater. Sol. Cells* **2019**, *193*, 7–12. [CrossRef]
11. Zhang, J.; Zhou, Z.; Quan, J.; Zhang, D.; Sui, J.; Yu, J.; Liu, J. A Flexible Film to Block Solar Radiation for Daytime Radiative Cooling. *Sol. Energy Mater. Sol. Cells* **2021**, *225*, 111029. [CrossRef]
12. Bao, H.; Yan, C.; Wang, B.; Fang, X.; Zhao, C.Y.; Ruan, X. Double-Layer Nanoparticle-Based Coatings for Efficient Terrestrial Radiative Cooling. *Sol. Energy Mater. Sol. Cells* **2017**, *168*, 78–84. [CrossRef]
13. Hossain, M.M.; Jia, B.; Gu, M. A Metamaterial Emitter for Highly Efficient Radiative Cooling. *Adv. Opt. Mater.* **2015**, *3*, 1047–1051. [CrossRef]
14. Zhai, Y.; Ma, Y.; David, S.N.; Zhao, D.; Lou, R.; Tan, G.; Yang, R.; Yin, X. Scalable-Manufactured Randomized Glass-Polymer Hybrid Metamaterial for Daytime Radiative Cooling. *Science* **2017**, *355*, 1062–1066. [CrossRef] [PubMed]

15. Cho, J.-W.; Lee, T.-I.; Kim, D.-S.; Park, K.-H.; Kim, Y.-S.; Kim, S.-K. Visible to Near-Infrared Thermal Radiation from Nanostructured Tungsten Anntennas. *J. Opt.* **2018**, *20*, 09LT01. [CrossRef]

16. Wu, D.; Liu, C.; Xu, Z.; Liu, Y.; Yu, Z.; Yu, L.; Chen, L.; Li, R.; Ma, R.; Ye, H. The Design of Ultra-Broadband Selective near-Perfect Absorber Based on Photonic Structures to Achieve near-Ideal Daytime Radiative Cooling. *Mater. Des.* **2018**, *139*, 104–111. [CrossRef]

17. Rephaeli, E.; Raman, A.; Fan, S. Ultrabroadband Photonic Structures to Achieve High-Performance Daytime Radiative Cooling. *Nano Lett.* **2013**, *13*, 1457–1461. [CrossRef]

18. Zhu, L.; Raman, A.P.; Fan, S. Radiative Cooling of Solar Absorbers Using a Visibly Transparent Photonic Crystal Thermal Blackbody. *Proc. Natl. Acad. Sci. USA* **2015**, *112*, 12282–12287. [CrossRef]

19. Gao, M.; Han, X.; Chen, F.; Zhou, W.; Liu, P.; Shan, Y.; Chen, Y.; Li, J.; Zhang, R.; Wang, S.; et al. Approach to Fabricating High-Performance Cooler with near-Ideal Emissive Spectrum for above-Ambient Air Temperature Radiative Cooling. *Sol. Energy Mater. Sol. Cells* **2019**, *200*, 110013. [CrossRef]

20. Vall, S.; Castell, A.; Medrano, M. Energy Savings Potential of a Novel Radiative Cooling and Solar Thermal Collection Concept in Buildings for Various World Climates. *Energy Technol.* **2018**, *6*, 2200–2209. [CrossRef]

21. Feng, J.; Santamouris, M.; Shah, K.W.; Ranzi, G. Thermal Analysis in Daytime Radiative Cooling. *IOP Conf. Ser. Mater. Sci. Eng.* **2019**, *609*, 072064. [CrossRef]

22. Bijarniya, J.P.; Sarkar, J.; Maiti, P. Environmental Effect on the Performance of Passive Daytime Photonic Radiative Cooling and Building Energy-Saving Potential. *J. Clean. Prod.* **2020**, *274*, 123119. [CrossRef]

23. Carlosena, L.; Ruiz-Pardo, Á.; Feng, J.; Irulegi, O.; Hernández-Minguillón, R.J.; Santamouris, M. On the Energy Potential of Daytime Radiative Cooling for Urban Heat Island Mitigation. *Sol. Energy* **2020**, *208*, 430–444. [CrossRef]

24. Argiriou, A.; Santamouris, M.; Balaras, C.; Jeter, S. Potential of Radiative Cooling in Southern Europe. *Int. J. Sol. Energy* **1992**, *13*, 189–203. [CrossRef]

25. Chang, K.; Zhang, Q. Modeling of Downward Longwave Radiation and Radiative Cooling Potential in China. *J. Renew. Sustain. Energy* **2019**, *11*, 066501. [CrossRef]

26. Li, M.; Peterson, H.B.; Coimbra, C.F.M. Radiative Cooling Resource Maps for the Contiguous United States. *J. Renew. Sustain. Energy* **2019**, *11*, 036501. [CrossRef]

27. Aubinet, M. Longwave Sky Radiation Parametrizations. *Sol. Energy* **1994**, *53*, 147–154. [CrossRef]

28. Hengl, T. A Practical Guide to Geostatistical Mapping. 2019, p. 15. Available online: http://spatial-analyst.net/book/system/files/Hengl_2009_GEOSTATe2c1w.pdf (accessed on 19 August 2021).

CHAPTER VIII

Climate change influences in the determination of the maximum power

potential of radiative cooling. Evolution and seasonal study in Europe

Chapter VIII. P5: Climate change influences in the determination of the maximum power potential of radiative cooling. Evolution and seasonal study in Europe

1. Introduction

Chapter VI and **Chapter VII** mapped out the potential for nocturnal and all-day radiative cooling. However, in these potentials only present or past meteorological data is considered. As it has been previously mentioned, the phenomenon of radiative cooling is very dependent on the weather conditions.

In the context of climate change, which is already a reality today, the meteorological variability associated with this problem may affect the potential of radiative cooling and, therefore, its resilience over time. As an example, the Intergovernmental Panel on Climate Change (IPCC) reports predict a rise in global ambient temperature. The fourth assessment report (AR4) of the IPCC proposed different emission scenarios based on carbon emissions [83]. In the case of scenario B1 (low emissions), it predicts an increase of 1.8 °C; in scenario A2 (high emissions), an increase of 3.4 °C; and in scenario A1B (middle emission), an increase of 2.8 °C.

In order to quantify how the global increase in temperature affects the potential of radiative cooling (night and all-day) in Europe over the years, in this chapter, which presents the article P5, the Kriging methodology - used in the chapters VI and VII – was applied to climate change projections between 2020 and 2050. These projections were based on IPCC emission scenarios and were available in the Meteonorm database [74].

At the same time, the article mapped the potential for radiative cooling splitting in seasons of the year, in order to identify which ones are more favorable to carry out radiative cooling.

CHAPTER VIII

Climate change influences in the determination of the maximum power potential of radiative cooling. Evolution and seasonal study in Europe

Universitat de Lleida

2. Contribution to the state of the art

To date, it has not been carried out in the literature a long-term analysis of the evolution of radiative cooling potential in the context of climate change. The paper presents a total of 40 radiative cooling resource maps: one for each year (2020, 2030, 2040, and 2050) and climate change scenario (B1, A2, and A1B), and also seasonal maps for both night and all-day radiative cooling. **Fig 24** shows an example of the generated maps. The maps could become an aid to drive public policies on the implementation and integration of radiative cooling-based technologies.
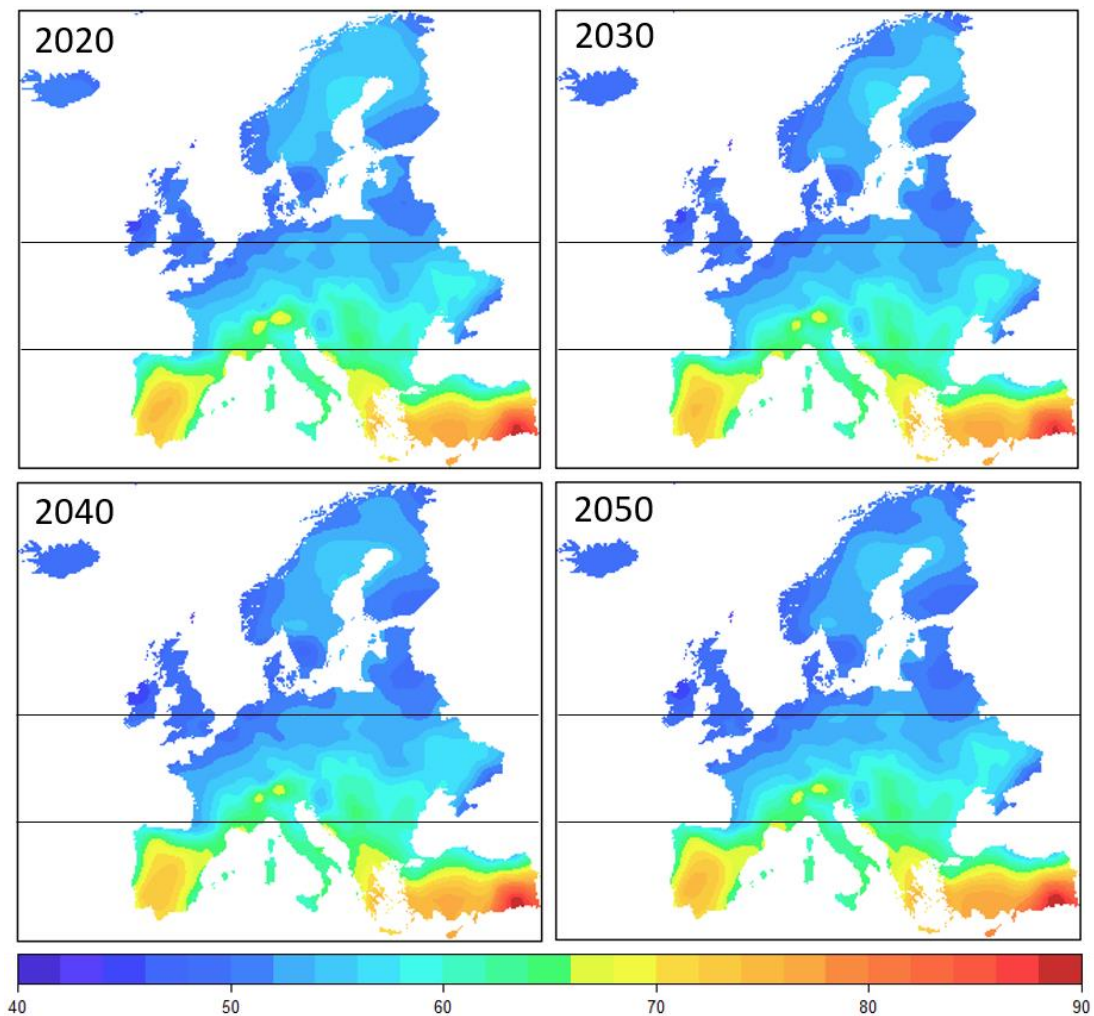

Fig 24. Resource maps of the evolution of the all-day radiative cooling power potential (in W/m^2) under the context of climate change. Study of the scenario A1B proposed in the AR4 by the IPCC. Black horizontal lines divide the map into three regions: north (53.55 N–71.15 N), centre (43.46 N–53.55 N) and south (34.60 N–43.46 N).

CHAPTER VIII

Climate change influences in the determination of the maximum power potential of radiative cooling. Evolution and seasonal study in Europe

The results show that between 2020 and 2050, the potential for radiative cooling remains practically invariable. In the paper it is shown that infrared atmospheric radiation absorbed by the surface increased; this increase compensates for the increase in upward radiation emitted by the surface, so that the net balance remains more or less constant during this period (**Fig 25**). With these results, we consider that RC technologies are robust over time, so that they can contribute to meet the increasing cooling demands in buildings in the short and long term.
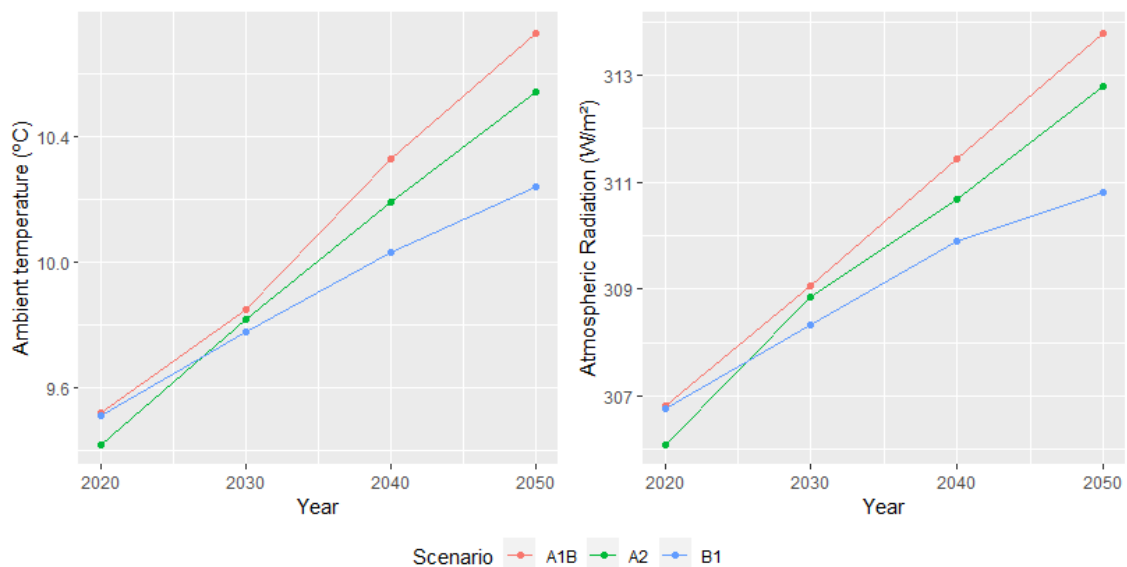
Fig 25. Evolution of the average ambient temperature (left) and atmospheric radiation (right) under the three different IPCC scenarios (A1B, B2 and B1).

Li et al. [69] already evaluated the seasonal performance of radiative cooling in the United States, and Aili et al. [71] compared winter and summer power potential all-over the word. A seasonal study in deep was still missing for Europe. From the seasonal study, spring became the season of the year where, on average, it had the highest nocturnal power potential; while winter was the season where more energy can be dissipated by radiative cooling, due to greater availability of night hours. In contrast, in all-day radiative cooling applications, summer was the season where the potential for energy and power was highest. In the summer, there is a higher production of cold by radiative cooling and it is also the season when the cooling loads are higher. The above enhances the idea set out in **Chapter VII**: to evolve towards an RCE capable of performing in either solar collection mode or radiative cooling mode during diurnal hours, in order to use the maximum

CHAPTER VIII

Climate change influences in the determination of the maximum power potential of radiative cooling. Evolution and seasonal study in Europe

potential of this technology. In all seasons, as expected, the south was the region in Europe with the greatest potential of radiative cooling.

3. Contribution to the objectives of the thesis

This chapter starts from hypothesis H3 and H4 and contributes to fulfil objective O4, O5 and O6, proving that the potential of radiative cooling is not affected by the evolution of meteorological conditions due to climate change, and it remains practically invariable between the period 2020-2050. This shows that radiative cooling is a resilient technology over the years.

From the seasonal study, a subsequently relevant conclusion has been drawn, which is that if the cold production is wanted to be coincident with the months of greatest cooling demands, the shift to all-day radiative cooling is required.

4. Contribution of the candidate

Roger Vilà Miró was in charge of the conceptualization and the definition of the methodology, the interpolation, the data validation and the analysis of the results. The candidate also led the discussion of the results and the writing of the paper.

5. Journal Paper

This chapter was submitted to the journal *Renewable*, published by Elsevier, and it is currently under a peer-review process.

Medrano, Marc and Vilà, Roger and Castell, Albert, Climate Change Influences in the Determination of the Maximum Power Potential of Radiative Cooling. Evolution and Seasonal Study in Europe. Available at SSRN: https://ssrn.com/abstract=4153299 or http://dx.doi.org/10.2139/ssrn.4153299

Climate Change Influences in the Determination of the Maximum Power Potential of Radiative Cooling. Evolution and Seasonal Study in Europe

Roger Vilà, Marc Medrano*, Albert Castell

Sustainable Energy, Machinery and Buildings (SEMB) Research Group, INSPIRES Research Centre, Universitat de Lleida, Pere de Cabrera s/n, 25001 Lleida, Spain; roger.vila@udl.cat (R.V.); albert.castell@udl.cat (A.C.)

* = corresponding author details: marc.medrano@udl.cat

Keywords *radiative cooling, nocturnal radiative cooling, all-day radiative cooling, potential maps, Kriging, climate change, renewable energy.*

Abstract

In the recent years, radiative cooling has emerged as a promising technology for space cooling applications. Nevertheless, radiative cooling phenomenon is dependent on weather conditions and it presents some performance limitations, meaning that the cooling capacity is limited in some climates. In this study we analyze the evolution of the radiative cooling potential in Europe under the context of climate changes. Radiative cooling potential maps for the period 2020-2050 are provided. The results reveal that radiative cooling potential remains constant for this period, evidencing a resilience of this technology during the following decades. We also provide a seasonal study of the potential by regions. Summer, when cooling needs are higher, is the season with the least nocturnal energy potential and the second with the highest nocturnal power potential. Shifting to all-day radiative cooling, the energy potential increases by 1.64 in winter; 2.97, in spring; 4.03, in summer and 2.2 in autumn.

Keywords: radiative cooling, cooling potential, nocturnal radiative cooling, all-day radiative cooling, renewable energy, Kriging, climate change, seasonal study, Europe

1. Introduction

Any surface at ambient temperature (~300K) emits infrared radiation, the majority of it in the wavelength range of 8-14 μm. The Earth's atmosphere is transparent into this range; this region is known as the atmospheric window. This means that almost all the radiation emitted by bodies on Earth can escape into outer space. This process, by which a body on Earth uses outer space - at a temperature close to 3K - as an energy sink, is known as radiative cooling (hereinafter referred to as RC).

Over the last decade, several authors have studied the integration of RC-based systems for space cooling. At the beginning it was only possible to achieve RC during the night, in absence of solar

radiation. New materials have been developed in the last decade which enable the achievement of RC during daytime hours [1–4]. These materials allow to reflect most of the solar radiation [5,6]. Other authors have studied the possibility of combining in a single device the features of solar collection, for water heating, and nocturnal radiative cooling, for water cooling, in a single device [7–9].

Radiative cooling is highly dependent on the weather conditions [10–12]. In the recent years, part of the researches on radiative cooling focus on the evaluation of the radiative cooling potential in various climates and regions. Vall et al. studied whether a combined system of solar heating and radiative cooling can meet the demands of DHW and space cooling in hotels, residential and commercial buildings in different climatic zones [13]. Li et al., using a deterministic interpolation model, presented radiative cooling resource maps in the USA [14]. Chang and Zhang used a stochastic interpolation model, called Kriging, to generate maps based on weather data from 351 stations in China [15]. Vilà et al.[16] also relayed on Kriging methods to generate daytime and night-time RC power and energy potential maps in Europe, based on data from 1791 weather stations, and performed a parametric study in order to define the influence of the solar reflectivity of the radiative surface in the determination of the maximum potential of RC. Aili et al. [17] produced global maps of net cooling power density, showing an uneven distribution of the cooling potential: the regions with the highest potential are uninhabited regions whereas dense areas present a low cooling potential in the order of 10~10^3 Watts per capita (WpP).

However, all studies presented to date only consider current or past weather conditions. Since radiative cooling is dependent on the climatology, changes in weather conditions must be considered in order to determine the resilience of this technology in the upcoming decades. Climate change has been predicted and is becoming a reality. In this context, the Intergovernmental Panel on Climate Change (IPCC) report predicts a rise of global ambient temperature. The fourth assessment report (AR4) of the IPCC proposed different emission scenarios based on the carbon emissions [18]. In the case of scenario B1 (low emissions), it predicts an increase of 1.8 °C; in scenario A2 (high emissions), an increase of 3.4 °C and, in scenario A1B (middle emission), an increase of 2.8 °C.

In order to determine the affectations in radiative cooling potential due to the global increase of the temperature, and whether radiative cooling-based technology are resilient to this variation, the application of Kriging to climate forecasts data for the period 2020-2050 under different emission scenarios proposed by the IPCC is performed in this paper in order to develop radiative cooling potential maps for Europe for the next three decades and considering different climate change scenarios.

In Europe cooling requirements are higher in summer. Another goal of this study is to present maps of RC potential in Europe in order to identify during which seasons of the year it is more favourable to carry out radiative cooling.

This paper is a continuation of the research published by Vilà et al. [16]. It presents power potential and energy potential maps for the four seasons and for the scenario A1B between 2020-2050. Maps for scenarios B1 and A2 are included in **Appendix**. The three scenarios present similar trends and only scenario A1B is discussed.

2. Methods

In the study Kriging was used as a tool for spatially continuous prediction of the power and the energy potential of radiative cooling in Europe based on data from known points. We define radiative cooling potential as the maximum possible cooling rate assuming the best design conditions, no heat losses and that the surface is at ambient temperature. The calculation methodology used, further developed in the following sections, is based on that already applied in the previous research [16]: obtainment of climatological data for different parts of Europe, then calculation of the radiative cooling power and energy at these points, elaboration of the Kriging interpolation model, validation of the model and prediction at new points (Fig 1).
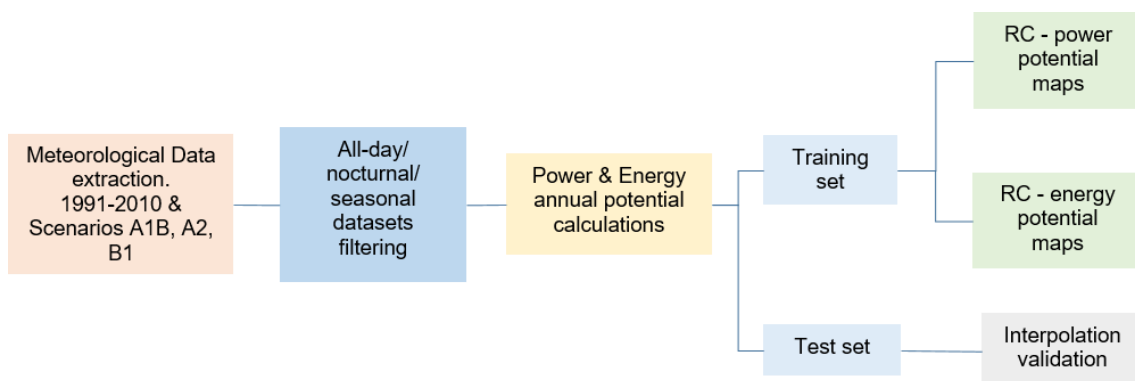
Fig 1. Workflow followed to generate radiative cooling potential maps.

Data analysis and processing, as well as the Kriging interpolation, was performed using the Rstudio, version 1.3. Sp and gstat packages, available for the R environment, were used in the geospatial analysis.

2.1. Origin of climatological data and data pre-processing.

Climatological data from 1831 locations were obtained from the Meteonorm database [19]. A total of thirteen different data sets were downloaded. The first corresponded to the data set for the period 1991-2010, the most recent period of data stored in the database. The other twelve sets corresponded to the forecasts for the years 2020, 2030, 2040 and 2050 under the climate change scenarios A1B, B1 and A2 proposed by the IPCC in the fourth assessment report (AR4) [18].

The data sets shared the same structure and included weather information, for each of the weather stations, aggregated hourly for the 365 days of the year. The stored variables included ambient temperature, atmospheric infrared radiation and global horizontal solar radiation, relative humidity, clearness index of the sky and atmospheric pressure.

Data was classified by seasons. December, January, and February have been classified as winter months; March, April, and May, as spring; June, July and August, as summer and September, October and November as autumn.

Each of the data sets described was divided into two subsets. The first, the training set, contained the observations corresponding to 80% of the points and were used for the construction of the interpolator. The second subset was the test set; containing the remaining 20% points and was used to evaluate the reliability of the predictions. The division process into the two subsets was randomized.

2.2. Climate Change Scenarios

The fourth assessment report (AR4) of the Intergovernmental Panel on Climate Change (IPCC) proposed different emission scenarios. The fifth evaluation report (AR5) presented new scenarios, which were improved with respect to those of the previous report (AR4), considering more ambitious concentration goals and wider assumptions about technology [20]. However, Meteonorm database only presents AR5 scenarios' data for large urban areas, which generated a very small data set. This is the reason why this study relies on predicted weather data under three emission scenarios (A1B, A2, and B1) from AR4 report. Scenario A1B predicts a future with rapid economic growth- reducing the income per capita gap- and the introduction of new and efficient technologies. Scenario A2 predicts high emission based in an independently operating world with a constant increase of population. Scenario B1 predicts an environmental stability as a result of a shift towards a global service and information economy and a reduction of material consumption.

2.3. Radiative cooling calculations

The radiative cooling power is the result of the energy balance between the infrared radiation emitted towards the atmosphere from a RC surface ($q_s(T_s)$ in W/m^2), the short wavelength solar radiation (0.3-2.5 μm) absorbed by the surface ($q_{sun}(T_{sun})$ in W/m^2), the infrared radiation emitted by the atmosphere and absorbed by the RC surface ($q_{atm}(T_{atm})$ in W/m^2) and the thermal gains/losses due to the convective (q_{conv} in W/m^2) and conductive (q_{cond} in W/m^2) thermal exchanges (Eq.1 and Eq.2).

$$q_{net} = q_s(T_s) - q_{atm}(T_{atm}) - q_{sun}(T_{sun}) - q_{cond} - q_{conv} \qquad (1)$$

$$q_{net} = \varepsilon_s \sigma T_s^4 - \alpha_s \varepsilon_{sky} \sigma T_{amb}^4 - (1 - \rho_{sun}) \cdot \varepsilon_{sun} \sigma T_{sun}^4 - q_{cond} - q_{conv} \qquad (2)$$

Where q_{net} is the net balance radiation expressed in W/m^2; ε_s, ε_{sky} and ε_{sun} represent the emissivity of the RC surface, the sky and the sun, respectively; σ is the Stefan – Boltzmann constant, expressed in $W/(m^2 \cdot K^4)$; ρ_{sun} is the reflectivity of the RC surface in the range of the solar radiation wavelength, T_s, T_{amb} and T_{sun} are the temperature of the RC surface, the ambient and the sun expressed in K, and q_{cond} and q_{conv} represent the convective and conductive exchanges, expressed in W/m^2.

Eq.2 expresses the radiative cooling power as a function of the surface reflectivity in the solar range. The literature points out that various researchers have developed metamaterials with reflectivity values close to 1 [21–23]. In the literature it also can be found that the use of windshields and convective covers enables the minimization of convective exchanges [24]. The assumptions accepted to calculate the radiative cooling power, both for night-time and all-day radiative cooling, are next listed:

a. The RC surface behaved as a black body ($\varepsilon_s = \alpha_s = 1$).
b. The RC surface was made of a metamaterial with $\rho_{sun} = 1$.
c. Parasitic thermal exchanges were minimized in the RC surface ($q_{cond} = q_{conv} = 0$).
   - The device was thermally isolated ($q_{cond} = 0$).
   - The device had a convective cover ($q_{conv} = 0$). Losses related to the optical properties of the cover were neglected.
d. The RC surface was placed horizontally; all the emitted radiation was projected towards the atmosphere. Infrared radiation absorbed by the device was coincident with the atmospheric radiation.
e. Temperature of the RC device was equal to the ambient temperature (T_{amb}).

With these assumptions, the maximum net radiative balance of the RC device in each location of the dataset was obtained as described in Eq.3:

$$q_{net,bb} = \sigma T_{amb}^4 - q_{atm} = \sigma T_{amb}^4 - L_{in} \ (W/m^2) \qquad (3)$$

In Eq.2 $q_{net,bb}$ represents the net balance radiation of the black-body surface, expressed in W/m^2; q_{atm}, the radiation emitted by the atmosphere and absorbed by the RC surface, expressed in W/m^2; σ, the Stefan – Boltzmann constant, expressed in $W/(m^2 K^4)$; T_{amb}, the ambient temperature, expressed in K; and L_{in} is the atmospheric radiation according to the Aubinet model [25], expressed in W/m^2.

Eq.3. was used to calculate the hourly radiative cooling potential. Then, two new datasets were created: the first one, corresponding to night-time RC observations, where there were filtered only

nocturnal observations where RC was achieved; the second dataset corresponded to all-day RC observations. The annual average power on each point of the sample was calculated according to Eq.4, where n is the total number of positive observations at each location.

$$q_{rc,annual} = \frac{\sum_i^n q_{net,bb}^+}{n} \ (W/m^2) \tag{4}$$

Every observation corresponded to a one-hour observation *(t = 1 h)*. The energy produced in a year was calculated according to Eq.5.

$$e_{rc,annual} = \frac{\sum_i^n (q_{net,bb}^+ \cdot t)}{1000} \ \left(\frac{kWh}{m^2 \cdot year}\right) \tag{5}$$

2.4. Kriging Interpolation

To predict values in unknown locations based on values from known locations, in this research we used Kriging methodologies. Kriging is a stochastic geographic interpolator, based on the covariance of the sample points, which allows to generate continuous resource maps and, in addition, it determines the reliability of the prediction [26].

The mathematical modelling of the Kriging interpolator was deeply explained in a previous research we published [16]. To summarise it, the Kriging interpolator worked as a linear regression applied to spatial data, used as regressor, *Z(s)*, to predict a dependent variable, $\hat{Z}(s_0)$, in a given point (Eq.6). Weights (λ_0) were determined as a function of the difference between the neighbouring values of the different points of the sample.

$$\hat{Z}(s_0) = \lambda_0 Z(s) \tag{6}$$

2.5. Validation of the prediction

In order to validate the performance of the interpolation, the Kriging prediction model was applied to the test set locations. We compared the values calculated at each of the points in the sample with the value predicted by the Kriging model at these same points. Two metrics were used to quantify the performance of the model: R^2 and RMSE (Eq.7 and Eq.8).

$$R^2 = 1 - \frac{\sum_{i=1}^N (X_{i,m} - X_{i,p})^2}{\sum_{i=1}^N (X_{i,m} - X_{avg,m})^2} \tag{7}$$

$$RMSE = \sqrt{\frac{1}{N} \sum_{i=1}^N (X_{i,m} - X_{i,p})^2} \tag{8}$$

Where N is the total number of locations; $X_{i,m}$ is the observed value of the sample; $X_{i,p}$ is the value estimated in the model and $X_{avg,m}$ is the average of the observed values at the location points. RMSE has the same units as the variable at interpolation while R^2 is dimensionless.

3. Results and Discussion

3.1. Seasonal Study

3.1.1. Night-time results

Fig 2¡**Error! No se encuentra el origen de la referencia.** and Fig 3 show the seasonal interpolation maps for nocturnal radiative cooling power and energy potential. The maps are divided into three regions: the southern region (34.60 N - 43.46 N); the central region (43.46 N - 53.55 N) and the northern region (53.55 N - 71.15 N).
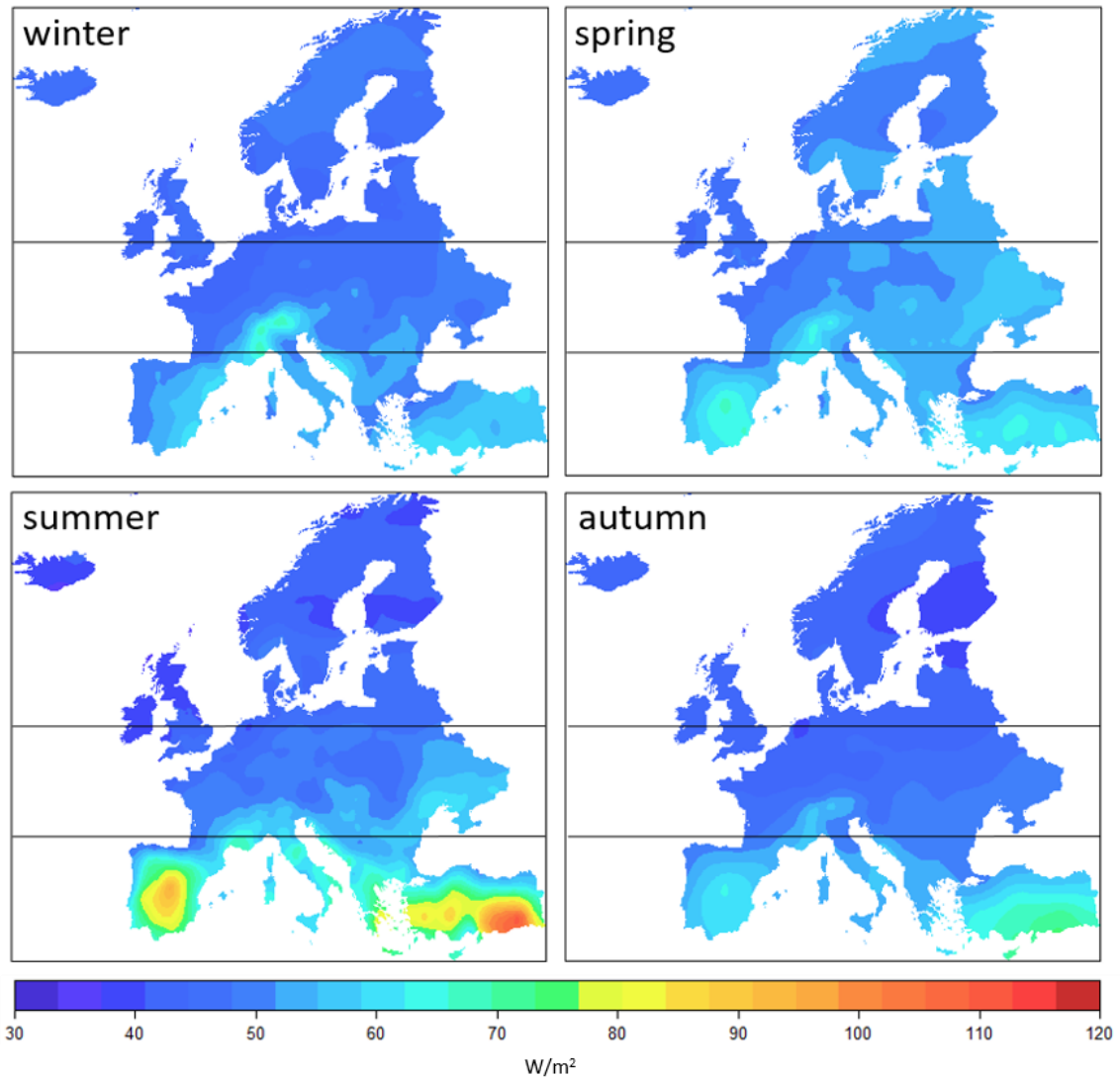

Fig 2. Night-time radiative cooling power potential resource maps for the different seasons in Europe (in W/m²). Black horizontal lines divide the map into three regions: north (53.55 N–71.15 N), centre (43.46 N–53.55 N) and south (34.60 N–43.46 N).

All the interpolations present a R^2 value above 0.73. The RMSE value is lower than 3.55 W/m^2, in the case of power; and lower than 4.91 kWh/m^2·year, in the case of energy (Table 1). The interpolations show off a good performance.

Table 1. Performance of the Kriging interpolations. Night-time evaluation.

	Power		Energy	
	R^2	RMSE	R^2	RMSE
	[-]	[W/m^2]	[-]	[kWh/(m^2·year)]
Winter	0.77	3.06	0.80	3.86
Spring	0.75	2.59	0.84	2.44
Summer	0.91	3.55	0.87	4.91
Autumn	0.80	3.12	0.73	3.66

Spring is the season when, on average, a higher power is potentially achieved (52.72 W/m^2), closely followed by summer (52.46 W/m^2) and, lastly, winter (49.17 W/m^2) and autumn (47.78 W/m^2) (Table 2). In the four maps (Fig 2) it is seen that the regions with the highest power potential are located in the south; specially during summer in Spain and Turkey, where power values higher than 100 W/m^2 can be achieved. The southern region holds higher variability among seasons: between winter and summer a maximum difference of 15.89 W/m^2 is achieved in this region. The northern and central regions exhibit lower variability: a maximum of 8.01 W/m^2 and 5.76 W/m^2, respectively.
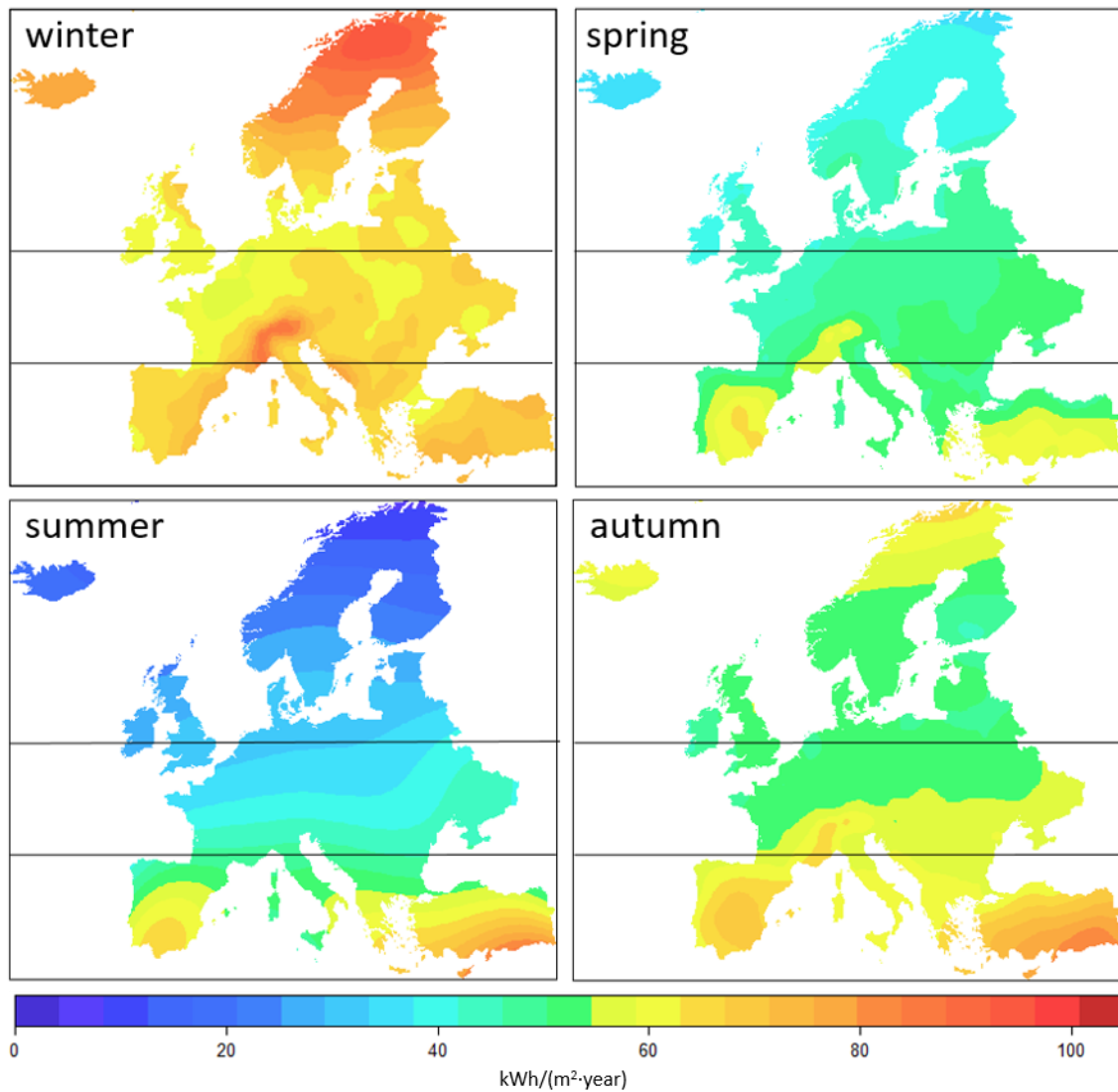
Fig 3. Night-time radiative cooling energy potential resource maps for the different seasons in Europe (in kWh/(m²·year)). Black horizontal lines divide the map into three regions: north (53.55 N–71.15 N), centre (43.46 N–53.55 N) and south (34.60 N–43.46 N).

Table 2. Seasonal average night-time radiative cooling power potential (in W/m²) disaggregated by region and season.

	Centre	North	South	Europe
Winter	48.45 ± 4.58	46.44 ± 4.74	54.50 ± 4.78	49.17 ± 4.68
Spring	52.38± 3.12	50.15 ± 3.22	57.16 ± 3.26	52.72 ± 3.19
Summer	50.66 ± 3.64	42.55 ± 3.79	70.39 ± 3.84	52.46 ± 3.74
Autumn	46.62 ±3.98	42.14 ± 4.07	58.25 ±4.08	47.78 ± 4.04

Regarding to the energy potential, Fig 3 shows the interpolated average energy production. Winter is the season of the year when more energy from radiative cooling sources can be generated (68.96 kWh/m²·year). This result contrast with the prediction of power: winter is the second season with

136

the lowest power potential. Similarly, although summer is the second season with the highest radiative cooling power potential, the results show that it is also the season when, on average, less radiative cooling energy can be generated (38.13 kWh/m²·year) (Fig 3). In Vilà et al.[16] we already analysed that a greater average power does not automatically translate into a greater energy. This value depends on the number of hours available during which radiative cooling can be achieved. During the summer, the days are longer and the nights are shorter, there are fewer hours available for radiative cooling. To compensate this lack of available cooling energy in summer months, a wise decision, proposed in this paper, is to move to all-day radiative cooling systems and use this renewable resource 24 h a day.

The data disaggregated by regions indicates that in the north, during winter, it is when the most energy can be produced on average (68.03 kWh/m²·year), while in northern Europe during the summer it is when it can be produced the least (22.57 kWh/m²·year). The northern region presents higher variability of energy between seasons. Between spring and summer, a maximum difference of 52.49 kWh/m²·year is achieved in this region. Table 3 shows the summary of the average annual energy potential by season and region.

Table 3. Seasonal average night-time radiative cooling energy potential (in kWh/(m²·year)) disaggregated by region and season.

	Centre	North	South	Europe
Winter	64.44 ± 6.13	75.06 ± 6.34	68.03 ± 6.35	68.96 ± 6.25
Spring	49.01 ±2.87	42.12 ± 2.96	55.30 ± 2.98	48.09 ± 2.93
Summer	39.14 ±3.08	22.57 ± 3.12	59.39 ± 3.13	38.13 ± 3.10
Autumn	54.37 ±4.19	53.83 ± 4.27	66.42 ± 4.29	53.83 ± 4.27

It is desirable that the seasons with the highest cooling demand coincide with the seasons with the greatest nocturnal RC potential. During the warm summer months, high cooling demands are expected; summer is the second season with the greatest potential in terms of power and the fourth in terms of energy. However, in southern Europe, where cooling needs are higher than in the rest of the continent [27], there is a coincidence, during summer, between the season with the greatest needs and the one with the greatest power potential. This fact justifies the usage of RC-based technology in these regions during the summer months. On the other hand, RC cooling potential presents a drawback during summer in the centre and the north, where the potential is much lower. Nevertheless, in these regions cooling needs are not as demanding and the lower powers can still be used to compensate for a portion of the cooling needs. Seasonal cold storage with RC in winter and spring months may be a good option as well for meeting the high summer cooling loads, especially in southern Europe.

This discussion suggests to adopt all-day radiative cooling-based technologies in order to benefit from greater cooling power and energy. In the following section the all-day radiative cooling potential is analysed for the different seasons.

3.1.2. All-Day Radiative Cooling

Similarly to the previous section, Fig 4 and Fig 5 show the seasonal interpolation resource maps for all-day radiative cooling power and energy potential. The interpolations show a high performance as prediction maps (Table 4), with values of R^2 higher than 0.78 and values of RMSE lower than 10.56 kWh/(m^2·year) for energy, and lower than 4.78 W/m^2 for power.

Table 4. Performance of the Kriging interpolations. All-Day evaluation.

	Power		Energy	
	R^2 [-]	RMSE [W/m^2]	R^2 [-]	RMSE [kWh/(m^2·year)]
Winter	0.80	3.52	0.78	7.98
Spring	0.78	3.02	0.78	6.67
Summer	0.90	4.78	0.90	10.56
Autumn	0.92	2.59	0.82	8.17

Table 5 summarises the average values of power potential and Table 6, the values of energy potential. Summer and spring are the seasons when the all-day radiative cooling power potential –on average in Europe- is higher (69.59 W/m^2 and 64.46 W/m^2), while autumn and winter show lower potential (54.49 W/m^2 and 52.24 W/m^2). As it is expected, compared to night-time radiative cooling results (section 3.1.1), seasonal power increased 6% in winter, 22% in spring, 33% in summer and 14% in autumn. A maximum source power can potentially be achieved during summer in the southern regions of the continent: 90.65 W/m^2 on average, with peak values of 136 W/m^2 in the south-east. On the other hand, during autumn in the north, minimum radiative cooling power is observed (48.04 W/m^2).

The energy potential also increases when shifting from night-time radiative cooling to all-day radiative cooling applications. In all-day radiative cooling, the number of hours available to perform radiative cooling no longer influences the season and the region, as all the hours of the day are available to achieve radiative cooling. Summer and spring are the season when more energy can be obtained. It is observed that, compared to night-time values, the average energy potential highly increases in all the four seasons (129% in winter, 196% spring, 303% in summer and 108% in autumn).

Focusing in the southern regions in summer, where more cooling is demanded, the shift from nocturnal RC to all-day RC systems multiples by 3.4 the cooling energy production potential. This is a significant increase and a strong potential for air conditioning electricity savings and summer electric peaks reductions and reinforces the proposed idea of moving to all-day radiative cooling systems, taking advantage of this renewable resource 24 h a day.

Table 5. Seasonal average all-day radiative cooling power potential (in W/m^2) disaggregated by region and season.

	Centre	North	South	Europe
Winter	51.22 ± 5.05	48.04 ± 5.17	60.30 ± 5.19	52.24 ± 5.12
Spring	63.82 ± 3.22	61.44 ± 3.33	70.80 ± 3.36	64.46 ± 3.29
Summer	66.60 ± 4.38	59.01 ± 4.58	90.65 ± 4.64	69.59 ± 4.51
Autumn	52.94 ± 4.09	46.58 ± 4.21	69.02 ± 4.23	54.49 ± 4.16

Table 6. Seasonal average all-day radiative cooling energy potential (in $kWh/(m^2 \cdot year)$) disaggregated by region and season.

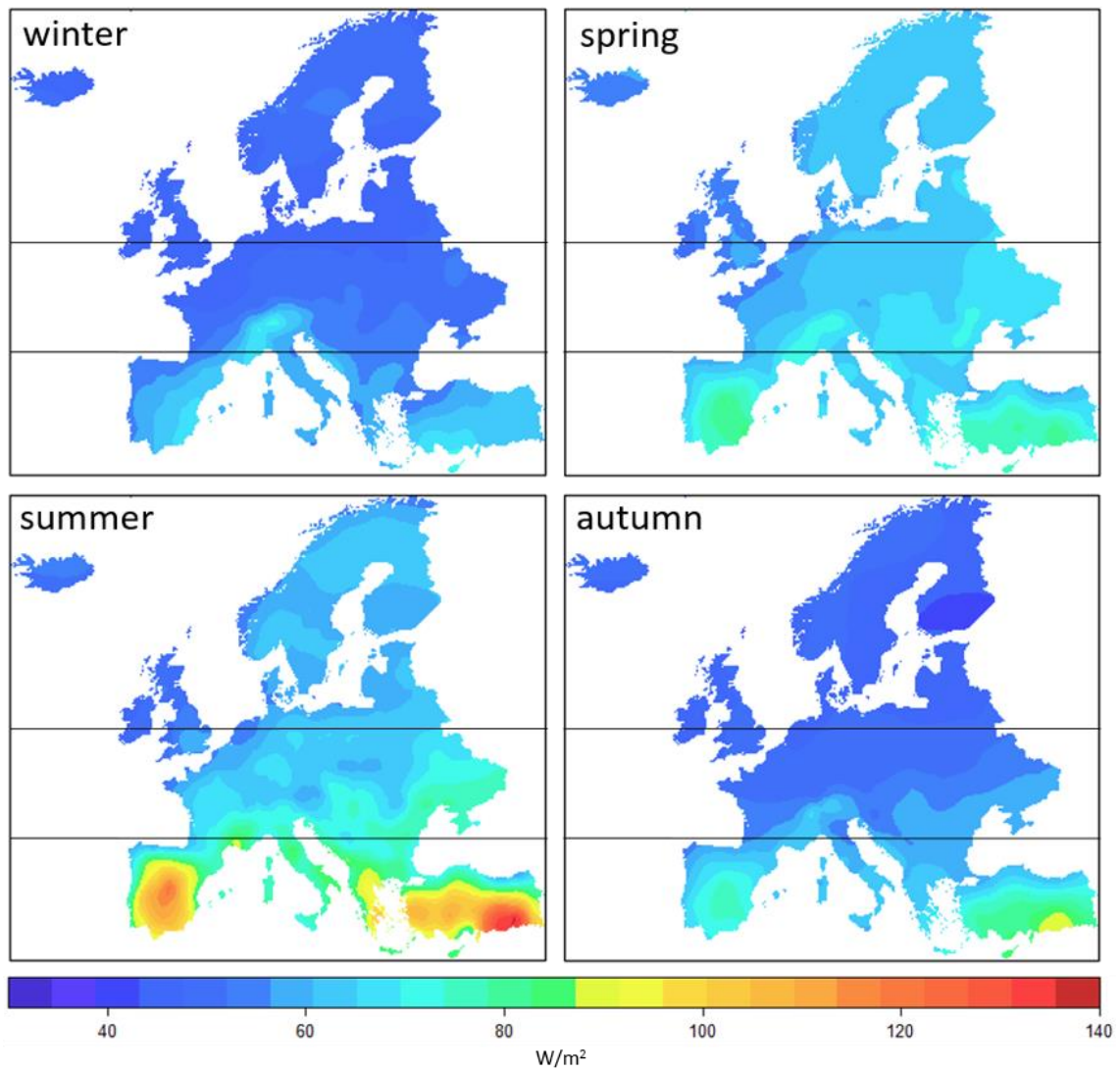|	Centre	North	South	Europe
Winter	110.64 ± 10.91	103.77 ± 11.16	130.24 ± 11.21	112.84 ± 11.07
Spring	140.92 ± 7.10	135.67 ± 7.35	154.73 ± 7.41	142.32 ± 7.26
Summer	147.04 ± 9.73	130.30 ± 10.17	200.15 ± 10.29	153.65 ± 10.01
Autumn	115.73 ± 8.73	101.47 ± 8.83	149.57 ± 8.84	118.69 ± 8.79

Fig 4. All-day radiative cooling power potential resource maps for the different seasons in Europe (in W/m²). Black horizontal lines divide the map into three regions: north (53.55 N–71.15 N), centre (43.46 N–53.55 N) and south (34.60 N–43.46 N).
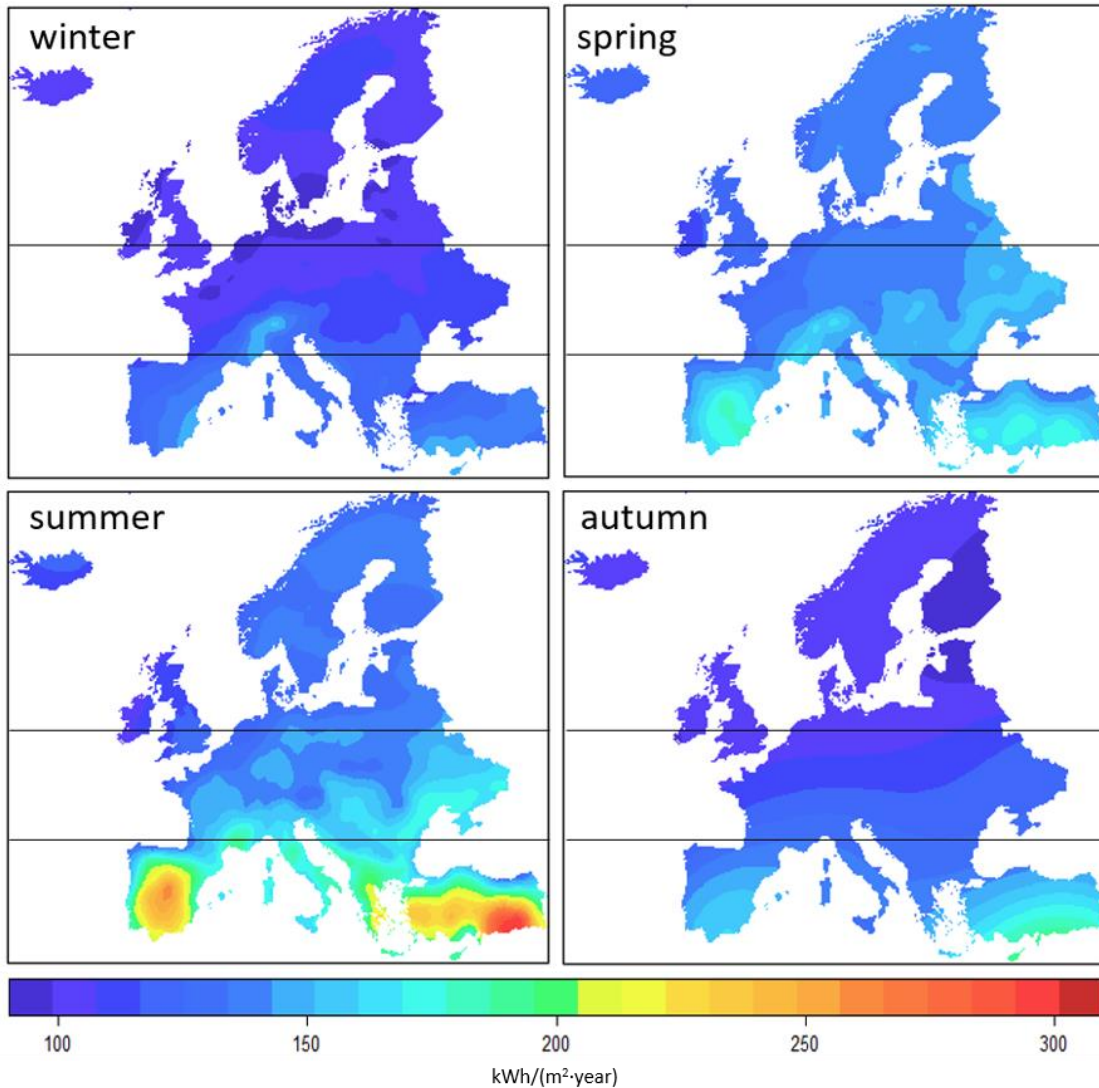
Fig 5. All-day radiative cooling energy potential resource maps for the different seasons in Europe (in kWh/(m²·year)). Black horizontal lines divide the map into three regions: north (53.55 N–71.15 N), centre (43.46 N–53.55 N) and south (34.60 N–43.46 N).

3.2. Evolution of radiative cooling under climate change

3.2.1. Radiative cooling power potential

Fig 6 and Fig 7 show the resource maps of night-time and all-day radiative cooling power potential for the decades 2020-2050 under the climate change scenario A1B of the IPCC. For the year 2020, the forecast of the average night-time is equal to 48.49 W/m²; 48.00 W/m², in 2030 and 2040; and 47.71 W/m², in 2050. Table 7 shows the annual average night-time power values across the continent. Similarly, in Table 8, the average daytime values are presented. No significant differences are observed in the decades analysed. To see better this phenomenon, the boxplots in Fig 8 and Fig 9 are presented. In the boxplots the value of the 50% of the observations are collected within the limits of the coloured boxes; the black horizontal line in each of the boxes represents the median, while the black dot inside each box represents the mean value. The black

dots outside the boxes represent atypical observations (outside the interquartile range). The graph exposes that the distribution of data does not vary significantly between decades in any region. The boxes show that the predicted values exhibit similar distribution: they have similar size and the average and median values remain close during the decades.
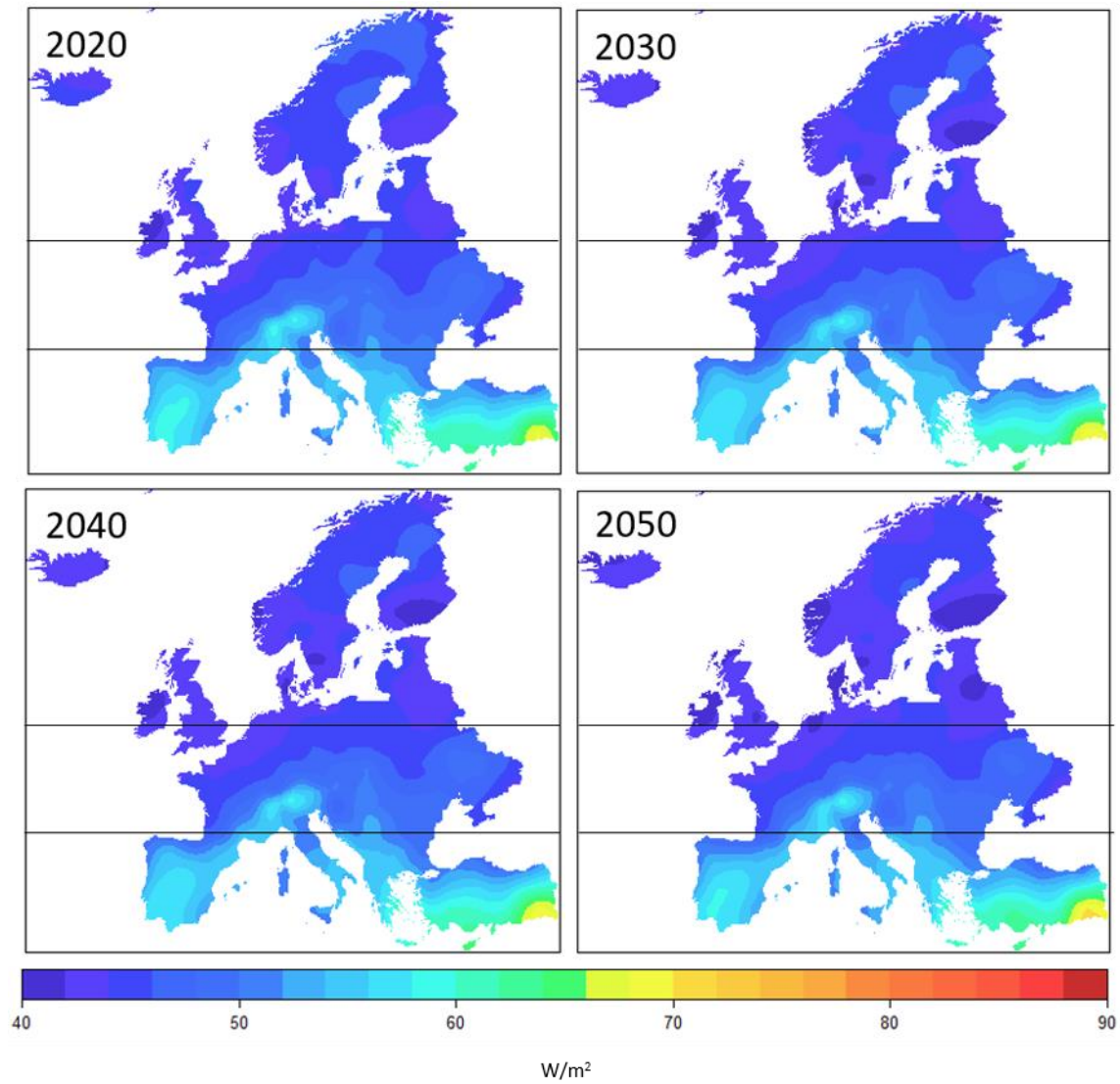
Fig 6. Resource maps of the evolution of the night-time radiative cooling power potential (in W/m^2) under the context of climate change. Study of the scenario A1B proposed in the AR4 by the IPCC. Black horizontal lines divide the map into three regions: north (53.55 N–71.15 N), centre (43.46 N–53.55 N) and south (34.60 N–43.46 N).

Table 7. Evolution of the annual average night-time radiative cooling power potential (in W/m^2) disaggregated by region. Study of scenario A1B of climate change.

| Zone	2020	2030	2040	2050
Centre	47.48 ± 3.44	47.14 ± 3.53	47.21 ± 3.57	46.89 ± 3.45
North	44.64 ± 3.52	43.83 ± 3.61	43.61 ± 3.65	43.20 ± 3.53
South	56.00 ± 3.53	55.70 ± 3.62	55.92 ± 3.68	55.87 ± 3.54
Europe	48.49 ± 3.49	48.00 ± 3.58	48.00 ± 3.62	47.71 ± 3.50
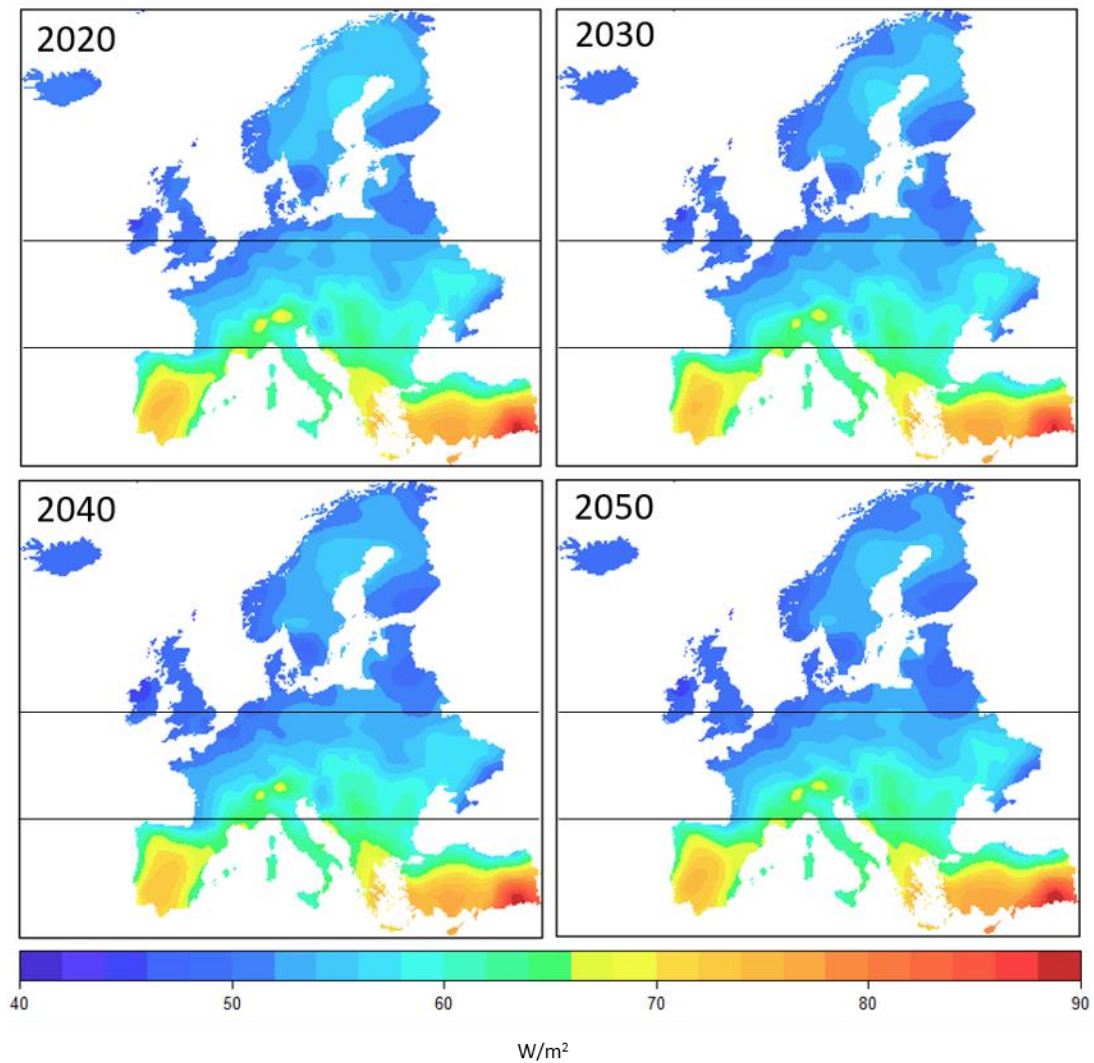
Fig 7. Resource maps of the evolution of the all-day radiative cooling power potential (in W/m^2) under the context of climate change. Study of the scenario A1B proposed in the AR4 by the IPCC. Black horizontal lines divide the map into three regions: north (53.55 N–71.15 N), centre (43.46 N–53.55 N) and south (34.60 N–43.46 N).

Table 8. Evolution of the annual average all-day radiative cooling power potential (in W/m^2) disaggregated by region. Study of scenario A1B of climate change

Zone	2020	2030	2040	2050
Centre	56.26 ± 2.94	56.02 ± 3.09	55.98 ± 3.06	55.92 ± 3.18
North	52.54 ± 3.06	51.69 ± 3.13	51.50 ± 3.11	51.13 ± 3.22
South	68.58 ± 3.08	68.03 ± 3.13	68.06 ± 3.11	68.36 ± 3.23
Europe	57.85 ± 3.01	57.33 ± 3.11	57.24 ± 3.09	57.17 ± 3.21
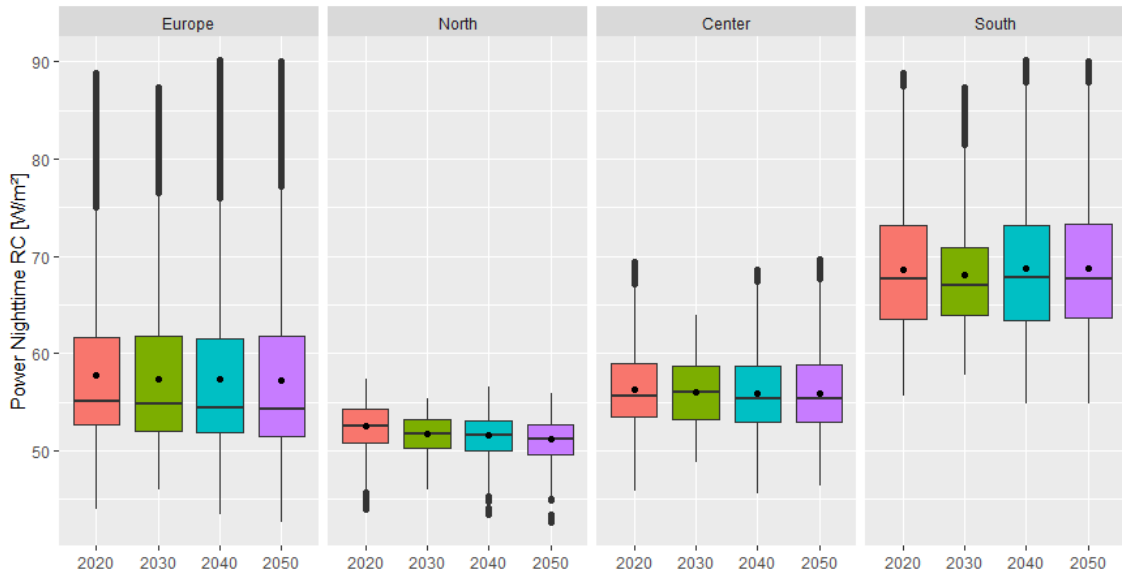
Fig 8. Boxplot with average values of the evolution of the night-time radiative cooling power potential along the years 2020-2050 in the scenario A1B of climate change proposed in the AR4 by the IPCC.

The average night-time power is only reduced by 1.61% between 2020 and 2050, being this reduction the greatest between 2020 and 2030 (1.01%). After disaggregating by regions, the north is the region where the potential decreases the most between 2020 and 2050 (3.23%) while in the south it only decreases by 0.23%; at the central region, the reduction is 1.24%. The values of R^2 are higher than 0.75 while the RMSE is below 2.95 W/m^2 (Table 9).

Similarly, the average all-day power decreases 0.68 W/m^2 (1.18%) in the studied period; being the north the region where the biggest reduction takes place (2.69%). The values of R^2 are higher than 0.91 and the RMSE is lower than 2.22 W/m^2 (Table 9).

Table 9. Performance of the interpolations of the evolution of night-time and all-day radiative cooling power potential between the years 2020-2050. Evaluation of the scenario A1B of climate change.

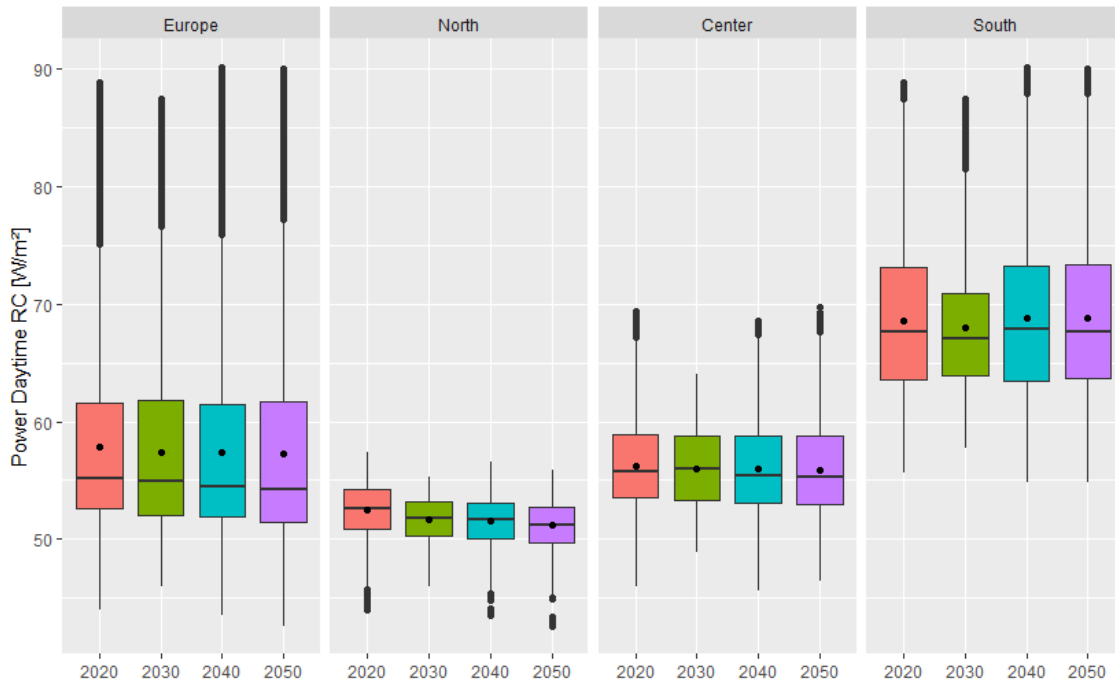|	Night-time		All-Day	
	R^2 [-]	RMSE [W/m^2]	R^2 [-]	RMSE [W/m^2]
2020	0.82	2.52	0.91	2.22
2030	0.75	2.95	0.92	2.13
2040	0.86	2.36	0.92	2.17
2050	0.80	2.73	0.93	2.16

Fig 9. Boxplot with average values of the evolution of the all-day radiative cooling power potential along the decades 2020-2050 in the scenario A1B of climate change proposed in the AR4 by the IPCC.

In this section we have seen that, despite the increase of ambient temperature and the consequent increase of the radiation emitted by a radiative cooling surface, it does not translate into an increase of the radiative cooling power potential. In section 3.2.2 this effect is analysed.

The results are similar for scenarios B1 and A2, so they will not be analysed in this section and we only offer the average value results in Table 10 and Table 11. The maps for these scenarios can be found in Appendix.

Table 10. Evolution of the annual average night-time radiative cooling power potential (in W/m^2) under different climate change scenarios (A1B, A2 and B1).

Scenario	2020	2030	2040	2050
A1B	48.49 ± 3.49	48.00 ± 3.58	48.00 ± 3.61	47.71 ± 3.50
A2	48.61 ± 3.31	48.16 ± 3.52	48.05 ± 3.42	47.80 ± 3.27
B1	48.57 ± 3.34	48.08 ± 3.50	47.92 ± 3.34	47.92 ± 3.34

Table 11. Evolution of the annual average all-time radiative cooling power potential (in W/m^2) under different climate change scenarios (A1B, A2 and B1).

Scenario	2020	2030	2040	2050
A1B	57.85 ± 3.01	57.33 ± 3.11	57.42 ± 3.05	57.28 ± 3.30
A2	57.93 ± 2.96	57.54 ± 3.06	57.43 ± 2.82	57.24 ± 2.99
B1	57.87 ± 3.10	57.54 ± 3.09	57.47 ± 3.07	57.46 ± 3.07

3.2.2. Evolution of the ambient temperature and the atmospheric radiation

We have applied Kriging interpolation to ambient temperature and atmospheric radiation meteorological data. In the case of scenario A1B, the average temperature in Europe in 2020 is 9.52 °C, while in 2050, it increases to 10.73 °C. This increase of 1.21 °C does not translate, as seen in the previous sections, into an increase of radiative cooling power. Conversely, during the period analysed, the power slightly decreased.

In scenario A1B, the predicted infrared radiation from atmosphere in 2020 is 306.82 W/m^2, while in 2050, an increase to 313.80 W/m^2 is predicted. The increase of the emitted radiation of a radiative cooling surface, due to the increase of the ambient temperature over the years, is balanced by the consequent increase of the atmospheric infrared radiation absorbed by the surface. As a result, the net balance remains almost constant during the studied period. The slight decrease in the potential between 2020 and 2050 means that the increase of the atmospheric radiation surpasses the increase of the radiation emitted by the radiative surface; the atmosphere becomes more absorptive and emissive. Scenarios A2 and B1 present the same trend, as exposed in Fig 10, which explains the almost constant radiative cooling potential among the decades studied in this paper.

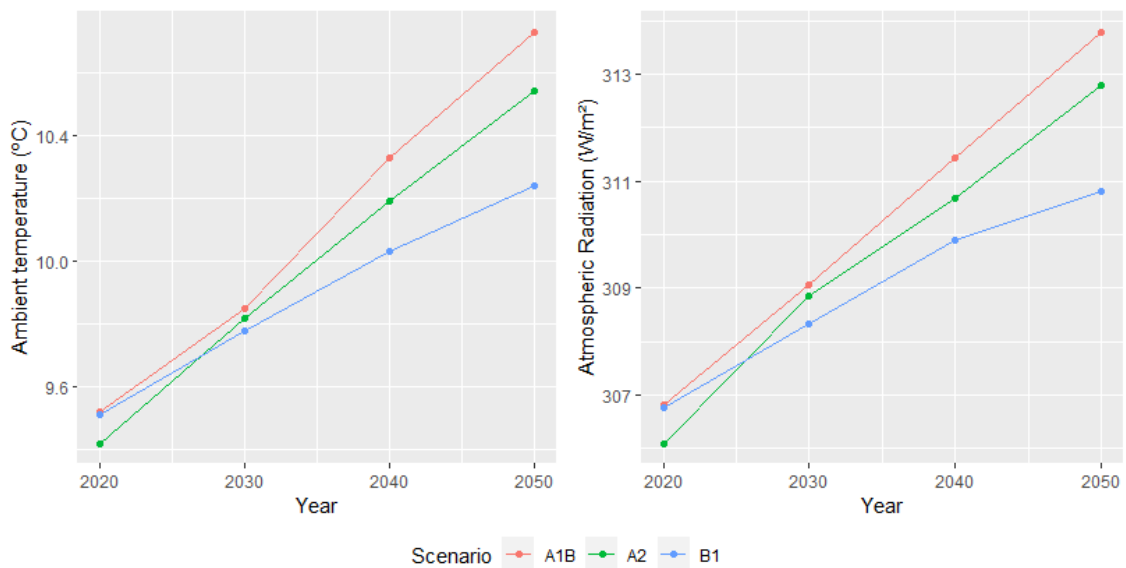Fig 10. Evolution of the average ambient temperature (left) and atmospheric radiation (right) under the three different IPCC scenarios (A1B, B2 and B1).

4. Conclusions

In this article we have presented resource maps in Europe of power and energy potential of night-time and all-day radiative cooling. In real applications, the performance of RC surfaces will fall below these potential values.

Kriging interpolation was used to predict values from known data. The interpolations performed well in terms of high R^2 (the models collected and explained most of the variability of the data) and low RMSE (the model gave accurate predictions).

For night-time applications, spring is identified as the season with the highest night-time performance in terms of power (52.72 W/m^2 on average). However, in southern Europe, where temperatures are warmer and there are more cooling requirements, the peak season occurs on summer (70.39 W/m^2 on average). Winter is the season of the year when more radiative cooling energy is produced (68.96 kWh/(m$^2\cdot$year)). Shifting towards all-day RC applications, summer is the season that presents the highest potential both in terms of power and energy (69.59 W/m^2 and 153.65 kWh/(m$^2\cdot$year)); enhancing the idea of using all-day RC applications in order to expand the full potential of this technology.

The study of the evolution of power and energy potential under climate change scenarios reveals that between the period 2020-2050, radiative cooling rates will decrease slightly both in night-time and daytime RC applications. Despite the increase in ambient temperature in all scenarios, the consequent increase in atmospheric radiation is slightly greater than the radiation emitted by the RC surface radiation.

However, as the radiative cooling potential remains barely constant during the studied period, we can consider RC technology as a reliable and robust present and future renewable energy technology, which can contribute to fulfill the increasing cooling demands in buildings, especially if all-day RC systems are used.

The maps presented in this study will be a helpful tool in the decision planning to implement radiative cooling technologies in Europe; especially in southern regions, where the greatest potentials of RC can assist supplying, totally or partially, the cooling demand associated with the warm climates of this region.

Acknowledgment

References

1. Catalanotti, S.; Cuomo, V.; Piro, G.; Ruggi, D.; Silvestrini, V.; Troise, G. The Radiative Cooling of Selective Surfaces. *Solar Energy* **1975**, *17*, 83–89, doi:10.1016/0038-092X(75)90062-6.
2. Kecebas, M.A.; Menguc, M.P.; Kosar, A.; Sendur, K. Passive Radiative Cooling Design with Broadband Optical Thin-Film Filters. *Journal of Quantitative Spectroscopy and Radiative Transfer* **2017**, *198*, 179–186, doi:10.1016/j.jqsrt.2017.03.046.

3. Mandal, J.; Fu, Y.; Overvig, A.C.; Jia, M.; Sun, K.; Shi, N.N.; Zhou, H.; Xiao, X.; Yu, N.; Yang, Y. Hierarchically Porous Polymer Coatings for Highly Efficient Passive Daytime Radiative Cooling. *Science* **2018**, *362*, 315–319, doi:10.1126/science.aat9513.

4. Cho, J.-W.; Lee, T.-I.; Kim, D.-S.; Park, K.-H.; Kim, Y.-S.; Kim, S.-K. Visible to Near-Infrared Thermal Radiation from Nanostructured Tungsten Anntennas. *J. Opt.* **2018**, *20*, 09LT01, doi:10.1088/2040-8986/aad708.

5. Ko, B.; Lee, D.; Badloe, T.; Rho, J. Metamaterial-Based Radiative Cooling: Towards Energy-Free All-Day Cooling. *Energies* **2018**, *12*, 89, doi:10.3390/en12010089.

6. Cui, Y.; Luo, X.; Zhang, F.; Sun, L.; Jin, N.; Yang, W. Progress of Passive Daytime Radiative Cooling Technologies towards Commercial Applications. *Particuology* **2022**, *67*, 57–67, doi:10.1016/j.partic.2021.10.004.

7. Vall, S.; Medrano, M.; Solé, C.; Castell, A. Combined Radiative Cooling and Solar Thermal Collection: Experimental Proof of Concept. *Energies* **2020**, *13*, 893, doi:10.3390/en13040893.

8. Matsuta, M.; Terada, S.; Ito, H. Solar Heating and Radiative Cooling Using a Solar Collector-Sky Radiator with a Spectrally Selective Surface. *Solar Energy* **1987**, *39*, 183–186.

9. Hu, M.; Pei, G.; Wang, Q.; Li, J.; Wang, Y.; Ji, J. Field Test and Preliminary Analysis of a Combined Diurnal Solar Heating and Nocturnal Radiative Cooling System. *Applied Energy* **2016**, *179*, 899–908, doi:10.1016/j.apenergy.2016.07.066.

10. Berdahl, P.; Fromberg, R. The Thermal Radiance of Clear Skies. *Solar Energy* **1982**, *29*, 299–314, doi:10.1016/0038-092X(82)90245-6.

11. Tang, R.; Etzion, Y.; Meir, I.A. Estimates of Clear Night Sky Emissivity in the Negev Highlands, Israel. *Energy Conversion and Management* **2004**, *45*, 1831–1843, doi:10.1016/j.enconman.2003.09.033.

12. Li, M.; Coimbra, C.F.M. On the Effective Spectral Emissivity of Clear Skies and the Radiative Cooling Potential of Selectively Designed Materials. *International Journal of Heat and Mass Transfer* **2019**, *135*, 1053–1062, doi:10.1016/j.ijheatmasstransfer.2019.02.040.

13. Vall, S.; Castell, A.; Medrano, M. Energy Savings Potential of a Novel Radiative Cooling and Solar Thermal Collection Concept in Buildings for Various World Climates. *Energy Technol.* **2018**, *6*, 2200–2209, doi:10.1002/ente.201800164.

14. Li, M.; Peterson, H.B.; Coimbra, C.F.M. Radiative Cooling Resource Maps for the Contiguous United States. *Journal of Renewable and Sustainable Energy* **2019**, *11*, 036501, doi:10.1063/1.5094510.

15. Chang, K.; Zhang, Q. Modeling of Downward Longwave Radiation and Radiative Cooling Potential in China. *Journal of Renewable and Sustainable Energy* **2019**, *11*, 066501, doi:10.1063/1.5117319.

16. Vilà, R.; Medrano, M.; Castell, A. Mapping Nighttime and All-Day Radiative Cooling Potential in Europe and the Influence of Solar Reflectivity. *Atmosphere* **2021**, *12*, 1119, doi:10.3390/atmos12091119.

17. Aili, A.; Yin, X.; Yang, R. Global Radiative Sky Cooling Potential Adjusted for Population Density and Cooling Demand. *Atmosphere* **2021**, *12*, 1379, doi:10.3390/atmos12111379.

18. *Special Report on Emissions Scenarios: A Special Report of Working Group III of the Intergovernmental Panel on Climate Change*; Nakićenović, N., Intergovernmental Panel on Climate Change, Eds.; Cambridge University Press: Cambridge ; New York, 2000; ISBN 978-0-521-80081-5.

19. Remund, J.; Müller, S.; Kunz, S.; Huguenin-Landl, B.; Studer, C.; Cattin, R. *Meteonorm*; Meteotest: Switzerland, 2019;

20. Intergovernmental Panel on Climate Change *Climate Change 2014 Mitigation of Climate Change: Working Group III Contribution to the Fifth Assessment Report of the Intergovernmental Panel on Climate Change*; Cambridge University Press: Cambridge, 2014; ISBN 978-1-107-41541-6.

21. Hossain, M.M.; Jia, B.; Gu, M. A Metamaterial Emitter for Highly Efficient Radiative Cooling. *Advanced Optical Materials* **2015**, *3*, 1047–1051, doi:10.1002/adom.201500119.

22. Zhai, Y.; Ma, Y.; David, S.N.; Zhao, D.; Lou, R.; Tan, G.; Yang, R.; Yin, X. Scalable-Manufactured Randomized Glass-Polymer Hybrid Metamaterial for Daytime Radiative Cooling. *Science* **2017**, *355*, 1062–1066, doi:10.1126/science.aai7899.

23. Rephaeli, E.; Raman, A.; Fan, S. Ultrabroadband Photonic Structures To Achieve High-Performance Daytime Radiative Cooling. *Nano Lett.* **2013**, *13*, 1457–1461, doi:10.1021/nl4004283.

24. Vilà, R.; Martorell, I.; Medrano, M.; Castell, A. Adaptive Covers for Combined Radiative Cooling and Solar Heating. A Review of Existing Technology and Materials. *Solar Energy Materials and Solar Cells* **2021**, *230*, 111275, doi:10.1016/j.solmat.2021.111275.

25. Aubinet, M. Longwave Sky Radiation Parametrizations. *Solar Energy* **1994**, *53*, 147–154, doi:10.1016/0038-092X(94)90475-8.

26. Hengl, T. A Practical Guide to Geostatistical Mapping of Enviromental Variables. *Office for Official Publications of the European Communities* **2007**, 165, doi:JRC38153.

27. Persson, U.; Werner, S. *Quantifying the Heating and Cooling Demand in Europe*; STRATEGO Enhanced Heating & Cooling Plans, 2015;
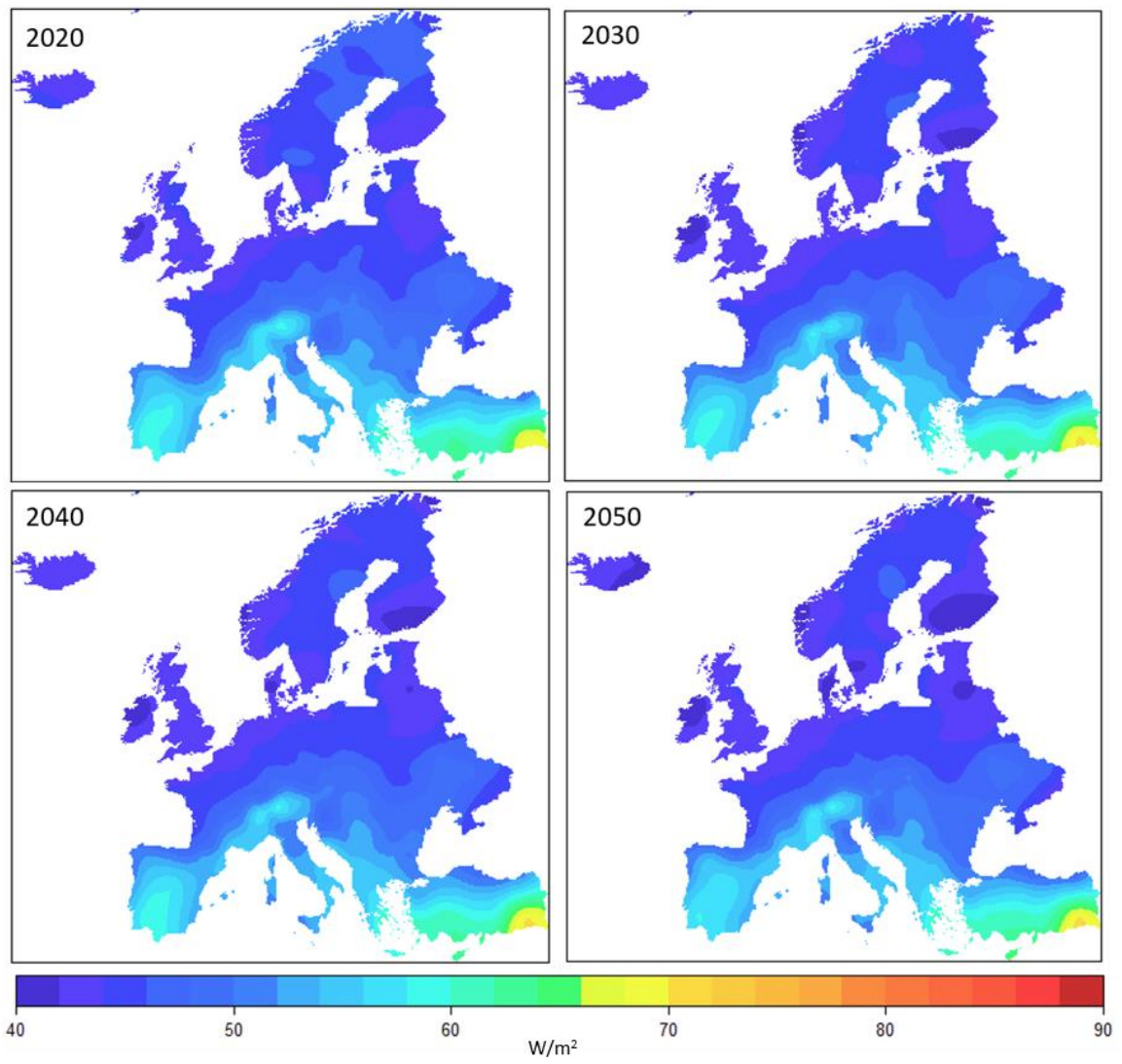
Appendix

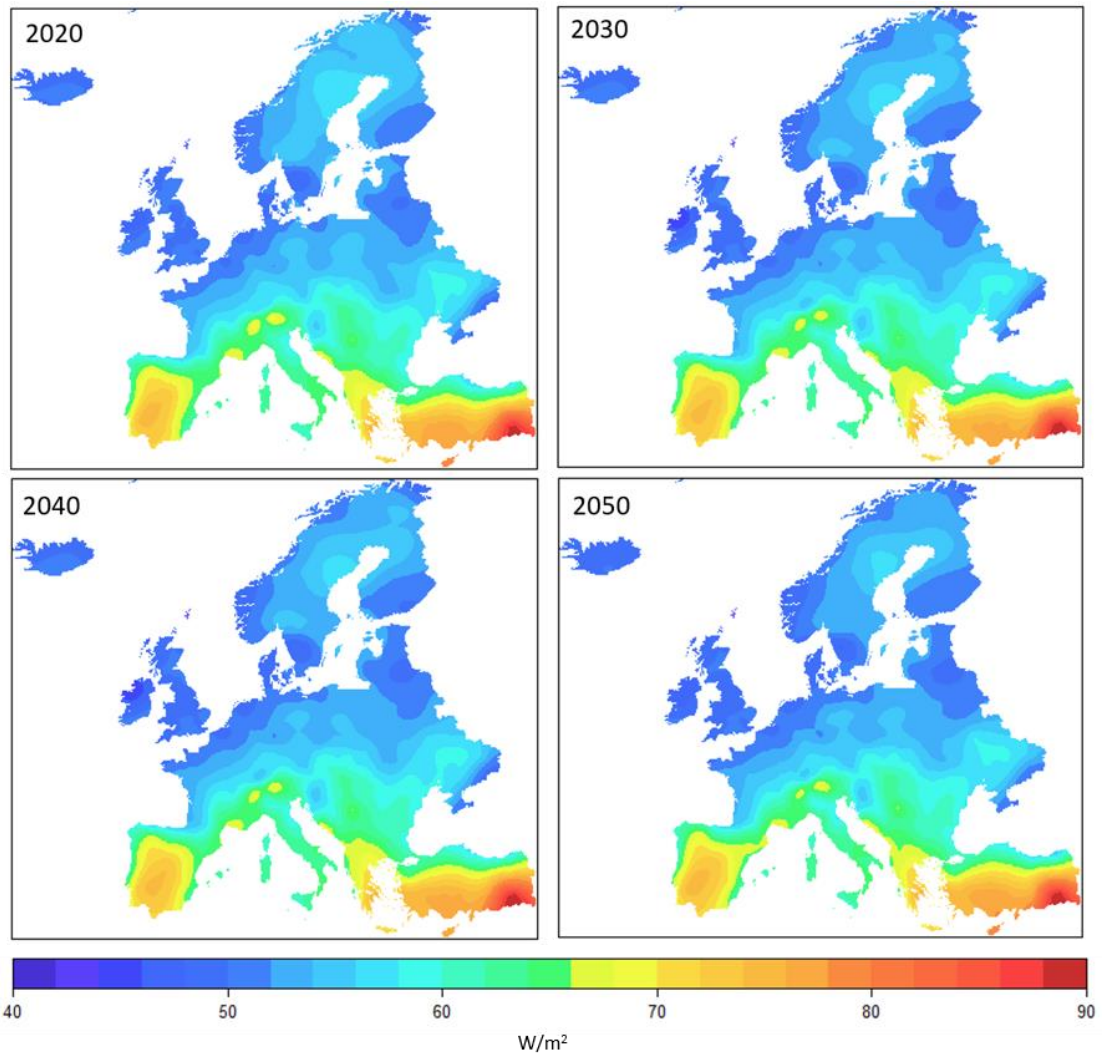1. Nocturnal power potential resource maps evolution for scenario A2
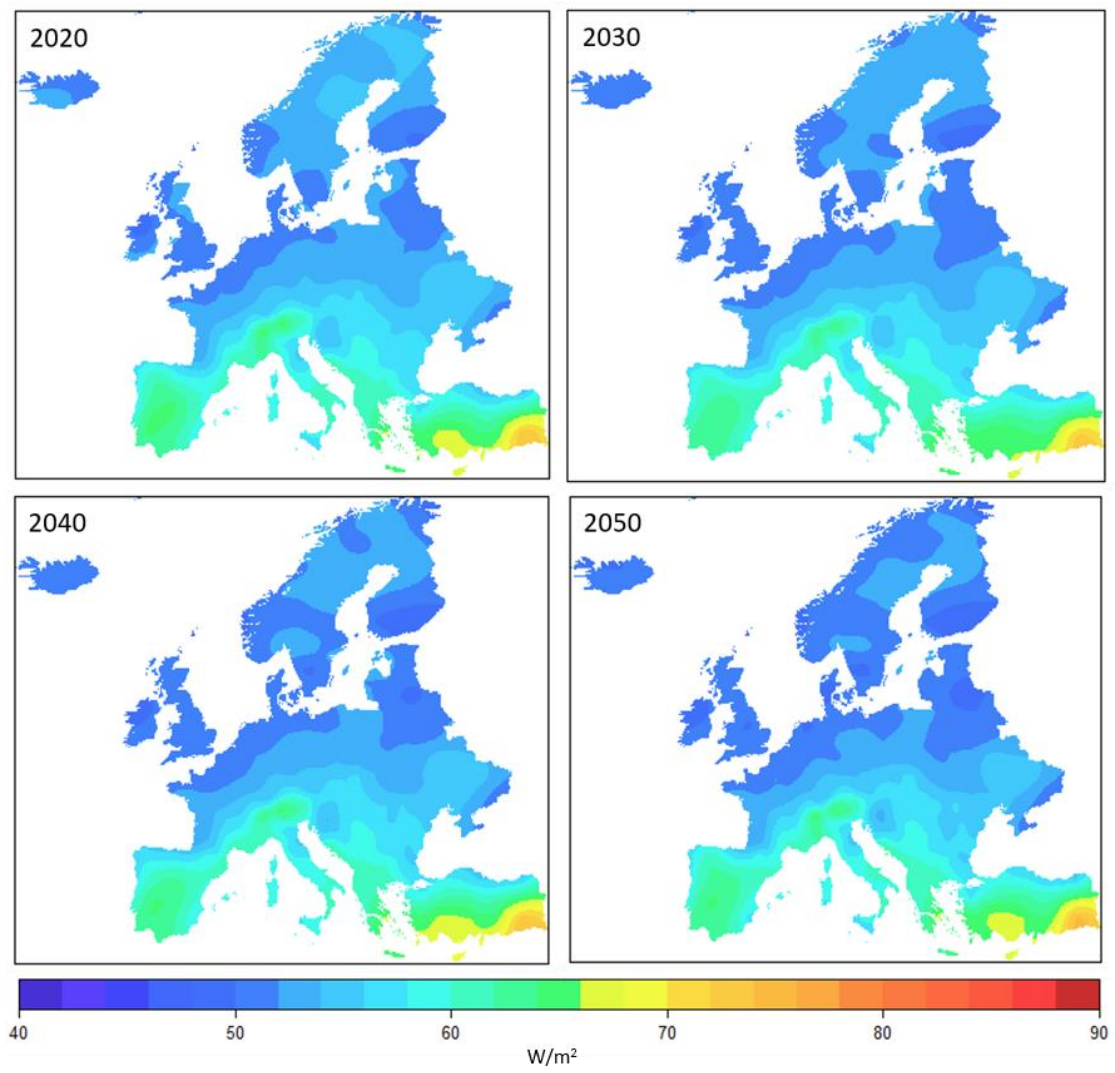
2. All-day power potential resource maps evolution for scenario A2
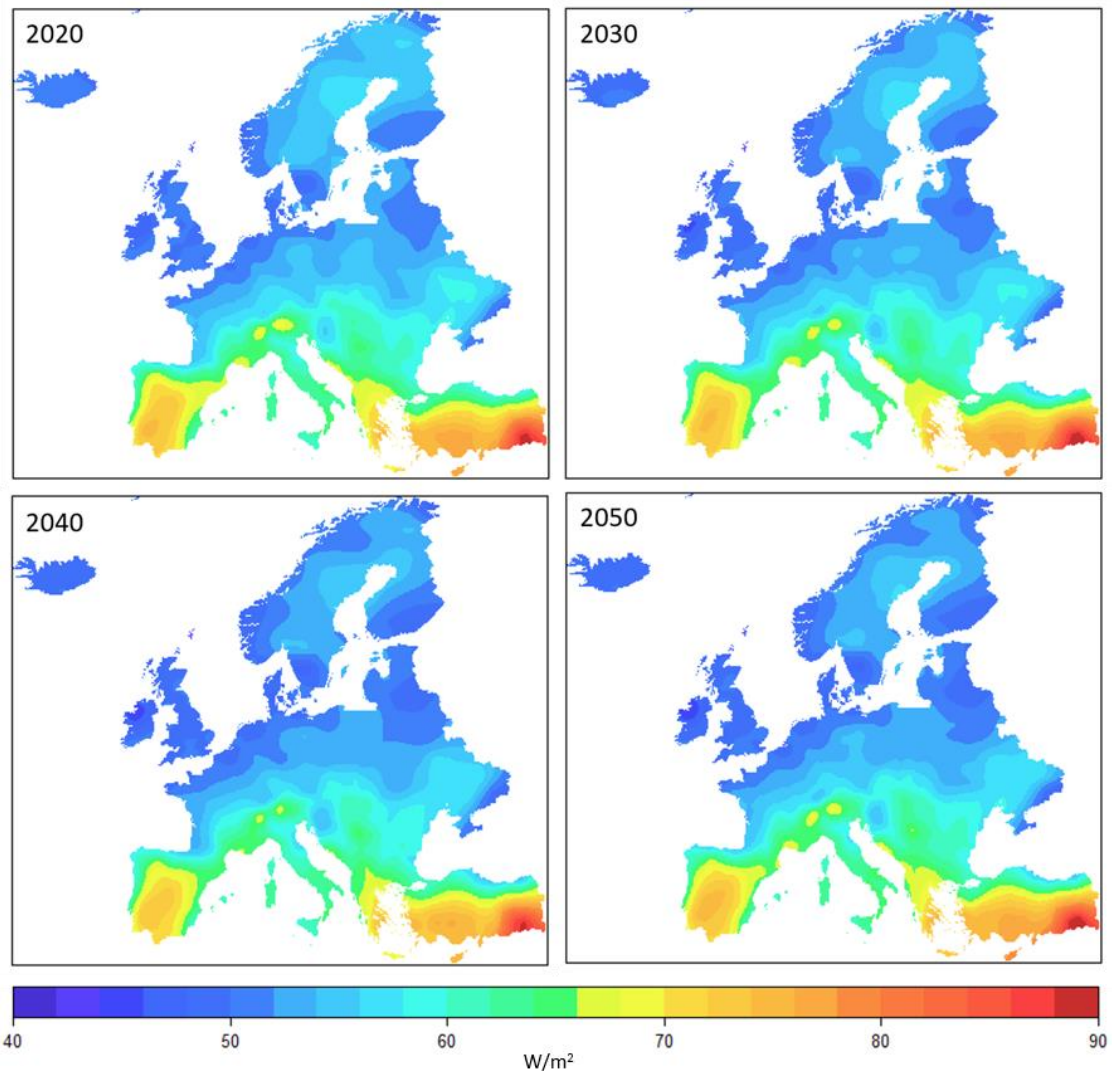
3. Nocturnal power potential resource maps evolution for scenario B1

4. All-day power potential resource maps evolution for scenario B1

Chapter IX.   Conclusions and future research

1. Conclusions of the thesis

The present PhD thesis has presented different strategies to take profit of the cold generated by radiative cooling in an innovative device, named Radiative Collector and Emitter (RCE), capable of producing both cold and heat in a renewable way. During the day the RCE is able to absorb solar radiation to heat up a heat transfer fluid, while during the night it radiates energy to the sky at a wavelength between 8 and 14 μm, allowing the heat transfer fluid to cool down to sub-ambient temperatures. The thesis brings new knowledge in the field of radiative cooling for space cooling, a field that is currently under development, which is presented as a possible solution to current society's energy problems.

The major achievements of the PhD are the following:

- A complete review of the state of the art of adaptive covers for combined radiative cooling and solar heating systems. The review presents the main design solutions for convective covers, with variable optical properties, in order to achieve dual functionality (radiative cooling and solar heating) and reduce convection heat losses. The main materials useful for this type of covers were also discussed.

- The proposal of two different designs for combined RC and HP and the analysis of their performance in a single-family house. Both designs were simulated and their performance was compared to a reference case, showing and improvement of the global performance and energy savings.

- The development of theoretical resource maps of the maximum potential of radiative cooling in Europe based on data recorded by weather stations across the continent. These maps have been used to identify the most suitable areas and seasons of year to use this technology. Maps have also proved the resilience of this technology over the years in different climate change scenarios. A methodology has also been proposed to study the combined potential of radiative cooling and solar heating.

154

The main conclusions from the second part of the thesis (convective covers) and the literature review (**Chapter IV**) are listed below:

- There are two strategies to achieve the dual function of radiative cooling/solar heating. The first strategy is to use adaptive covers on a black surface. The second strategy is based on the use of a selective surface that can control the emissivity/absorptivity properties in different wavelength ranges.

- Adaptive covers provide an improvement over selective surfaces, they reduce parasitic convective exchanges in sub-ambient radiative cooling applications. Adaptive covers can be classified into two different types: exchangeable adaptive covers, which use different materials, with different optical properties, depending on the mode of operation, and smart material covers capable of changing their optical properties.

- The research carried out so far in the field of radiative cooling has not studied in depth the improvement associated to convective covers, and is only presented as a complement. While much of the effort is focused on manufacturing new materials for the emitting surface. In solar heating, on the other hand, the improvement due to the covers has been studied and glass has become a standard material in commercial applications.

- The covers used can be classified into polymeric covers, pigmented covers, deposited films and non-polymeric covers (zinc and cadmium based).

- Polyethylene covers are the most used in radiative cooling applications as they present high transmittance in the atmospheric window and also have a good transmittance to solar radiation. The constant exposure of polyethylene to solar radiation causes structural disadvantages due to aging.

- Pigmented covers and deposited film covers have low transmissivity in the solar range so they are not suitable as covers for combined solar collection and radiative cooling.

- Non-polymeric covers made of zinc crystals have high transmittance in the atmospheric window and medium transmittance in the solar, so they could be used in RCE applications. These materials do not have the structural disadvantages of polyethylene. These are expensive solutions.

- There is not information in the literature of the application of smart chromic materials in RC or RCE applications and more research should be done.

The conclusions derived from the review have confirmed the hypothesis H1. However, it has not been possible to quantify the improvement due to the use of adaptive covers in RCE applications. Finally, although different materials have been selected as RCE cover candidates, structural problems are still a major issue.

From the third part of the thesis (**Chapter V**), related to the integration of RCE systems with heat-pumps, the following was concluded:

- It was proved numerically that RCE can both provide heat and cold during the hottest months of the year in the northern hemisphere.
- The cold generated by the RCE during the night demonstrated to be a useful to dissipate the heat produced in the condenser of a heat pump, increasing the COP of the system and saving electricity.
- The two proposed designs for combining RCE and heat pumps (Peak Load Shifting (PL) and Intermediate Tank (IT)) demonstrated to increase the performance of the system in all the simulated cities (except in PL configuration in Caracas).
- In cities with dry climate and middle-low cooling requirements the improvement of the system is greater (Denver, Lleida and Rome).
- Sub-ambient temperatures were achieved only in IT configurations.
- PL configurations present higher radiative cooling efficiencies in the RCE compared to IT configurations.
- In solar heating mode the RCE field is underused.

The conclusions derived from **Chapter V** have confirmed the hypothesis H2. The combination of RCE with compression heat pumps showed and improvement of the performance of this system. This chapter brings more knowledge on how to integrate radiative cooling technology (in this case RCE technology) with energy systems.

Furthermore, from the study of the potential of implementation of RC and RCE technologies in the fourth part of the thesis (**Chapter VI**, **Chapter VII** and **Chapter VIII**), using the Kriging interpolation methodology, resource maps for radiative cooling and solar heating in Europe have been generated, and the areas of the continent more suitable have been characterized. These studies concluded:

- Kriging is a good methodology to predict unknown power and energy, with high values of R^2 and low RMSE values in Europe.
- The thesis proposes an index to combine both RC + SH maps. Under restrictive criteria only the south and east of the continent are suitable for applying RCE technology, while with medium criteria, the whole continent is suitable.
- The potential of radiative cooling is an order of magnitude lower than in solar heating. The average annual nocturnal potential of radiative cooling in Europe is 50.24 W/m^2 and 212.21 kWh/m^2, and the average annual solar heating potential is 225.08 W/m^2 and 1152.36 kWh/m^2.
- Spring is the season with the highest power (52.72 W/m^2 on average), followed by summer (52.46 W/m^2), winter (49.17 W/m^2), and autumn (47.78 W/m^2). In the south the peak season occurs on summer (70.39 W/m^2 on average).
- In terms of energy, winter is the season with the highest nocturnal potential, while summer is the season with the least potential. The results are influenced by the number of night hours available in each season: in summer the nights are shorter than in winter. The above suggests the use of all-day RC technology to boost its maximum potential.

After studying the potential of all-day radiative cooling, the following conclusions were drawn:

- The best performance is achieved when solar reflectivity is equal to one.
- The maximum potential increases when switching from nocturnal to all-day radiative cooling:
  - On average, the energy potential can increase 127% in Europe.
  - Summer is the season of the year with the highest power potential (65.59 W/m^2 on average) and energy potential (153.65 kWh/m^2 on average) while

in winter the potential is lower (52.24 W/m^2 and 112.84 kWh/m^2 on average).

- o Energy potential increases in all seasons: 1.64 times in winter; 2.97, in spring; 4.03, in summer; and 2.2 in autumn.

- For solar reflectivity values below 0.5, the behavior of the surface can be assimilated to a nocturnal radiative cooler.

- For low values of solar reflectivity, maps tend to show homogeneous patterns all over the continent.

- Small variations in solar reflectivity have greater impacts on the radiative cooling potential at higher reflectivity values than lower ones: in the range of 1–0.8, the reduction of the average power potential is 29.19% and that of the annual energy is 38.83%.

- Performance in radiative cooling remains almost constant between the period 2020-2050. Radiative cooling rates slightly decrease both in nocturnal and all-day applications.

The conclusions derived from part IV (**Chapter VI**, **Chapter VII** and **Chapter VIII**) validated hypothesis H3 and H4. The south of Europe showed the highest potential for implementing RCE technology. From **Chapter V** and **Chapter VII,** the candidate concluded that, in order to achieve the full potential of radiative cooling to meet the cooling demands in buildings, and still be able to perform both solar heating and radiative cooling, a radiative surface able to achieve, during different moments of the day, all-day radiative cooling and diurnal solar heating is required.

1.1 Global conclusion of the thesis

From the conclusions described previously, five global conclusions of the thesis can be extracted:

1. Convective covers can improve the performance of the RCE in two ways: allowing the double function of both solar heating and radiative cooling in a single device, and increasing the efficiency of both processes as they reduce the convective heat exchanges. Nevertheless, structural problems are still an issue to solve in convective covers.

2. The combination of RCE with water-water heat pumps increases the performance of the heat pump in the majority of the studied cases.

3.   According to the potential production, southern Europe is the region which shows the highest potential of implementation of RCE technologies in the continent.

4. The radiative cooling potential will remain barely constant from 2020 to 2050 in Europe.

5. Switching from nocturnal radiative cooling to all-day radiative cooling can drastically improve the production of radiative cooling, up to 127% on average in Europe.

2. Recommendations for future work

Different topics have been identified during the development of the thesis, which felt out of the scope of the thesis, but which the candidate considers appropriate to study in the future in order to make RCE a feasible technology. These topics are listed below:

2.1   Materials

After reviewing the existing literature, a suitable cover material for combined radiative cooling and solar heating could not be found. The combination of a glass cover with a polyethylene cover resulted a good option but it still presents two main drawbacks: (1) it occupies double of its surface and (2) the degradation of polymer makes it not a proper long-term solution. The candidate suggests to characterize chromic materials in both atmospheric window and solar range to see if they are good candidates.

2.2   All-day RCE

Up until this point, the investigations in combined applications have focused on developing a combined system to generate cold during the night and heat during the day. From **Chapter V** it was concluded that RCE was underused for the production of DHW, and from **Chapter VII** it was concluded that all-day radiative cooling can deliver more cooling power and energy. As the heat is still a requirement and its production should not be suppressed, the candidate proposes to investigate the combination of nocturnal radiative cooling with an adaptive diurnal solar heating or radiative cooling depending on the load requirements.

This means that new designs of the RCE should be developed and that the metamaterials, which are now being developed, should be studied in depth and integrated in the new RCE design.

2.3   Control

The control of the system used experimentally was a simple control which only distinguished between night and day, but any other input was not taken into account. This causes that during certain hours of the night, when the meteorological conditions are not favorable for RC, the system is still working and wasting electricity. In the simulations in **Chapter V**, the control also considered that, if the cooling power achieved was low, the system stopped. This was still a simple control.

The candidate recommends to study the possibility of developing a new optimized control system which could consider the prediction of parameters of different nature such as environmental, user consumption, and cost production and it could decide whether or not the activation of the system, in a given time of the night, generates benefits.

2.4   Mapping the potential

The candidate recommends two actions related to the mapping of the potential:

- Using the methodology used in papers P3, P4 and P5 it is possible to generate world hourly source maps of radiative cooling. The candidate proposes to generate these maps which could be a more powerful decision and design tool.
- Radiative cooling source maps provide the maximum potential that can be achieved in a certain location, but they do not give information on whether the cold produced can cover or not the cooling demands at that point. The candidate recommends to go one step further and to cross the source maps of radiative cooling potential with maps of cooling demand, in order to identify how much of the demand can be covered by radiative cooling.

2.5   Integration of the RCE

The candidate recommends two actions related to the integration of the RCE to energy systems and facilities:

- During the thesis the candidate realized that there is a gap of knowledge related to the integration of RCE with systems. The optimal for the main operational parameter (flow rate inside the RCE) and the main installation parameters (volume of the storage tank, tilt of the RCE and type of connection of the different RCE) are unknown until the moment. These parameters affect the performance of the system. The optimal of these parameters should be studied in the next steps of the research.

- In this thesis the integration of the RCE with other cooling systems was only studied in a single-family house. The candidate suggests to investigate the performance of the systems in different buildings and industries with different load profiles.

Chapter X.   List of contributions

1. Journal papers included in the thesis

- **Vilà, R.**, Martorell, I., Medrano, M., Castell, A., 2021. Adaptive covers for combined radiative cooling and solar heating. A review of existing technology and materials. Solar Energy Materials and Solar Cells 230, 111275. doi.org/10.1016/j.solmat.2021.111275

- **Vilà, R.**, Medrano, M., Castell, A., 2021. Mapping Nighttime and All-Day Radiative Cooling Potential in Europe and the Influence of Solar Reflectivity. Atmosphere 12, 1119. doi.org/10.3390/atmos12091119

- **Vilà, R.**, Rincón, L., Medrano, M., Castell, A, 2022. Potential Maps for Combined Nocturnal Radiative Cooling and Diurnal Solar Heating Applications in Europe. Renewable Energy (Under peer-review process).

- **Vilà, R.**, Medrano, M., Castell, A., 2022. Climate change influences in the determination of the maximum power potential of radiative cooling. Evolution and seasonal study in Europe. Renewable Energy (Under peer-review process).

- **Vilà, R.**, Medrano, M., Castell, A., 2022. Numerical Analysis of the Combination of Radiative Collectors and Emitters to Improve the Performance of Water-Water Compression Heat Pumps under Different Climates. Energy. (Under peer-review process).

2. Other journal papers contributions

- Martorell, I., Camarasa, J., **Vilà, R.**, Solé, C., Castell, A., 2022. RCE as a device to produce heating and cooling. Transmittance and aging study for cover materials suitable for radiative cooling. (Under peer-review process).

3. Conference contributions

The PhD candidate contributed to the following international conferences:

- **Vilà, R.**, Martorell, I., Medrano, M., Castell, A., 2020a. Optimal Characteristics of an Adaptive Windshield for a Solar Collector and Radiative Cooling Combined System', in: Proceedings of the ISES EuroSun 2020 Conference – 13th International Conference on Solar Energy for Buildings and Industry. Presented at the Eurosun2020, International Solar Energy Society, Athens (Greece), p. 8. doi.org/10.18086/eurosun.2020.06.04

- **Vilà, R.**, Rincón, L., Medrano, M., Castell, A., 2020b. Radiative Cooling Potential Maps for Spain, in: Proceedings of the ISES EuroSun 2020 Conference – 13th International Conference on Solar Energy for Buildings and Industry. Presented at the EuroSun 2020, International Solar Energy Society, Athens (Greece), pp. 1–9. doi.org/10.18086/eurosun.2020.09.01

- **Vilà, R.**, Garcia, M., Medrano, M., Martorell, I., Castell, A., 2020. Combining Radiative Collector and Emitter with Compression Heat Pump: Numerical Analysis, in: Proceedings of the ISES EuroSun 2020 Conference – 13th International Conference on Solar Energy for Buildings and Industry. Presented at the EuroSun 2020, International Solar Energy Society, Athens (Greece), pp. 1–7. doi.org/10.18086/eurosun.2020.06.01

- Castell, A., Medrano, M., Martorell, I., Solé, C., Rincón, L., Saladin, A., Carrobé, A., **Vilà, R.**, 2021. Development and evaluation of a radiative cooling and solar heating system for combined heat and cold production. Phase 1. Presented at the EXCO'21. International Itinerant Exhibition, Valencia (Spain).

- Martorell, I., Camarasa, J., **Vilà, R.**, Solé, C., Castell, A., 2021. RCE as a device to produce heating and cooling. Transmittance and aging study for cover materials suitable for radiative cooling, in: Proceedings of the 6th International Conference on Polygeneration. Presented at the ICP 2021, International Conference on Poligeneration, Zaragoza (Spain).

- **Vilà, R.**, Rincón, L., Medrano, M., Castell, A., 2021. Potential Maps for Combined Nocturnal Radiative Cooling and Diurnal Solar Heating Applications. Cases of Spain, Switzerland, Germany and Sweden., in: Proceedings of the 6th International Conference on Polygeneration. Presented at the ICP 2021, International Conference on Poligeneration, Zaragoza (Spain).

- Medrano, M., Saladin, A., Solé, C., Martorell, I., **Vilà, R.**, Castell, A., 2021. Potential for Integration of a Renewable Combined Heating and Cooling System in Food Industries requiring Heat and Cold. Presented at the ISES Solar World Congress 2021, Kassel (Germany).

- Castell, A., Delgado, M., **Vilà, R.**, Rincón, L., Martorell, I., 2021. Domestic Hot Water and cooling demand coverage for nearly Zero Energy Buildings applying combined solar heating and radiative cooling. Presented at the ISES Solar World Congress 2021, Kassel (Germany).

- Féat, N., Castell, A., Medrano, M., **Vilà, R.**, 2021. Improving cooling production combining Radiative Cooling and Phase Change Materials. Presented at the ICAE International Conference on Applied Energy 2021, Bangkok (Thailand).

- **Vilà, R.**, Medrano, M., Martorell, I., Castell, A., 2022. Radiative Collectors and Emitters to Improve the Efficiency of Compression Heat Pumps. Presented at the XII

National and III International Conference on Engineering Thermodynamics (12CNIT) 2022, Madrid (Spain).

- Medrano, M., Saladin, A., Solé, C., Martorell, I., Vilà, R., Castell, A., 2021. Potential for Integration of a Renewable Combined Heating and Cooling System in Food Industries requiring Heat and Cold. Presented at the ISES Solar World Congress 2021, Kassel (Germany).

- Castell, A., Delgado, M., Vilà, R., Rincón, L., Martorell, I., 2021. Domestic Hot Water and cooling demand coverage for nearly Zero Energy Buildings applying combined solar heating and radiative cooling. Presented at the ISES Solar World Congress 2021, Kassel (Germany).

4. Participation in projects

The PhD candidate participated in the following founded projects:

- SGR SEMB (Sustainable Energy, Machinery and Buildings). AGAUR, grup de recerca consolidat nº 2017 SGR 00659.
- Desarrollo y evaluación de un sistema de refrigeración radiante y captación para producción combinada de frío y calor. Ministerio de Ciencia, Innovación y Universidades, RAD-CHC (RTI2018-097669-A-I00).
- Desarrollo y evaluación de un equipo para producción combinada de frío y calor mediante refrigeración radiante y captación solar. Fundación Iberdrola.
- Poligeneración adaptativa de calor y frío renovables mediante la combinación de captación solar y refrigeración radiante diurna. Ministerio de Ciencia, Innovación y Universidades, PID2021-126643OB-I00.
- Mejora de la potencia de un sistema de producción de frío y calor renovables combinando enfriamiento radiante y captación solar, TED2021-131446B-I00.
- Economía circular en la construcción con tierra y catalogación de suelos idóneos. Ministerio de Ciencia, Innovación y Universidades, TED2021-129705B-C31

5. Book chapters contributions

- Martorell, I., Rincón, L., Castell, A., Medrano, M., Solé, C., Carrobé, A., **Vilà, R**. Análisis térmico de un edificio Earthbag en clima continental Mediterráneo. Monitorización y simulación. Monitorización y evaluación de la habitabilidad, calidad del aire y eficiencia energética de los edificios. Experiencias en España. BIA2017-90912-REDT. pp.119-126. ISBN: 978-84-122767-4-9.
- Castell, A., Medrano, M., Martorell, I., Solé, C., Rincón, L., Saladin, A., Carrobé, A., **Vilà, R.**, 2021. Development and evaluation of a radiative cooling and solar

heating system for combined heat and cold production. Phase 1. Research in Building Engineering EXCO'21. ISBN: 978-84-12-45182-5.

6. Other contributions

- **Vilà, R.**, Castell, A., Martorell, I., Medrano, M., Rincón, L., Solé, C., 2021. Refrigeració radiant per a la climatització d'espais. Estudi del potencial a Europa. Presented at the European Research Night. Available at: https://researchersnight.udl.cat/la-nostra-recerca-2021
- Medrano, M., Martorell, I., Castell, A., **Vilà, R.** Una refrigeració sostenible és possible:la refrigeració radiant. Pensem.cat. Available at: ttps://www.pensem.cat/noticia/252/refrigeracio-sostenible-es-possible-la-refrigeracio-radiant (accessed Jul. 12, 2022).

References

[1] IEA, "Global energy demand rose by 2.3% in 2018, its fastest pace in the last decade," *IEA*, Mar. 26, 2019. https://www.iea.org/news/global-energy-demand-rose-by-23-in-2018-its-fastest-pace-in-the-last-decade (accessed Jan. 23, 2020).

[2] J. Cook *et al.*, "Consensus on consensus: a synthesis of consensus estimates on human-caused global warming," *Environ. Res. Lett.*, vol. 11, no. 4, p. 048002, Apr. 2016, doi: 10.1088/1748-9326/11/4/048002.

[3] "A European Green Deal," *European Commission - European Commission*. https://ec.europa.eu/info/strategy/priorities-2019-2024/european-green-deal_en (accessed Apr. 25, 2022).

[4] Eurostat, "Energy consumption in households," May 2019. https://ec.europa.eu/eurostat/statistics-explained/index.php?title=Energy_consumption_in_households#Use_of_energy_products_in_households_by_purpose

[5] Eurostat, "Energy consumption in households," May 2019. https://ec.europa.eu/eurostat/statistics-explained/index.php?title=Energy_consumption_in_households#Use_of_energy_products_in_households_by_purpose

[6] D. F. Birol, "The Future of Cooling," p. 92, 2018.

[7] A. Gautam, S. Chamoli, A. Kumar, and S. Singh, "A review on technical improvements, economic feasibility and world scenario of solar water heating system," *Renewable and Sustainable Energy Reviews*, vol. 68, pp. 541–562, Feb. 2017, doi: 10.1016/j.rser.2016.09.104.

[8] J. Steven Brown and P. A. Domanski, "Review of alternative cooling technologies," *Applied Thermal Engineering*, vol. 64, no. 1–2, pp. 252–262, Mar. 2014, doi: 10.1016/j.applthermaleng.2013.12.014.

[9] R. Gomri, "Investigation of the potential of application of single effect and multiple effect absorption cooling systems," *Energy Conversion and Management*, vol. 51, no. 8, pp. 1629–1636, Aug. 2010, doi: 10.1016/j.enconman.2009.12.039.

[10] M. Santamouris and J. Feng, "Recent Progress in Daytime Radiative Cooling: Is It the Air Conditioner of the Future?," *Buildings*, vol. 8, no. 12, p. 168, Dec. 2018, doi: 10.3390/buildings8120168.

[11] N. Fernandez, W. Wang, K. J. Alvine, and S. Katipamula, "Energy Savings Potential of Radiative Cooling Technologies," PNNL--24904, 1234791, Nov. 2015. doi: 10.2172/1234791.

[12] M. Santamouris, "Passive cooling of buildings," in *Advances in Solar Energy1*, 1st ed., 2005.

[13] D. J. Fixsen, "The temperature of the cosmic microwave background," *ApJ*, vol. 707, no. 2, pp. 916–920, Dec. 2009, doi: 10.1088/0004-637X/707/2/916.

[14] S. Vall and A. Castell, "Radiative cooling as low-grade energy source: A literature review," *Renewable and Sustainable Energy Reviews*, vol. 77, pp. 803–820, Sep. 2017, doi: 10.1016/j.rser.2017.04.010.

[15] M. M. Hossain and M. Gu, "Radiative cooling: Principles, progress, and potentials," *Advanced Science*, vol. 3, no. 7, pp. 1–10, 2016, doi: 10.1002/advs.201500360.

[16] C. G. Granqvist and A. Hjortsberg, "Radiative cooling to low temperatures: General considerations and application to selectively emitting SiO films," *Journal of Applied Physics*, vol. 52, no. 6, pp. 4205–4220, 1981, doi: 10.1063/1.329270.

[17] C. G. Granqvist, A. Hjortsberg, and T. S. Eriksson, "Radiative Cooling to Low Temperatures with Selectively IR-Emitting Surfaces," *Thin Solid Films*, vol. 90, pp. 187–190, 1982.

[18] M. N. Bahadori, "Passive Cooling Systems in Iranian Architecture," *SCIENTIFIC AMERICAN*, vol. 238, pp. 144–154, 1978.

[19] E. E. Bell, L. Eisner, J. Young, and R. A. Oetjen, "Spectral Radiance of Sky and Terrain at Wavelengths between 1 and 20 Microns II Sky Measurements*," *J. Opt. Soc. Am.*, vol. 50, no. 12, p. 1313, Dec. 1960, doi: 10.1364/JOSA.50.001313.

[20] D. Zhao *et al.*, "Radiative sky cooling: Fundamental principles, materials, and applications," *Applied Physics Reviews*, vol. 6, p. 021306, Jun. 2019, doi: 10.1063/1.5087281.

[21] A. P. Raman, M. A. Anoma, L. Zhu, E. Rephaeli, and S. Fan, "Passive radiative cooling below ambient air temperature under direct sunlight," *Nature*, vol. 515, no. 7528, pp. 540–544, Nov. 2014, doi: 10.1038/nature13883.

[22] E. Rephaeli, A. Raman, and S. Fan, "Ultrabroadband Photonic Structures To Achieve High-Performance Daytime Radiative Cooling," *Nano Lett.*, vol. 13, no. 4, pp. 1457–1461, Apr. 2013, doi: 10.1021/nl4004283.

[23] Y. Zhai *et al.*, "Scalable-manufactured randomized glass-polymer hybrid metamaterial for daytime radiative cooling," *Science*, vol. 355, no. 6329, pp. 1062–1066, Mar. 2017, doi: 10.1126/science.aai7899.

[24] B. Ko, D. Lee, T. Badloe, and J. Rho, "Metamaterial-Based Radiative Cooling: Towards Energy-Free All-Day Cooling," *Energies*, vol. 12, no. 1, p. 89, Dec. 2018, doi: 10.3390/en12010089.

[25] A. S. Farooq, P. Zhang, Y. Gao, and R. Gulfam, "Emerging radiative materials and prospective applications of radiative sky cooling - A review," *Renewable and Sustainable Energy Reviews*, vol. 144, p. 110910, Jul. 2021, doi: 10.1016/j.rser.2021.110910.

[26] A. Khan *et al.*, "Optically Modulated Passive Broadband Daytime Radiative Cooling Materials Can Cool Cities in Summer and Heat Cities in Winter," *Sustainability*, vol. 14, no. 3, p. 1110, Jan. 2022, doi: 10.3390/su14031110.

[27] K.-T. Lin, J. Han, K. Li, C. Guo, H. Lin, and B. Jia, "Radiative cooling: Fundamental physics, atmospheric influences, materials and structural engineering, applications and beyond," *Nano Energy*, vol. 80, p. 105517, Feb. 2021, doi: 10.1016/j.nanoen.2020.105517.

[28] X. Lu, P. Xu, H. Wang, T. Yang, and J. Hou, "Cooling potential and applications prospects of passive radiative cooling in buildings: The current state-of-the-art," *Renewable and Sustainable Energy Reviews*, vol. 65, no. 4800, pp. 1079–1097, 2016, doi: 10.1016/j.rser.2016.07.058.

[29] S. Vall, M. Medrano, C. Solé, and A. Castell, "Combined Radiative Cooling and Solar Thermal Collection: Experimental Proof of Concept," *Energies*, vol. 13, no. 4, p. 893, Feb. 2020, doi: 10.3390/en13040893.

[30] U. Eicker and A. Dalibard, "Photovoltaic-thermal collectors for night radiative cooling of buildings," *Solar Energy*, vol. 85, no. 7, pp. 1322–1335, 2011, doi: 10.1016/j.solener.2011.03.015.

167

[31] G. Mihalakakou, A. Ferrante, and J. O. Lewis, "The cooling potential of a metallic nocturnal radiator," *Energy and Buildings*, vol. 28, no. 3, pp. 251–256, Nov. 1998, doi: 10.1016/S0378-7788(98)00006-1.

[32] M. Sugawara, M. Tago, Y. Komatsu, and H. Beer, "Water freezing at outdoor temperatures higher than 0 °C by the effect of radiative cooling," *Heat Mass Transfer*, vol. 54, no. 1, pp. 1–6, Jan. 2018, doi: 10.1007/s00231-017-2096-2.

[33] D. Zhao *et al.*, "Subambient Cooling of Water: Toward Real-World Applications of Daytime Radiative Cooling," *Joule*, vol. 3, no. 1, pp. 111–123, Jan. 2019, doi: 10.1016/j.joule.2018.10.006.

[34] S. Vall, A. Castell, and M. Medrano, "Energy Savings Potential of a Novel Radiative Cooling and Solar Thermal Collection Concept in Buildings for Various World Climates," *Energy Technol.*, vol. 6, no. 11, pp. 2200–2209, Nov. 2018, doi: 10.1002/ente.201800164.

[35] B. Zhao, M. Hu, X. Ao, X. Huang, X. Ren, and G. Pei, "Conventional photovoltaic panel for nocturnal radiative cooling and preliminary performance analysis," *Energy*, vol. 175, pp. 677–686, May 2019, doi: 10.1016/j.energy.2019.03.106.

[36] W. Li, Y. Shi, K. Chen, L. Zhu, and S. Fan, "A Comprehensive Photonic Approach for Solar Cell Cooling," *ACS Photonics*, vol. 4, no. 4, pp. 774–782, Apr. 2017, doi: 10.1021/acsphotonics.7b00089.

[37] T. S. Safi and J. N. Munday, "Improving photovoltaic performance through radiative cooling in both terrestrial and extraterrestrial environments," *Opt. Express*, vol. 23, no. 19, p. A1120, Sep. 2015, doi: 10.1364/OE.23.0A1120.

[38] M. Matsuta, S. Terada, and H. Ito, "Solar Heating and radiative cooling using a solar collector-sky radiator with a spectrally selective surface," *Solar Energy*, vol. 39, no. 3, pp. 183–186, 1987.

[39] M. Hu, G. Pei, Q. Wang, J. Li, Y. Wang, and J. Ji, "Field test and preliminary analysis of a combined diurnal solar heating and nocturnal radiative cooling system," *Applied Energy*, vol. 179, pp. 899–908, 2016, doi: 10.1016/j.apenergy.2016.07.066.

[40] L. Long, Y. Yang, and L. Wang, "Simultaneously enhanced solar absorption and radiative cooling with thin silica micro-grating coatings for silicon solar cells," *Solar Energy Materials and Solar Cells*, vol. 197, pp. 19–24, Aug. 2019, doi: 10.1016/j.solmat.2019.04.006.

[41] E. Erell and Y. Etzion, "Heating experiments with a radiative cooling system," *Building and Environment*, vol. 31, no. 6, pp. 509–517, Nov. 1996, doi: 10.1016/0360-1323(96)00030-3.

[42] E. Erell and Y. Etzion, "Radiative cooling of buildings with flat-plate solar collectors," *Building and Environment*, vol. 35, no. 4, pp. 297–305, May 2000, doi: 10.1016/S0360-1323(99)00019-0.

[43] J. Liu *et al.*, "Research on the performance of radiative cooling and solar heating coupling module to direct control indoor temperature," *Energy Conversion and Management*, vol. 205, p. 112395, Feb. 2020, doi: 10.1016/j.enconman.2019.112395.

[44] T. E. Johnson, "Radiation cooling of structures with infrared transparent wind screens," *Solar Energy*, vol. 17, no. 3, pp. 173–178, 1975, doi: 10.1016/0038-092X(75)90056-0.

[45] F. Trombe, "Perspectives sur l'utilisation des rayonnements solaires et terrestres dans certaines régions du monde.," *Revue Générale de Thermique*, vol. 6, pp. 1285–1314, 1967.

[46] M. Muselli, "Passive cooling for air-conditioning energy savings with new radiative low-cost coatings," *Energy and Buildings*, vol. 42, no. 6, pp. 945–954, Jun. 2010, doi: 10.1016/j.enbuild.2010.01.006.

[47] M. G. Meir, J. B. Rekstad, and O. M. LØvvik, "A study of a polymer-based radiative cooling system," *Solar Energy*, vol. 73, no. 6, pp. 403–417, Dec. 2002, doi: 10.1016/S0038-092X(03)00019-7.

[48] T. S. Eriksson, S.-J. Jiang, and C. G. Granqvist, "Surface coatings for radiative cooling applications: silicon dioxide and silicon nitride made by reactive RF-sputtering," *Solar Energy Materials*, vol. 12, pp. 319–325, 1985.

[49] T. S. Eriksson and C. G. Granqvist, "Infrared optical properties of electron-beam evaporated silicon oxynitride films," *Applied Optics*, vol. 22, no. 2, pp. 3204–3206, 1983.

[50] A. Hjortsberg and C. G. Granqvist, "Infrared optical properties of silicon monoxide films," *Applied Optics*, vol. 19, no. 10, pp. 1694–1696, 1980.

[51] E. M. Lushiku, T. S. Eriksson, A. Hjortsberg, and C. G. Granqvist, "Radiative cooling to low temperatures with selectively infrared-emitting gases," *Solar & Wind Technology*, vol. 1, no. 2, pp. 115–121, 1984, doi: 10.1016/0741-983X(84)90013-4.

[52] A. Hjortsberg and C. G. Granqvist, "Radiative cooling with selectively emitting ethylene gas," *Applied Physics Letters*, vol. 39, no. 6, pp. 507–509, 1981, doi: 10.1063/1.92783.

[53] J. Song, J. Seo, J. Han, J. Lee, and B. J. Lee, "Ultrahigh emissivity of grating-patterned PDMS film from 8 to 13 μ m wavelength regime," *Appl. Phys. Lett.*, vol. 117, no. 9, p. 094101, Aug. 2020, doi: 10.1063/5.0017838.

[54] M. M. Hossain, B. Jia, and M. Gu, "A Metamaterial Emitter for Highly Efficient Radiative Cooling," *Advanced Optical Materials*, vol. 3, no. 8, pp. 1047–1051, Aug. 2015, doi: 10.1002/adom.201500119.

[55] E. Lee and T. Luo, "Black body-like radiative cooling for flexible thin-film solar cells," *Solar Energy Materials and Solar Cells*, vol. 194, pp. 222–228, Jun. 2019, doi: 10.1016/j.solmat.2019.02.015.

[56] R. Vilà, I. Martorell, M. Medrano, and A. Castell, "Adaptive covers for combined radiative cooling and solar heating. A review of existing technology and materials," *Solar Energy Materials and Solar Cells*, vol. 230, p. 111275, Sep. 2021, doi: 10.1016/j.solmat.2021.111275.

[57] W. Wang, N. Fernandez, and S. Katipamula, "Parametric analysis of a photonic radiative cooling system," presented at the ISES Solar World Congress 2017, 2017. doi: doi:10.18086/swc.2017.17.05.

[58] Z. Cui, C. Guo, and D. Zhao, "Energy-saving and economic analysis of passive radiative sky cooling for telecommunication base station in China," *Build. Simul.*, Mar. 2022, doi: 10.1007/s12273-022-0894-z.

[59] M. Medrano, A. Salandin, C. Solé, I. Martorell, R. Vilà, and A. Castell, "Potential for Integration of a Renewable Combined Heating and Cooling System in Food Industries requiring Heat and Cold," *ISES Solar World Congress 2021*, 2021.

[60] K. Zhang, D. Zhao, X. Yin, R. Yang, and G. Tan, "Energy saving and economic analysis of a new hybrid radiative cooling system for single-family houses in the

USA," *Applied Energy*, vol. 224, pp. 371–381, Aug. 2018, doi: 10.1016/j.apenergy.2018.04.115.

[61] S. Zhang, "Cooling performance of nocturnal radiative cooling combined with microencapsulated phase change material (MPCM) slurry storage," *Energy and Buildings*, p. 9, 2012.

[62] L.-Y. Yang, "Flexible shape-stabilized phase change materials with passive radiative cooling capability for thermal management," *Chemical Engineering Journal*, p. 9, 2021.

[63] N. Féat, A. Castell, M. Medrano, and R. Vilà, "Improving cooling production combining Radiative Cooling and Phase Change Materials," Thailand, 2021, p. 4.

[64] T. Facius and B. Aircoil, "Benefits of Water Cooled vs Air Cooled Equipment in Air Conditioning Applications," *Cooling Technology Institute*, p. 50, 2011.

[65] E. A. Goldstein, A. P. Raman, and S. Fan, "Sub-ambient non-evaporative fluid cooling with the sky," *Nature Energy*, vol. 2, no. 9, p. 17143, Sep. 2017, doi: 10.1038/nenergy.2017.143.

[66] T. Hu, T. H. Kwan, and G. Pei, "An all-day cooling system that combines solar absorption chiller and radiative cooling," *Renewable Energy*, vol. 186, pp. 831–844, Mar. 2022, doi: 10.1016/j.renene.2022.01.058.

[67] A. Argiriou, M. Santamouris, C. Balaras, and S. Jeter, "Potential of radiative cooling in southern Europe," *International Journal of Solar Energy*, vol. 13, no. 3, pp. 189–203, Jan. 1992, doi: 10.1080/01425919208909784.

[68] J. P. Bijarniya, J. Sarkar, and P. Maiti, "Environmental effect on the performance of passive daytime photonic radiative cooling and building energy-saving potential," *Journal of Cleaner Production*, vol. 274, p. 123119, Nov. 2020, doi: 10.1016/j.jclepro.2020.123119.

[69] M. Li, H. B. Peterson, and C. F. M. Coimbra, "Radiative cooling resource maps for the contiguous United States," *Journal of Renewable and Sustainable Energy*, vol. 11, no. 3, p. 036501, May 2019, doi: 10.1063/1.5094510.

[70] K. Chang and Q. Zhang, "Modeling of downward longwave radiation and radiative cooling potential in China," *Journal of Renewable and Sustainable Energy*, vol. 11, no. 6, p. 066501, Nov. 2019, doi: 10.1063/1.5117319.

[71] A. Aili, X. Yin, and R. Yang, "Global Radiative Sky Cooling Potential Adjusted for Population Density and Cooling Demand," *Atmosphere*, vol. 12, no. 11, p. 1379, Oct. 2021, doi: 10.3390/atmos12111379.

[72] "TRNSYS : Transient System Simulation Tool." https://www.trnsys.com/ (accessed Mar. 23, 2022).

[73] S. Vall, K. Johannes, D. David, and A. Castell, "A new flat-plate radiative cooling and solar collector numerical model: Evaluation and metamodeling," *Energy*, vol. 202, p. 117750, Jul. 2020, doi: 10.1016/j.energy.2020.117750.

[74] J. Remund, S. Müller, S. Kunz, B. Huguenin-Landl, C. Studer, and R. Cattin, "Meteonorm." Meteotest, Switzerland, Jul. 23, 2019. [Windows Vista/7/8/10 32/64 bit]. Available: https://meteonorm.com/en/download

[75] C. G. Granqvist and G. A. Niklasson, "Solar energy materials for thermal applications: A primer," *Solar Energy Materials and Solar Cells*, vol. 180, pp. 213–226, Jun. 2018, doi: 10.1016/j.solmat.2018.02.004.

[76] Y. Etzion and E. Erell, "Thermal storage mass in radiative cooling systems," *Building and Environment*, vol. 26, no. 4, pp. 389–394, Jan. 1991, doi: 10.1016/0360-1323(91)90065-J.

[77] A. Carrobé, M. Medrano, C. Solé, I. Martorell, L. Rincón, and A. Castell, "Experimental Study of a Combined Solar Heating and Radiative Cooling Device with an Adaptive Cover," in *Proceedings of the ISES EuroSun 2020 Conference – 13th International Conference on Solar Energy for Buildings and Industry*, Online, 2020, pp. 1–10. doi: 10.18086/eurosun.2020.06.03.

[78] A. Carrobé, I. Martorell, C. Solé, and A. Castell, "Transmittance analysis for materials suitable as radiative cooling windshield and aging study for polyethylene," in *Proceedings of the ISES EuroSun 2020 Conference – 13th International Conference on Solar Energy for Buildings and Industry*, Online, 2020, pp. 1–9. doi: 10.18086/eurosun.2020.06.02.

[79] J. Zhang *et al.*, "Cover shields for sub-ambient radiative cooling: A literature review," *Renewable and Sustainable Energy Reviews*, vol. 143, p. 110959, Jun. 2021, doi: 10.1016/j.rser.2021.110959.

[80] P. Berdahl and R. Fromberg, "The thermal radiance of clear skies," *Solar Energy*, vol. 29, no. 4, pp. 299–314, 1982, doi: 10.1016/0038-092X(82)90245-6.

[81] R. Tang, Y. Etzion, and I. A. Meir, "Estimates of clear night sky emissivity in the Negev Highlands, Israel," *Energy Conversion and Management*, vol. 45, no. 11–12, pp. 1831–1843, 2004, doi: 10.1016/j.enconman.2003.09.033.

[82] N. ur Rehman, M. Uzair, M. A. Siddiqui, and M. Khamooshi, "Regression Models and Sensitivity Analysis for the Thermal Performance of Solar Flat-Plate Collectors," *Arab J Sci Eng*, vol. 44, no. 2, pp. 1119–1127, Feb. 2019, doi: 10.1007/s13369-018-3432-7.

[83] N. Nakićenović and Intergovernmental Panel on Climate Change, Eds., *Special report on emissions scenarios: a special report of Working Group III of the Intergovernmental Panel on Climate Change*. Cambridge ; New York: Cambridge University Press, 2000.